Spring 2022

# The utilization and loss of available energy in aerospace systems

Mohammad Abbas



Department: Mechanical and Aerospace Engineering

# THE UTILIZATION AND LOSS OF AVAILABLE ENERGY IN AEROSPACE SYSTEMS

by

MOHAMMAD ABBAS

A DISSERTATION

Presented to the Graduate Faculty of the

MISSOURI UNIVERSITY OF SCIENCE AND TECHNOLOGY

In Partial Fulfillment of the Requirements for the Degree

DOCTOR OF PHILOSOPHY

in

AEROSPACE ENGINEERING

2022

Approved by:

David W. Riggins, Advisor
Kelly O. Homan
Serhat Hosder
Henry J. Pernicka
Aleksandr V. Chernatynskiy

## PUBLICATION DISSERTATION OPTION

This dissertation consists of the following four articles, formatted in the style used by the Missouri University of Science and Technology:

Paper I, found on pages 23–76, has been published in the *Aerospace Journal* in Nov 2021.

Paper II, found on pages 77–127, has been published in the *AIAA Journal of Spacecraft and Rockets* in May 2019.

Paper III, found on pages 128–179, has been published in the *AIAA Journal of Spacecraft and Rockets* in Aug 2021.

Paper IV, found on pages 180–227, is intended to be submitted to the *International Journal of Exergy*.

## ABSTRACT

Theoretical principles and analytical methodology for the control volume-based energy availability methodology for aerospace vehicles are developed; applications are made to jet-propelled and rocket-propelled vehicles as well as to stand-alone engine systems. Energy availability utilization characteristics of a modeled turbojet engine are studied across a wide range of operating conditions of throttle setting, flight altitude, and flight Mach number. The method is also extended to consider jet-powered vehicles. Fundamental principles regarding entropy generation and energy availability are developed, including directly linking entropy generation and maximum range and endurance of a powered aircraft. Theory and application of the energy utilization methodology with allocation of losses and productive usage are also developed and shown for atmospheric accelerating and climbing (access-to-space) rockets both at specific flight points as well as across missions. Flight conditions required for optimal performance in terms of energy utilization and entropy generation are theoretically derived and verified with applications. Performance impact of entropy generation both in the engine and in the wake on vehicle performance are studied; studies are made for representative rocket systems. In addition, mission-integrated form of the theoretical availability balance formulation has been derived and generalized for an *N*-stage rocket and cast in both dimensional and non-dimensional forms; theory for special cases and optimization criteria are defined and tested. The primary objective of this work has been to formulate, characterize, and investigate performance of airbreathing and rocket-powered aerospace systems, specifically from the standpoint of energy availability utilization.

# ACKNOWLEDGMENTS

The author wishes to express his most sincere gratitude and appreciation to his doctoral advisor, Professor David W. Riggins, for his constant support, patience, and understanding. His guidance, advice, and wealth of knowledge were essential for the completion of this work. It was a great privilege and an absolute pleasure working with him. I have enjoyed the many thought-provoking discussions we had in his office.

My earnest gratitude also goes to the esteemed members of the doctoral advisory committee, Professors Kelly Homan, Serhat Hosder, Henry Pernicka, and Aleksandr Chernatynskiy for their continuous support.

This work is dedicated to my parents, to whom I am eternally indebted. Their unabating love and unwavering support were crucial throughout the course of this work. This work would not have been possible without them. Many thanks also go to my siblings for their encouragement and support over the years.

I would also like to extend my cordial thanks to my colleague and friend Pratheek Bagivalu Prasanna for his comradeship throughout my time as a graduate student at Missouri S&T.

Lastly, I wish to express my heartfelt thanks to my friend Jack Tuchschmidt for being inspirational and for the many intellectual conversations we had.

# TABLE OF CONTENTS

Page

# LIST OF ILLUSTRATIONS

SECTION Page

# LIST OF TABLES

Page

PAPER I



PAPER II



PAPER IV

# NOMENCLATURE

| Symbol | Description |
|---|---|
| $C$ | Effective exhaust velocity, m/s |
| $C_D$ | Aircraft drag coefficient |
| $C_L$ | Aircraft lift coefficient |
| $\dot{E}$ | Net rate of energy transfer rate into a control volume (both heat and work), W |
| $F_{x(\text{flight})}$ | Net force in the direction of flight, N |
| $H^*$ | Total thermochemical availability, J/kg |
| $h$ | Specific enthalpy, J/kg |
| $I_{sp}$ | Engine specific impulse, s |
| $K$ | Parametric engine entropy generation ratio |
| $\dot{m}$ | Mass flow rate, kg/s |
| $\dot{m}_P$ | Propellant mass flow rate, kg/s |
| $\dot{S}$ | Time rate change in entropy (generation for most cases) across a streamtube, W/K |
| $s$ | Specific entropy, J/kg-K |
| $T$ | Static temperature, K |
| $u_\infty$ | Flight/freestream velocity, m/s |
| $\eta$ | Instantaneous energy utilization effectiveness |
| $\mu_{\text{engine}}$ | Fraction of propellant mass flow rate used to overcome losses in the engine |
| $\mu_{\text{overall}}$ | Fraction of propellant mass flow rate used to overcome all losses in global control volume |

Subscripts

| | |
|---|---|
| $s$ | Exit plane of side-bounding sub-control volume |
| $w$ | Exit plane of wake sub-control volume |
| $\infty$ | Free-stream conditions; upstream (entrance) plane of global control volume |

# 1. INTRODUCTION

The combination of the first and second laws of thermodynamics imply that energy not only has quantity but also has ‘quality.’ This fundamental principle specifically indicates that when a system that is initially not in thermodynamic (thermal, mechanical, and chemical) equilibrium with its surroundings is brought to a state of equilibrium with its surroundings, it is physically not possible to extract all the resulting energy transferred in that process in the form of a work interaction. While the second law, unlike the first law, does differentiate between energy transfer as a heat interaction and energy transfer as a work interaction, the engineering view considers work to be the superior (useful) form. Indeed, many if not most mechanical engineering systems are centered around generating and productively utilizing mechanical work (including vehicles of all types). It should not be overlooked that the science of thermodynamics traces its roots back to engineering applications, such as demonstrated by the pioneering work of Sadi Carnot, as focused on heat engines and available work interactions [1].

Any system that is not in equilibrium with its surroundings can be brought to equilibrium with its surroundings through any number of different processes. The maximum amount of work that can be produced by the system as it undergoes such processes is known as ‘exergy,’ or historically as ‘energy availability’ or ‘available energy,’ as in ‘available to be extracted’ in the form of a work interaction. Exergy is therefore the system’s potential to do work. This maximum amount of ‘producible’ work is obtained for a reversible process that takes the system to the dead state (in which the system is in equilibrium with its surroundings). Regardless of how the system arrives at

the dead state, at that state no more changes can occur and therefore no more work (energy as a work interaction) can be extracted.

Changes in state and accompanying energy interactions between systems can only occur when there is a state of non-equilibrium, as a system in a state of equilibrium will not experience any changes. Furthermore, systems that are not in equilibrium with each other will naturally and spontaneously tend to a state of mutual equilibrium if allowed to interact. Transport phenomena, viz., mass, energy, and momentum transport (diffusion), are the mechanisms by which this natural equilibration process takes place (e.g., friction). Processes involving transport phenomena are inherently irreversible and therefore invariably result in entropy generation. Irreversibilities cause a degradation in the systems' potential to do work. Specifically, then, exergy destruction is proportional to entropy generation.

Exergy analysis has seen wide use and utility for design, analysis, and optimization of ground-based systems, such as powerplants [2]. It has not been as universally accepted or used for aerospace systems, probably due to the lack of a direct link between exergy and traditional vehicle performance metrics (i.e., thrust, drag, lift and other metrics). Nonetheless, due to the importance of the concept, especially when studying the efficiency of systems, a number of works throughout the years have applied exergy analysis, in one form or another, to aerospace systems, see for example Ref. [3-9]. Most of these previous works have focused on airbreathing propulsion systems (i.e., gas turbine cycles) due to the historical connection of exergy (available work) to heat engines [10-17]. Generally speaking, however, there has been limited direct connection of exergy losses made to

classic engine/vehicle performance metrics in most previous works. A more detailed overview of the literature can be found in the introductions of the individual papers.

The research undertaken in this work has focused on furthering the development of the theory and application of second law-based energy utilization methodology and supporting analyses to aerospace systems. In this work, energy utilization analysis specifically refers to analysis that is based on a global control volume approach for an aerospace vehicle (or system) in flight. The resulting energy utilization balance for the flight system (embedded within the fluid defining the global control volume) represents a powerful combination of the first and second laws of thermodynamics, also incorporating momentum and mass principles. The global control volume necessarily includes the wake equilibration region (generally downstream of the vehicle) and most generally propellant feed sub-systems, including propellant tankage. The approach is a form of exergy/availability analysis that has been (largely) developed by Riggins, Moorhouse, and Camberos in recent years [18]. However, because it is based on the global control volume approach and explicitly provides the direct analytical linkage between conventional vehicle/propulsion system performance and entropy generation within the global control volume, it provides a useful (and essentially new) approach for assessing performance characterization of aerospace systems. It inherently allows the fundamental and complete characterization of losses and performance for aerospace vehicles of all types, powered and unpowered. This approach provides additional information beyond conventional analysis. The main objective of this work was to 1) further develop and refine the basic theory of the energy utilization approach, particularly with respect to how the methodology applies

to specific aerospace vehicle systems, 2) develop, tailor, and systemize the approach for these specific applications, and 3) to provide case studies for these applications.

Research and scholarly articles resulting from the overall effort undertaken in this work may be primarily categorized by the two types of aerospace propulsion systems that have been examined (both in conjunction with a vehicle, or as nominal 'stand-alone' flight systems for separate analysis). These two categories of propulsion systems are 1) airbreathing engines, and 2) chemical rocket engines.

Work documented in Paper I is focused on energy utilization analysis involving gas turbine engines (jet engines) and engine-airframe integrated systems (vehicles) with gas turbine propulsion systems. This work, as indicated above, has continued and built on previous preliminary work on this topic completed during the author's MS degree program. Specifically for the effort represented by Paper I, the simplified and approximate turbojet engine model utilized in the earlier work was significantly strengthened and improved and theoretical extensions for specific flight regimes/modes were developed. Engine additive drag and capture issues as relevant to stand-alone and airframe-integrated engine energy utilization analysis were studied. A thermofluid-dynamic model was developed in order to allow the assessment of the installed (as well as the uninstalled) energy utilization characteristics of a turbojet engine. As a result of this effort, the capability was developed to assess a stand-alone turbojet engine in terms of its energy utilization and performance characterization across both on-design and off-design operating conditions, representing the full operational envelope of the engine (in terms of flight Mach, altitudes, and fuel throttle settings). Note that this model and the analytical work presented in this paper represent new capability in terms of enabling the global control volume-based analysis of

the utilization of available energy of nominal ‘stand-alone’ gas turbine engines. Related works on exergy in gas turbines in the literature are generally not based on the global control volume approach and therefore do not explicitly account for wake losses. More significantly, most generally have relied on either approximation involving off-design operation of engines or have not considered off-design operation at all. The theoretical basis for a fundamental superposition principle involving entropy generation has also been developed; this principle mandates that the wake losses (in terms of wake entropy generation) of an integrated airframe/propulsion system (i.e., a powered vehicle) are equal to the combined (separately assessed) losses (entropy generation) in the (separately assessed) wakes of the stand-alone propulsion system and the unpowered airframe; this can be useful in building comprehensive loss audits of powered vehicles from individual stand-alone aerodynamic and propulsive subsystems. In addition, in Paper I, the theoretical basis for describing required conditions for maximum range and endurance in terms of entropy generation in the global control volume are established. This is believed to represent the first explicit description of the direct analytical linkage between entropy generation to range and endurance for a jet-powered vehicle and showcases the utility of the energy utilization methodology and entropy generation analysis for characterizing optimization of aerospace vehicles and missions.

In Paper II, III, and IV, the energy utilization approach has been applied to chemical rocket engines and vehicles utilizing chemical rocket engines. Paper II provides the initial theoretical framework for the comprehensive application of the energy utilization methodology for a staged rocket in flight and presented a preliminary case study of a legacy two-stage access-to-space system. Paper III provides further theoretical development as

well as significantly improved modeling; specifically, a chemical rocket engine model was developed for both hydrogen-fueled and kerosene-fueled rockets (with oxygen as oxidizer) in order to better characterize engine losses. This model utilizes specified tank and injector manifold conditions, nozzle geometry, and propellant flow rates, and returns rocket performance parameters (e.g., thrust, $I_{sp}$, as well as flow conditions and chemical composition at the nozzle's exit). Incorporating this engine model with the global control volume analysis then yields energy availability utilization characteristics of the rocket. This was done both on an instantaneous rate basis as well as on a mission-integrated basis (in the latter, the availability balance is combined with the vehicle's equation of motion). Fundamental metrics are developed which describe the energy availability utilization performance of rockets, and flight conditions that optimize various aspects of energy utilization performance are identified. This work represents the first comprehensive study of the global energy utilization approach for chemical rockets and allows the complete auditing of stack (vehicle) performance for staged systems, with engine modeling. Finally, Paper IV establishes the generalization of the energy utilization methodology for *N*-stage rocket systems, as well as optimization and validation issues for special cases. This paper analytically investigates staging optimization for two special cases: the operation of a two-stage rocket in 1) free-space and 2) vertical climb in a constant gravitational field. Two case studies are also conducted to validate and illustrate the analytical results.

As discussed earlier, this body of work is based on the energy availability utilization methodology, as rooted in a global control volume approach to a vehicle in flight. This technique differs from other works that employed exergy to study aerospace systems in several ways. One important distinction is that this method explicitly includes the wake of

the vehicle in the analysis. This directly accounts for the losses incurred by the system in that region (which represents a large proportion of overall losses). Another distinction is that this method is inherently based on a ‘wholistic’ approach, studying the entire vehicle as one system. Most other works that utilize exergy for aerospace applications focus on the propulsion subsystem alone. In addition, this methodology establishes a direct mathematical relation between the ‘classic’ force-based performance of an aerospace system and losses (in terms of either entropy generation or equivalently losses in exergy). Of the many works that studied gas turbine-engines using exergy, the vast majority employ standard exergy analysis as found in basic thermodynamic textbooks (difference in exergy flow rate between two stations), and as such, do not explicitly establish a direct relation between engine/vehicle traditional performance and loss in availability/exergy. The present work also employs exergetic analysis to a specific gas-turbine engine model incorporating detailed on- and off-design methodology, across a wide range of off-design operating points. Other related works do not generally incorporate the modeling of a single engine with the varying response of various components to change in operating conditions (e.g., the change in compressor ratio, mass capture, etc.). Therefore, when they present performance at different operating conditions, they are effectively studying different engines, or, equivalently, a family of engines. This work, then, constitutes a more accurate representation of a real engine and its exergetic performance over the entire operating range of that (given engine). In addition, it is believed that this is the first work that explicitly and directly delineates the relationship between losses (entropy generation) and aircraft cruise performance in terms of range and endurance.

For rockets, there is relatively very little published work regarding availability/exergy and rocket engines and vehicles. The few publications, other than those presented here, that have attempted to use exergy to study conventional chemical rockets, are based on the energy availability methodology developed at Missouri S&T (and the Air Force Research Laboratory), albeit with very simplified and approximate models. The work presented here on rockets is believed to be new and unique among exergetic studies of aerospace applications. This has also been noted by reviewers of the published journal articles produced.

## 1.1. OVERVIEW OF THE ENERGY AVAILABILITY UTILIZATION METHODOLOGY

Energy availability, or exergy, and entropy generation are well-established concepts in thermodynamics. The application of these concepts in engineering design and analysis, however, has been somewhat limited, particularly in aerospace engineering. The research described in this work constitutes an addition to previous works that have incorporated or have attempted to incorporate the thermodynamic concepts of entropy, exergy, losses, and related ideas to the analysis of aerospace systems (focusing most often on propulsion systems). These works are diverse but do not use a unified approach in terms of formulation (see literature reviews in the papers). The research work described here, however, entirely follows and builds upon the specific approach for analyzing energy utilization that is based on the global control volume approach for vehicle (or flight system) analysis. This approach (termed here energy availability utilization) was first introduced to the scientific community in a paper by Riggins, Moorhouse, and Camberos [18].

As noted, the energy availability methodology is based on a control volume analysis. The aerospace vehicle is embedded in a fluid control volume, designated the global control volume, that encompasses the fluid within the vehicle itself, in the vehicle's zone of influence and in any side-bounding free-stream flow (relevant to supersonic flight), as well as the entire wake region of the vehicle including the exhaust plume(s) of the propulsion system. In the axial direction (i.e., direction of flight), the inflow plane to the control volume is the uniform and undisturbed freestream, sufficiently upstream of the vehicle, and the (equilibrated) outflow plane is at a location sufficiently downstream of the vehicle such that the flow properties are uniform (and infinitesimally displaced from those at the inflow plane). The global control volume is further divided into several streamtubes or sub-volumes. As seen in Figure 1.1, the first of these subdivisions is the vehicle sub-volume, which totally encompasses the vehicle's zone of influence in all directions. Axially, it extends from the uniform freestream, plane ∞, to a location just aft of the vehicle where the flow ceases to directly affect the vehicle, plane $s$. Within this sub-volume the propulsive flowpath(s), which include the fuel/propellant lines all the way to the tanks, constitute separate streamtubes. The wake sub-volume envelopes the vehicle's wake, which includes the exhaust plume(s) of the propulsion system, where the equilibration process between the disturbed flow (by the presence of the vehicle), the exhaust plume(s), and the surrounding ambient is taking place. The side-bounding sub-volume is what remains of the global control volume and encompasses an undisturbed flow. The boundary between the vehicle sub-volume and the side-bounding sub-volume is well defined for supersonic flows.

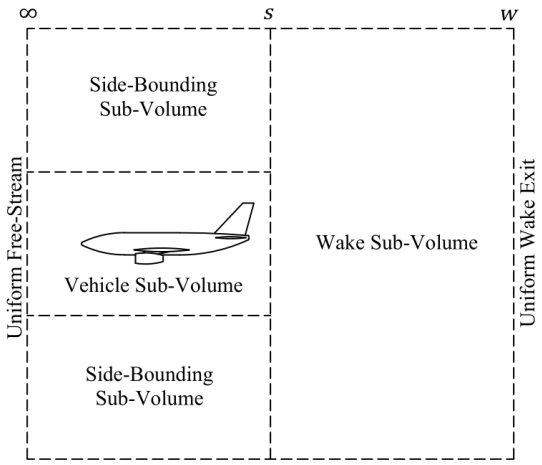


Figure 1.1. Global control volume with major sub-volumes shown.

The analysis invokes the governing equations, applied to the global control volumes, namely: the conservation of mass (continuity), the conservation of energy (first law of thermodynamics), the entropy balance (second law of thermodynamics), and the momentum equation. These relations are combined into a single expression designated the energy availability utilization balance, Eq. (1), which is the central mathematical relation in the energy availability methodology of aerospace systems.

$$u_\infty F_{x(\text{flight})} = \dot{E} + \dot{m}_P \left( H^* + \frac{u_\infty^2}{2} \right) - T_\infty \dot{S}_{\text{total}} \tag{1}$$

The left-hand side of Eq. (1) represents the net force-based power delivered to the vehicle, where $u_\infty$ is the flight velocity magnitude, and $F_{x(\text{flight})}$ is the axial (direction of flight) component of the net fluid dynamic force experienced by the vehicle. This force is the result of the distribution of pressure and shear stress on all wetted surfaces of the vehicle both external and internal (including the fuel/propellant lines). This force is equivalent to thrust minus drag for simple vehicle configurations. This left-hand side term represents the

energy availability utilized (i.e., realized as productive work). The first term on the right-hand side, $\dot{E}$, represents the net rate of energy supply (both heat and work) to the flow from sources outside the global control volume not associated with the propellant (e.g., batteries on board). Note that the vehicle's structure is not part of the global control volume. The second term on the right-hand side is the total energy availability rate associated with the propellant and includes the total thermochemical availability, $H^*$ (to be discussed shortly), and the kinetic energy availability, $u_\infty^2/2$, of the fuel/propellant that is carried onboard the vehicle. In the last term, $T_\infty$ denotes the ambient temperature, while $\dot{S}_{\text{total}}$, as defined in Eq. (2), denotes the change in entropy flow rate across the global control volume, which is predominantly due to entropy generation (irreversibilities) within the global control volume.

$$\dot{S}_{\text{total}} = \Delta\dot{S}_{\infty\to s} + \Delta\dot{S}_{s\to w} = \dot{S}_w - \dot{S}_\infty - \dot{S}_{P(\text{tanks})} = \dot{S}_{\text{vehicle}} + \dot{S}_{\text{wake}} \qquad (2)$$

This entropy term, $T_\infty\dot{S}_{\text{total}}$, represents the loss in energy availability (exergy destruction), while the first two terms on the right-hand side constitute the rate of energy availability (exergy). Care must be taken when there exists a net heat interaction (as part of $\dot{E}$) between the fluid in the global control volume and the surroundings, especially when interpreting the terms previously discussed. That is because energy transferred to/from a system in the form of heat is not entirely available to do work (exergy transferred ≠ heat transferred), and the change in entropy flow rate across the global control volume is not due solely to entropy generation (entropy is transferred by heat). Therefore, for such a case, a reorganization of terms is necessary to keep the interpretation of energy availability and losses precise and correct in accordance with thermodynamics. Nonetheless, the research work presented here nowhere involves a net heat interaction but always assumes a

thermally balanced vehicle where any heat lost by the flow somewhere is eventually reabsorbed by it elsewhere and vice versa. The total thermochemical availability, $H^*$, is defined mathematically in Eq. (3). It constitutes the change in thermochemical availability between 1) the ambient air and propellant/fuel and 2) the equilibrated mixture at the wake's exit plane [19]. The lower heating value of the propellant/fuel may be used as an approximation in lieu of $H^*$ as the difference between the two values is small, especially for low ambient temperatures and moderate tank pressures [19].

$$\begin{aligned} &\dot{m}_P H^* \\ &= \dot{m}_{\text{fuel}} \left(h_{\text{fuel (tank)}} - T_\infty s_{\text{fuel(tank)}}\right) \\ &+ \dot{m}_{\text{oxidizer}} \left(h_{\text{oxidizer(tank)}} - T_\infty s_{\text{oxidizer(tank)}}\right) + \dot{m}_\infty (h_\infty - T_\infty s_\infty) \\ &- \dot{m}_w (h_w - T_\infty s_w) \end{aligned} \tag{3}$$

An efficiency-like parameter, termed the instantaneous energy availability utilization effectiveness $\eta$, is defined in Eq. (4). It is a measure of how much (the fraction) of the available energy (that) is utilized/realized as propulsive power:

$$\eta \equiv \frac{u_\infty F_{x(\text{flight})}}{\dot{m}_P \left(H^* + \frac{u_\infty^2}{2}\right)} \tag{4}$$

## 1.2. OVERVIEW OF WORK

**1.2.1. Paper I: Analysis of Energy Utilization and Losses for Jet-Propelled Vehicles.** A single-spool turbojet engine is modeled with the ability to assess overall as well as component performance for both on-design and off-design operating points spanning a wide range of operating conditions. An operating point is defined by the specification of flight Mach number, flight altitude, and fuel throttle setting. The turbojet

is first analyzed in the stand-alone configuration, i.e., with no airframe integration. Both conventional performance metrics as well as energy availability utilization characteristics are studied, with the focus on the latter.

In addition to the work pertaining to a stand-alone engine, a superposition principle is derived from the theory which states that the wake entropy generations of a stand-alone engine and an unpowered airframe (separately modeled) are shown to be additive when the engine is integrated with the airframe (i.e., forming a powered aircraft) as seen in Eq. (5). This principle allows the easy incorporation of the stand-alone engine model previously developed into an analysis of a complete vehicle.

$$\dot{S}_{\text{wake}} = \dot{S}_{\text{wake(engine alone)}} + \dot{S}_{\text{wake(airframe alone)}} \tag{5}$$

The energy availability balance is then applied to assess the performance of a powered aircraft in cruise flight, specifically in terms of range $R$ and endurance $E$. Note that for a vehicle in cruise flight, the net axial force developed on the vehicle is zero (i.e., $F_{x(\text{flight})} = 0$). Traditional parameters and conditions required to maximize range and endurance are directly correlated with the corresponding conditions associated with total entropy generation in the global control volume. These conditions are summarized as follows: (Note that these conditions, unlike the traditional range and endurance formulations related to the lift and drag coefficients, are exact.)

At max $E$: $\dot{S}_{\text{total (vehicle)}}$ is minimized (exact); $C_L/C_D$ is maximized (approximate)

At max $R$: $\frac{\dot{S}_{\text{total (vehicle)}}}{u_\infty}$ is minimized (exact); $C_L^{1/2}/C_D$ is maximized (approximate)

In a case study that applies the theoretical and analytical formulations developed in this part of the work, the airframe of the Northrop F-5E Tiger II fighter aircraft is integrated

with two turbojet engines (the turbojet engine developed and modeled for this work). Results for this sample application validate the theoretical formulations and provide comparison to traditional formulations for range and endurance.

**1.2.2. Paper II: Analysis of Energy Utilization for Chemical Rockets.** The energy availability balance provided by Eq. (1) is written in instantaneous rate form. This balance can be combined with the vehicle equation of motion (in the direction of flight) utilizing the net force on the vehicle, $F_{x(\text{flight})}$ and integrated over a mission (i.e., across time). Paper II develops the theory for this approach and studies the energy availability and utilization characteristics over an entire mission with specialization to a two-stage access to space system, i.e., focus is on an accelerating and climbing rocket stack from launch to orbit. The rocket is considered to consist of the two stages (effecting two separate burns) along with a 'final' mass, defined as the payload (obviously including all mass of the system after the second stage burnout and stage mass discard or separation). Productive energy utilized for such a mission is defined as the energy imparted to the payload (final mass) and is reflected in the changes of its velocity and its altitude (i.e., change in kinetic and gravitational potential energies) from first stage ignition on the launch pad to mission completion (here identified as occurring at second stage burnout and separation). Losses for this system fall under one of three categories: 1) losses due to irreversibilities (entropy generation) everywhere within the global control volume of fluid that the vehicle is embedded in including internal propulsion system and wake region, 2) kinetic and potential energies imparted to structural mass that is discarded during staging events and 3) potential energy change associated with raising propellant to the altitude it is exhausted from the rocket. Note that the kinetic energy imparted to the propellant up to the point that it is

discharged from the rocket is a loss that is inherently incorporated in the irreversibility term, since the velocity of the plume becomes equilibrated with that of the freestream within the wake mixing process itself (at the given altitude it is expelled).

The losses are further sub-divided into eight contributions (four for each stage): energy utilized to effect 1) change in kinetic energy of the discarded mass at staging, 2) change in gravitational potential energy of the discarded mass at staging, 3) change in the gravitational potential energy of the expelled propellant at altitude, and 4) losses due to irreversibilities. These eight loss terms along with the productive energy utilization associated with kinetic and potential energy changes for the final mass of the vehicle (payload), sum to the overall mission-integrated energy availability. The formulation for how available energy is utilized during the mission (providing a time evolution of losses and energy utilization) is also developed. The analysis and resulting formulations are then applied to the legacy mission for the Apollo 11 Saturn V ascent from launch to second stage separation, using nominal engine performance parameters. Mission (rocket) operational parameters, drag, and trajectory information are obtained from the flight log This study demonstrates that only about 8% of the initially available energy associated with the propellant on the launch pad is actually realized as productive energy availability utilization (providing changes to the kinetic and gravitational potential energies of the final mass, or payload); 86% is lost due to irreversibilities during the operation of both stages, with the remaining balance being associated with the various other losses.

**1.2.3. Paper III: Utilization and Loss of Available Energy for Chemical Rockets in Atmospheric Flight.** This work continues and extends the work documented in Paper II and provides a theoretical study of the (instantaneous) energy availability

characteristics of chemical rockets in flight in the atmosphere, as well as relevant applications. In this work, both hydrogen fuel systems and kerosene-based fuel systems for rockets are modeled and analyzed, with detailed models of combustion and propulsion developed and formulated for extraction of entropy generation and actual computations of entropy generation in the wake performed. Initially in this work, the energy availability balance, Eq. (1), is applied to a stand-alone rocket engine with these detailed internal models and the effects on resulting entropy generations in the engine itself as well as in the wake of the rocket are studied as flight condition is varied (specifically velocity and altitude). For a given rocket, the thrust developed at higher altitudes where atmospheric pressure effects become negligible becomes virtually constant, and as such, the productively utilized available energy (specifically the propulsive power delivered) has essentially a linear dependence on flight velocity. The other terms in the energy utilization balance, including the overall energy availability (see Eq. (1)) which is the sum of the thermochemical availability $H^*$ of the propellant as well as the kinetic energy associated with the stored propellant can, however, vary considerably with flight conditions. This is because $H^*$ has a strong dependence on the ambient temperature (although $H^*$ has no dependence on flight velocity). The paper points out the fact that the contribution of the kinetic energy of the stored propellant on the overall availability grows quadratically with flight velocity, and in fact exceeds the contribution of $H^*$ at high flight velocities. It is found that for any given altitude, there exists a flight velocity that maximizes the instantaneous energy availability utilization effectiveness $\eta$; that velocity is $\sqrt{2H^*}$ (if drag is negligible). This condition does not coincide with the condition at which the entropy generation rate in the global control volume is minimized, which -for negligible drag-

occurs at a flight velocity that equals the effective exhaust velocity of the rocket $C$ (where $C = \text{Thrust}/\dot{m}_P$).

As part of this work, two models of legacy rocket systems were developed to allow the study of the energy availability characteristics (along with the traditional performance metrics) of chemical rocket engines. These two systems are the Rocketdyne J-2 (liquid hydrogen fuel, liquid oxygen oxidizer) and the Rocketdyne F-1 (RP-1 fuel, liquid oxygen oxidizer) which powered the Apollo space program's Saturn V second (as well as third) and first stages, respectively. The models employ quasi-1D analysis with simplified chemistry to account for the combustion. With known tank and injector conditions, the flow conditions and chemical composition in the combustion chamber, at the nozzles throat, and at the nozzle's exit are determined. The study investigated performance parameters and entropy generation and energy utilization metrics over a wide range of operating conditions defined by the combination of flight velocity, flight altitude, and oxidizer-to-fuel ($O/F$) ratio.

In Paper III, the theory, formulations, and engine modeling are then applied to the ascent of Apollo 11 Saturn V stack from launch to second stage separation. Trajectory information from an after-mission report coupled with the modeled engines are combined to assess the energy availability utilization characteristics of this mission. Note that along with the engine modeling and entropy generation computed in the engine and in the wake of the vehicle, the investigation here differs from that presented in Paper II in that the Paper III tracks the instantaneous energy availability balance and associated parameters (including $\eta$), whereas Paper II looks at the mission-integrated energy availability balance.

A study of the effects of irreversibilities inside the rocket engine on performance is also conducted in this work (Paper III). To facilitate this study, a parametric entropy generation ratio $K$ is defined in Eq. (6). This ratio is a measure of how much more or less entropy generation a reference engine has compared to the actual engine studied. This means that $K$ = 1 corresponds to the actual engine. For an isentropic flowfield in the engine, termed the 'ideal engine,' for which the entropy generation in the engine is zero (but still with entropy generation in the wake), $K$ = 0.

$$K \equiv \frac{\dot{S}_{\text{engine (reference)}}}{\dot{S}_{\text{actual engine}}} \tag{6}$$

As compared to the actual engine, the performance of reference engines covering a span of $K$ values from 0 to 1.15 (which includes the actual engine with $K$ = 1) is analyzed from three standpoints: 1) the entropy generation rate in the wake, 2) the lost thrust, and 3) the propellant usage associated with entropy generation. Entropy generation in the wake is affected by the entropy generation upstream, including inside the engine. It is found that the effect is highly nonlinear. Performance for engines with high internal losses are more sensitive to changes in entropy generation within the engines than the performance for engines with low losses. Lost thrust is the measure of the reduction in developed thrust from that produced by the isentropic ideal engine operating at the same propellant flow rate (the ideal engine produces the maximum amount of thrust).

The relationship of propellant usage to losses is also investigated. This is done by using two mass fractions $\mu_{\text{engine}}$ and $\mu_{\text{overall}}$. For $\mu_{\text{engine}}$, any reference engine studied is compared to the ideal engine (one for which there is no entropy generation inside the engine). For the reference engine to produce as much thrust as the ideal engine, it must

operate at a higher propellant flow rate. The fraction $\mu_{\text{engine}}$, defined in Eq. (7), is the amount of additional propellant mass flow rate necessary to produce the same thrust as the ideal engine normalized by the ideal engine's nominal propellant flow rate that produces that thrust value. The fraction $\mu_{\text{overall}}$ is similarly defined [in Eq. (8)] but instead of the ideal engine being used as the base-line, a theoretically absolutely ideal device is defined which is completely reversible even in the wake (i.e., referring to a global control volume with no entropy generation anywhere; note that the ideal engine described above has losses in its wake, even though there are no losses in the engine itself). For such a device, the entirety of the available energy is converted/realized into a propulsive power (i.e., $\eta$ = 1), and thus produces the maximum theoretically possible amount of thrust for the nominal propellant flow rate. The key difference between the two parameters is whereas $\mu_{\text{engine}}$ only identifies the propellant mass required to overcome losses only in the engine (with no accounting for how that effects the losses in the wake), $\mu_{\text{overall}}$ identifies the amount of propellant required to overcome all losses everywhere in the global control volume. Note that $\mu_{\text{overall}}$ is identically equal to $1-\eta$. The main conclusion from this part of the study is the fact that there is a diminishing improvement of performance as losses are 'removed.'

$$\mu_{\text{engine}} \equiv \frac{\dot{m}_{P\ \text{associated with entropy generation in engine}}}{\dot{m}_{P\ \text{total}}} \tag{7}$$

$$\mu_{\text{overall}} \equiv \frac{\dot{m}_{P\ \text{associated with all entropy generation}}}{\dot{m}_{P\ \text{total}}} = 1-\eta \tag{8}$$

**1.2.4. Paper IV: Generalization and Validation of Energy Availability Utilization Methodology to *N*-Stage Rockets.** The work done in this paper also builds upon the work presented in Paper II as it employs the mission integrated energy utilization balance for a rocket coupled with the vehicle equation of motion. The first objective of the

paper is to establish the formulation and notation for the mission-integrated energy availability utilization balance and all associated terms for an *N*-stage rocket, first in dimensional form, and then in non-dimensional form. The non-dimensional form is then employed to analytically investigate staging optimization for a two-stage rocket operating in: 1) free-space, and 2) vertical climb in a constant gravitational field.

The staging optimization problem studied is concerned with identifying the staging velocity (velocity at which staging must occur) that would maximize the fraction of initially available, mission-integrated overall energy availability for a mandated change of total impulse imparted on the rocket (i.e., mandated change in velocity). This staging velocity, in turn, indirectly identifies the proportion of propellant mass for both stages (i.e., how big each stage needs to be). Analytical expressions are derived that yield the optimal staging velocity for both special cases. The work presented in the paper also proves that the analytical expression obtained from the energy availability balance approach is mathematically equivalent to the expression obtained in traditional, mass-based analysis, specifically the analysis presented in Ref. [20]. The equivalence of the availability-based optimization and the mass-based optimization for the free-space case is again proven numerically in the case study conducted. The two approaches are not equivalent, however, for the case of vertical climb in a constant gravitational field, as the final altitude (at stage-2 separation) is not fixed in the analysis, only the final velocity of the rocket.

### 1.3. AUTHOR'S CONTRIBUTION TO THE RESEARCH EFFORT

The entirety of the work presented in this dissertation has been a joint effort between the author and his doctoral advisor, Professor David W. Riggins. Much of the

groundwork related to the basis and theory of energy utilization has been previously done by Dr. Riggins. However, as described in the papers discussed here, the present work significantly extends this previous work. In terms of writing and organization of the papers, the author wrote initial drafts of Papers I, III, and IV; editing was performed primarily by Dr. Riggins, with other co-authors contributing some to the revision process.

All engine models that have been developed (modeling, coding and details of physics and second-law evaluation of components) and all base-line applications that are described in Papers I, III, and IV were the responsibility of the author. All other coding for all papers and analysis for all papers were done by the author, with the exception of aspects of Paper II ("Analysis of Energy Utilization of Chemical Rockets)." For the effort documented in that paper, the author was instead responsible for the evaluation of the complete energy utilization balance, specifically in assessing and validating the formal definition and quantification of the thermochemical availability ($H^*$) for use in the energy utilization balance. In terms of the theory outlined in Papers III and IV, the author developed and validated the methodology for assessing the metrics (and physical reasoning behind those metrics) associated with optimization of various aspects of energy utilization for rocket systems. For Paper IV that describes the generalization of the methodology to *N*-stage rockets, the author developed the approach and modified the notation used in previous work to be applicable to any *N*-stage rocket. Nondimensional forms of the equations and terms developed by Dr. Riggins have also been modified by the author and notation and mathematical expressions are subsequently developed for *N*-stage rockets. For the application of this methodology to the optimization of the staging velocity to a 2-stage rocket, the author derived the analytical expressions that yield the optimum staging velocity

for rocket operation in both free-space and vertical flight in a constant gravitational field. For the air-breathing aspect of the work (most notably Paper I), the author was primarily responsible for developing the theoretical linkage between entropy generation and range and endurance, as well as formulating the physics behind the energy utilization characteristics of combined airframe/jet engine aircraft systems.

# PAPER

## I. ANALYSIS OF ENERGY UTILIZATION AND LOSSES FOR JET-PROPELLED VEHICLES

Mohammad Abbas and David W. Riggins

Department of Mechanical and Aerospace Engineering, Missouri University of Science and Technology, Rolla, MO 65409

## ABSTRACT

The global control volume-based energy utilization balance for an aerospace vehicle is extended to allow analysis of jet-propelled vehicles. Methodology is first developed for analyzing energy utilization and entropy generation characteristics for jet engines without airframe considerations. This methodology, when combined with separate energy utilization analysis for an unpowered airframe, allows assessment of a powered vehicle. Wake entropy generation for a powered vehicle is shown to be the summation of the wake entropy generations associated with the propulsion system (no airframe) and with the unpowered airframe. The fundamental relationships between overall entropy generation and the flight conditions required for maximum range and endurance of a powered vehicle are also derived. Example energy utilization results obtained for a modeled turbojet engine in off-design operation are provided; wake and engine component entropy generation characteristics are directly related to engine operation and flight conditions. This engine model is then integrated with a legacy (twin-engine) Northrop

F-5E Tiger II airframe. The overall entropy generation temporal rate for the vehicle is minimized, as predicted by analysis, at flight conditions corresponding to maximum endurance. For flight conditions corresponding to maximum range, the overall entropy spatial rate is minimized.

## NOMENCLATURE

| Symbol | Description |
|---|---|
| $A$ | Cross-sectional area, $m^2$ |
| $AR$ | Aspect ratio |
| $C_D$ | Aircraft drag coefficient |
| $C_{Di}$ | Induced drag coefficient |
| $C_{D0}$ | Parasitic (zero-lift) drag coefficient |
| $C_L$ | Aircraft lift coefficient |
| $c_t$ | Thrust specific fuel consumption, kg/N-s |
| $D$ | Aerodynamic drag, N |
| $D_{add}$ | Additive drag, N |
| $E$ | Aircraft cruise endurance, sec |
| $\dot{E}$ | Net rate of energy transfer rate into a control volume (both heat and work), W |
| $e$ | Oswald efficiency factor |
| $F_x$ | Net force in the direction of flight, N |
| $H_f$ | Lower heating value of the fuel, J/kg |

| | |
|---|---|
| $H^*$ | Total thermochemical availability, J/kg |
| $L$ | Lift, N |
| $m_f$ | Fuel mass, kg |
| $\dot{m}$ | Mass flow rate, kg/s |
| $\dot{m}_f$ | Fuel mass flow rate, kg/s |
| $\hat{n}_x$ | Unit vector in the direction of flight |
| $P$ | Static pressure, N/m$^2$ |
| $q_\infty$ | Dynamic pressure, N/m$^2$ |
| $R$ | Aircraft cruise range, m |
| $S$ | Planform area or control surface area, m$^2$ |
| $\dot{S}$ | Time rate change in entropy (generation for most cases) across a streamtube, W/K |
| $T$ | Static temperature, K |
| $u$ | Flow velocity, m/s |
| $u_\infty$ | Flight/freestream velocity, m/s |
| $W$ | Aircraft gross weight, N |
| $\eta$ | Instantaneous energy utilization effectiveness |
| $\rho$ | Mass density, kg/m$^3$ |
| $\tau$ | Shear stress |

Subscripts

| | |
|---|---|
| $e$ | Engine (nozzle) exit plane |
| $i$ | Engine inlet plane |

| | |
|---|---|
| $s$ | Exit plane of side-bounding sub-control volume |
| $w$ | Exit plane of wake sub-control volume |
| $x$ | axial direction; direction of flight axial direction; direction of flight |
| $\infty$ | Free-stream conditions; upstream (entrance) plane of global control volume |

## 1. INTRODUCTION

The effective utilization of available energy for an aerospace vehicle in flight is necessary in order to satisfy performance and mission requirements. These requirements are met primarily by generating suitable thrust and lift forces from available energy, as well as by the proper management of aerodynamic drag. While in some flight systems there are stored or acquired sources of available energy other than the propellant, the propellant is generally the only significant source of available energy for most powered aerospace vehicles. Furthermore, while there may be some usage of available energy in subsystems other than the propulsive and aerodynamic subsystems, such subsystems are usually thermodynamically tied into the propulsive and/or aerodynamic flowpaths. Propulsive and aerodynamic flows ultimately then serve as thermal sinks for energy not explicitly associated with thrust/lift production and/or drag mitigation.

The analytical development of the fundamental rate-based energy utilization balance for powered aerospace flight vehicles, based on the global control volume approach, has enabled the direct assessment of the impact of available energy losses on vehicle performance at discrete flight conditions [1]. In addition, the energy utilization rate balance has been combined with vehicle equations of motion to provide time-integrated

energy utilization balances, allowing assessment of energy utilization across vehicle missions and mission segments in terms of vehicle kinetic and potential energy changes [2]. Energy utilization formulations that are based on the global control volume approach have been used and validated for a wide range of applications and flow regimes, including multi-dimensional flows and chemically reacting flows [3]. Most applications have focused on hypersonic air-breathing vehicles with ram/scramjet propulsion systems [4] and rocket-powered vehicles [5,6].

Exergy analysis, and systematic application of entropy generation minimization techniques for performance improvements and optimization, are very well-established and widely utilized for ground-based systems; less so for aerospace flight vehicles, due in part to the lack of direct (analytical) linkage between exergy losses and classic vehicle performance characteristics and design objectives. Although energy utilization analysis based on the global control volume approach is a form of exergy analysis, the balance that results is specifically based on traditional vehicle performance (i.e., net propulsive and aerodynamic forces, changes in vehicle kinetic and potential energies, etc.). It (analytically) links losses in traditional performance metrics to entropy generation in the global control volume in which the vehicle is embedded, at the specific flight condition of the vehicle. Nevertheless, both traditional exergy methods and the global control volume-based energy utilization balances are linked by their respective assessment of losses in terms of entropy generation. Entropy generation is the most fundamental measure of losses for all physical processes, and hence provides the common (single) currency of losses for all sub-systems and processes associated with aerospace vehicles.

The earliest development of the global control volume-based approach for relating forces on aerodynamic shapes to entropy generation was by Ostawitch [7], who characterized the drag of an unpowered shape in fluid flow in terms of overall entropy generation. Subsequent developments of the approach are essentially extensions and refinements, applied to increasingly complex aerospace systems. The approach is also used by Giles and Cummings [8], who characterized the energy availability balance for a vehicle using a simple heating model for fuel energy release. The present work is related as well to previous investigations ([9,10]) that sought to characterize gas turbine (turbojet and ramjet) transient behavior utilizing energy utilization/entropy generation analysis. Abbas and Riggins [11], in earlier work prior to that reported in the current paper, investigated energy utilization and entropy generation for a turbojet engine model without airframe considerations; focusing primarily on presenting uninstalled performance and providing related energy utilization information.

The earliest work in the area of performance assessment of jet engines includes that of Foa [12], Builder [13], and Lewis [14]; the latter reference provides a basic description of the framework of exergy methods applicable to jet engines, and hence is a precursor to later exergy-based investigations of aerospace propulsion systems. Clarke and Horlock [15] provided a pioneering treatment of availability and thrust power losses for aerospace jet engines, including a single operation point application of the method for a modeled turbojet engine. Their work, in terms of control volume-based analysis of stand-alone engines, is closely related to the global control volume-based energy utilization approach used in the present work, especially as applied to jet engines without airframe considerations. Subsequent interest in applying exergy methodology to aerospace

propulsion systems, including airbreathing scramjet engines during the 1990s, led to work such as that by Czysz and Murthy [16], Murthy [17], and Brilliant [18]. A parallel effort (again with initial emphasis on high-speed systems) focused on analysis and optimization based on the minimization of engine thrust losses. This engineering performance-based approach was first pioneered by Curran and Craig [19] who provided the basis of the thrust-potential methodology later developed by Riggins, et al. (see, for example, [20-22]). In these and related investigations the thrust for a high-speed engine was explicitly linked to entropy production occurring inside the engine. A parallel and related methodology was developed using work potential methods as applied to engines (see, for example, Roth [23,24]). Unlike exergy-based analyses, both thrust potential and work potential methods avoid wake entropy generation (wake exergy destruction) issues, due to their direct assessment of forces and work potential specific to an engine flow-field itself. In more recent work using traditional exergy analysis, Ehyaei, et al. [25] performed an exergy analysis of an afterburning turbojet engine at two altitudes and identified the exergetic efficiencies of the various engine components. Etele and Rosen [26] explored the important issue of the sensitivity of exergy analysis for aerospace systems to the choice of reference state. Discussion and examples of benefits of exergy-based analysis when applied to general (and specific) aerospace applications are reported by Doty, et al. [27]. A recent detailed and comprehensive description of the exergy-based formulation for aircraft aerodynamic-propulsive performance assessment is provided by Arntz, Atinault, and Merlen [28]. Additional work analyzing exergetic aspects of gas turbine engines is done in references [29-33].

There are three main objectives of the present work: the first objective is to extend the global control volume-based energy utilization balance to enable the analysis of aerospace vehicles with gas turbine (jet) engines, operating at either subsonic or supersonic flight Mach numbers. The second objective is to use the control-volume based energy utilization balance to analytically investigate the overall entropy generation characteristics of a jet-powered vehicle in cruise. The third objective is to provide performance and energy utilization results for specific applications (i.e., first for a specified engine without an airframe and then for a powered vehicle with a specified airframe, with focus on cruise flight; range and endurance).

The approach taken in this work to accomplish these objectives is to develop a turbojet engine model that correctly accounts for (hardware-specific) engine off-design operation; this requires the identification or use of component performance maps and loss models, and the implementation of component matching. The component-matched engine model then allows the assessment of performance and energy utilization for the specific engine for all fuel throttle settings, flight Mach number, and altitudes across the off-design flight envelope. Most previous studies using conventional exergy techniques do not fully account for off-design engine operation but rely on traditional cycle analysis approximations and assumptions. The specific engine used in the application example for this work is selected and sized based on nominal on-design operation at flight Mach of 0.85, altitude 9 km, and a thrust requirement of 9.3 kN; off-design operation and performance for this engine is then calculated appropriately from the engine operating line information as obtained through the component matching process.

In conjunction with the installed thrust and additive drag models for this turbojet engine, a drag model for a legacy airframe with known aerodynamic and weight characteristics is defined; the Northrop F-5E Tiger II airframe (with twin turbojet engines) has been selected in this work. This airframe provides a good match in terms of its drag envelope to the modeled installed engine thrust performance envelope. Finally, combination of the airframe and the modeled engines provides a complete (powered) vehicle model thus allowing quantitative assessment of cruise flight in terms of energy utilization characteristics (and in terms of conventional principles).

This work (along with earlier complementary work described in Ref. [11]) is unique in employing a control volume/energy utilization analysis that explicitly includes the wake (and the entropy generation occurring therein) for the analysis of a gas turbine engine from a second-law/exergetic perspective. It is also the first exergy analysis of a turbojet engine utilizing that approach that analyzes a given engine over a range of 'off-design' conditions, as opposed to employing cycle analysis assumptions and limitations. In addition, the work is believed to provide the first fundamental derivation and case study showing the direct relation between overall entropy generation and maximum range and endurance conditions for an aircraft; this derivation results from the comprehensive nature of the global control volume/energy utilization approach.

Section 2 of this paper provides a brief summary and discussion of the global control volume-derived energy utilization balance for an aerospace vehicle in flight. Subsequent sections of this paper develop the analytical basis for using this energy availability balance in order to 1) assess conventional gas turbine engines without airframe considerations (Section 3), 2) assess integrated airframe and air-breathing (jet) propulsion

systems, i.e., powered vehicles (Sections 4 and 5), and 3) develop fundamental range and endurance considerations that result from the energy utilization balance (Section 6). Section 7 describes specifics of the gas turbine modeling (with emphasis on correctly accounting for off-design performance using component matching) and the specific configuration for a modeled turbojet engine. Section 8 provides information regarding the airframe, the airframe drag model, and specifics of the selected airframe used in this study. Performance and energy utilization results are shown in Section 9 for both the stand-alone turbojet engine and for the integrated airframe and engines, with focus on cruise implications for energy utilization and considerations related to flight for maximum range and endurance of a jet-propelled vehicle.

## 2. ENERGY UTILIZATION ANALYSIS OF AEROSPACE VEHICLE SYSTEMS

The energy utilization rate balance for an air-breathing aerospace vehicle in flight is written as:

$$u_\infty F_{x(\text{flight})} = \dot{E} + \dot{m}_f \left( H^* + \frac{u_\infty^2}{2} \right) - T_\infty \dot{S}_{\text{total}} \tag{1}$$

This fundamental relationship represents the combination of the first and second laws of thermodynamics, as well as momentum and continuity principles, applied to a global control volume containing fluid in which the vehicle is embedded (see Figure 1 for a 2-D representation). The boundary of the global control volume is defined to envelope all fluid wetted solid surfaces of the vehicle. This includes both external and internal surfaces of the vehicle (i.e., all wetted surfaces associated with aerodynamic, propulsive,

fuel feed, and tankage systems). The balance equation given by Eq. (1) mandates that the vehicle (net) force power that is realized (the productive utilization of energy) is equal to the overall energy availability rate (primarily associated with fuel flow rate) minus all losses in available energy that occur within the global control volume.

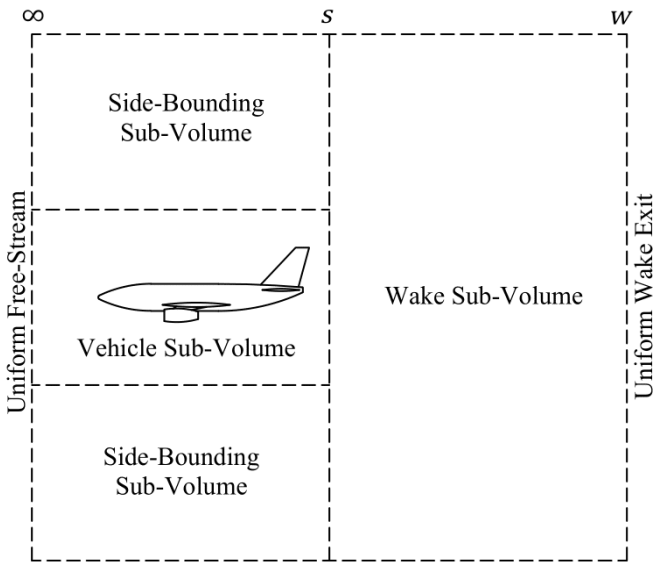


Figure 1. Global control volume for vehicle exergy analysis.

In the energy utilization balance (Eq. (1)), $u_\infty$ is the vehicle flight velocity, $F_{x(\text{flight})}$ is the net resultant force component on all solid surfaces of the vehicle in the direction of flight (traditionally the 'thrust – drag,' or net accelerative force in the instantaneous flight direction). The first term on the right-hand side, $\dot{E}$, represents possible (net) rate of energy interactions (heat and/or work) into the fluid in the global control volume. This is energy supplied to (or extracted from) the fluid within the global control volume from sources external to said control volume (e.g., batteries on board the vehicle). $\dot{E}$, however, will be

assumed to be negligible in this work; all available energy will be strictly associated with the fuel. The second term on the right-hand side represents the overall energy availability rate associated with the fuel flow rate leaving the fuel tank(s). $H^*$ is the total thermochemical availability of the fuel (maximum chemical and thermal work potential as measured with respect to the ambient conditions) [1], and $u_\infty^2/2$ is the energy availability associated with the kinetic energy of the on-board fuel (this latter term, however, is negligible in comparison with $H^*$ for the conventional flight atmospheric systems/vehicles considered in the present work). The third term on the right-hand side of Eq. (1) represents the rate of loss of available energy. $T_\infty$ is the free-stream ambient temperature, and $\dot{S}_{\text{total}}$ is the net rate of entropy change across the global control volume from $\infty$ to $w$.

For analysis, the global control volume is divided into three sub-control volumes (see Figure 1). The first sub-control volume is that associated with the vehicle zone of influence (i.e., the flowfield surrounding the vehicle and directly impacted or influenced by the vehicle, extending axially from $\infty$ to $s$, and including the internal propulsion and propellant flowpaths and all fluid in propellant feed systems and tankage). The second sub-control volume is that region defined by the side-bounding 'far-field' flow that is at free-stream conditions (especially relevant for high-speed systems), theoretically extending to infinity in the lateral plane and extending axially from $\infty$ to $s$. The third sub-control volume is that associated with the vehicle wake; it is downstream of the vehicle exit plane (extending from station $s$ to station $w$). The inflow to the global control volume at station $\infty$ is undisturbed and uniform at the free-stream conditions. The outflow of the global control volume at $w$ is uniform (i.e., equilibrated) and the flow properties at $w$ are (for very

large lateral extent of the global control volume), by definition, infinitesimally displaced from those of the free stream.

There are two contributions to the total entropy generation in the global control volume: 1) entropy generated in (and transferred to) the fluid associated with the sub-control volume encompassing the vehicle zone of influence (which can be further sub-divided into contributions from the propulsion system and from the external aerodynamic system), and 2) entropy generated in the unconstrained wake sub-control volume:

$$\dot{S}_{\text{total}} = \Delta\dot{S}_{\infty\rightarrow s} + \Delta\dot{S}_{s\rightarrow w} = \dot{S}_{\text{vehicle}} + \dot{S}_{\text{wake}} \tag{2}$$

The entropy generated in the wake equilibration process generally significantly exceeds the total entropy generated in the vehicle zone of influence, including within the propulsive system. Entropy generation due to irreversibilities and non-ideal effects in other non-propulsive and non-aerodynamic subsystems on board the vehicle most generally result in the transfer of rejected heat to the fluid within the control volume, and hence the energy utilization balance is inclusive of such effects.

The energy availability balance mandates that if the total entropy generation rate can be quantified at a known fuel flow rate and for a known thermochemical availability, the net resultant force acting on the vehicle in the direction of flight can be determined using Eq. (1). Conversely, if the net force power is known, the entropy generation rate is then necessarily fixed. Furthermore, the complete quantification and composition of expended energy associated with the fuel can be assessed in terms of both realized productive force power and the specific performance losses associated with entropy generation details (identifiable in terms of individual loss mechanisms, components,

processes, and sub-systems). The level of detail available for such quantification depends on the level of modeling used.

In terms of the energy utilization balance, an energy utilization effectiveness, $\eta$ can be defined to assess the degree to which the overall energy availability associated with the fuel is realized as force-based power at any given flight condition for a powered vehicle:

$$\eta = \frac{u_\infty F_{x(\text{flight})}}{\dot{m}_f \left( H^* + \frac{u_\infty^2}{2} \right)} \tag{3}$$

## 3. ENERGY AVAILABILITY ANALYSIS OF A STAND-ALONE GAS TURBINE ENGINE

The general energy availability balance for aerospace vehicles as summarized in the previous section can be readily adapted to a stand-alone gas turbine engine operating in either subsonic or supersonic flow. Here, the term stand-alone refers to an engine in flight without considerations of an airframe and with the constraint that all losses (entropy generation) occur only in the engine flowpath itself, as well as in the wake downstream of the engine. In such an application and reflective of the approach described in the last section, the global control volume is again divided into three sub-control volumes (see Figure 2): 1) the 'outer' or side-bounding sub-control volume (streamtube) from $\infty$ to $s$ and of asymptotically large (lateral) extent in which the fluid external to the engine is taken to be isentropically processed, 2) the sub-control volume (streamtube) associated with the air that is inducted into the engine, and 3) the downstream wake mixing sub-control volume in which the disparate flows at station $s$ are eventually equilibrated (at station $w$).

Upstream of an engine, whether it is considered ‘stand-alone’ as defined above or attached to an airframe, external acceleration or deceleration of the captured airflow (for subsonic or subcritical engine operation) dictates that the propulsive flowpath extends forward of the inlet face (station $i$) to the free stream (plane $\infty$). The actual (installed) thrust force delivered by an engine is the uninstalled thrust less the sum of the additive and external cowl drags.

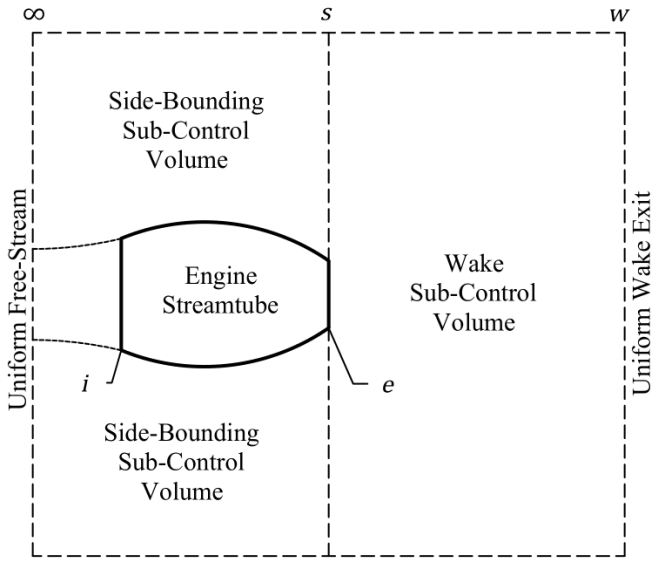


Figure 2. Global control volume for stand-alone gas turbine engine exergy analysis.

$$F_{x(\text{engine})} = \text{installed engine thrust}$$
$$= \text{uninstalled engine thrust} - D_{add} - D_{\text{external cowl}} \tag{4}$$

where,

$$D_{add} = \int_{\infty}^{i} (P - P_{\infty}) \hat{n}_x dS \tag{5}$$

$$D_{\text{external cowl}} = \int_i^e (P_{\text{external cowl}} - P_\infty)\hat{n}_x dS + \int_i^e \tau_{x(\text{external cowl})}\, dS \qquad (6)$$

$$\text{uninstalled engine thrust} = \left(\dot{m}_f + \dot{m}_{air}\right)u_e - \dot{m}_{air}u_\infty + (P_e - P_\infty)A_e \qquad (7)$$

From momentum considerations for the upstream captured streamtube entering an engine, the additive drag can be found as:

$$D_{add} = \dot{m}_{air}(u_i - u_\infty) + (P_i - P_\infty)A_i \qquad (8)$$

Furthermore, for a stand-alone engine configuration, with the requirement of isentropic flow in the side-bounding streamtube (mandating a frictionless external cowl) and the large lateral extent of this streamtube, $P_{\text{external cowl}} = P_\infty$, hence $D_{\text{external cowl}} \approx 0$. Therefore:

$$F_{x(\text{flight}),\text{engine alone}} = \left(\dot{m}_f + \dot{m}_{air}\right)u_e - \dot{m}_{air}u_i + (P_e - P_\infty)A_e - (P_i - P_\infty)A_i \qquad (9)$$

For air-breathing (jet) engines, the thermochemical availability $H^*$ can be very closely approximated as the heating value of the fuel $H_f$ [1]. The installed thrust of the stand-alone jet engine in terms of heating value of fuel and total entropy generation rate (here subdivided between entropy generation in the engine streamtube from $\infty$ to $e$, $\dot{S}_{\text{engine}}$, and entropy generation in the wake mixing zone from $s$ to $w$, $\dot{S}_{\text{wake(engine alone)}}$) can then be determined with a known (or computed) wake entropy generation rate as:

$$F_{x(\text{flight}),\text{engine alone}} = \frac{1}{u_\infty}\left[\dot{m}_f\left(H^* + \frac{u_\infty^2}{2}\right) - T_\infty(\dot{S}_{\text{engine}} + \dot{S}_{\text{wake(engine alone)}})\right] \qquad (10)$$

Conversely, the entropy generation in the wake can be determined from a given (or computed) thrust using Eq. (10). However, when it is desired to directly compute wake

entropy generation from (upstream) flow rates at station $s$ (for instance to independently check the force obtained using the availability balance against the force obtained using engine flow-field modeling), a sufficiently large lateral dimension of the global streamtube must be used. The wake equilibration process (from plane $s$ to plane $w$, where the flow is equilibrated and uniform) can then be modeled by enforcing conservation of mass flow rate, axial stream thrust, and total enthalpy flow rate between $s$ and $w$, and solving for wake equilibrated conditions at station $w$ (thus allowing the computation of $\dot{S}_{\text{wake(engine alone)}}$). With sufficiently large lateral extent of the global control volume, comparisons of the values of engine thrust obtained through momentum analysis (i.e., via classic cycle analysis) to values of engine thrust obtained independently from the energy availability balance have percent differences less than $10^{-6}$. In the current study, the ratio of cross-sectional area of the global control volume to the engine inlet entrance cross-sectional area is taken to be $10^9$ for any direct computations of the wake entropy generation rate; this value is significantly larger than necessary but ensures asymptotic convergence (this corresponds to a square area of roughly 8 km for the modeled engine that has a nozzle exit diameter of about 0.3 m).

## 4. ENERGY AVAILABILITY ANALYSIS OF AN UNPOWERED AIRFRAME

The overall energy availability balance can also be readily applied when considering the aerodynamics (drag characteristics) of an unpowered airframe; in fact, this situation corresponds to the first specific formulation and application of the global control volume approach with second law analysis by Oswatitsch [7]. The net axial force

component developed on an unpowered airframe (colinear with the instantaneous flight direction) is the airframe drag, $D_{\text{airframe}}$. In the absence of fuel usage, the energy availability balance for the unpowered airframe (with $\dot{S}_{\text{airframe}}$ designating the entropy generation associated with the aerodynamics of the unpowered airframe from $\infty$ to $s$), simplifies to:

$$u_\infty D_{\text{airframe}} = T_\infty\left(\dot{S}_{\text{airframe}} + \dot{S}_{\text{wake(airframe alone)}}\right) \tag{11}$$

## 5. VEHICLE PERFORMANCE MODEL IN TERMS OF PROPULSIVE AND AIRFRAME ENTROPY GENERATION RATES

From the standpoint of flight performance, the dominant fluid dynamic force components experienced by a vehicle in atmospheric powered flight are associated with the airframe and with the propulsion system. For purposes here, conventional lift and drag are considered to be solely associated with the airframe, while the thrust is specifically associated with the defined propulsive flowpath (the propulsion system), i.e., no consideration of thrust vectoring is made in the following development, although it can be incorporated readily. Note that the analysis is inclusive of airframe-engine integrated configurations as well, although care has to be taken to properly account for and allocate forces, based on the specifics of the performance accounting system being used and the exact delineations of engine and airframe boundaries and interfaces.

Consider the global control volume around a powered vehicle; the flow through the global control volume can be separated into a propulsive streamtube and an aerodynamic streamtube interacting with the airframe. These streamtubes can interact with each other

but are separable in terms of both the mass flow rates of air they process and their respective (exclusive) force interactions with either the engine solid surfaces or the airframe solid surfaces. The net instantaneous axial force developed on the vehicle in the flight direction is then written as:

$$F_{x\,(\text{vehicle})} = F_{x\,(\text{engine})} - D_{\text{airframe}} \tag{12}$$

or

$$F_{x\,(\text{vehicle})} = \text{uninstalled engine thrust} - D_{add} - D_{\text{external cowl}} - D_{\text{airframe}} \tag{13}$$

The energy availability balance for the vehicle is written as:

$$u_\infty F_{x(\text{vehicle})} = \dot{m}_f \left( H^* + \frac{u_\infty^2}{2} \right) - T_\infty \dot{S}_{\text{total (vehicle in flight)}} \tag{14}$$

The total entropy generation rate in the global control volume, $\dot{S}_{\text{total (vehicle in flight)}}$, is composed of three contributions as follows:

$$\dot{S}_{\text{total (vehicle in flight)}} = \dot{S}_{\text{engine}} + \dot{S}_{\text{airframe}} + \dot{S}_{\text{wake}} \tag{15}$$

If $D_{\text{external cowl}}$ is considered small or, for convenience, is included in $D_{\text{airframe}}$, a fundamental superposition principle for wake entropy generation can then be written as:

$$\dot{S}_{\text{wake}} = \dot{S}_{\text{wake(engine alone)}} + \dot{S}_{\text{wake(airframe alone)}} \tag{16}$$

This wake entropy generation superposition principle states that the overall entropy generation in the wake of a powered vehicle is the summation of the entropy generation in the wake of the independently analyzed ‘stand-alone’ propulsion system and the entropy generation in the wake of the independently analyzed unpowered airframe.

# 6. ENTROPY GENERATION AND CRUISE; RANGE AND ENDURANCE

The performance of a powered vehicle in flight in terms of endurance, $E$, and range, $R$, are both related to the expenditure of fuel. The time traveled in cruise on a given amount of fuel is defined as the endurance, $E$, of the vehicle. Endurance, by definition, is maximized when the time rate of fuel burned $\left(\frac{d}{dt}m_f = \dot{m}_f\right)$ is minimized across the cruise leg. The distance traveled in cruise on a given amount of fuel is defined as the range, $R$, of the vehicle. Range, by definition, is maximized when the fuel burned per unit distance travelled is minimized $\left(\frac{d}{dx}m_f = \frac{\dot{m}_f}{u_\infty}\right)$ across the cruise leg. Flight conditions necessary for maximizing range and endurance for jet-propelled vehicles have traditionally been obtained in preliminary design by extension of the classic Breguet range and endurance methodology for propeller-driven vehicles, based on cruise flight [34]. The range and endurance relationships that result are functions of thrust specific fuel consumption as well as specific aerodynamic flight characteristics of a jet-propelled vehicle in cruise. To an approximation, the time per unit mass of fuel burned in cruise is proportional to $C_L/C_D$ (the lift-to-drag ratio of the vehicle). Thus, when the vehicle is flown in cruise at an angle of attack and flight velocity corresponding to maximum $C_L/C_D$, the endurance is approximately maximized. Likewise, the distance traveled per unit mass of fuel burned in cruise is approximately proportional to $C_L^{1/2}/C_D$, such that range is maximized when this ratio is maximized, i.e., when the vehicle is flown in cruise at an angle of attack and flight velocity corresponding to this condition.

For a vehicle in cruise (i.e., neither accelerating nor decelerating in the flight direction), the net axial force developed on the vehicle is necessarily zero ($F_{x(\text{engine})} = D_{\text{airframe}}$). The energy availability balance then becomes:

$$\dot{m}_f \left( H^* + \frac{u_\infty^2}{2} \right) = T_\infty \dot{S}_{\text{total(vehicle in cruise flight)}} \tag{17}$$

This states that all availability associated with fuel usage (thermochemical and kinetic energy of the on-board stored fuel) is entirely lost. From Eq. (17), flight at conditions corresponding to maximum endurance and maximum range, respectively, occur when the time rate of overall entropy generation is minimized and when the spatial rate of overall entropy generation is minimized, i.e.:

$$\text{At max } E: \quad \dot{S}_{\text{total (vehicle)}} \text{ is minimized (exact); } C_L/C_D \text{ is maximized (approx.)} \tag{18}$$

$$\text{At max } R: \quad \frac{\dot{S}_{\text{total (vehicle)}}}{u_\infty} \text{ is minimized (exact); } C_L^{1/2}/C_D \text{ is maximized (approx.)} \tag{19}$$

In addition, Eq. (17) can be rewritten based on the superposition principle in terms of separate contributions of the airframe and engine (evaluated at cruise flight conditions for the vehicle):

$$\dot{m}_f \left( H^* + \frac{u_\infty^2}{2} \right) = T_\infty \dot{S}_{\text{total (engine alone)}} + T_\infty \dot{S}_{\text{total (airframe alone)}} \tag{20}$$

The total entropy generation rates on the right-hand side of Eq. (20) are in turn composed of contributions occurring within the respective systems from $\infty$ to $s$ (again, evaluated at cruise flight conditions for the vehicle) and contributions occurring in the respective wake processes:

$$\dot{S}_{\text{total (engine alone)}} = \dot{S}_{\text{engine}} + \dot{S}_{\text{wake (engine alone)}} \tag{21}$$

$$\dot{S}_{\text{total (airframe alone)}} = \dot{S}_{\text{airframe}} + \dot{S}_{\text{wake (airframe alone)}} \quad (22)$$

## 7. TURBOJET ENGINE SPECIFICATIONS AND MODELING SUMMARY

This section provides the rationale and specifications for the fixed area single-spool turbojet engine modeled in this work, as well as a brief summary of the methodology used to characterize its performance across its operability envelope of allowable fuel throttle setting, flight Mach number, and altitude. Previous studies of availability and exergy in turbojet engines have generally performed cycle analysis (often simply assuming full mass capture without accounting for additive drag at all operational points). This effectively models the uninstalled performance of a family of engines as operating conditions are varied, rather than the installed performance of a given engine. As an example, if compressor pressure ratio is kept constant as flight Mach number and altitude are varied, this is not reflective of the performance of a given engine, but rather actually models a family of engines with necessarily different compressors, since the performance of a given compressor (i.e., the compressor pressure ratio and efficiency) will necessarily change with flight Mach and/or altitude. Such analysis, then, does not account for individual engine component characteristics and the required matching of those components that is necessary to predict the performance of a given engine across the operational ranges of fuel throttle setting, flight Mach number, and altitude for that given engine. In addition, previous works on exergy/availability and gas turbine engine performance often assume that the static pressure at nozzle exit is equal to the ambient pressure at all operational points of interest.

This assumption thus implicitly mandates a ‘flexible’ (non-constant) exit area of the engine, rather than a given (specified) engine with fixed cross-sectional areas.

In addition, the specific values of $\dot{m}_f$, altitude, and flight Mach number at which a given engine is operated determine the mass flow rate of air inducted into the engine, i.e., the engine will accelerate or decelerate the upstream captured streamtube of air as necessary (determining the spillage characteristics and additive drag of that engine at those conditions). This information, for a given engine, must be obtained by a process of correctly matching components within the engine, in order to correctly evaluate off-design performance. The component-matching methodology is applied for this work by utilizing a generic compressor performance map along with models for inlet, burner, turbine, and nozzle loss characteristics, and a defined ‘on-design’ operating point, in order to develop the full matched-component operating line for the engine. This in turn allows the analysis of the component-integrated engine performance (in terms of engine thrust, spillage, and RPM of the spool, as well as the energy availability characteristics) across the operational ranges of fuel throttle setting, flight Mach number, and altitude.

## 7.1. TURBOJET ENGINE SELECTION AND ON-DESIGN POINT SPECIFICATIONS

The gas turbine engine modeled in this study is a single-spool turbojet engine with no afterburner, fixed geometry throughout, and a convergent nozzle with fixed exit area. The simplicity of such an engine selection when coupled with the appropriate component matching required for accurate off-design analysis facilitates the straight-forward application and demonstration of the energy availability methodology discussed in earlier sections. Furthermore, the use of generic component performance maps and loss models in

the analysis allows for accurate generation of engine performance in terms of engine thrust, mass capture (spillage), and spool RPM across the allowable (off-design) ranges of fuel throttle setting, flight Mach number, and altitude. Engine component characteristics and (physical) sizing are chosen to be consistent with necessary required thrust requirements (for performance integration) for a specific airframe (vehicle airframe), to be described subsequently.

The on-design operational point for the defined turbojet corresponds to a flight Mach number of 0.85 at a standard altitude of 9 kilometers and a fuel flow rate of 0.279 kg/sec. For this defined on-design operational point, the compressor pressure ratio is 10 and compressor efficiency is 0.85; the engine produces 9.31 kN of thrust, mass flow rate of air inducted is 14.49 kg/sec, and the spool RPM is 15,000. The total temperature at burner exit is 1400K. The inlet has a cross-sectional area of 0.1332 $m^2$ (inlet area is sized to minimize spillage at the on-design point while avoiding excessive upstream acceleration at low-altitude low-speed operation) and the (convergent) nozzle exit has a cross-sectional area of 0.0666 $m^2$ (with choked flow).

## 7.2. TURBOJET ENGINE CONTROL SYSTEM LIMITS (OFF-DESIGN)

In calculation of off-design performance and losses, temperatures at turbine entrance greater than 1600 K were prohibited; this limit (along with the range on the generic compressor map that was utilized in this study) then produced the limitations on the possible ranges of flight Mach number, fuel throttle setting, and altitude for the modeled engine.

## 7.3. SUMMARY OF COMPONENT MATCHING AND PERFORMANCE EVALUATION PROCESS FOR OFF-DESIGN ENGINE OPERATION

In order to be able to correctly predict the on and off-design performance of a specified engine, the coupling between integrated components (inlet, compressor, burner, turbine, and nozzle) must first be established, i.e., the individual components must be integrated ('matched') with each other. This drives the integrated-engine component operation lines on individual component performance maps. The information associated with this process then allows the correct prediction of the thrust, mass capture, and RPM across the off-design engine operational space of allowable flight Mach number, fuel throttle setting, and altitude. The methodology of component matching and off-design performance evaluation is well-known and extensively documented in propulsion textbooks (see Ref. [35,36]). This section therefore provides only information relevant to specific modeling and component characterizations used in this particular work for the component matching for the defined turbojet engine.

**7.3.1. Inlet.** The adiabatic inlet total pressure loss model used for the turbojet engine is taken from [6]; this approximate model was developed by curve fitting over a wide representation of inlet data versus flight Mach number, as obtained from [35]. Captured streamtube characteristics, including spillage and additive drag, are determined by the specific fuel throttling, flight Mach number, and altitude operating point.

**7.3.2. Compressor.** The on and off-design component performance of the single-spool compressor integrated into the turbojet engine model is characterized, through component matching methodology as summarized in the previous section, by the development of a steady-state operating line on a selected generic compressor performance map. The modeled compressor allows for a wide operating range in terms of resulting

component/engine performance. Specifically, for the selected compressor, the off-design variability in compressor pressure ratio ranges from 50% to 130% of the on-design value. Off-design corrected mass flow rates range from 55% to 115% of the on-design value and off-design corrected RPM range from 76% to 106% of the on-design RPM.

**7.3.3. Burner.** In order to simplify the analysis in this work (focused on demonstrating energy availability analysis for the overall engine), a burner map was not used; instead, the burner here is assumed to have negligible total pressure drop and no losses due to incomplete combustion or cooling of the flow.

**7.3.4. Turbine.** For the present work, the general turbine efficiency was assumed to be constant at 0.86 for both on-design and off-design performance; cooling of the turbine was also not considered. A more detailed analysis would incorporate an individual turbine performance map. This would allow for variations in the turbine efficiency as well as possible unchoking at turbine entrance, however turbine efficiency remains relatively constant and the flow at turbine entrance usually remains choked across the engine on-off design operating envelope for a turbojet [36]. The inclusion of more detailed modeling of the turbine (i.e., utilization of the turbine performance map) is not necessary in the present work, which is focused on energy availability methodology and demonstration for a simple model of an engine.

**7.3.5. Nozzle.** Due to a relatively short length of the adiabatic nozzle required for the modeled turbojet and the lack of afterburning, the simplifying assumption is made in the current work that there is negligible total pressure loss through the nozzle.

**7.3.6. Summary.** Based on the engine operating line and loss information developed in the component matching methodology, as well as the fixed geometry (fixed

cross-sectional areas throughout the engine) determined from on-design flight point requirements, flow properties at all engine stations are then readily computed, for all possible fuel throttle settings, flight Mach numbers, and altitudes. This also allows the computation of individual entropy generation rates for all individual engine components; energy availability losses for these individual engine components are then found by multiplying the specific entropy generation rate by the ambient temperature. Engine performance in terms of thrust (both uninstalled and installed), spool RPM, spillage, and overall entropy generation in the engine from $\infty$ to $e$ can then be computed as well (again, at all possible fuel throttle settings, flight Mach numbers, and altitudes, hence defining the performance-operability envelope for the given engine).

## 8. AIRFRAME SPECIFICATIONS AND MODELING SUMMARY FOR CRUISE FLIGHT

Airframe and aerodynamic specifications in this work are based on the Northrop F-5E Tiger II. The F-5E is a legacy vehicle with well-documented aerodynamic characteristics; it was powered by two General Electric J85-GE-21 turbojet engines, each rated at 15.6 kN of dry thrust at sea-level (22.2 kN with afterburner), similar in terms of thrust performance to the turbojet engine modeled in this work. Specifically, thrust requirements and available thrust levels for cruise for this airframe are well matched using the respective engine model with this selected airframe. Specifications for the F-5E airframe [37] are given below:

Table 1. Northrop F-5E Tiger II Specifications.

| | | |
|---|---|---|
| Parasite Drag Coefficient | $C_{D0}$ | 0.02 |
| Aspect Ratio | $AR$ | 3.86 |
| Planform Area | $S$ | 17.28 m$^2$ |
| Oswald Efficiency Factor[1] | $e$ | 0.86 |
| Gross Weight | $W$ | 70.208 kN |

[1] Estimated using Schaufele's correlation [38].

The airframe drag, $D_{\text{airframe}}$, is calculated using the following classical airframe drag model [39]:

$$D_{\text{airframe}} = C_D q_\infty S = (C_{D0} + \frac{C_L^2}{\pi e AR}) q_\infty S \tag{23}$$

For cruising flight, aerodynamic lift ($L$) = vehicle weight ($W$) and airframe drag ($D_{\text{airframe}}$) = engine installed thrust ($F_{x\,(\text{engine})}$). The thrust specific fuel consumption at a given fuel throttle setting, flight Mach number, and altitude is defined as:

$$c_t = \frac{\dot{m}_f}{F_{x(\text{engine})}} \tag{24}$$

Using the drag model given above and solving the energy availability balance for cruising flight (Eq. (17)) in terms of $\dot{S}_{\text{total(vehicle in cruise flight)}}$, the following expression is obtained for $\dot{S}_{\text{total(vehicle in cruise flight)}}$ in terms of airframe aerodynamic parameters, $c_t$, vehicle weight $W$, and freestream dynamic pressure $q_\infty$:

$$u_\infty F_{x(\text{flight})} = \dot{E} + \dot{m}_f \left( H^* + \frac{u_\infty^2}{2} \right) - T_\infty \dot{S}_{\text{total}} \tag{25}$$

From Eq. (18), $\dot{S}_{\text{total(vehicle in cruise flight)}}$ is minimized at the flight condition (flight velocity and vehicle angle of attack) corresponding to flight for maximum endurance. The thrust specific fuel consumption, $c_t$, for a specific engine is, strictly speaking, a function of flight Mach number, altitude, and fuel throttle setting. At a flight/engine operational

point, it can be estimated from simple engine cycle analysis or found using the higher-level methodology of component matching and subsequent off-design performance analysis for an engine (as described and applied in this paper). However, it is generally assumed to be approximately constant in basic range and endurance analysis, i.e., when finding the flight velocity required for maximum range and endurance. With this assumption, when $\dot{S}_{\text{total(vehicle in cruise flight)}}$ is differentiated with respect to flight velocity and set to zero (and also noting that $\frac{u_\infty^2}{2} \ll H^*$ for gas turbine engines in general), the well-known requirement for flight for maximum endurance is obtained that parasite drag must be exactly balanced by the induced drag, i.e. $C_{D0} = C_L^2/\pi eAR = C_{Di}$.

Similarly, from Eq. (17), $\frac{\dot{S}_{\text{total (vehicle in cruise flight)}}}{u_\infty}$ can be written in terms of airframe aerodynamic parameters, $c_t$, vehicle weight, and freestream dynamic pressure $q_\infty$:

$$\frac{\dot{S}_{\text{total(vehicle in cruise flight)}}}{u_\infty} = \left[\frac{1}{2} q_\infty S C_{D0} + \frac{2W^2}{3\pi eAR q_\infty S}\right] \frac{c_t}{T_\infty} \sqrt{\frac{\rho_\infty}{2}} \left(H^* + \frac{u_\infty^2}{2}\right) \quad (26)$$

From Eq. (19), this quantity must be minimized at the flight condition corresponding to maximum range. Furthermore, if this relationship is differentiated with respect to flight velocity and set to zero (again, $\frac{u_\infty^2}{2} \ll H^*$), the classic requirement for flight for maximum range is then obtained that the parasite drag is exactly three times the induced drag, i.e., $C_{D0} = 3C_L^2/\pi eAR$. This analysis, along with the discussion in Section 6, therefore, provides the theoretical equivalence between the energy availability methodology (quantified in terms of entropy generation) and classic range and endurance relationships, and flight conditions required to maximize range and endurance.

# 9. RESULTS

This section of the paper provides quantitative results obtained using the energy utilization methodology as applied to specific engine and vehicle configurations. Selected details of the energy availability characteristics (and performance) of a defined turbojet engine in flight without airframe considerations are first presented. The modeling for this engine, and the resulting performance of the engine, has incorporated component matching (hence allowing the correct representation of actual on and off-design performance for a given engine, unlike most previous exergy studies which have not accounted for off-design engine behavior). This allows for the complete definition of the actual energy availability characteristics of a given engine across the complete range of off-design operational fuel throttle settings, flight Mach numbers, and altitudes for that engine. Representative results are then presented for the energy utilization characteristics (entropy generation) associated with a vehicle in cruise, in terms of endurance and range. The airframe and propulsive models used in the range and endurance analysis are based on the aerodynamic and configurational characteristics of the F-5E Tiger II fighter and the defined turbojet engine, respectively, as discussed in previous sections.

## 9.1. TURBOJET ENGINE ENERGY UTILIZATION (NO AIRFRAME)

Table 2 provides a summary of five cases of engine-alone operation (each case representing operation at a specific fuel throttle setting, flight Mach number, and altitude). These cases were selected to provide representative results from the complete engine on/off-design performance/energy utilization study, with emphasis on energy utilization

and losses. Case 1 is the base-line nominal ‘on-design’ flight and engine operation condition (altitude 9 km, flight Mach number of 0.85, fuel flow rate of 0.279 kg/sec, corresponding to a defined ‘100% on-design’ throttle setting, etc.). Cases 2 through 5 represent four distinct off-design operation points. Case 2 has the same flight Mach number and throttle setting as Case 1, but is for an altitude of 4.5 km. Case 3 corresponds to the same altitude and fuel throttle setting as Case 1 but is at a reduced flight Mach number of 0.6. Case 4 describes a flight Mach number of 1.25, while keeping altitude and fuel throttle at the on-design values. Case 5 denotes a 50% reduction in fuel throttle setting at on-design flight Mach number and altitude.

Table 2. Comparative parameter values between the on-design case and the four off-design cases studied.

| Conditions | | Altitude | Flight Mach No. | Fuel Throttle |
|---|---|---|---|---|
| On-Design Case 1 | | 9000 m | 0.85 | 100% |
| Off-Design Case 2 | Altitude Reduction | 4500 m | 0.85 | 100% |
| Off-Design Case 3 | Flight Mach No. Reduction | 9000 m | 0.60 | 100% |
| Off-Design Case 4 | Flight Mach No. Increase | 9000 m | 1.25 | 100% |
| Off-Design Case 5 | Fuel Throttle Reduction | 9000 m | 0.85 | 50% |

Figure 3 provides results for energy availability and losses for Cases 1 through 5. These results use relative values (as percent of overall energy availability) to facilitate comparisons and observations between the cases in subsequent discussion. In this figure, the far left-hand bar (in orange) represents the overall (initial) energy availability rate for all cases. This corresponds to 12.34 MW for Cases 1 thru 4 and 6.17 MW for Case 5. The energy availability rate is decomposed for each case into contributions associated with

individual engine component losses, wake loss, and the productive thrust power realized. Table 3 provides additional information for these five cases: including values of installed thrust, RPM, and spillage information, as well as compressor pressure ratios, fluid property ratios, etc. Examination of the information given in both Figure 3 and Table 3 allows the comparative analysis of energy utilization and losses between these five cases. Because the data and information generated in these results are based on the operating line-determined performance of a specific engine (with integrated and matched components), comparative analysis of the energy utilization increments between these cases can then be specifically related to changes in fuel throttle setting, altitude, and flight Mach number for that engine.

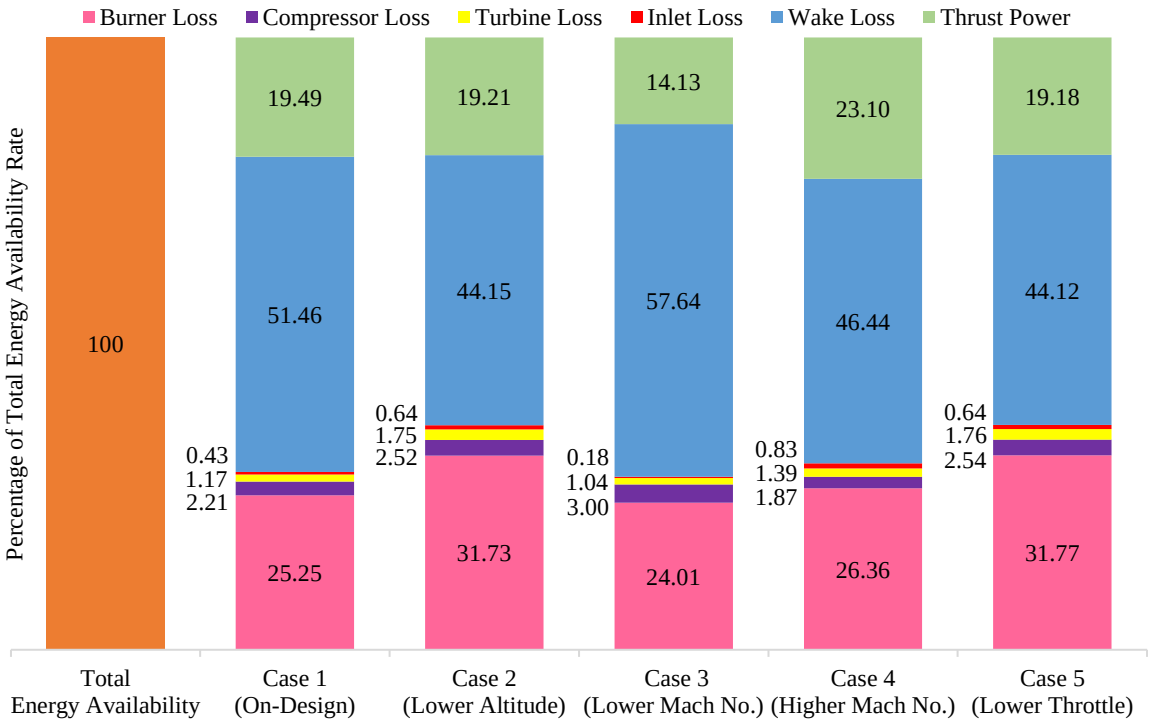


Figure 3. Comparative energy availability breakdown for the different engine operating conditions.

Figure 3 and Table 3 show that for Case 1, the on-design operating point, the wake mixing (equilibration) process is dominant in terms of entropy generation (losses). Wake loss represents approximately 64% of the total energy availability loss incurred by the engine at this condition. Wake entropy generation is driven by the degree of non-uniformity in the flow (the degree of non-equilibrium) between the propulsive and the side-bounding streamtubes at station $s$ (Section 2). The degree of this distortion entering the wake region for a given case is particularly indicated by the velocity ratio (nozzle exit to free stream) as provided in Table 3. Previous work has demonstrated the importance of the velocity ratio in terms of driving wake entropy generation behind powered aerospace vehicles in flight [15]. By the same token, the temperature and pressure ratios contribute as well to wake entropy generation.

For all individual engine component losses as well as the overall engine loss rate, loss rates in energy availability as given in Figure 3 (and Table 3) are directly proportional to the mass flow rate of air inducted into the engine (determined by flight and operating condition and resulting spillage characteristics upstream of the inlet face), as well as the individual component loss characteristics. Inlet energy availability losses are due to shocks, friction, etc.; inlet losses scale with flight Mach number via the inlet (diffuser) total pressure recovery model used. Compressor and turbine losses are functions of compressor and turbine efficiency, respectively, at a given operating point (in turn dependent on the operating line developed by the component matching for off-design performance analysis). Figure 5 shows that for Case 1, inlet and turbomachinery together account for only around 5% of the total lost availability rate; the compressor loss is larger than the turbine loss while the inlet loss is very small, as expected at a flight Mach of 0.85. Although significantly

smaller than the wake loss, the burner generates the largest engine component loss (accounting for approximately 31% of overall lost energy availability) in comparison to all other engine components. As a consequence of all losses, only about 20% of the total initial available energy rate for the on-design point is realized as thrust power. This fraction represents the instantaneous energy availability utilization effectiveness $\eta$.

The comparative (relative) values of the various losses in the individual components at the on-design condition (i.e., the burner clearly representing the largest engine component loss, followed by the compressor, etc.) are well-established by previous exergy and availability studies of gas turbine (jet) engines. However, because off-design engine performance is appropriately modeled using component matching in the present work, variations in individual component and wake energy availability loss rates can be directly associated with (and explained in terms of) changes in fuel throttle setting, flight Mach number, and altitude for a given engine. Hence, Case 2, which represents an off-design condition at the same fuel throttle setting and flight Mach as Case 1 (on-design), but at lower altitude, has markedly larger respective burner losses (39%) and less wake losses (55%) than those same losses experienced in Case 1. This is due to the fact that Case 2, even with the increase in total temperature entering the compressor due to the lower altitude, represents engine operation at significantly lower RPM and lower compressor pressure ratio than Case 1 (i.e., it is operating lower on the engine operating line on the compressor map). The reduced compression results in a reduction in the thermal efficiency in the burner ($\eta_{\text{thermal}} = 1 - (T_\infty / T_{t3})$, where $T_{t3}$ is the total/stagnation temperature at compressor exit), therefore generating higher entropy in that component. Concurrently, wake losses decrease for Case 2 (relative to Case 1; on-design) since the nozzle exit

conditions are closer to the free-stream conditions for this spooled-down engine operation point. Due to the trade between wake loss and burner losses, thrust power contribution to the overall energy availability balance does not change appreciably between Case 1 and Case 2.

Case 3 (for a lower flight Mach number) in comparison to Case 1 demonstrates reduced burner losses and much greater wake loss (i.e., the increase in wake loss is significantly greater than the drop in burner losses). There are negligible inlet losses, due to the low subsonic flight Mach number. The decreased burner losses as well as the increased wake loss are primarily because Case 3 represents a high RPM, high compressor pressure ratio condition for the engine (i.e., is higher on the operating line than the on-design operating point), see Table 3. The high compression results in increased thermal efficiency, hence lower losses in the burner. However, the larger gradients that then inherently exist at the nozzle exit (i.e., as seen in the velocity ratio between nozzle exit and free stream, etc.) and the increased mass flow rate of air generate increased entropy in the wake. Also, as flight Mach is reduced, the thrust power contribution necessarily drops (due to the lower flight velocity); thrust may increase marginally (as it does in this case) but thrust power drops overall, with the increased entropy generation necessarily appearing in the wake.

Case 4 (for a higher flight Mach number of 1.25) in comparison to Case 1 shows the expected increase in thrust power due to the increase in flight velocity; this occurs even though thrust has decreased. All loss increments in the energy availability balance are therefore necessarily reduced in part because of this effect (increased productive utilization of available energy, due to the higher flight velocity). However, this case represents a

spooled-down operation point for this engine in terms of compressor pressure ratio, RPM, and inducted mass flow rate (high spillage). Wake loss is noticeably decreased; this is due again to the reduction in entropy generation associated with reduced fluid properties' gradients between engine exit flow and the side-bounding flow at plane $s$. Wake loss, however, still remains the largest loss contribution at 60%; burner losses represent 34% of total losses. Inlet loss increases markedly at this supersonic flight Mach number as expected due to shock losses.

Case 5 (50% reduction in fuel throttling rate while maintaining on-design flight Mach number and altitude) in comparison to Case 1 inherently provides for loss rate reductions across the board of around a factor of two, due to the proportional reduction in heat release in the burner. However, for this case, there is a relative increase in the burner loss as compared to the wake loss. This is driven by the fact that this low-throttle engine condition represents a very low RPM, spooled down operating point (lower proportional mass flow rate of air inducted). This drives down the thermal efficiency (due to decreased pressure and temperature in the burner). This same effect, however, reduces gradients and resulting entropy generation in the wake, relative to the burner entropy generation, and relative to the wake entropy generation contribution to losses seen for Case 1.

Table 3. Comparative parameter values for engine on- and off-design operation.

| Parameter | Units | Case 1<br>Alt = 9000m<br>M = 0.85<br>mf = 100% | Case 2<br>Alt = 4500m<br>M = 0.85<br>mf = 100% | Case 3<br>Alt = 9000m<br>M = 0.60<br>mf = 100% | Case 4<br>Alt = 9000m<br>M = 1.25<br>mf = 100% | Case 5<br>Alt = 9000m<br>M = 0.85<br>mf = 50% |
|---|---|---|---|---|---|---|
| Thrust | kN | 9.31 | 8.64 | 9.56 | 7.51 | 4.58 |
| Thrust Power | MW | 2.40 | 2.37 | 1.74 | 2.85 | 1.18 |
| Total Availability Loss Rate | MW | 9.94 | 9.97 | 10.60 | 9.49 | 4.99 |
| $\dot{S}_{\text{wake}}/\dot{S}_{\text{engine}}$ | | 1.77 | 1.20 | 2.04 | 1.52 | 1.20 |

Table 3. Comparative parameter values for engine on- and off-design operation. (cont.)

| Parameter | Units | Case 1<br>Alt = 9000m<br>M = 0.85<br>mf = 100% | Case 2<br>Alt = 4500m<br>M = 0.85<br>mf = 100% | Case 3<br>Alt = 9000m<br>M = 0.60<br>mf = 100% | Case 4<br>Alt = 9000m<br>M = 1.25<br>mf = 100% | Case 5<br>Alt = 9000m<br>M = 0.85<br>mf = 50% |
|---|---|---|---|---|---|---|
| $T_\infty \dot{S}_{\text{total}}/\dot{m}_f H_f$ | | 0.81 | 0.81 | 0.86 | 0.77 | 0.81 |
| $\eta$ | | 0.19 | 0.19 | 0.14 | 0.23 | 0.19 |
| TSFC | kg/kN-s | 0.0300 | 0.0323 | 0.0292 | 0.0372 | 0.0304 |
| RPM | | 15,000 | 13,323 | 15,053 | 14,087 | 12,534 |
| $\dot{S}_{\text{inlet/diffuserr}}$ | W/K | 229.5 | 305.3 | 97.6 | 444.0 | 172.0 |
| $\dot{S}_{\text{compressor}}$ | W/K | 1,188.5 | 1,202.3 | 1,613.6 | 1,006.9 | 681.1 |
| $\dot{S}_{\text{burner}}$ | W/K | 13,562.6 | 15,121.4 | 12,895.9 | 14,161.7 | 8,531.5 |
| $\dot{S}_{\text{turbine}}$ | W/K | 627.7 | 834.9 | 557.4 | 748.9 | 471.4 |
| $\dot{S}_{\text{wake}}$ | W/K | 27,639.9 | 21,039.3 | 30,960.2 | 24,943.3 | 11,849.6 |
| $\pi_c$ | | 10.0 | 6.5 | 11.3 | 7.3 | 6.5 |
| $u_e/u_\infty$ | | 2.36 | 2.04 | 3.48 | 1.53 | 2.04 |
| $P_e/P_\infty$ | | 3.08 | 2.00 | 2.84 | 3.51 | 2.00 |
| $T_e/T_\infty$ | | 4.03 | 3.01 | 4.36 | 3.67 | 3.00 |
| Spillage | kg/s | 1.59 | 9.14 | -1.51 | 6.35 | 5.19 |
| Spillage Ratio | | 0.90 | 0.68 | 1.13 | 0.73 | 0.68 |
| $\dot{m}_{air}$ | kg/s | 14.49 | 19.3 | 12.9 | 17.3 | 10.9 |
| $\eta_{\text{thermal}}$ | | 0.58 | 0.52 | 0.59 | 0.59 | 0.52 |
| $D_{add}$ | kN | 0.049 | 0.701 | 0.033 | 1.130 | 0.375 |

## 9.2. SELECTED GRAPHICAL RESULTS OF ENGINE PERFORMANCE/ENERGY AVAILABILITY CHARACTERISTICS ACROSS THE OPERATING RANGE

Previous results and analysis (Figure 3, Table 3 and associated discussion) give significant insight in terms of understanding (diagnosing) basic performance and corresponding energy availability losses for this engine. This was done by choosing five (discrete) off-design operation points, including the nominal on-design point. However, complete engine performance descriptions (i.e., thrust, RPM, mass capture, losses, and details of energy availability balances and relative loss contributions) are complex constructs defined at every point within the engine operational envelope of fuel throttle setting, flight Mach number, and altitude.

Figures 4 and 5 illustrate selected energy availability information in terms of slices through the operational space of the engine. Specifically, Figure 4 provides contours of the ratio of entropy generation in the wake to the entropy generation in the engine, $\dot{S}_{\text{wake}}/\dot{S}_{\text{engine}}$ , for the modeled turbojet at 9 km altitude, across ranges of flight Mach number and fuel throttle setting. Figure 5 provides contours of the same ratio for 100% (nominal) fuel flow rate across ranges of flight Mach number and altitude. Recall that the entropy generation in the engine is dominated by burner losses.

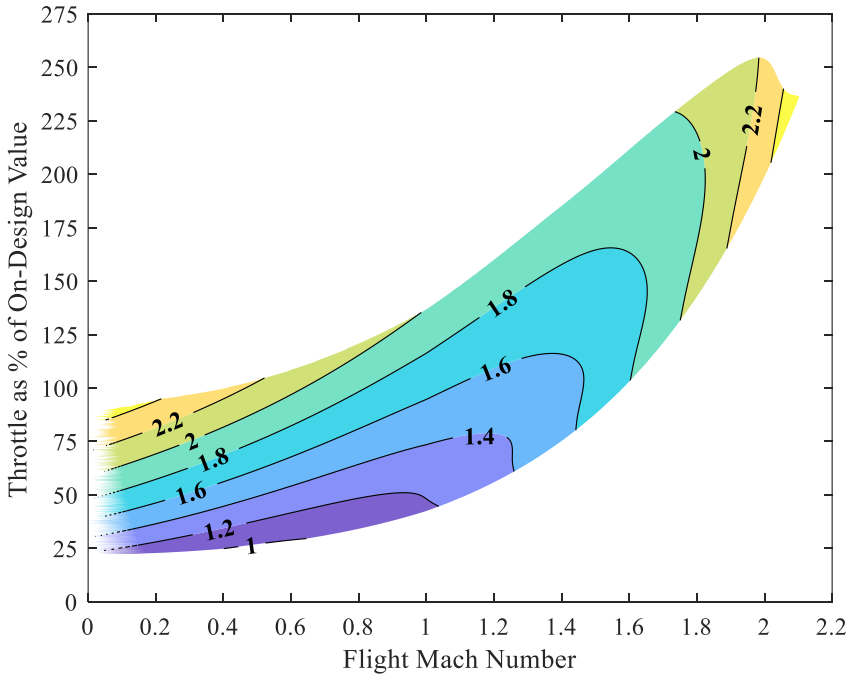


Figure 4. Ratio of entropy generation rate in the wake to entropy generation rate in the engine, $\dot{S}_{\text{wake}}/\dot{S}_{\text{engine}}$, at 9 km altitude.

These figures show that the ratio of wake entropy to engine entropy generation monotonically increases with increasing throttle and altitude, while decreasing with

increasing flight Mach number. Within the entire envelope of engine operation, this quantity has a minimum that is close to unity (i.e., the wake and engine losses in availability are approximately the same) and has a maximum of around 2.5. As discussed at length in the more detailed analysis of specific off-design cases in the previous section, variance in this ratio (wake to engine loss) is mainly due to effects of changing thermal efficiency, increased or decreased spooling of the engine and movement on the engine operating line, and changing fluid/thermodynamic gradients between engine exhaust flow and ambient.

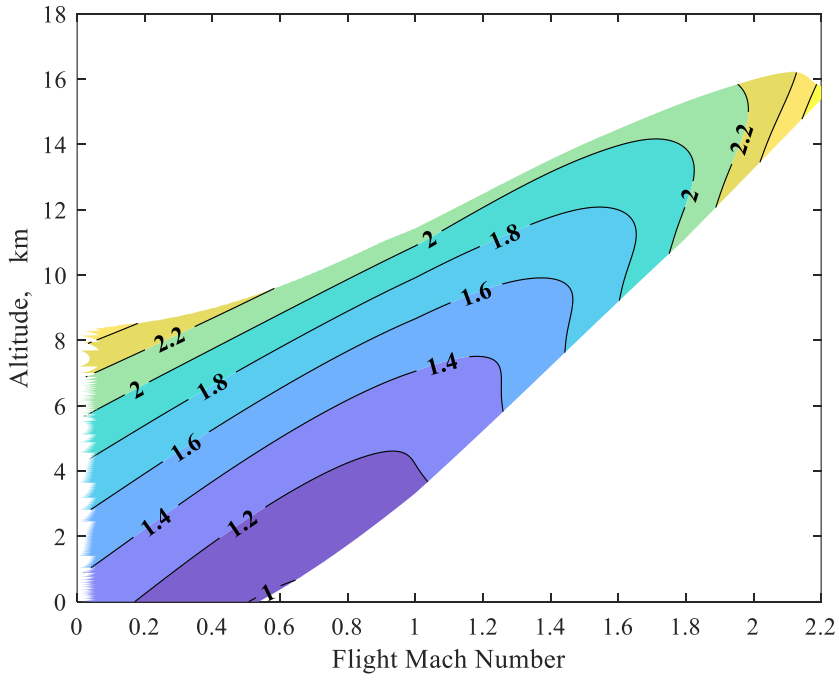


Figure 5. Ratio of entropy generation rate in the wake to entropy generation rate in the engine, $\dot{S}_{\text{wake}}/\dot{S}_{\text{engine}}$, at 100% of on-design fuel throttle setting.

## 9.3. ENDURANCE, RANGE, AND ENTROPY GENERATION; A CASE STUDY (AIRFRAME-ENGINE INTEGRATION)

Previous sections (6,8) have developed and described the relationships between energy availability (entropy generation) and the endurance and range of a jet-powered vehicle in flight. Flight conditions for maximum endurance and range have been shown to correspond to the minimum time rate and the minimum spatial rate of overall entropy generation, respectively, within the global control volume in which a vehicle is embedded. In addition, classic maximum endurance and range parameters such as lift to drag relationships and the balances between parasite and induced drag have been shown to be directly related to energy availability considerations. The analysis developed in this paper also provides the methodology for separately assessing and then combining entropy generations and energy utilization for the airframe and for the propulsion system. A quantitative case study of energy utilization and range and endurance in cruise flight is now performed for a specific vehicle configuration for which a selected legacy airframe drag model (based on the twin-engine Northrop F-5E Tiger II, as described in Section 8) is integrated with the turbojet engine model developed in this work. Specifically, two turbojet engines are integrated with the F-5E airframe to provide a complete powered vehicle model for this study. Entropy generation characteristics for cruise flight are then assessed in conjunction with classic relationships and parameters for range and endurance.

The parabolic curve in Figure 6 shows the aerodynamic drag generated by the F-5E airframe at 9 km altitude versus flight velocity. This drag is based on the aerodynamic parameters for the F-5E airframe and the nominal vehicle gross weight as given in Section 8. The magnitude of drag at a given flight velocity is, by definition, the engine thrust required for the vehicle (consisting of both engine and airframe) to cruise; there is a

minimum in thrust required (airframe drag) at a specific velocity, due to the trade between induced drag and parasite drag. In Figure 6, the line defining the thrust required for cruise is shown overlaid on a carpet plot of actual (available) thrusts provided by the two turbojet engines at this altitude for various fuel throttling rates, across the range of flight velocities. This underlying carpet plot of engine performance (shown as lines of constant $\dot{m}_f$) is generated using the component-matched (off-design) turbojet analysis and methodology described earlier; the required thrust distribution for cruise across a wide range of flight velocities for the F-5E airframe is seen to lie within the envelope of the performance of the engine. The flight velocity associated with the minimum thrust required is also seen to be very close to the minimum fuel flow rate, as expected.

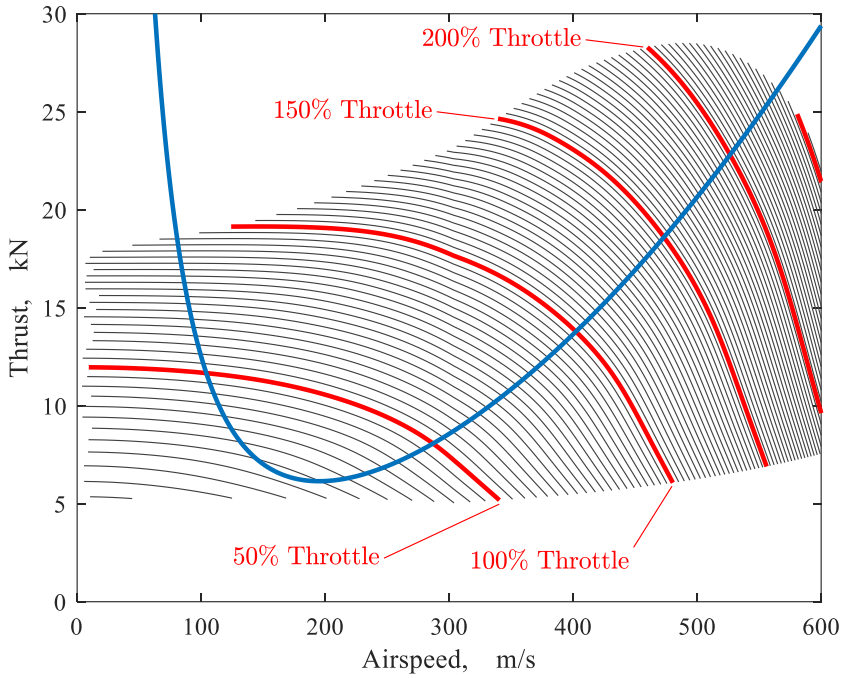


Figure 6. Thrust required (blue line) for cruise for F-5E airframe overlaid on twin turbojets performance envelope (thrust versus fuel flow rate). 9 km altitude.

In Figure 7, four parameters associated with endurance in cruise for this aircraft configuration (integrated airframe and turbojet engines together) are plotted over a range of flight velocities at an altitude of 9 km. These parameters are mass flow rate of fuel $\dot{m}_f$ required to cruise (obtained from the off-design engine analysis at the required thrust), overall entropy generation $\dot{S}_{\text{total}}$ in the global control volume (also obtained from the off-design engine and airframe analysis), lift-to-drag ratio $C_L/C_D$, and the required thrust (which is the airframe drag). Endurance for 1 gram of fuel consumed at the nominal gross weight is also plotted. All parameters are normalized by their respective extrema in order to clearly and easily compare characteristics. $\dot{m}_f$, $\dot{S}_{\text{total}}$, and thrust required are normalized by their minimum values of 174.4 g/s, 33.57 kW/K, and 6.15 kN, respectively. $C_L/C_D$ and endurance are normalized by their maximum values of 11.42 and 0.00573 sec/g. It is seen that all four parameters, as expected from classic endurance relationships and from the energy availability analysis as developed and described in this work, give approximately similar results for the flight condition for maximum endurance. There is, however, as expected, a difference in terms of the flight velocity at which maximum lift-to-drag ratio and minimum thrust required occurs (as compared to the actual flight velocity required for maximum endurance, i.e., at minimum $\dot{m}_f$ and minimum $\dot{S}_{\text{total}}$). Whereas the flight velocity corresponding to maximum endurance is 168 m/s, the flight velocity corresponding to maximum lift-to-drag ratio is 195 m/s. This difference is due to the approximation in the classic endurance formulation that thrust specific fuel consumption ($c_t$) is constant with flight velocity, this approximation results in the condition that $C_L/C_D$ be maximized (and hence thrust required minimized) for flight conditions corresponding to maximum endurance (see the discussion in Section 8).

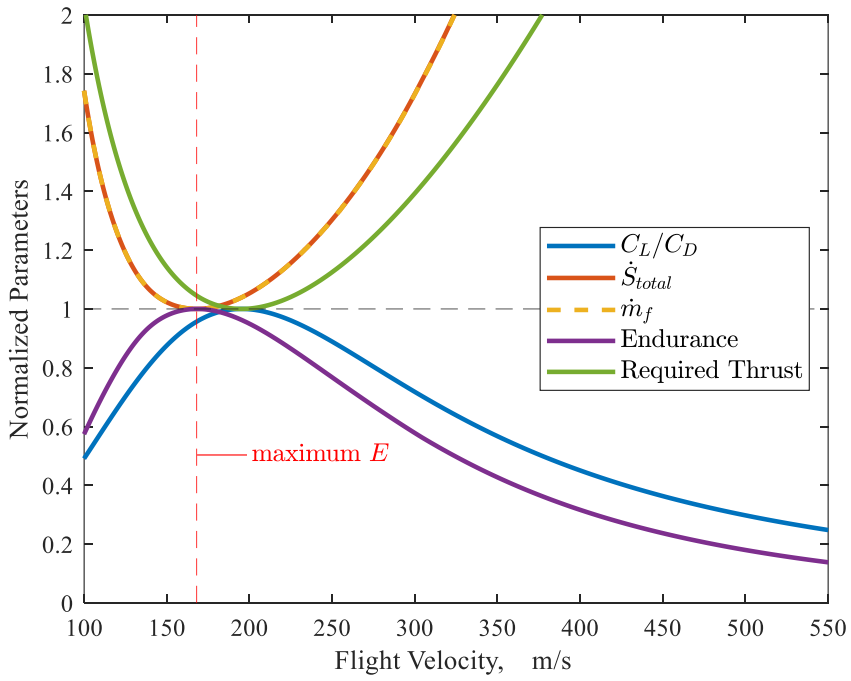


Figure 7. Normalized endurance related parameters over range of flight velocities. F-5E airframe with modeled turbojet engines; 9 km altitude.

Figure 8 provides a plot of three parameters associated with range in cruise for the modeled vehicle (the F-5E airframe powered by a pair of the modeled turbojet) across the flight velocity range. These parameters are mass of fuel per distance traveled, $\dot{m}_f/u_\infty$ (obtained from the off-design engine analysis at the required thrust), overall entropy generated per distance traveled, $\dot{S}_{\text{total}}/u_\infty$ (also obtained from the off-design engine analysis), and the ratio $C_L^{1/2}/C_D$ (obtained from the airframe model). The range for 1 gram of fuel consumed at the nominal gross weight is also plotted. These parameters are normalized by their respective extrema; $\dot{m}_f/u_\infty$ and $\dot{S}_{\text{total}}/u_\infty$ are normalized by their minimum values of 0.896 g/m and 172.5 N/K, respectively. $C_L^{1/2}/C_D$ and range are normalized by their maximum values of 19.3 and 1.116 m/g, respectively. For range

(similar to observations regarding endurance in Figure 7), all four parameters in Figure 8, as expected from classic range relationships and from the energy availability analysis as developed and described in this work, yield approximately similar results for the flight condition required for maximum range. Referring to the discussion of Figure 7, however, and for the same reason that maximum $C_L/C_D$ is an approximate condition for maximum endurance, maximum $C_L^{1/2}/C_D$ also occurs at a somewhat different flight velocity (257 m/s) than that corresponding to maximum range (226 m/s).

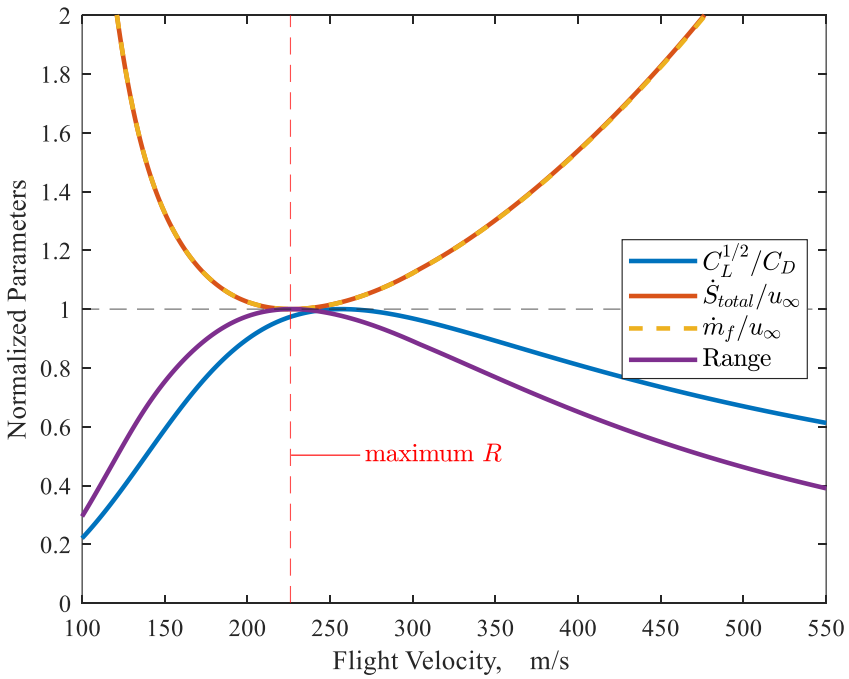


Figure 8. Normalized range related parameters over range of flight velocities. F-5E airframe with modeled turbojet engines; 9 km altitude.

Figure 9 shows the total entropy generation rate versus flight velocity for the powered vehicle in cruise as the summation of the respective contributions associated with

propulsion system and airframe, reflecting the superposition principle for losses described in Section 6. In Figure 9, the top (yellow) line represents the total entropy generation rate that occurs in the overall global control volume that encompasses the powered vehicle, from freestream ∞ to wake exit plane $w$ (see Figure 2 for station designations). The bottom (blue) line represents the entropy generation rate within the propulsive flowpaths (not including wake), i.e., from freestream ∞ to wake region entrance plane $s$. The increment between the blue (bottom) line and the middle (orange) line represents the entropy generation that specifically occurs in the wakes of the (twin-engine) propulsion system (analyzed without an airframe). Therefore, the middle (orange) line provides the total entropy generation rate associated with the propulsion system without airframe considerations, encompassing all losses: 1) in the upstream acceleration/deceleration captured streamtubes from ∞ to $i$ (inlet face), 2) inside the engines from $i$ to $e$ (engine exit), and 3) in the wakes of the stand-alone engines (from $e$ to $w$). Finally, the increment between the orange (middle) and yellow (top) lines represents the total entropy generation associated with the unpowered airframe. This increment includes losses upstream of the unpowered airframe wake, as well as losses within that wake. At a flight velocity of 168 m/s, corresponding to the minimum total entropy generation rate for the vehicle (which, as demonstrated in this work, also corresponds to maximum endurance), the propulsion system accounts for approximately 86% of the overall entropy generation (with the remaining 14% of losses associated with the airframe). Also, at this flight velocity, the propulsive system alone (no airframe) wake losses are seen to be approximately equal to the propulsive flowpath losses occurring upstream of the wake. This relatively low ratio (approximately 1) of wake to engine entropy generations in the propulsive system analysis

is entirely due to the low throttle operation of the engines at this point (i.e., at very near minimum thrust required, as described in previous discussion).

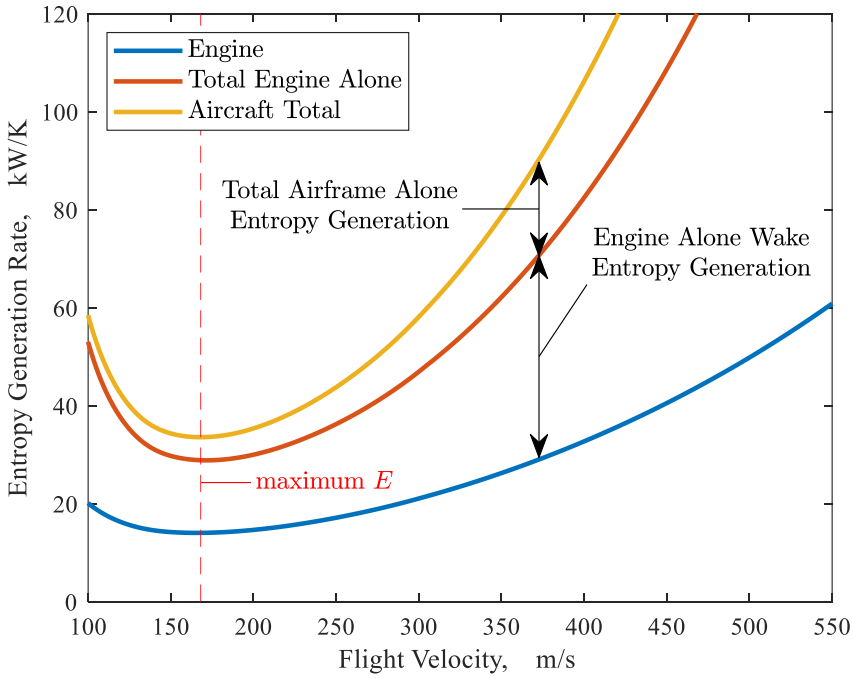


Figure 9. Total aircraft entropy generation rate breakdown over range of flight velocities. F-5E airframe with modeled turbojet engines; 9 km altitude.

## 10. DISCUSSION

The fundamental energy utilization balance for an air-breathing aerospace vehicle in flight represents the synthesis of both first and second laws of thermodynamics and flight mechanics. This balance, as derived from the global control volume approach, directly (analytically) links classic vehicle force-based performance at a given flight condition to available energy associated with the propellant, and to losses in that available energy.

While the global control volume approach and the resulting energy utilization balances (both rate-based and mission-integrated) have been previously described and applied in a number of works, including detailed analyses of scramjets and rockets, it has not been previously applied to the analysis of airframe/jet engine configurations in terms of cruise requirements.

In this paper, the energy availability balance is first specialized to allow the full analysis of the performance and energy utilization of a stand-alone gas turbine (jet) engine (without airframe considerations); this analysis accounts for additive drag effects and characterizes wake impacts as well as the contributions of individual engine components, in terms of entropy generation and resultant losses in installed engine thrust. Detailed results for five selected cases of engine-alone operation are obtained. These cases include the on-design point (defined by its specific fuel throttle rate, flight Mach number, and altitude) and four off-design points, each representing a variation in fuel throttle setting, flight Mach, and altitude from the design point values. Results obtained incorporate, for all five cases, both conventional off-design engine performance (installed thrust, spillage, additive drag, component performance, thermal efficiency, etc.) as well as significant parameters and information related to energy utilization and the energy utilization balance for the engine. For both on and off-design engine operation, the loss in overall energy availability (reflecting a reduction in delivered thrust) is dominated by the wake entropy generation. Within the engine itself, relative to other engine components, the burner is dominant in terms of entropy generation. Other component losses are generally very small in comparison to the burner loss. These results are expected, based on previous exergetic studies of similar gas turbines using, for instance, cycle analysis. However, because the

results obtained in this study accurately reflect actual off-design performance of the (given) engine (rather than cycle analysis results), direct assessments of the linkage and drivers between energy utilization and entropy generation and the observed performance of the engine can be made in a consistent fashion between on and off-design points.

Specifically, by examining and comparing (stand-alone) engine conventional performance in conjunction with energy utilization results for the off-design cases, the two dominant influences on wake entropy generation are seen to be: 1) the degree of distortion at the (engine) exit plane and 2) the (related) engine operating point, RPM and spooling characteristics; these factors all determined by the specific fuel throttle setting, flight Mach number, and altitude for any particular case. In terms of the impact of the degree of distortion at engine exit plane, the wake entropy generation is observed to be (especially) correlated with the nozzle exit velocity to freestream velocity ratio, in line with previous energy availability studies for aerospace systems. The burner entropy generation, representing by far the largest loss within the engine itself, is driven (as expected) primarily by the thermal efficiency, which in turn is strongly related to the specific engine operating point, RPM, and spooling characteristics (as well as flight conditions).

In order to more comprehensively illustrate the actual envelope of off-design engine performance and energy utilization behavior obtained by the analysis in this paper, selected contour plots of the ratio of entropy generation in the wake to entropy generation in the engine are provided. These results are shown for varying flight Mach number and varying fuel flow rate at a given altitude and for varying flight Mach number and varying altitude at a given fuel throttle setting and emphasize the dominant role of the losses in the wake in terms of overall utilization of available energy.

In addition to the employment of the energy availability balance to the study of a stand-alone engine, the balance is also applied to provide the energy utilization characteristics of an unpowered airframe, in terms of drag of the airframe and resulting entropy generation. These engine-only and airframe-only energy utilization formulations are then combined analytically. This combination provides the capability to assess the overall performance of a jet-powered aircraft in terms of energy utilization. A superposition principal results from the analysis: the entropy generation that actually occurs in the wake of a powered vehicle is the summation of the entropy generations that (separately) occur in the modeled wake of its stand-alone (analyzed with no airframe) propulsion system and in the modeled wake of its airframe (analyzed with no propulsion system).

Entropy generation and energy utilization that are experienced by a vehicle in cruise are next formulated, utilizing the airframe drag model, with focus on the flight conditions corresponding to maximum endurance and maximum range. The relationship of entropy generation and energy availability to classic range and endurance conditions is described. The theoretical requirement that overall entropy generation temporal rate in the global control volume must be minimized for a jet-powered vehicle at the flight condition for maximum endurance results from this analysis; similarly, the fundamental requirement that overall entropy generation spatial rate be minimized for maximum range is also shown. Additionally, energy utilization analysis in terms of entropy generation is shown to give the well-known (classic) balances between induced and parasite drag contributions required for maximum endurance and range, respectively. These characteristics of the entropy generation at cruise, as developed theoretically and then illustrated in this application, are fundamental requirements that emerge from the energy availability

balance. Furthermore, the classic maximum endurance and range flight conditions involving the necessary balances of lift and drag, are shown in this vehicle application to also correlate with the energy availability (entropy generation) results. These results also provide verification of theoretical derivations in this paper; the well-known lift and drag balances required for maximum endurance and maximum range, as well as the associated balances between parasite drag and induced drag, can be obtained directly from energy utilization analysis and global control volume-based considerations of entropy generation.

The work described in this paper provides the methodology necessary to apply the global control volume/energy utilization approach to both stand-alone gas turbine engines and to powered airframes with jet propulsion in the atmosphere. This methodology supplements (but does not replace) both traditional momentum-based analysis and conventional exergetic methods. Specifically, it allows new insight into the second-law aspects of powered flight. For instance, as shown in this paper, the approach uniquely enables the derivation of the necessary conditions for maximum range and endurance for cruise flight in terms of overall entropy generation. It is believed that the most promising use of this methodology undoubtably is in system-level analysis and optimization of aerospace flight systems. Entropy generation inherently provides a single universal metric of losses for all components, processes, and sub-systems associated with the flight of a vehicle. The methodology described in this paper enables the comprehensive global and complete assessment of system-level performance losses, and relationships to overall entropy generation, including wake effects, for the applications of interest.

# REFERENCES


[1] Riggins, D., Taylor, T., and Moorhouse, D., "Methodology for Performance Analysis of Aerospace Vehicles Using the Laws of Thermodynamics", *AIAA Journal of Aircraft,* Vol. 43, No. 4, 2006, pp. 953-963. DOI: 10.2514/1.16426

[2] Riggins, D.W., Camberos, J., and Moorhouse, D., "The Characterization of Aerospace Vehicle Performance and Mission Analysis Using Thermodynamic Availability", *AIAA Journal of Aircraft,* Vol. 47, No. 3, 2010, pp. 904-916. DOI: 10.2514/1.46420

[3] Riggins, D., Taylor, T., Moorhouse, D., and Terhune, L., "Methods for the Design of Energy Efficient High-Speed Aerospace Vehicles", *Aeronautical Journal of the Royal Aeronautical Society,* May 2007, pp 297-309. DOI: 10.1017/S0001924000004541

[4] Riggins, D. W., Camberos, J., Wolff, M., and Bowcutt, K., "Mission-Integrated Exergy Analysis for Hypersonic Vehicles: Methodology and Application", *Journal of Propulsion and Power,* Vol. 29, No. 3, pp. 610-620, May-June 2013. DOI: 10.2514/1.B34733

[5] Riggins, D. W., Abbas, M., Wainwright, M., and Camberos, J., "Analysis of Energy Utilization for Chemical Rockets", *AIAA Journal of Spacecraft and Rockets,* Vol.56, No.3, May–June 2019. DOI 10.2514/1.A34296

[6] Abbas, M., Riggins, D., and Watson, M., "Entropy-Based Performance Analysis of Chemical Rockets", *AIAA SciTech 2020 Forum,* AIAA Paper 2020-0759, Orlando, FL, January 2020. DOI: 10.2514/6.2020-0759

[7] Oswatitsch, K., "General Equations and Theorems", *Gas Dynamics,* Academic Press Inc., New York, 1956, pp. 177-210

[8] Giles, M. and Cummings, R., "Wake Integration for Three-Dimensional Flowfield Computations: Theoretical Development," *Journal of Aircraft*, Vol. 36, No. 2, 1999, pp. 357–365. DOI: 10.2514/2.2465

[9] Marley, C., and Riggins, D., "The thermodynamics of Exergy Losses and Thrust Production in Gas Turbine engines," *47th AIAA/ASME/SAE/ASEE Joint Propulsion Conference & Exhibit,* AIAA Paper 2011-6130, San Diego, CA, July 2011. DOI: 10.2514/6.2011-6130

[10] Marley, C., and Riggins, D., "Exergy Analysis of a Turbojet Engine Modeled as a Lumped Parameter System," *50th AIAA Aerospace Sciences Meeting including the New Horizons Forum and Aerospace Exposition,* AIAA Paper 2012-1122, Nashville, TN, January 2012. DOI: 10.2514/6.2012-1122

[11] Abbas, M., and Riggins, D., "Exergy-Based Performance Analysis of a Turbojet Engine," *52nd AIAA/SAE/ASEE Joint Propulsion Conference*, AIAA Paper 2016-4638, Salt Lake City, UT, July 2016. DOI: 10.2514/6.2016-4638

[12] Foa, J., "Efficiencies: Propulsive Cycles," *Elements of Flight Propulsion*, Wiley, New York, 1960, pp. 274–287.

[13] Builder, C. H., "On the Thermodynamic Spectrum of Air-Breathing Propulsion," *1st Annual Meeting*, AIAA Paper 64-243, Washington, DC, June 1964. DOI: 10.2514/6.1964-243

[14] Lewis, J. H., "Propulsive Efficiency from an Energy Utilization Standpoint," *Journal of Aircraft*, Vol. 13, No. 4, 1976, pp. 299–302. DOI: 10.2514/3.44525

[15] Clarke, J., and Horlock, J., "Availability and Propulsion," *Journal of Mechanical Engineering Science*, Vol. 17, No. 4, 1975, pp. 223–232. DOI: 10.1243/JMES_JOUR_1975_017_033_02

[16] Czysz, P. and Murthy, S. N. B., "Energy Analysis of High-Speed Flight Systems," Chapter 3 in *High-Speed Flight Propulsion Systems*. Progress in Astronautics and Aeronautics Series, AIAA, Volume 137. DOI: 10.2514/5.9781600866104.0143.0235

[17] Murthy, S. N. B., "Effectiveness of a Scram Engine," *30th Joint Propulsion Conference and Exhibition*, AIAA Paper 94-3087, Indianapolis, IN, June 1994. DOI: 10.2514/6.1994-3087

[18] Brilliant, H. M., "Analysis of Scramjet Engines Using Exergy Methods," *31st Joint Propulsion Conference and Exhibition*, AIAA Paper 95-2767, San Diego, CA, June 1995. DOI: 10.2514/6.1995-2767

[19] Curran, E. T. and Craig, R. R., "The Use of Stream Thrust Concepts for the Approximate Evaluation of Hypersonic Ramjet Engine Performance," Air Force Aero Propulsion Laboratory, Technical Report AFAPL-TR-73-38, July 1973.

[20] Riggins, D. W., "The Thermodynamic Continuum of Jet Engine Performance; The Principle of Lost Work due to Irreversibility in Aerospace Systems," *International Journal of Thermodynamics*, Vol. 6, No. 3, 2003, pp. 107–120. DOI: 10.5541/ijot.1034000113

[21] Riggins, D., McClinton, C. R., and Vitt, P., "Thrust Losses in Hypersonic Engines Part 1: Methodology," *Journal of Propulsion and Power*, Vol. 13, No. 2, 1997, pp. 281–287. DOI: 10.2514/2.5160

[22] Riggins, D., "Thrust Losses in Hypersonic Engines Part 2: Applications," *Journal of Propulsion and Power*, Vol. 13, No. 2, 1997, pp. 288–295. DOI: 10.2514/2.5161

[23] Roth, B., and Mavris, D., “Comparison of Thermodynamic Loss Models Suitable for Gas Turbine Propulsion,” *Journal of Propulsion and Power*, Vol. 17, No. 2, 2001, pp. 324–332. DOI: 10.2514/2.5745

[24] Roth, B., “A Work Potential Perspective of Engine Component Performance,” *Journal of Propulsion and Power*, Vol. 18, No. 6, 2002, pp. 1183–1190. DOI: 10.2514/2.6077

[25] Ehyaei, M., Anjiridezfuli, A. and Rosen, M.. "Exergetic Analysis of an Aircraft Turbojet Engine with an Afterburner." *Thermal Science*, Vol. 17, No. 4, pp. 1181-194. DOI: 10.2298/TSCI110911043E

[26] Etele, J. and Rosen, M. “Sensitivity of Exergy Efficiencies of Aerospace Engines to Reference Environmental Selection”, *Exergy, An International Journal*, Vol. 1, Issue 2, 2001, pp. 91-99. DOI: 10.1016/S1164-0235(01)00014-0

[27] Doty, J., Camberos, J., and Moorhouse, D., "Benefits of Exergy-Based Analysis for Aerospace Engineering Applications: Part 1." *40th Thermophysics Conference*, AIAA Paper 2008-4355, Seattle, WA, June 2008. DOI: 10.2514/6.2008-4355

[28] Arntz, A., Atinault, O., and Merlen, A., “Exergy-Based Formulation of Aircraft Aeropropulsive Performance Assessment: Theoretical Development,” *AIAA Journal*, Vol. 53, No. 6, June 2015, pp. 1627-1639. DOI: 10.2514/1.J053467

[29] Bastani, M., Jafari, R., and Ghasemi, H., “Exergy Analysis of an Aircraft Turbojet Engine,” *International Journal of Engineering Sciences and Research Technology*, Vol. 4, No. 4, April 2015, pp. 380–386.

[30] Karakoc, T., and Turan, O., “Exergetic Destruction Effects of Operating Conditions on the Turbojet Engine Components,” *Applied Mechanics and Materials*, Vols. 110-116, October 2011, pp. 2390-2394.

[31] Turan, O. and Karakoc, T., “Exergetic and Energetic Response Surfaces for Small Turbojet Engine,” *Applied Mechanics and Materials*, Vol. 110-116, pp. 1054-1058.

[32] Yuksel, B., Balli, O., Gunerhan, H., Hepbasli, A., and Atalay, H., “Exergetic and Environmental Analyses of Turbojet Engine,” *7th Global Conference on Global Warming (GCGW-2018)*, June 24-28, 2018, Izmir, Turkey.

[33] Gronstedt, T., Irannezhad, M., Lei, X., Thulin, O., and Lundbladh, A., “First and Second Law Analysis of Future Aircraft Engines,” *Journal of Engineering for Gas Turbines and Power*, Vol. 136, March 2014, pp. 031202 1-10.

[34] Anderson, J. D., *Introduction to Flight (7th Edition)*, McGraw-Hill, New York, 2012, pp. 506-513.

[35] Mattingly, J. D., *Elements of Propulsion: Gas Turbines and Rockets*, AIAA Education Series, Virginia, 2006, pp. 358-359, pp. 437-769.

[36] Oates, G. C., *Aerothermodynamics of Gas Turbine and Rocket Propulsion (3rd Edition)*, AIAA Education Series, Virginia, 1997, pp. 277-322.

[37] Loftin, L. K., *Quest for Performance: The Evolution of Modern Aircraft*, National Aeronautics and Space Administration, History Office, 1985, pp. 488–492.

[38] Schaufele, R. D., *The Elements of Aircraft Preliminary Design*, Aries Publications, California, 2000, pp. 238.

[39] Anderson, J. D., *Fundamentals of Aerodynamics (5th Edition)*, McGraw-Hill, New York, 2011, pp. 502-503.

# II. ANALYSIS OF ENERGY UTILIZATION FOR CHEMICAL ROCKETS

David W. Riggins, Mohammad Abbas, and Mitchell Wainwright

Department of Mechanical and Aerospace Engineering, Missouri University of Science and Technology, Rolla, MO 65409

and

Jose Camberos

Air Force Research Laboratory, Wright Patterson AFB, Dayton, OH 45433

## ABSTRACT

Methodology is developed for the comprehensive analysis and quantification of energy utilization in chemical rockets, based on the overall thermochemical and kinetic energy availability of the stored propellant. The energy utilization balances for both single and two stage rockets operating in a gravitational field and with external atmospheric drag are derived and discussed in terms of contributors to that balance, including irreversibility occurring in the rocket engine and external to the vehicle, work required to lift expended propellant to altitude, and the productive utilization of energy as realized by kinetic and potential energy changes achieved by the final rocket mass. For multiple stage systems, additional contributors are the energy utilizations associated with kinetic and potential energies of discarded structural masses at staging. The energy utilization balance can be tracked in time through a given mission. Calculation of the thermochemical availability for chemical rockets necessary for a complete thermodynamic analysis of energy utilization is

described. A case study for 1st and 2nd stage operation of the legacy Saturn V access-to-space launch vehicle using Apollo 11 data is performed. Details of the time evolution and final balance of energy utilization are provided for this system using the methodology developed.

## NOMENCLATURE

| Symbol | Description |
|---|---|
| $C$ | Effective exhaust velocity, m/s |
| $D$ | Aerodynamic drag, N |
| $E_{\mathrm{AV}}$ | Total energy availability of propellant at beginning of mission, J |
| $F$ | Net fluid dynamic force component on vehicle in flight direction, N |
| $g$ | Gravitational acceleration, m/s$^2$ |
| $H_f$ | Heating value of fuel, J/kg |
| $H_P$ | Heating value of propellant, J/kg |
| $H^*_{\mathrm{eff}}$ | Effective thermochemical energy availability of propellant (mission integrated), J/kg |
| $H^*$ | Total thermochemical energy availability of propellant, J/kg |
| $h$ | Altitude, m |
| $m$ | Mass of vehicle, with subscript denoting specific condition, kg |
| $m_R$ | (Instantaneous) mass of rocket, kg |
| $\dot{m}_P$ | Mass flow rate of propellant, kg/s |
| $R$ | Mixture ratio (oxidizer to fuel mass flow rates) |

| | |
|---|---|
| $S$ | Entropy, J/K |
| $\dot{S}$ | Entropy flow rate, with subscript denoting specific location, J/K-s |
| $s$ | Entropy per mass, with subscript denoting specific location, J/K-kg |
| $T$ | Temperature, K |
| Thrust | Thrust provided by rocket engine, N |
| $V$ | Vehicle flight velocity, m/s |
| $W$ | Vehicle flight velocity, m/s |
| $\beta$ | Energy availability remaining in propellant tanks at time $t$, J |
| $\theta$ | Vehicle climb angle |
| $\tau_b$ | Time of burn, s |
| $\phi$ | Productive energy used (kinetic energy and potential energy change realized by final vehicle mass), J/kg |

Subscripts

| | |
|---|---|
| discard | Mass discarded at staging event |
| $f$ | Final condition (end of mission) |
| $i$ | Initial condition (where $t$ is equal to zero; beginning of mission) |
| irr | Irreversibility |
| $P$, prop | Propellant |
| $s$ | Condition at staging |
| $w$ | Wake exit plane of global control volume in which vehicle is embedded |
| 1, 2 | Stage 1 and stage 2, respectively |

| | |
|---|---|
| $\infty$ | Freestream (inflow) plane of global control volume in which vehicle is embedded |

## 1. INTRODUCTION

This paper describes methodology for the analysis of energy utilization in missions performed by single-stage and two-stage chemical rockets operating in the atmosphere. This methodology is based on the fundamental physical principle of work availability (variously termed exergy or availability in the literature). The concept of availability results from the combination of the first and second laws of thermodynamics, and hence has complete generality in terms of systems and processes to which it applies. Specifically, the correct application of availability analysis to aerospace vehicles, including rockets, can provide the well-ordered and generalized analytical treatment of the utilization of available energy at any given flight condition, as well as across an entire mission. The purpose of this paper is to provide a detailed treatment of the topic of energy utilization in chemical rockets, as well as to illustrate its use by analyzing the energy utilization during the flight of the first two stages of the legacy Apollo 11 vehicle.

To describe the energy utilization of a rocket, consider a chemical rocket with initial mass that initiates firing of the propulsion system at a given altitude and at a given velocity. The energy availability (or exergy) associated with the stored propellant at the beginning of the burn is, by definition, the maximum available work that is realizable through equilibration of the stored propellant with the environment in which the rocket is operating. This requirement of equilibration implies that the propellant achieves complete chemical, thermal, and mechanical equilibrium with the ambient environment. However, as the

rocket burns propellant, accelerates, and changes altitude, the availability of the propellant (per mass of propellant) remaining in the tanks therefore changes. This is due to changing ambient (atmospheric) conditions as well as changes in vehicle velocity (resulting in changes in stored propellant kinetic energy). Therefore, across a specific mission, there results a total mission-integrated availability of energy (integration in time of the availability per mass of propellant multiplied by the mass flow rate of propellant) that is associated with the propellant used during the mission. This total mission-integrated availability necessarily accounts for the changing atmospheric conditions that the rocket experiences in its flight (along with possible changes in tank conditions) and possible changes in mass flow rates of propellant during the mission.

The total mission-integrated availability is progressively used during the mission in order to 1) overcome losses associated with various irreversibilities both internal and external to the vehicle, including in the wake equilibration process downstream of the vehicle; 2) perform geopotential work in lifting to altitude the propellant mass that is expended during the burn; and 3) effect the productive (desired) changes in the kinetic energy and gravitational potential energy of the nonpropellant mass (i.e., the final mass of the rocket for a given burn). For a multistage rocket with discard of structural mass, a portion of the initially available energy also necessarily goes into the work required to lift the discarded structural mass to altitude as well as to effect kinetic energy and potential energy changes of the discarded mass before discard. Although not attributable to irreversibilities, the energy needs that are associated with the discarded mass in staged systems nevertheless represent a real and quantifiable loss that reduces the (final) realized productive energy utilization described previously in item 3.

If all stored propellant is used within the burn, there results a thermodynamically mandated energy utilization balance at the end of the burn. Specifically, the total mission-integrated availability associated with stored propellant will be exactly equal to the sum of the various losses (previous items 1 and 2 for a single-stage burn) and the productive energy utilization (previously item 3) realized in achieving the final velocity and altitude of the final mass of the vehicle. It should be noted that, during the burn itself, the balance also exists; however, the (progressively decreasing) amount of still available energy associated with unburned propellant must also be included with the (progressively increasing) losses and productive energy utilization. For multistage systems, the energy used to lift and accelerate discarded structural mass must also be included as a loss.

The concept of thermodynamic availability, or exergy, combines both first law and second law principles. The concept encapsulates the fundamental balance between maximum (force-based) work potential available from a process, actual realized work within the process, and the balance of losses associated with entropy generation due to all mechanisms during that process. A foundational reference for availability theory, methods, and analysis is that provided by Bejan [1]. Availability has a long history and has been widely accepted and used in analyzing and optimizing energy management in ground-based systems and processes

The use of availability for aerospace systems and vehicles has less of an extensive track record than that for ground-based systems. A recent review of work done in this area was provided by Hayes et al. [2]. Probably the earliest reference that incorporated availability methodology in terms of analysis of a body in motion in a fluid was by Oswatitsch [3] in 1956, who first derived the relationship between fluid dynamic drag and

entropy generation over and downstream of a nonpowered object in fluid flow using a global control volume approach. Clark and Horlock [4] also developed the basic availability balance for propulsion systems using a control volume approach. Lewis [5] applied conventional availability methods to airbreathing engines in order to characterize engine efficiencies. Riggins et al. [6–8], due to issues with conventional availability when applied to engines, focused on related thrust potential concepts for aerospace airbreathing engines. This followed earlier work by Curran and Craig [9], who applied stream thrust methods for the optimization of ramjets. Etele and Rosen [10] identified the two major complicating issues when applying availability to aerospace propulsion systems; these issues were the open-cycle character of jet engines and the variable thermodynamic reference condition(s) that were necessary for availability analysis. Giles and Cummings [11] and Hunt et al. [12] developed the availability balance via a control volume approach to powered aerospace vehicles using a simplified heat model for combustion. They clearly showed the significance of the vehicle wake in terms of entropy generation and the relationship to vehicle force-based performance using a computational fluid dynamics case study. Riggins et al. [13–15] also derived and applied the generalized availability balance for an aerospace vehicle in terms of the global control volume in which a vehicle was embedded and combined that balance with the vehicle equation of motion in order to provide the general treatment of mission-integrated availability, including the effects of the combustion of propellants. Additional details of the derivation for the generalized balance can be found in the work of Terhune [16]. Riggins et al. [17] applied this methodology to the modeling and analysis of a hypersonic airbreathing vehicle and tracked its energy utilization throughout an acceleration and climb mission. Exergy mapping for aircraft

systems design and reference state issues was investigated by Berg et al. [18]. Arntz et al. [19] recently provided an exergy-based formulation and evaluation for aircraft, which was focused on the integrated aerodynamic and propulsive systems. Moorhouse and Camberos [20] and Moorhouse [21] articulated the need for refinement and further development in order to make availability truly useful for aerospace applications. Additional work in the area of (airbreathing) jet engines and availability included that of Ehyaei et al. [22], in which a conventional exergy analysis of a turbojet with an afterburner was performed. Marley and Riggins [23] first applied the global control volume approach developed in Ref. [13] to a turbojet engine, whereas more recently, Abbas and Riggins [24] analyzed the entropy generation of a turbojet in both on- and off-design conditions: again, using the global control volume method.

The use of availability in the analysis of rockets, particularly launch systems, was sparsely documented in the literature. Riggins et al. [15] provided an initial and preliminary assessment of availability of the Saturn V stack across the operation of the first three stages using the heating value of propellant as the exergy baseline with the overall global availability balance rather than the actual thermochemical availability of the propellant. This issue is explored in more detail in the present work. Availability issues for chemical rockets versus airbreathers were also addressed in the same work. The most significant body of work in the area of availability as applied to rocket-based systems was recent work involving complete systems engineering for launch systems, which was led by Dr. Michael Watson at the NASA Marshall Space Flight Center and presented in various recent references, including Ref. [25–27]. Watson [28] provided exergy (availability) methodology based in part on the exhaust kinetic energy of the rocket as the exergy

baseline rather than the full thermochemical and kinetic energy availability of the stored propellant. This was done to relate more directly to conventional rocket analysis and design methodologies that directly incorporated the nozzle exit velocity; this allowed a comparative assessment of launch systems and a calculation of an exergetic efficiency, but it did not provide the fundamental baseline necessary for the assessment of energy availability increments (productive utilization and various losses) as developed in the present work. The effort described in the preceding references also incorporated the use of exergy in spaceflight as well as for launch systems. In Ref. [28], the flight of the Apollo 17 Saturn V stack through third-stage operation using actual flight and operational data was analyzed in order to produce a time history of exergetic efficiency through the defined mission.

The current work is an extension of the use of the global availability balance as previously derived in Refs. [13,16] and then applied using approximate methods in subsequent work [15] for rockets and, more extensively, in other works for hypersonic airbreathing vehicles. Specifically, the current work focuses on developing a comprehensive energy utilization methodology for single- and two-stage chemical rockets operating in the atmosphere; this methodology incorporates the overall fundamental thermochemical and kinetic energy availability of stored propellant. The actual thermochemical availability of propellant referenced to the changing ambient conditions for a rocket in flight is developed and analyzed; and it is used within the balance, both for end-of-mission quantification of energy utilization characteristics as well as for the time-dependent evolution of energy utilization throughout a mission. A case study of the flight

of the first two stages of the Apollo 11 stack using the energy availability methodology is provided.

The organization of subsequent sections of this paper is as follows: In the second section, a review of the general theory necessary for fully describing the energy utilization of rockets is presented. The third section develops the methodology for analyzing energy utilization for a single-stage rocket across a burn. The energy utilization balance that results is expressed in terms of the overall thermochemical and kinetic availability of propellant, losses, and the productive energy utilization actually realized through kinetic and potential energy changes of the rocket. The fourth section provides similar development for a two-stage rocket, with the resulting energy utilization including discarded mass effects. The fifth section describes the evolution of energy utilization across missions, i.e., it characterizes the time-dependent behavior of the energy utilization for both single- and two-stage rockets. The sixth section of this paper presents a discussion of the definition and calculation of the thermochemical availability of propellant at given altitude and tank conditions, for use in the global control volume availability balance. A case study of energy utilization for the flight of the first two stages of the Apollo 11 mission is presented in the seventh section. This case study uses detailed flight and trajectory information to present both the time history of energy utilization as well as the final energy utilization balance for this legacy mission. The final section provides a summary of the paper, including a review of the methodology developed and the results obtained for the case study.

# 2. ENERGY UTILIZATION FOR ROCKETS: GENERAL ANALYTICAL FORMULATION

This section reviews the fundamental laws that allow the description of the utilization of energy for aerospace vehicles in flight within the atmosphere. These laws are 1) the general equation of motion (Newton's Law) for a vehicle that, for a rocket, can be integrated in time in order to provide the generalized rocket equation; and 2) the availability or exergy balance for an aerospace vehicle that results from combining mass, momentum, energy, and entropy considerations across a global control volume that contains the vehicle. These two laws are combined and integrated in time to provide the mission-integrated availability balance, which then allows the rigorous assessment of losses and energy utilization.

## 2.1. GENERAL EQUATION OF MOTION AND RESULTING ROCKET EQUATION

The general equation of motion in the direction of flight for an aerospace vehicle in the atmosphere (without thrust vectoring) is written as follows (see Figure 1):

$$m_R \frac{dV}{dt} = \text{Thrust} - D - m_R \text{g} \sin\theta \tag{1}$$

$V$ is the flight velocity of the vehicle; $D$ is the (external) drag on the vehicle; $m_R$ is the mass of the vehicle at time $t$; and $\theta$ is the climb angle of the vehicle, measured from the horizontal.

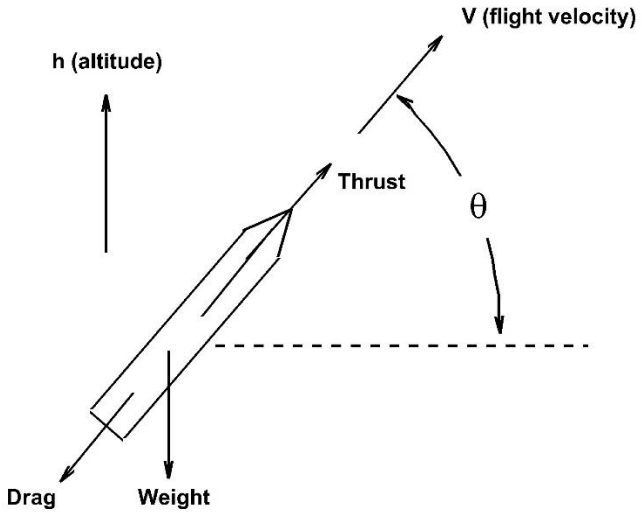


Figure 1. Rocket in flight in atmosphere.

For a rocket, the thrust is equal to $\dot{m}_P C$, where $C$ is defined as the effective exhaust velocity of the rocket. Note that the specific impulse $I_{sp}$ is equal to $C/\mathrm{g}_0$ and that $C$ is the actual velocity at nozzle exit only when the nozzle exhaust static pressure is exactly equal to the ambient pressure. Furthermore, by definition, $\dot{m}_P = -\frac{dm_R}{dt}$.

Integrating the equation of motion between initial $i$ and final $f$ states across a single stage burn for a rocket-powered vehicle, the following equation (the generalized rocket equation) is obtained:

$$\frac{V_f - V_i}{C} = ln\left(\frac{m_i}{m_i - m_P}\right) - \int_0^{\tau_b} \frac{\mathrm{g}\sin\theta}{C}\,dt - \int_0^{\tau_b} \frac{D}{m_R C}\,dt \qquad (2)$$

where $\tau_b$ is the firing (burn) time of the rocket (between initial $t = t_0 = 0$ and final $t = t_f$ states), and $m_P$ is the total mass of propellant expended during the firing. The initial rocket mass (at $t = 0$) is $m_i$.

## 2.2. FORCE-ENTROPY-AVAILABILITY BALANCE FOR VEHICLE IN ATMOSPHERIC FLIGHT

The balance between the aerospace vehicle net force power, the thermochemical and kinetic energy availability of propellant, and the overall entropy generation has been derived in detail and used extensively in previous work [13,16,17]. The balance is developed using a global control volume in which the vehicle is embedded, as depicted in a side view in Figure 2, resulting in the following relationship for a thermally balanced vehicle:

$$FV = \dot{m}_P \left( H^* + \frac{V^2}{2} \right) - T_\infty (\dot{S}_w - \dot{S}_\infty - \dot{S}_{P(tanks)}) \tag{3}$$

$FV$ is the net vehicle force power, where $F$ is the overall net fluid dynamic force component on the vehicle in the direction of flight and $V$ is the flight velocity. $F$ is (for negligible thrust vectoring angle) simply the conventional net (thrust–drag) force on a vehicle.

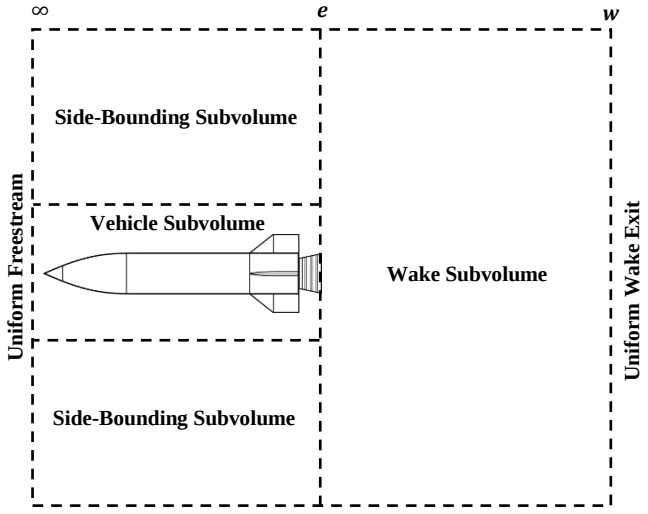


Figure 2. Global control volume for force and availability analysis of a vehicle in atmospheric flight.

Equation (3) is valid for a vehicle in any condition of general atmospheric flight (climbing, accelerating, etc.). If a vehicle has an overall nonzero (net) heat transfer to or from the fluid of the control volume (i.e., it is not thermally balanced), the relationship can be readily modified as discussed in Ref. [13].

The entropy flow rates in Eq. (3) are, respectively, referenced to the inflow plane $\infty$ of the global control volume, the actual equilibrated wake exit plane $w$ of the global control volume, and the entropy flow rate of propellant exiting the fuel/oxidizer tanks. Note that $\dot{m}_P$ is the mass flow rate of propellant (both fuel and oxidizer) and $H^* + (V^2/2)$ is the sum of the overall thermochemical energy availability and the kinetic energy per mass of the fuel and oxidizer in vehicle propellant tanks, referenced to the local atmospheric conditions at a given altitude (with ambient temperature, $T_\infty$). The quantity $H^* + (V^2/2)$ is, fundamentally, the maximum possible available work realizable per propellant mass that can be obtained by complete equilibration of stored propellant with the ambient environment; this quantity is called either exergy or availability. The exact definition of the thermochemical availability (or propellant exergy) $H^*$ and associated discussion will be given in a subsequent section of this paper.

The balance described by Eq. (3) is the direct analytical resultant of combining fundamental principles of continuity, fluid momentum and forces on the vehicle, energy (first law), and availability (second law) across the control volume. It is therefore, itself, as fundamental as these underlying principles. Note, however, that the global control volume must be taken large enough to ensure asymptotic convergence of the balance, as discussed in Ref. [13].

## 2.3. MISSION-INTEGRATED ENERGY UTILIZATION BALANCE FOR AEROSPACE VEHICLE

The energy utilization balance across a mission (from $t_i$ to $t_f$) for a general aerospace vehicle in atmospheric flight can be formally derived from combining Eq. (1) [or Eq. (2)] and Eq. (3) and then integrating across the time of a mission or mission segment in which the only mass drop is propellant expended (see Ref. [15]) to obtain

$$\left[\int H^* dm_P\right]_{\text{mission}} - \left[\int T_\infty dS_{\text{irr(total)}}\right]_{\text{mission}} = \Delta\left(m_R \frac{V^2}{2}\right) + \left[\int m_R \mathrm{g}\, dh\right]_{\text{mission}} \tag{4}$$

In Eq. (4),

$$\left[\int H^* dm_P\right]_{\text{mission}}$$

is the overall (mission-integrated) thermochemical availability of the propellant (available energy associated with the propellant) that is expended during the mission,

$$\Delta\left(m_R \frac{V^2}{2}\right)$$

is the overall change in kinetic energy of the vehicle during the mission,

$$\left[\int m_R \mathrm{g}\, dh\right]_{\text{mission}}$$

is the overall change in the geopotential energy of the vehicle during the mission, and

$$\left[\int T_\infty\, dS_{\text{irr(total)}}\right]_{\text{mission}}$$

is the overall loss associated with all entropy generation (including within the vehicle wake) during the mission.

The overall thermochemical availability term can, for convenience, be written (for subsequent analytical development within this work) in terms of a constant effective availability $H^*_{\text{eff}}$ as follows:

$$\left[\int H^* dm_P\right]_{\text{mission}} = H^*_{\text{eff}}\, m_P \tag{5}$$

Here, the value of $H^*_{\text{eff}}$ is simply chosen to mandate the equality. The formal definition of $H^*$ (and hence $H^*_{\text{eff}}$) for liquid propellant rockets operating within the atmosphere (to altitudes up to low Earth orbit) will be discussed in detail in a later section of this paper. Subsequently, comprehensive results for the availability characteristics of kerosene/oxygen and hydrogen/oxygen stages of a representative historical access-to-space system (Saturn V) will also be provided in the case study presented in the results.

Using the definition of $H^*_{\text{eff}}$, Eq. (4) is rearranged to identify the overall loss term as follows:

$$\begin{aligned}&\left[\int T_\infty\, dS_{\text{irr(total)}}\right]_{\text{mission}} \\ &= H^*_{\text{eff}}\, m_P - \left[(m_i - m_P)\frac{V_f^2}{2} - m_i\frac{V_i^2}{2}\right] - \left[\int m_R \text{g}\, dh\right]_{\text{mission}}\end{aligned} \tag{6}$$

## 3. ENERGY UTILIZATION ANALYSIS FOR A SINGLE-STAGE ROCKET

The previous section developed the fundamental characterization necessary for the assessment of energy utilization for a general mission of a general aerospace vehicle and defined an effective thermochemical availability for mission-integrated analysis. This section provides elaboration of that balance of energy utilization from the standpoint of a

defined mission for a single-stage rocket with no discard of mass (other than burned propellant). For purposes of discussion, it is assumed that the rocket is accelerating and climbing during the propellant burn, although the analysis is completely general.

From Eq. (4), the overall mission-integrated available thermochemical energy associated with stored propellant in vehicle tanks is written as the sum of the loss term, the kinetic energy term, and the geopotential energy term or

$$H^*_{\text{eff}}\, m_P = \left[\int T_\infty\, dS_{\text{irr(total)}}\right]_{\text{burn}} + \Delta\left(m_R \frac{V^2}{2}\right) + \left[\int m_R \text{g}\, dh\right]_{\text{burn}} \tag{7}$$

Equivalently,

$$\begin{aligned} &H^*_{\text{eff}}\, m_P \\ &= \left[\int T_\infty\, dS_{\text{irr(total)}}\right]_{\text{burn}} + \left[(m_i - m_P)\frac{V_f^2}{2} - m_i \frac{V_i^2}{2}\right] + \left[\int m_R \text{g}\, dh\right]_{\text{burn}} \end{aligned} \tag{8}$$

The productive metric in terms of energy utilization for a rocket across a single-stage burn is, by definition, the summation of the kinetic and potential energy changes achieved during the burn by the final vehicle mass (i.e., the final mass of the vehicle after all propellant is expended). This summation thus represents the productive energy utilization during the burn. Note that the last two terms in Eq. (8) include these productive kinetic and potential energy terms, but they also include loss contributions associated with kinetic and potential energy changes imparted to propellant before it exhausts from the vehicle. Therefore, the productive energy utilization must be correctly parsed from these terms.

Specifically, the productive energy utilization (where $m_i - m_P = m_f$), designated here as $\phi$, is defined as follows:

$$\phi = m_f \frac{V_f^2}{2} - m_f \frac{V_i^2}{2} + m_f \mathrm{g}(h_f - h_i) \tag{9}$$

where $\phi$ describes the absolute change (from beginning to end of the burn) in the kinetic and geopotential energy of the final vehicle (i.e., the vehicle with mass $m_f$) at the end of the burn. It is this quantity that represents the productive utilization of energy in the mission. Hence, it will be desirable (in general) to maximize $\phi$, i.e., to maximize the sum of the kinetic and potential energy changes experienced by the final vehicle across the mission (here, a single-stage burn).

Equation (8) is then rewritten in terms of $\phi$:

$$\begin{aligned} & H_{\mathrm{eff}}^* \, m_P \\ & = \left[\int T_\infty \, dS_{\mathrm{irr(total)}}\right]_{\mathrm{burn}} + \phi - m_P \frac{V_i^2}{2} + \left[\int m_R \mathrm{g} \, dh\right]_{\mathrm{burn}} \\ & - (m_i - m_P)\mathrm{g}(h_f - h_i) \end{aligned} \tag{10}$$

Rearranging Eq. (10), the following representation of the energy utilization balance is obtained:

$$\begin{aligned} & m_P \left(H_{\mathrm{eff}}^* + \frac{V_i^2}{2}\right) \\ & = \phi + \left[\int T_\infty \, dS_{\mathrm{irr(total)}}\right]_{\mathrm{burn}} + \left\{\left[\int m_R \mathrm{g} \, dh\right]_{\mathrm{burn}} - (m_i - m_P)\mathrm{g}(h_f - h_i)\right\} \end{aligned} \tag{11}$$

Equation (11) describes the fundamental energy utilization balance across the burn for a single-stage rocket. Specifically, this balance states that the total available energy associated with the propellant (both thermochemical and the initial kinetic energy) is equal to the sum of 1) the productive energy utilization associated with the increase in kinetic and potential energies of the final rocket mass during the burn, 2) the energy expended due

to losses associated with irreversibility (internal and external to the vehicle, including losses associated with wake entropy generation), and 3) the work done in lifting expended propellant to altitude. As noted earlier, the third term (work done in lifting expended propellant to the altitude at which it is exhausted from the vehicle) is a realized loss that must be tracked, although it is not associated with entropy generation. It is also important to realize that the second term (that term associated with irreversibility) necessarily includes the energy that must be used to increase the kinetic energy of onboard propellant mass before it is expended (because, for an accelerator, the vehicle is increasing its flight velocity). This particular energy utilization contribution is ultimately associated with irreversibility (and hence is properly represented within the second term) because wake dissipative processes eventually completely attenuate the velocity of the expelled propellant.

For optimization in terms of the utilization of the total thermochemical and kinetic energy of stored propellant, it is therefore necessary to maximize $\phi$. Equation (11) shows that maximizing $\phi$ is equivalent to minimizing the sum of 1) losses associated with all irreversibilities during the burn and 2) the work performed in the lifting of expended propellant.

## 4. ENERGY UTILIZATION ANALYSIS FOR A TWO-STAGE ROCKET

The methodology developed for a rocket single stage in the previous sections can be readily extended to the analysis of energy utilization for multiple-stage systems. A multiple-stage system is characterized by the discard of structural mass at the time(s) of

staging. For convenience, the following methodology is specifically developed for a two-stage rocket. This methodology can be directly extended for staged systems with more than two stages.

In the following analysis, $V_s$ denotes the staging velocity at which the two-stage rocket transitions between stage 1 and stage 2; specifically, at this velocity, the rocket discards stage 1 "discard (structural) mass," here for simplicity assumed to occur "instantaneously" at the time of stage 1 burnout. At the end of the considered two-stage mission (for present purposes), stage 2 burnout is similarly followed by the instantaneous discard of stage 2 discard (structural) mass, thus resulting in the final rocket mass. The complete loss of kinetic and potential energies associated with discard masses must therefore be accounted for in a multiple-stage analysis; however, the form of the energy utilization balance during each individual stage burn exactly reflects the balance developed previously for the individual (single) stage.

Using Eq. (4), which provides the formulation of the time-integrated energy utilization balance across a burn for a single stage, the following is written for the first-stage burn of a two-stage system:

$$\begin{aligned} & H^*_{\mathrm{eff},1} m_{P1} - \left[\int T_\infty dS_{\mathrm{irr(total)}}\right]_{\text{stage 1}} \\ & = (m_i - m_{P1})\frac{V_s^2}{2} - m_i \frac{V_i^2}{2} + \left[\int m_R \mathrm{g}\, dh\right]_{\text{stage 1}} \end{aligned} \tag{12}$$

Note that this balance applies only during the first-stage burn in which propellant is being used; it does not incorporate mass discard during staging, which must be accounted for separately. Define the mass of the rocket after stage-1 discard (i.e., the "initial" mass for stage-2 burn) as $m_{\text{stage}}$, such that

$$m_{\text{stage}} = m_i - m_{P1} - m_{\text{discard}(1)} \tag{13}$$

Therefore,

$$\begin{aligned} &H^*_{\text{eff},1} m_{P1} - \left[\int T_\infty dS_{\text{irr(total)}}\right]_{\text{stage 1}} \\ &= m_{\text{stage}} \frac{V_s^2}{2} - m_i \frac{V_i^2}{2} + m_{\text{discard}(1)} \frac{V_s^2}{2} + \left[\int m_R \text{g}\, dh\right]_{\text{stage 1}} \end{aligned} \tag{14}$$

Using the same approach, the stage 2 energy utilization balance across the stage-2 burn is written:

$$\begin{aligned} &H^*_{\text{eff},2} m_{P2} - \left[\int T_\infty dS_{\text{irr(total)}}\right]_{\text{stage 2}} \\ &= (m_{\text{stage}} - m_{P2} - m_{\text{discard}(2)}) \frac{V_f^2}{2} - m_{\text{stage}} \frac{V_s^2}{2} + m_{\text{discard}(2)} \frac{V_f^2}{2} \\ &+ \left[\int m_R \text{g}\, dh\right]_{\text{stage 2}} \end{aligned} \tag{15}$$

The productive energy utilization $\phi$ for the two-stage system is again the sum of the kinetic and geopotential energy changes achieved by the final rocket mass after second-stage burnout and the subsequent mass discard (i.e., the mass of the rocket excluding all burned/expended propellant and structural mass discarded during the mission). This specific summation then necessarily represents the productive utilization of energy achieved during a two-stage mission. Therefore, the definition of $\phi$ given in Eq. (5) is now based on the final mass, velocity, and altitude achieved after second-stage burnout and mass discard such that $m_f = m_{\text{stage}} - m_{P2} - m_{\text{discard}(2)}$.

Hence,

$$\phi$$

$$= \left(m_{\text{stage}} - m_{P2} - m_{\text{discard}(2)}\right)\frac{V_f^2}{2} - \left(m_{\text{stage}} - m_{P2} - m_{\text{discard}(2)}\right)\frac{V_i^2}{2} \quad (16)$$

$$+ \left(m_{\text{stage}} - m_{P2} - m_{\text{discard}(2)}\right)\mathrm{g}(h_f - h_i)$$

Note that

$$m_i \frac{V_i^2}{2}$$

$$= \left(m_{\text{stage}} - m_{P2} - m_{\text{discard}(2)}\right)\frac{V_i^2}{2} \quad (17)$$

$$+ \left(m_{P1} + m_{\text{discard}(1)} + m_{P2} + m_{\text{discard}(2)}\right)\frac{V_i^2}{2}$$

Substituting Eq. (17) into Eq. (14) and rearranging,

$$-\left(m_{\text{stage}} - m_{P2} - m_{\text{discard}(2)}\right)\frac{V_i^2}{2}$$

$$= H^*_{\text{eff},1} m_{P1} - \left[\int T_\infty dS_{\text{irr(total)}}\right]_{\text{stage 1}} - m_{\text{stage}}\frac{V_s^2}{2} - m_{\text{discard}(1)}\frac{V_s^2}{2} \quad (18)$$

$$- \left[\int m_R \mathrm{g}\, dh\right]_{\text{stage 1}} + \left(m_{P1} + m_{\text{discard}(1)} + m_{P2} + m_{\text{discard}(2)}\right)\frac{V_i^2}{2}$$

Rearranging Eq. (15),

$$\left(m_{\text{stage}} - m_{P2} - m_{\text{discard}(2)}\right)\frac{V_f^2}{2}$$

$$= H^*_{\text{eff},2} m_{P2} - \left[\int T_\infty dS_{\text{irr(total)}}\right]_{\text{stage 2}} + m_{\text{stage}}\frac{V_s^2}{2} - m_{\text{discard}(2)}\frac{V_f^2}{2} \quad (19)$$

$$- \left[\int m_R \mathrm{g}\, dh\right]_{\text{stage 2}}$$

Using Eqs. (18) and (19) in Eq. (16), $\phi$ is then written as

$$\begin{aligned}\phi &= H^*_{\text{eff},1} m_{P1} - \left[\int T_\infty dS_{\text{irr(total)}}\right]_{\text{stage 1}} + H^*_{\text{eff},2} m_{P2} - \left[\int T_\infty dS_{\text{irr(total)}}\right]_{\text{stage 2}} \\ &- m_{\text{discard(1)}} \frac{V_s^2}{2} - m_{\text{discard(2)}} \frac{V_f^2}{2} - \left[\int m_R \text{g}\, dh\right]_{\text{stage 1}} - \left[\int m_R \text{g}\, dh\right]_{\text{stage 2}} \\ &+ \left(m_{P1} + m_{\text{discard(1)}} + m_{P2} + m_{\text{discard(2)}}\right)\frac{V_i^2}{2} \\ &+ (m_{\text{stage}} - m_{P2} - m_{\text{discard(2)}})\text{g}(h_f - h_i)\end{aligned} \tag{20}$$

Because $h_f - h_i = \left(h_f - h_s\right) + (h_s - h_i)$,

$$\begin{aligned}\phi &= \left(H^*_{\text{eff},1} + \frac{V_i^2}{2}\right) m_{P1} - \left[\int T_\infty dS_{\text{irr(total)}}\right]_{\text{stage 1}} + \left(H^*_{\text{eff},2} + \frac{V_i^2}{2}\right) m_{P2} \\ &- \left[\int T_\infty dS_{\text{irr(total)}}\right]_{\text{stage 2}} - m_{\text{discard(1)}}\left(\frac{V_s^2}{2} - \frac{V_i^2}{2}\right) - m_{\text{discard(2)}}\left(\frac{V_f^2}{2} - \frac{V_i^2}{2}\right) \\ &- \left\{\left[\int m_R \text{g}\, dh\right]_{\text{stage 1}} - \left(m_{\text{stage}} - m_{P2} - m_{\text{discard(2)}}\right)\text{g}(h_s - h_i)\right\} \\ &- \left\{\left[\int m_R \text{g}\, dh\right]_{\text{stage 2}} - \left(m_{\text{stage}} - m_{P2} - m_{\text{discard(2)}}\right)\text{g}(h_f - h_s)\right\}\end{aligned} \tag{21}$$

The following relationship [Eq. (22)] is then obtained by rearranging Eq. (21) such that the total mission-integrated available energy associated with both stage-1 and stage-2 stored propellants (both thermochemical and kinetic energies) is moved to the left-hand side. This quantity is equal to the summation of the productive energy utilization $\phi$ and all losses, i.e., losses associated with entropy generation as well as the losses associated with lifting of both burned propellant and discarded structural/nonpropellant mass:

$$\left(H^*_{\text{eff},1}+\frac{V_i^2}{2}\right)m_{P1}+\left(H^*_{\text{eff},2}+\frac{V_i^2}{2}\right)m_{P2}$$

$$=\left[\int T_\infty dS_{\text{irr(total)}}\right]_{\text{stage 1}}+\left[\int T_\infty dS_{\text{irr(total)}}\right]_{\text{stage 2}}$$

$$+m_{\text{discard(1)}}\left(\frac{V_s^2}{2}-\frac{V_i^2}{2}\right)+m_{\text{discard(2)}}\left(\frac{V_f^2}{2}-\frac{V_i^2}{2}\right) \tag{22}$$

$$+\left\{\left[\int m_R \text{g}\, dh\right]_{\text{stage 1}}-\left(m_{\text{stage}}-m_{P2}-m_{\text{discard(2)}}\right)\text{g}(h_s-h_i)\right\}$$

$$+\left\{\left[\int m_R \text{g}\, dh\right]_{\text{stage 2}}-\left(m_{\text{stage}}-m_{P2}-m_{\text{discard(2)}}\right)\text{g}(h_f-h_s)\right\}+\phi$$

Optimization in terms of energy utilization for the two-stage system described in Eq. (22) mandates maximizing $\phi$.

Denote the total mission-integrated available energy associated with both stage-1 and stage-2 stored propellants as $E_{\text{AV}}$ such that

$$E_{\text{AV}}=\left(H^*_{\text{eff},1}+\frac{V_i^2}{2}\right)m_{P1}+\left(H^*_{\text{eff},2}+\frac{V_i^2}{2}\right)m_{P2}$$

Equation (22) can be further reorganized in order to separate individual loss terms associated with geopotential energy changes:

$$
\begin{aligned}
&E_{\mathrm{AV}} \\
&= \left[\int T_\infty dS_{\mathrm{irr(total)}}\right]_{\text{stage 1}} + \left[\int T_\infty dS_{\mathrm{irr(total)}}\right]_{\text{stage 2}} \\
&+ m_{\mathrm{discard(1)}}\left(\frac{V_s^2}{2} - \frac{V_i^2}{2}\right) + m_{\mathrm{discard(2)}}\left(\frac{V_f^2}{2} - \frac{V_i^2}{2}\right) \\
&+ \left\{\left[\int m_R \mathrm{g}\, dh\right]_{\text{stage 1}} - (m_i - m_{P1} - m_{P2})\mathrm{g}(h_s - h_i)\right. \\
&\left. + \left(m_{\mathrm{discard(1)}} + m_{\mathrm{discard(2)}}\right)\mathrm{g}(h_s - h_i)\right\} \\
&+ \left\{\left[\int m_R \mathrm{g}\, dh\right]_{\text{stage 2}} - \left(m_i - m_{P1} - m_{P2} - m_{\mathrm{discard(1)}}\right)\mathrm{g}\left(h_f - h_s\right)\right. \\
&\left. + m_{\mathrm{discard(2)}}\mathrm{g}(h_f - h_s)\right\} + \phi
\end{aligned}
\tag{23}
$$

Finally, summarizing the energy utilization balance for the two-stage rocket as represented in Eq. (23),

$$E_{\mathrm{AV}} = L1 + L2 + L3 + L4 + L5 + L6 + L7 + L8 + \phi \tag{24}$$

Table 1 provides a detailed description of the terms in Eq. (24). However, in summary, the $L$ terms all represent various losses, either associated with irreversibility (terms $L1$ and $L2$), work done to lift propellant ($L5$ and $L7$), or staging losses ($L3$, $L4$, $L6$, $L8$). Note that $\phi$ is the productive energy utilization, whereas $E_{\mathrm{AV}}$ is the total mission-integrated available energy.

Table 1. Energy utilization balance summary for Eq. (24) terms.

| Term designator in Eq. (24) | Description of term | Analytical expression for term |
|---|---|---|
| $E_{\mathrm{AV}}$ | Overall mission-integrated energy availability (stages 1 and 2) | $\left(H^{*}_{\mathrm{eff},1}+\frac{V_i^2}{2}\right)m_{P1}+\left(H^{*}_{\mathrm{eff},2}+\frac{V_i^2}{2}\right)m_{P2}$ |
| $L1$ | Available energy used to overcome stage-1 irreversibility | $\left[\int T_\infty dS_{\mathrm{irr(total)}}\right]_{\mathrm{stage\ 1}}$ |
| $L2$ | Available energy used to overcome stage-2 irreversibility | $\left[\int T_\infty dS_{\mathrm{irr(total)}}\right]_{\mathrm{stage\ 2}}$ |
| $L3$ | Kinetic energy loss due to stage-1 discarded mass | $m_{\mathrm{discard(1)}}\left(\frac{V_s^2}{2}-\frac{V_i^2}{2}\right)$ |
| $L4$ | Kinetic energy loss due to stage-2 discarded mass | $m_{\mathrm{discard(2)}}\left(\frac{V_f^2}{2}-\frac{V_i^2}{2}\right)$ |
| $L5$ | Work done by stage 1 to lift propellant expended | $\left[\int m_R \mathrm{g}\, dh\right]_{\mathrm{stage\ 1}} - (m_i-m_{P1}-m_{P2})\mathrm{g}(h_s-h_i)$ |
| $L6$ | Work done by stage 1 to lift discarded mass | $(m_{\mathrm{discard(1)}}+m_{\mathrm{discard(2)}})\mathrm{g}(h_s-h_i)$ |
| $L7$ | Work done by stage 2 to lift propellant expended | $\left[\int m_R \mathrm{g}\, dh\right]_{\mathrm{stage\ 2}} - (m_i-m_{P1}-m_{P2}-m_{\mathrm{discard(1)}})\mathrm{g}(h_f-h_s)$ |
| $L8$ | Work done by stage 2 to lift discarded mass | $m_{\mathrm{discard(2)}}\mathrm{g}(h_f-h_s)$ |
| $\phi$ | Productive energy utilization (change in kinetic and potential energies of final mass of vehicle) | $m_{\mathrm{final}}\left(\frac{V_f^2}{2}-\frac{V_i^2}{2}\right)+m_{\mathrm{final}}\mathrm{g}(h_f-h_i)$ $(m_{\mathrm{final}}=m_{\mathrm{stage}}-m_{P2}-m_{\mathrm{discard(2)}})$ |

In Eq. (24) and Table 1, $L1$ and $L2$ represent the energy usage due to all irreversibilities (internal and external to vehicle, including in the wake) associated with stage-1 and stage-2 operations, respectively. Specifically [see Eqs. (12) and (15)], these terms are given by the following:

$$\left[\int T_\infty dS_{\text{irr(total)}}\right]_{\text{stage 1}} = H^*_{\text{eff},1} m_{P1} - (m_i - m_{P1})\frac{V_s^2}{2} + m_i \frac{V_i^2}{2} - \left[\int m_R \text{g}\, dh\right]_{\text{stage 1}}$$

$$\left[\int T_\infty dS_{\text{irr(total)}}\right]_{\text{stage 2}}$$

$$= H^*_{\text{eff},2} m_{P2} - \left(m_{\text{stage}} - m_{P2}\right)\frac{V_f^2}{2} + m_{\text{stage}} \frac{V_s^2}{2} - \left[\int m_R \text{g}\, dh\right]_{\text{stage 2}}$$

## 5. TIME EVOLUTION ANALYSIS OF ENERGY UTILIZATION ACROSS A MISSION

A given rocket mission has an overall mission-integrated available energy (both thermochemical and initial kinetic energy) associated with all propellant expelled during the mission; this is represented by the left-hand side of 1) Eq. (11) for a rocket single stage and 2) Eq. (24) for a two-stage rocket. The analysis thus far has considered only the energy utilization over the complete (overall) mission, i.e., providing the various contributions to energy utilization at the end of the burn; at which point, all availability associated with expended propellant has been completely used. (Specifically, this availability is used to effect productive kinetic and potential energy changes of the final mass of the vehicle, or it is used in overcoming various losses as previously described.) It is also useful to describe

the evolution of the various energy utilization terms as the mission progresses over time; this is described in the current section.

## 5.1. SINGLE-STAGE ROCKET TIME EVOLUTION OF ENERGY UTILIZATION

First, consider the time evolution of the energy utilization for a single-stage rocket stage in an accelerating climb without discard of mass (other than propellant burned), i.e., consider the character of the various energy utilization terms as the burn progresses. Over time, losses associated with both irreversibilities and work done to lift expended propellant both increase (these terms, respectively, are the second and third terms on the right-hand side of Eq. (11) across the entire burn). In addition, as time increases, the instantaneous productive energy utilization $\phi(t)$ (the change in the kinetic and potential energies of the final rocket mass from the initial state conditions to the time of interest) also changes; this term progressively and monotonically increases for an accelerating climb, although the analysis is valid for any mission, whether or not accelerating and/or climbing.

The required balance for energy utilization at any time during the mission dictates that the actual available energy remaining in stored fuel is progressively decreasing with time, ranging from the total (mission-integrated) available energy (at beginning of burn, or at time = 0) to zero (at the end of the burn).

Define this time-dependent (remaining) available energy as $\beta(t)$. The instantaneous (transient) energy utilization balance at any time $t$ during the burn is then written as follows:

$$m_{P(\text{total})}\left(H_{\text{eff}}^{*}+\frac{V_i^2}{2}\right)$$

$$=\phi(t)+\left[\int T_\infty dS_{\text{irr(total)}}\right]_{\text{from } t=0 \text{ to } t} \tag{25}$$

$$+\left\{\left[\int m_R \text{g}\, dh\right]_{\text{from } t=0 \text{ to } t}-m_{\text{final}}\text{g}(h(t)-h_i)\right\}+\beta(i)$$

This formulation therefore allows the energy utilization to be "tracked" in time.

Care must be taken with the individual terms. For instance, the entropy generation term for use in Eq. (25) is found from

$$\left[\int T_\infty dS_{\text{irr(total)}}\right]_{\text{from } t=0 \text{ to } t}$$

$$=H_{\text{eff}}^{*}\big(m_i-m_R(t)\big)-\left[m_R(t)\frac{V(t)^2}{2}-m_i\frac{V_i^2}{2}\right]-\left[\int m_R \text{g}\, dh\right]_{\text{from } t=0 \text{ to } t} \tag{26}$$

Furthermore, in Eq. (25),

$$\phi(t)=m_{\text{final}}\left(\frac{V(t)^2}{2}-\frac{V_i^2}{2}\right)+m_{\text{final}}\text{g}(h(t)-h_i) \tag{27}$$

## 5.2. TWO-STAGE ROCKET TIME EVOLUTION OF ENERGY UTILIZATION

For a two-stage system, the kinetic and potential energy loss terms involving discarded structural masses are considered here to be instantaneous events, occurring first at first-stage burnout and then at second-stage burnout (mission end for present work). Hence, $\beta$ drops discontinuously at staging times.

The same eight contributions to losses as described in Eq. (24) for the two-stage system over the complete mission can be used in a time evolution analysis such that

$$\left(H^*_{\text{eff},1} + \frac{V_i^2}{2}\right) m_{P1} + \left(H^*_{\text{eff},2} + \frac{V_i^2}{2}\right) m_{P2} = E_{\text{AV}}$$
$$= L1(t) + L2(t) + L3(t) + L4(t) + L5(t) + L6(t) + L7(t) + L8(t) \quad (28)$$
$$+ \phi(t) + \beta(t)$$

For all $t$,

$$\phi(t) = m_{\text{final}} \left(\frac{V(t)^2}{2} - \frac{V_i^2}{2}\right) + m_{\text{final}} \text{g}(h(t) - h_i) \quad (29)$$

Progressive losses $L1$ through $L8$ are quantified over the time of flight using the following time evolution:

From $t$ = 0 to $t_{\text{stage}}$,

$$L1(t) = \left[\int T_\infty dS_{\text{irr(total)}}\right]_{\text{stage 1}} (t)$$

$$= H^*_{\text{eff},1}\big(m_i - m_R(t)\big) - \left[m_R(t)\frac{V(t)^2}{2} - m_i\frac{V_i^2}{2}\right] - \left[\int m_R \text{g}\, dh\right](t)$$

$$L2(t) = L3(t) = L4(t) = L6(t) = L7(t) = L8(t) = 0$$

$$L5(t) = \left[\int m_R \text{g}\, dh\right](t) - (m_i - m_{P1} - m_{P2})\text{g}(h(t) - h_i)$$

At $t = t_{\text{stage}}$,

$$L3\big(t = t_{\text{stage}}\big) = m_{\text{discard(1)}} \left(\frac{V_s^2}{2} - \frac{V_i^2}{2}\right)$$

$$L6\big(t = t_{\text{stage}}\big) = \big(m_{\text{discard(1)}} + m_{\text{discard(2)}}\big)\text{g}(h_s - h_i)$$

From $t = t_{\text{stage}}$ to $t = t_{\text{final}}$

$$L1(t) = \text{constant} = L1(t = t_{\text{stage}})$$

$$L5(t) = \text{constant} = L5(t = t_{\text{stage}})$$

$$L3(t) = \text{constant} = L3(t = t_{\text{stage}})$$

$$L6(t) = \text{constant} = L6(t = t_{\text{stage}})$$

$$L4(t) = L8(t) = 0$$

$$L2(t) = \left[\int T_{\infty} dS_{\text{irr(total)}}\right]_{\text{stage 2}}(t)$$

$$= H^{*}_{\text{eff,2}}\left(m_{\text{stage}} - m_R(t)\right) - \left[m_R(t)\frac{V(t)^2}{2} - m_{\text{stage}}\frac{V_s^2}{2}\right] - \left[\int m_R \text{g}\, dh\right](t)$$

$$L7(t) = \left[\int m_R \text{g}\, dh\right](t) - \left(m_i - m_{P1} - m_{P2} - m_{\text{discard(1)}}\right)\text{g}(h(t) - h_s)$$

At $t = t_{\text{final}}$,

$$L4(t) = m_{\text{discard(2)}}\left(\frac{V_f^2}{2} - \frac{V_i^2}{2}\right)$$

$$L8(t) = m_{\text{discard(2)}}\text{g}\left(h_f - h_i\right)$$

Note that $\phi$ must, by definition, exactly equal the total initially available energy minus the sum of all losses (losses represented by $L1$ through $L8$) at the end of mission, where $\beta$ = 0, i.e., after second-stage burnout and structural mass discard.

## 6. ANALYSIS AND CALCULATION OF PROPELLANT AVAILABILITY OF ATMOSPHERIC CHEMICAL ROCKETS

To correctly analyze energy utilization for rockets using the methodology described in the previous sections, it is necessary to quantitatively describe and compute the overall thermochemical availability $H^*$ for the propellant stored in the vehicle propellant tanks [see Eqs. (3) and (4)]. As noted earlier, the overall (time-integrated) mission-integrated availability of the propellant [appearing in Eq. (4)] is then used to usefully define a constant

effective availability $H^*_{\text{eff}}$ [see Eq. (5)]. Riggins et al. [13] derived the expression for $H^*$ from global control volume considerations for a vehicle in flight in the atmosphere; this development used the global control volume shown in Figure 2. The global control volume must be defined to envelope a very large domain extending from upstream of the vehicle (at station ∞) to a far downstream plane (station $w$), where the wake from the vehicle may be assumed to be equilibrated with the surroundings. To correctly derive the relationship between propellant availability and vehicle performance, the domain must also extend laterally to very large distances.

In terms of the development of Eq. (3), the thermochemical availability associated with propellant (fuel and oxidizer) at a given altitude and flight velocity is derived as the following:

$$\begin{aligned} &\dot{m}_P H^* \\ &= \dot{m}_{\text{fuel}}\left(h_{\text{fuel(tank)}} - T_\infty s_{\text{fuel(tank)}}\right) \\ &+ \dot{m}_{\text{oxidizer}}\left(h_{\text{oxidizer(tank)}} - T_\infty s_{\text{oxidizer(tank)}}\right) \\ &+ \dot{m}_{\infty\text{(global c.v.)}}\left(h_{\infty\text{(global c.v.)}} - T_\infty s_{\infty\text{(global c.v.)}}\right) \\ &- \dot{m}_{w\text{(global c.v.)}}\left(h_{w\text{(global c.v.)}} - T_\infty s_{w\text{(global c.v.)}}\right) \end{aligned} \tag{30}$$

In this equation, the mixture enthalpy per mass $h$ and entropy per mass $s$ of the air entering the global control volume (at station ∞ of the global control volume) are evaluated at the ambient atmospheric temperature and pressure. The enthalpy per mass and entropy per mass at exit station $w$ of the global control volume in Eq. (30) are also evaluated at the ambient atmospheric temperature and pressure. However, these terms must be assessed with the proper reacted mixture species mass and mole fractions at the wake exit plane

associated with complete mixing and equilibrium chemistry. Similarly, the fuel and oxidizer contributions in terms of both enthalpy and entropy (per unit mass) are evaluated at their respective tank temperatures and pressures. Although (as shown and discussed in Ref. [13]), in principle, the global control volume must be made infinitely large to yield an exact limiting analysis relating vehicle performance and entropy production and availability, in practice, there is asymptotic convergence to values of interest (vehicle performance, wake subvolume entropy production, and thermochemical availability) using large but finite control volume dimensions.

From the standpoint of the overall global control volume, the mixture ratio (available oxygen to fuel) in the overall system is inherently extremely fuel lean, regardless of whether the mixture ratio in the engine is fuel rich or lean. The product species of combustion at the wake exit are represented by infinitesimal mass fractions compared to the mass fractions associated with air composition at a given altitude (generally diatomic nitrogen; diatomic oxygen; and for altitudes above 100 km, monatomic oxygen).

The magnitude of the thermochemical availability of the propellant as expressed in Eq. (30) can be compared to the lower heating value of propellant. The heating value is most often expressed in terms of the standard heating value of fuel, i.e., per unit mass of fuel $H_f$. For energy utilization methodology as developed in this work, however, the heating value is more usefully characterized per unit mass of propellant (fuel and oxidizer), which is here designated as $H_P$. This quantity provides a direct comparison with the propellant availability $H^*$ as derived in the preceding sections. The relationship between the heating value per mass of fuel $H_f$ and the heating value per mass of propellant (fuel and oxidizer) $H_P$ is given as follows:

$$H_P = \left[\frac{1}{R+1}\right] H_f \tag{31}$$

Here, $R$ is the engine mixture ratio for the onboard propellant, i.e., the ratio of the mass flow rate of oxidizer to the mass flow rate of fuel in the engine. For hydrogen fuel at a standard temperature and pressure, the approximate lower heating value per mass of fuel is $H_f$ ($H_2$) = $1.2 \times 10^8$ J/kg (fuel) [29]. For typical kerosene-based fuels (such as RP-1) at standard conditions, the lower heating value per mass of fuel is $H_f$ (hydrocarbon), which is approximately $4.45 \times 10^7$ J/kg (fuel) [29].

The exact relationship between the thermochemical availability $H^*$ and $H_P$ is given in detail in Ref. [13]. However, to an approximation (i.e., depending on tank and ambient conditions), the thermochemical availability often lies between the lower and upper heating values (see Refs. [13,30,31]). This is particularly true for fuels (hydrogen and hydrocarbon fuel) at low ambient temperatures (lower altitudes), where $H^*$ is typically only a few percent different than $H_P$, as shown in [13].

The heating value per unit mass of propellant using ambient conditions can be formally derived from considerations of the global control volume (see Ref. [13] for more detail) as follows:

$$\begin{aligned} &\dot{m}_P H_P \\ &= \dot{m}_{\text{fuel}} h_{\text{fuel at } T_\infty} + \dot{m}_{\text{oxidizer}} h_{\text{oxidizer at } T_\infty} + \dot{m}_\infty h_{\infty(\text{global c.v.})} \\ &- \dot{m}_w h_{w(\text{global c.v.})} \end{aligned} \tag{32}$$

In general, the heating value of propellant per unit mass of propellant is a function of the fuel and oxidizer mass flow rates, the ambient temperature $T_\infty$, and the species mass fractions of the air entering the global control volume and at the wake exit plane.

# 7. RESULTS: CASE STUDY FOR ENERGY UTILIZATION FOR APOLLO 11

This section implements the formulations developed in this paper in order to analyze the energy utilization of a legacy Apollo access-to space system, with focus on the operation of the first two stages, from launch to second-stage burnout and mass discard. In this section, a preliminary discussion of the general (and nominal) characteristics of the propulsion system and flight history is first provided for context. The thermochemical availability term $H^*$ is then computed across the altitude range of the defined mission and used to define effective thermochemical availabilities $H^*_{\text{eff}}$ for both stage 1 and stage 2. These are used to assess quantitatively the details of the energy utilization throughout the mission.

## 7.1. GENERAL DESCRIPTION OF VEHICLE AND MISSION CHARACTERISTICS

The following information on the general vehicle and mission characteristics of the Apollo 11 mission can be readily extracted from the flight logs and summaries available for the Apollo 11 flight [32,33]. The thrust for the first stage of this system was provided by five Rocketdyne F-1 rocket engines. These engines used RP-1 (kerosene-based) fuel and oxygen as propellant. For this work, the liquid fuel in the tanks was approximated to have been at standard temperature and a pressure of slightly less than 2 atm during first-stage operation, whereas the (liquid) oxygen was held at 90 K and at a pressure of about 1.5 atm. The nominal oxygen to fuel ratio $R$ during the operation of the F-1 engines was 2.27. First-stage operation extended through 162 s from time of launch; at which time, the vehicle achieved an altitude of 66.5 km and an inertial flight velocity of around 2747 m/s.

Thrust for the second stage was provided by J-2 engines using hydrogen fuel and oxygen as propellant. The hydrogen tank conditions were 20 K and 2.5 atm (liquid fuel). Oxygen tank conditions were 90 K and 2.8 atm. The nominal mixture ratio $R$ during second-stage operation was 5.5. Second-stage burnout and mass discard occurred at approximately 550 s after launch; this represented the end of the defined mission for energy utilization for the present work.

## 7.2. COMPUTATION OF THERMOCHEMICAL AVAILABILITY $H^*$ FOR APOLLO MISSION

The atmospheric model described in [34] is used to generate atmospheric species mass fraction, density, and ambient temperature distributions versus altitude; modeled species are diatomic nitrogen (N2), diatomic oxygen (O2), argon, and atomic oxygen (O). The ambient temperature climbing rapidly above a 100 km altitude and reaches approximately 900 K at a 200 km altitude. Also, above a 100 km altitude, atomic oxygen begins to become significant. For all calculations of (gaseous) species enthalpies and entropies on both the inflow and the wake exit plane, the 2002 NASA Lewis Research Center curve fits [35] are used. For calculations of liquid fuel and oxidizer enthalpies and entropies in vehicle tanks, the NASA curve fits are supplemented using the extensive database provided by the National Institute of Standards and Technology [36]. In this work, $C_{12}H_{23}$ is used as a representative model of RP-1 due to the availability of curve fits and other thermochemical data. RP-1 is a complex kerosene blend but can be adequately represented in a simple one-dimensional analysis (particularly relevant to the present methodology) using long-chain hydrocarbons such as $C_{12}H_{23}$. For example, in this context,

Magee et al. [37] suggested that RP-1 could be represented for specific purposes by $C_{11.8}H_{23}$, whereas Wang [38] used $C_{12}H_{24}$ as a surrogate for RP-1.

Species compositions at the wake exit plane are computed in the present work using the simplifying assumption of complete reaction. Due to the relatively low temperature of the ambient air, complete reaction should adequately approximate the (actual) equilibrium composition in the wake for much of the trajectory. In terms of the very large global control volume that must be taken to obtain a converged value of $H^*$, the species composition at the wake exit plane is essentially very close to the air entering the global control volume. This is because the mass fractions of $CO_2$ and $H_2O$ (for stage 1) or $H_2O$ (for stage 2) necessarily become increasingly small as the control volume is enlarged. Nevertheless, as indicated, asymptotic convergence at very large cross-sectional areas of the global control volume is obtained for all values of interest, such as $H^*$ and $H_P$ (as well as thrust as computed from basic availability–performance relationships, as described in Ref. [13]).

Figure 3 provides the variation of the thermochemical availability of the fuel and oxidizer propellant $H^*$ versus altitude for the flight of the Apollo 11 vehicle from launch through second-stage burnout and discard. This quantity is computed using Eq. (30). $H^*$ versus altitude for the first-stage F-1 engine operation is fairly flat at around 15 MJ/kg (propellant) across the range of altitudes. For the initial operation of the second-stage J-2 engines after first-stage separation at around 166 s, $H^*$ is significantly larger than the $H^*$ value for the first stage, which is expected due to the hydrogen fuel. Specifically, immediately after first-stage separation, the $H^*$ for the J-2 engines is around 22 MJ/kg (propellant). It is somewhat flat with increasing altitude until an altitude of 100 km, when it begins to climb rapidly. Also shown for reference in Figure 3 is the heating value per

mass of propellant (based on sea level standard (STP) conditions rather than ambient conditions) for both stage 1 (RP-1 fuel at $R$ = 2.27) and stage 2 ($H_2$ fuel at $R$ = 5.5).

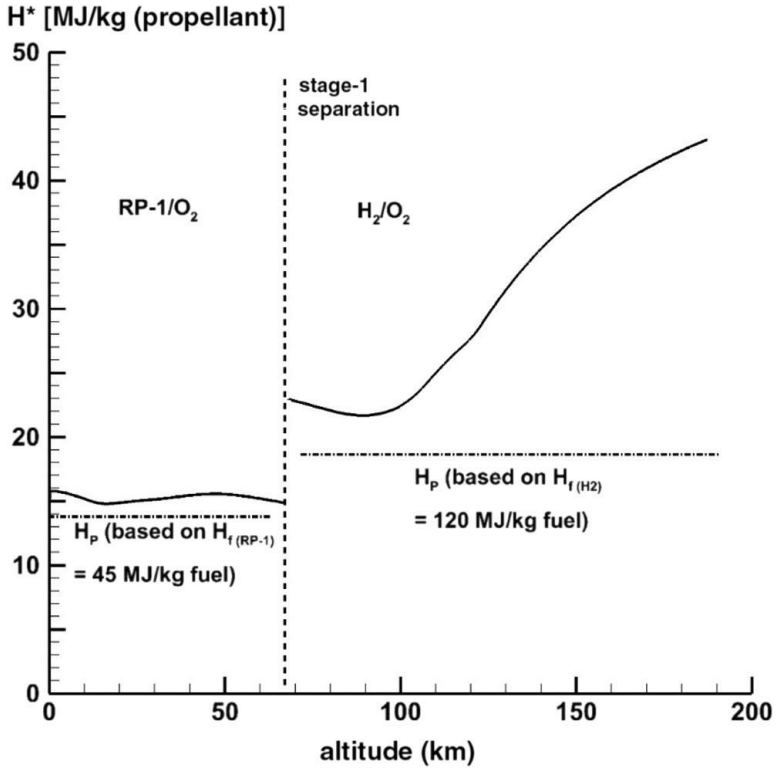


Figure 3. Thermochemical energy availability of propellant $H^*$ for Apollo first- and second-stage operations (also shown is $H_P$ based on $H_f$ evaluated at STP for stages 1 and 2).

Figure 4 shows the ratio of the thermochemical availability of the fuel and oxidizer $H^*$ to the lower heating value of the propellant $H_P$ (both quantities are based on the ambient conditions at altitude) across the altitude range. This ratio is approximately 1.15 for stage-1 operation (RP1-LOX) and 1.2 for stage-2 operation ($LH_2$-LOX) until a 100 km altitude; above that altitude, the ratio climbs significantly due to the increase in $H^*$.

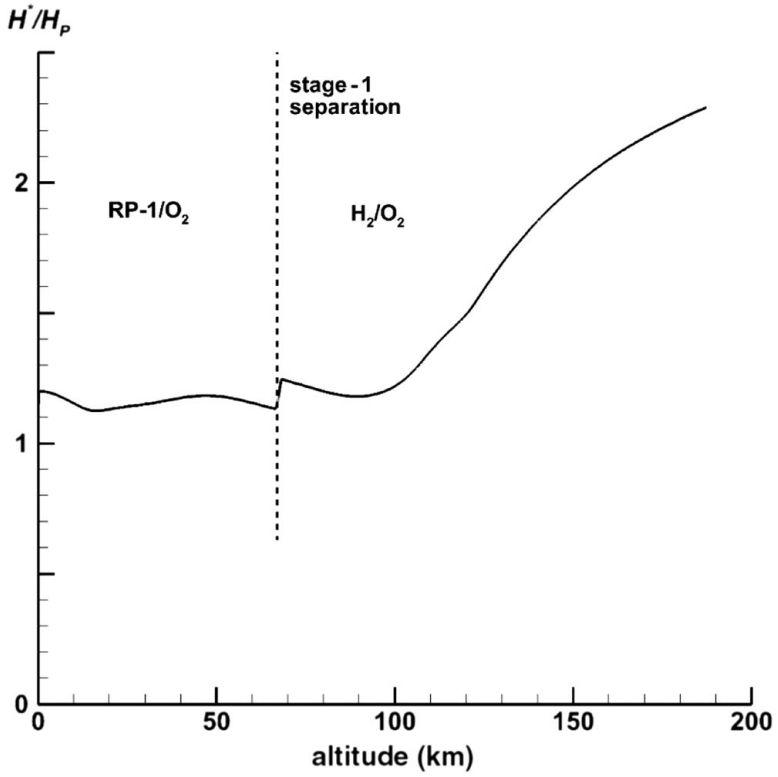


Figure 4. Ratio of thermochemical energy availability $H^*$ to heating value of propellant (per unit mass of propellant) $H_P$ for Apollo first- and second stage operations.

### 7.3. TIME-DEPENDENT ENERGY UTILIZATION OF THE APOLLO 11 STACK (STAGES 1 AND 2)

To perform the time-dependent energy utilization analysis developed in earlier sections and to quantify the various terms appearing in Eq. (28), the necessary mass, altitude, and velocity information are obtained from the flight logs and summaries available for the Apollo 11 flight [32,33]. Specifically, the information required includes the detailed time histories of the mass of the vehicle, the mass of propellant used, the velocity, and the altitude; this information is readily extracted and digitized from these databases. Using this vehicle and flight information and the altitude-dependent variation of the overall thermochemical energy availability $H^*$ developed and presented earlier in Figure 3, it is

now possible to evaluate all energy utilization terms appearing in Eq. (28). Note, however, that the development of the methodology is characterized using "effective" $H^*_{\text{eff}}$ for stage 1 and stage 2 that, when properly defined using Eq. (5), exactly represents the integrated $H^*$ behavior across a given stage operation. These values (for use in characterizing the Apollo 11 mission) are calculated as follows: $H^*_{\text{eff},1}$ = 15.375 MJ/kg (propellant), and $H^*_{\text{eff},2}$ = 36.298 MJ/kg (propellant). As discussed earlier, these quantities are defined per the mass of the propellant (i.e., both fuel and oxidizer).

Figure 5 provides the time history of the energy utilization for the Apollo 11 mission from launch to second-stage burnout and mass discard. Specifically, the mission productive energy utilization as defined by $\phi$ (the change in the kinetic energy and potential energy of the final mass of the vehicle) is based on the mass, altitude, and velocity of the vehicle subsequent to second-stage mass discard (at 550 s from launch). In conjunction with Figure 5, Table 2 provides a listing describing the final balance of energy availability at the end of the defined mission.

In Figure 5, the top horizontal line is the value of the total mission-integrated available thermochemical energy associated with the stored propellant in stage 1 and stage 2 at launch, or $E_{\text{AV}}$ (for this case, there is no initially available kinetic energy associated with stored propellant due to the zero initial velocity of the vehicle at launch). During the stage-1 burn (from time 0 to time ~162 s), this available energy is progressively used (decreased) via three mechanisms as shown in the figure. The first mechanism is that available energy usage associated with the thermochemical/fluid dynamic irreversibility losses within (stage 1) rocket motors, as well as in the flow external to the vehicle including in the vehicle wake. This mechanism corresponds to term $L1(t)$ within Eq. (28); see also

Eq. (24) for the end-of-mission balance in terms of the (final) time-integrated $L1$. Energy utilization associated with irreversibility involving the first-stage burn represents by far the largest contributor to energy utilization throughout the mission. The second mechanism contributing to progressive energy utilization during the first-stage burn is the work done to lift expended propellant to altitude [corresponding to term $L5$ in earlier sections; see Eqs. (28) and (24)]. As can be seen in Figure 5, both stage-1 energy utilization associated with thermochemical/fluid dynamic losses and stage-1 energy utilization due to lifting of expended propellant increase monotonically through stage-1 burn to their final values when stage-1 burn is complete at a time of ~162 s. For the rest of the mission [time of ~162 s to end of (defined) mission at time of ~550 s], there is then no further increase for either of these contributions to energy utilization.

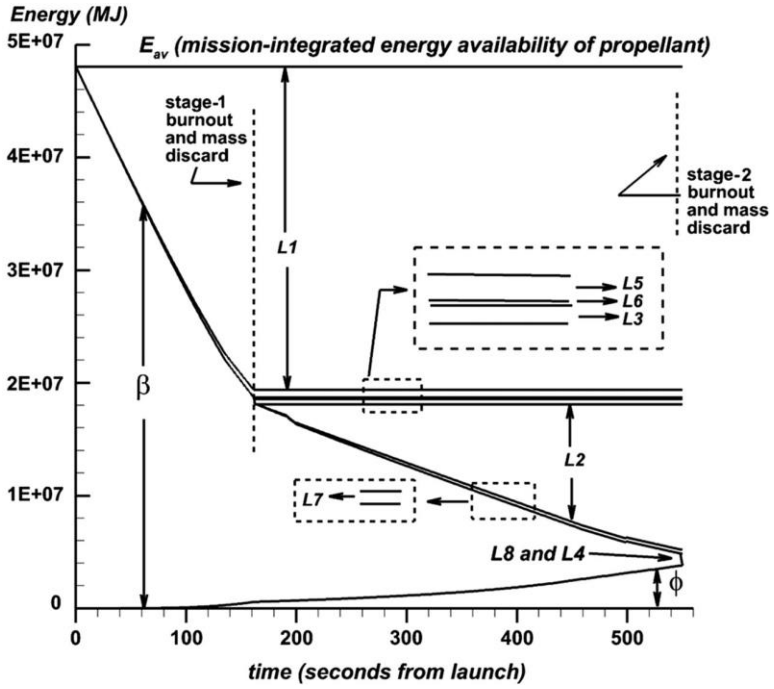


Figure 5. Saturn V stack energy utilization time history; $L$ denote losses, $\phi$ denotes productive energy utilization, and $\beta$ denotes remaining energy availability; see Table 2.

The third mechanism contributing to energy utilization during the first-stage burn is the progressively increasing (vehicle) productive energy utilization for the mission (specifically, as defined in this work, the kinetic and potential energy changes at any time $t$ during the mission experienced by the final mass of the vehicle). This contribution is denoted by $\phi(t)$ in Eq. (28) and is represented by the bottom (monotonically increasing) line in Figure 5. It increases very slowly at the beginning of the burn due to the low initial acceleration of the stack; as the vehicle mass drops and the acceleration and velocity increase, the rate of increase of $\phi$ with time begins to increase. Note that $\beta(t)$, which is the remaining available energy associated with unburned propellant [see Eq. (28)], is also shown in Figure 5, in which it is seen as the progressively decreasing increment between the (vehicle) productive energy utilization and the sum of all progressively mounting losses at a given time during the mission.

At the end of the first-stage burn, the structural mass associated with stage-1 expended propellant is discarded. The effect of this mass discard is that two instantaneous increments of energy utilization appear in Figure 5 at the time of staging ($t$ = 162 s). These increments represent the potential and kinetic energy, respectively, associated with the discarded mass; the thermochemical energy of the stored propellant is used to accelerate this discarded mass to the velocity and altitude at staging (from conditions at launch). Hence, the geopotential and kinetic energy of the discarded mass at staging are real losses in terms of reducing the productive energy utilization of the final vehicle mass. These two energy utilization contributions correspond in Eq. (28) to terms $L6$ (work done by stage 1 to lift discarded structural mass) and $L3$ (loss of kinetic energy due to discard of structural mass after stage 1 burnout). As can be seen in the Figure 5, work done by stage 1 to lift

discard mass (potential energy loss) is significantly smaller than the kinetic energy loss associated with that (discarded) mass.

Energy utilization time evolution during the second-stage burn (from $t$ = 162 s to end of defined mission at $t$ = 550 s) is similar in terms of contributions and trends as seen for the first-stage burn. Hence, the energy used due to stage-2 irreversibilities (term $L2$) and the work done by the second stage to lift expended propellant to altitude (term $L7$) are seen as progressively increasing increments during the second-stage burn. Additionally, at the end of the defined mission after stage-2 burnout (when all initially stored propellant in stage 1 and stage 2 have been used), two instantaneous additional energy utilization contributions associated with stage-2 discard mass kinetic energy (term $L4$) and potential energy (term $L8$) take place, again representing losses to productive energy utilization realized for the mission.

Throughout the second-stage burn, the productive energy utilization $\phi$ (the bottom line in Figure 5) monotonically increases as kinetic and potential energies (altitude) associated with the final mass of the vehicle increase. It is important to stress that, at the end of the mission, the energy utilization must and does necessarily balance, i.e., the balance described in Eq. (24) is exactly satisfied. At this point, $\beta$ is equal to zero; all propellant (in first and second stages) has been used, and hence there is no remaining availability of energy associated with those stages.

Table 2 provides the percentages associated with the various increments for energy utilization at the end of the tracked mission (at 550 s after launch). These increments are associated with the various terms ($\phi$, $L1$, $L2$, $L3$, $L4$, $L5$, $L6$, $L7$, and $L8$) that appear in the energy utilization balance given in Eq. (28).

Table 2. Energy utilization summary for Apollo mission (Apollo 11) after second-stage separation ($t$ = 550 s).

| Description of term in energy utilization balance Eq. (28) | Term designation | Fraction of overall mission-integrated energy availability (stages 1 and 2) used |
|---|---|---|
| Overall mission-integrated energy availability (stages 1 and 2) | $E_{\mathrm{AV}}$ | 1.0 (summation of all the fractions below) |
| Available energy used to overcome stage-1 irreversibility | $L1$ | 0.5965 |
| Available energy used to overcome stage-2 irreversibility | $L2$ | 0.2680 |
| Kinetic energy (KE) loss due to stage-1 discarded mass | $L3$ | 0.0097 |
| Kinetic energy (KE) loss due to stage-2 discarded mass | $L4$ | 0.0212 |
| Work done by stage 1 to lift propellant expended | $L5$ | 0.0142 |
| Work done by stage 1 to lift discarded mass | $L6$ | 0.0030 |
| Work done by stage 2 to lift propellant expended | $L7$ | 0.0073 |
| Work done by stage 2 to lift discarded mass | $L8$ | 0.0012 |
| Productive energy utilization (change in KE and potential energy of final mass of vehicle) | $\phi$ | 0.0790 |

At the end of the defined mission (and hence where the remaining propellant associated with stage 1 and stage 2 is zero), irreversibility (occurring in, around, and in the wake of the vehicle) accounts for a total of 86% of the energy utilization, with stage 1 responsible for somewhat over double that associated with stage 2. Slightly less than 8% of the energy is realized productively in the kinetic and potential energy changes of the final mass of the vehicle (i.e., the vehicle after stage-2 mass discard). As can be seen in Table 2 for the end of the defined mission (as well as in the time evolution presented in Figure 5), all other losses are very small; the largest losses other than that associated with

irreversibilities are the kinetic energy loss due to stage-2 discarded mass (2%) and the work done by stage 1 to lift propellant expended (1.5%).

The results shown here represent a larger loss due to irreversibility than that described in earlier preliminary results presented in Ref. [15] for a generic Saturn V mission. Specifically, in the previous work, irreversibility was estimated to account for approximately 76% of the overall energy utilization for this system. The main reason for this difference is that, in the current work, the actual thermochemical availability distribution is computed versus altitude for the mission. In Ref. [15], the thermochemical availabilities were also simply approximated based on the lower heating values of propellants at STP. Although such an estimation is often used and is usually considered sufficient for airbreathing engines and most (lower altitude) atmospheric rocket applications, it is seen to be inaccurate at high altitudes (here identified as above 100 km). Above 100 km, the ratio between the thermochemical availability $H^*$ and the heating value of the propellant $H_P$ increases significantly, as shown in Figure 4 for stage-2 flight. This necessarily results in a considerably increased energy utilization increment associated with stage-2 irreversibility when the actual thermochemical availability is used. In addition, the example developed in Ref. [13] used approximations to define potential energy contributions, whereas the present analysis is based on detailed time-dependent flight and trajectory data.

# 8. CONCLUSIONS

This paper provides the general analytical formulation necessary for comprehensively describing the utilization of energy in single and two-stage rocket missions. The analysis includes the effects of flight in a gravitational field and with atmospheric drag. The formulation is constructed from first principles, necessitating the systematic combination of the equation of motion with the universal exergy (available energy) balance for a rocket in flight. The analysis shows that the sum of the mission-integrated available thermochemical and kinetic energies (associated with the overall propellant that is loaded in all rocket stages at the beginning of a defined mission) is progressively used through the mission. This utilization is then precisely quantified by a number of contributors; these contributors are 1) the energy utilization associated with irreversibility, 2) work done in lifting expended propellant to the altitude at which it is expelled from the rocket, and 3) the energy used to productively increase the kinetic and potential energies of the actual final (end-of-mission) vehicle mass. In addition, for multiple-stage systems (in this work, explicitly shown for two-stage systems only), other contributions in energy utilization must also include the initially available energy that is needed to effect kinetic and geopotential energy changes of the discarded (structural) masses associated with staging. The resultant exact balance of energy utilization (in which all contributors with the exception of the productive energy utilization are viewed as losses) can be analyzed at the end of a defined mission or, alternatively, can be tracked in time through a mission. This capability is developed for both single- and two-stage systems. However, extension of the methodology to rockets with more than two stages is

straightforward. The analysis is relevant to any rocket mission, including those involving gravitational and drag effects, turning and maneuvering flight, etc.; hence, it most generally must be coupled with a rocket trajectory/mission simulation or flight data (as is done here).

A case study of energy utilization is then performed for the flight of the Apollo 11 vehicle from launch to second-stage burnout and staging (mass discard). To perform the analysis, the detailed formulation and quantification of the thermochemical availability associated with the fuels and oxidizer across the altitude range and for both stage 1 and stage 2 for the flight of the Apollo 11 are performed and compared to the lower heating values of the propellant. Necessary atmospheric, flight, and vehicle data are obtained from available databases for this mission. This case study is performed in order to provide a demonstration of the energy utilization methodology developed in this work. The impact of the losses due to irreversibility, particularly in stage 1, is by far the most pronounced contributor to energy utilization. Thermodynamic losses representing the generation of entropy through irreversible processes are responsible for 86% of the energy utilization for this mission. Productive energy utilization for the mission, defined as the kinetic and geopotential changes in energy of the final realized rocket mass (after second-stage burnout and discard of second-stage mass), represents only around 8% of the available mission-integrated thermochemical energy associated with stage-1 and stage-2 (loaded) propellants at launch.

The benefits of considering the energy utilization characteristics of access-to-space chemical rockets as described in this work include the precise quantification of how the initially available energy is being allocated or distributed within a rocket mission, the detailed representation of the explicit balancing of losses versus the productive (desired)

utilization of energy, and the possible use of the results in providing additional useful information in existing and future optimization techniques for rocket design and missions.

## ACKNOWLEDGMENTS

The authors would like to thank Larry Lambe of the Multidisciplinary Software Systems Research Corporation who provided funding under U.S. Air Force contract number FA8650-17-C-2418 for a portion of this work, which was performed during the summer of 2017. In addition, we thank Michael Watson at NASA Marshall Space Flight Center for his leadership in the area of system-level application of exergy to launch and space-based vehicles.

## REFERENCES

[1] Bejan, A., "Entropy Generation and Exergy Destruction," *Entropy Generation Minimization: The Method of Thermodynamic Optimization of Finite-Size Systems and Finite-Time Processes*, CRC Press, New York, 1996.

[2] Hayes, D., Lone, M., and Whidborne, J., "Entropy Generation Minimization and Exergy Analysis Approaches for Aerospace Applications—A Review," AIAA Paper 2016-0866, Jan. 2016.

[3] Oswatitsch, K., "General Equations and Theorems," *Gas Dynamics*, Academic Press, New York, 1956, pp. 177–210.

[4] Clarke, J., and Horlock, J., "Availability and Propulsion," *Journal of Mechanical Engineering Science*, Vol. 17, No. 4, 1975, pp. 223–232.

[5] Lewis, J. H., "Propulsive Efficiency from an Energy Utilization Standpoint," *Journal of Aircraft*, Vol. 13, No. 4, 1976, pp. 299–302.

[6] Riggins, D., McClinton, C. R., and Vitt, P., "Thrust Losses in Hypersonic Engines Part 1: Methodology," *Journal of Propulsion and Power*, Vol. 13, No. 2, 1997, pp. 281–287.

[7] Riggins, D., "Thrust Losses in Hypersonic Engines Part 2: Applications," *Journal of Propulsion and Power*, Vol. 13, No. 2, 1997, pp. 288–295.

[8] Riggins, D., "Evaluation of Performance Loss Methods for High-Speed Engines and Engine Components," *Journal of Propulsion and Power*, Vol. 13, No. 2, 1997, pp. 296–304.

[9] Curran, T., and Craig, R., "The Use of Stream Thrust Concepts for the Approximate Evaluation of Hypersonic Ramjet Engine Performance," U.S. Air Force Aero-Propulsion Lab. TR-73-38, 1978.

[10] Etele, J., and Rosen, M., "Sensitivity of Exergy Efficiencies of Aerospace Engines to Reference Environment Selection," *Exergy International Journal*, Vol. 1, No. 2, 2001, pp. 91–99.

[11] Giles, M., and Cummings, R., "Wake Integration for Three-Dimensional Flowfield Computations: Theoretical Development," *Journal of Aircraft*, Vol. 36, No. 2, 1999, pp. 357–365.

[12] Hunt, D., Giles, M., and Cummings, R., "Wake Integration for Three-Dimensional Flowfield Computations: Applications," *Journal of Aircraft*, Vol. 36, No. 2, 1999, pp. 366–373.

[13] Riggins, D., Taylor, T., and Moorhouse, D., "Methodology for Performance Analysis of Aerospace Vehicles Using the Laws of Thermodynamics," *Journal of Aircraft*, Vol. 43, No. 4, 2006, pp. 953–963.

[14] Riggins, D., Camberos, J., and Moorhouse, D., "Entropy Generation and Aerospace Vehicle Performance," *Exergy Analysis and Design Optimization for Aerospace Vehicles and Systems*, AIAA Progress in Astronautics and Aeronautics Series, AIAA, Reston, VA, 2011, pp. 181–227.

[15] Riggins, D. W., Camberos, J., and Moorhouse, D., "The Characterization of Aerospace Vehicle Performance and Mission Analysis Using Thermodynamic Availability," *Journal of Aircraft*, Vol. 47, No. 3, 2010, pp. 904–916.

[16] Terhune, L., "Drag and Fuel Minimization and Entropy-Based Performance Analysis of Hypersonic Vehicles," M.S. Thesis, Univ. of Missouri–Rolla, Rolla, MO, 2006.

[17] Riggins, D., Camberos, J., Wolff, M., and Bowcutt, K., "Mission-Integrated Exergy Analysis for Hypersonic Vehicles: Methodology and Application," *Journal of Propulsion and Power*, Vol. 29, No. 3, 2013, pp. 610–620.

[18] Berg, F., Balchin, M., and Keogh, P., "New Principles for Dynamic Aircraft Exergy Mapping," *Journal of Aircraft*, Vol. 50, No. 4, 2013, pp. 1088–1098.

[19] Arntz, A., Atinault, O., and Merlen, A., "Exergy-Based Formulation of Aircraft Aeropropulsive Performance Assessment: Theoretical Development," *AIAA Journal*, Vol. 53, No. 6, 2015, pp. 1627–1639. DOI:10.2514/1.J053467

[20] Moorhouse, D., and Camberos, J., "Introduction," *Exergy Analysis and Design Optimization for Aerospace Vehicles and Systems*, Vol. 238, AIAA Progress in Astronautics and Aeronautics Series, AIAA, Reston, VA, 2011, pp. 1–8. DOI:10.2514/5.9781600868405.0001

[21] Moorhouse, D. J., "Proposed System-Level Multidisciplinary Analysis Technique Based on Exergy Methods," *Journal of Aircraft*, Vol. 40, No. 1, 2003, pp. 11–15. DOI:10.2514/2.3088

[22] Ehyaei, M., Anjiridezfuli, A., and Rosen, M., "Exergetic Analysis of an Aircraft Turbojet Engine with an Afterburner," *Thermal Science*, Vol. 17, No. 4, 2013, pp. 1181–1194. DOI:10.2298/TSCI110911043E

[23] Marley, C., and Riggins, D., "The Thermodynamics of Exergy Losses and Thrust Production in Gas Turbine Engines," AIAA Paper 2011- 6130, July 2011.

[24] Abbas, M., and Riggins, D., "Exergy-Based Performance Analysis of aTurbojet Engine," AIAA Paper 2016-4638, July 2016.

[25] Gilbert, A., Mesmer, B., and Watson, M., "Exergy Analysis of Rocket Systems," *Proceedings of 9th Annual IEEE International Systems Conference*, IEEE Publ., Piscataway, NJ, April 2015, pp. 283–288.

[26] Watson, M. D., Gilbert, A., and Mesmer, B., "Launch Vehicle Exergy Efficiency Analysis," *JANNAF 43rd SMBS/39th PEDCS/30th RNTS/28th SEPS Joint Subcommittee Meeting*, Paper 2015-0003DX, Salt Lake City, UT, Dec. 2015.

[27] Gilbert, A., Mesmer, B., and Watson, M. D., "Exergy Based Optimization of Rocket System Staging Times," *IEEE International Systems Conference*, IEEE Publ., Piscataway, NJ, April 2016, pp. 1–7.

[28] Watson, M., "System Exergy: System Integrating Physics of Launch Vehicles and Spacecraft," *Journal of Spacecraft and Rockets*, Vol. 55, No. 2, 2018, pp. 451–461.

[29] Farokhi, S., *Aircraft Propulsion*, Wiley, Hoboken, NJ, 2009, pp. 379–382.

[30] Sohret, Y., Ekici, S., Altuntas, O., Hepbasli, A., and Karakoc, T., "Exergy as a Useful Tool for the Performance Assessment of Aircraft Gas Turbine Engines: A Key Review," *Progress in Aeronautical Sciences*, Vol. 83, May 2016, pp. 57–69

[31] Wu, Z., Zhou, S., and An, L., "The Second Law (Exergy) Analysis of Hydrogen," *Journal of Sustainable Development*, Vol. 4, No. 1, Feb. 2011, pp. 260–263.

[32] “Saturn V Launch Vehicle Flight Evaluation Report,” NASA TM-62558, Sept. 1969.

[33] “Apollo/Saturn V Post-Flight Trajectory-AS-506,” The Boeing Company Rept. D5-15560-6, Huntsville, AL, Oct. 1969.

[34] “MSIS-E-90 Atmosphere Model (online database),” Community Coordinated Modeling Center, NASA Goddard Space Flight Center, Greenbelt, MD, https://ccmc.gsfc.nasa.gov/modelweb/models/msis_vitmo.php [retrieved 09 March 2018].

[35] McBride, B., Zehe, M., and Gordon, S., “NASA Glenn Coefficients for Calculating Thermodynamic Properties of Individual Species,” NASA TP-2002-211556, Sept. 2002.

[36] Lemmon, E., McLinden, M., and Friend, D., “Thermophysical Properties of Fluid Systems,” *NIST Chemistry WebBook, NIST Standard Reference Database Number 69*, edited by P. J. Linstrom, and W. G. Mallard, National Inst. of Standards and Technology, Gaithersburg, MD, April 2018. DOI:10.18434/T4D303

[37] Magee, J., Bruno, T., Friend, D., Huber, M., Laesecke, A., Lemmon, E., McLinden, M., Perkins, R., Baranski, J., and Widegren, J., “Thermophysical Properties Measurements and Models for Rocket Propellant RP-1: Phase 1,” National Inst. of Standards and Technology, Gaithersburg, MD, Feb. 2007, p. 7.

[38] Wang, T.-S., “Thermophysics Characterization of Kerosene Combustion,” *Journal of Thermophysics and Heat Transfer*, Vol. 15, No. 2, May 2001. DOI:10.2514/2.6602

# III. UTILIZATION AND LOSS OF AVAILABLE ENERGY FOR CHEMICAL ROCKETS IN ATMOSPHERIC FLIGHT

Mohammad Abbas and David W. Riggins

Department of Mechanical and Aerospace Engineering, Missouri University of Science and Technology, Rolla, MO 65409

and

Michael D. Watson

NASA Marshall Space Flight Center, Huntsville, AL 35808

## ABSTRACT

The physical basis and application of the fundamental relationship governing the balance and utilization of available energy for a chemical rocket operating within the atmosphere is described. The relative contributions of the thermochemical availability and the kinetic energy of the stored propellant to the overall energy availability are shown. There are optimal flight velocities for which 1) overall entropy generation is minimized and 2) effectiveness of the conversion of available energy to vehicle force power is maximized. The fundamental impacts of entropy generation within a rocket engine flow-field on energy utilization and thrust/performance characteristics of a rocket-powered vehicle is studied analytically. Highly non-linear coupling between entropy generation in the engine and entropy generation in the wake is observed; this is true as well as for other energy utilization parameters such as thrust losses. Representative energy utilization-based performance maps for selected (example) legacy rocket systems across altitude/flight

velocity confirm the theoretical results. Propulsion models and available flight data are then utilized to provide the time evolution of energy utilization characteristics for the flight of the Apollo 11 (Saturn V).

## NOMENCLATURE

| Symbol | Description |
|---|---|
| $A$ | Cross-sectional area of streamtube/flowpath, $m^2$ |
| $C$ | Effective exhaust velocity, m/s |
| $D$ | Aerodynamic drag, N |
| $\dot{E}$ | Net energy transfer rate, W |
| $F_{\text{engine}}$ | Raw (uninstalled) thrust of engine, N |
| $F_{x(\text{flight})}$ | Net fluid-dynamic force acting on the vehicle in flight (axial) direction, N |
| $F_{x(\text{propulsion})}$ | Net axial fluid-dynamic force on all internal wetted surfaces of the engine, N |
| $g_0$ | Gravitational acceleration constant at sea-level, $m/s^2$ |
| $H^*$ | Total thermochemical energy availability of propellant, J/kg |
| $h$ | Specific enthalpy (per unit mass), J/kg |
| $I_{sp}$ | Specific impulse, s |

| | |
|---|---|
| $K$ | Parametric engine entropy generation ratio |
| $\dot{m}$ | Mass flow rate, kg/s |
| $O/F$ | Oxidizer-to-fuel mixture (mass flow rate) ratio |
| $P$ | Static pressure, Pa |
| $\dot{S}$ | Entropy flow/change rate, W/K |
| $s$ | Specific entropy (per unit mass), J/K-kg |
| $T$ | Static temperature, K |
| $u$ | Fluid axial velocity component (in the $x$ direction), m/s |
| $u_\infty$ | Flight velocity, m/s |
| $\eta$ | Instantaneous energy availability effectiveness |
| $\mu_{\text{engine}}$ | Fraction of propellant mass flow rate used to overcome losses in the engine |
| $\mu_{\text{overall}}$ | Fraction of propellant mass flow rate used to overcome all losses in global control volume |

Subscripts

| | |
|---|---|
| $e$ | Nozzle exit/exhaust conditions |
| $P$ | Propellant (both fuel and oxidizer) |

| | |
|---|---|
| $s$ | Plane $s$, wake zone inlet conditions |
| $w$ | Plane $w$, wake zone exit conditions |
| $x$ | In flight (axial) direction |
| $\infty$ | Plane $\infty$, global control volume inlet (freestream) conditions |

## 1. INTRODUCTION

Effective utilization and transfer of energy are the core requirements for the meaningful design, analysis, and optimization of an aerospace vehicle of any type. In a chemically based propulsion system, the bulk of energy initially available to produce useful thrust work is generally associated with the chemical bonds of fuel and oxidizer, and the overall exothermic heat release that occurs as product species are formed from reactant species. However, at high-enough flight velocities, the kinetic energy associated with the stored propellant being carried at the flight velocity of a vehicle (not related to the thermochemical availability of fuel and oxidizer) also becomes an important contributor to energy availability and utilization. A fraction of the total available energy onboard the vehicle is ultimately realized in the development of a (force-based) work interaction upon the vehicle. The remainder is entirely lost in terms of realizing productive work. This lost work is measurable in terms of the 1) generation of entropy within (and transfer of entropy to) the rocket propulsion system and the vehicle zone of influence (associated with external aerodynamic drag) and 2) generation of entropy within the wake of the vehicle. The entropy

generation that occurs in the wake is primarily a result of the equilibration process between the wake of the rocket (which includes the exhaust plume of the engine) and the ambient atmosphere. The overall purpose of this paper is to explore basic issues relating to thermochemical and directed kinetic energy availabilities of onboard propellant, entropy generation, and the performance of a rocket-powered vehicle.

Fundamental relationships that link the comprehensive utilization of available energy to classic aerospace vehicle and engine performance using global control volume analysis have been developed, validated, and applied in recent years [1–5]. Although these relationships are valid for both airbreathing and rocket-powered vehicles and have been applied to both types of vehicles, focus in the present work is on chemical rockets. Previous work in this area (energy availability applied to classic chemical rocket performance) has focused on single- and two-stage (generically defined) systems [2,4]. For mission-based (time-integrated) performance using energy utilization [2,3], entropy generation as well as staging phenomena are shown in Ref. [4] to be directly relatable to changes in vehicle kinetic and geopotential energies across a defined mission for a single-stage or a two-stage chemical rocket operating in a gravitational field with external drag. Reference [4] also used this approach to study the time evolution of the energy utilization balance over a legacy mission for the Saturn V system, using a simplified model. Other rocket-specific work, partially based on the global control volume formulations developed in [1–5], provides system-level comparative studies of access to space rocket systems [6], with emphasis on providing engineering-level exergy quantification and analysis of relevant systems.

Other work based on the global control volume approach includes the early derivation of the relationship between drag and entropy generation for an unpowered object in fluid flow, by Oswatitsch [7]. Giles and Cummings [8] also derived and used a simplified airbreathing powered vehicle formulation for energy availability, using a simplified heating model for fuel–air combustion. Abbas and Riggins [9] have employed the energy utilization balance based on the same control volume formulation of energy availability to study turbojet performance.

The maximum amount of thermodynamic work that can be obtained from a system operating in a given environment is known as exergy (historically known in thermodynamics as availability); exergy analysis represents the synthesis of the first and second laws of thermodynamics. Exergy destruction is due to irreversibility and is directly proportional to entropy generation. Therefore, entropy generation provides the single and universal measure of losses associated with all processes and mechanisms (mechanical, electrical, thermodynamic, chemical, etc.). Exergy analysis is a mature and well-accepted tool for analysis, design, and optimization of ground-based energy systems of all types [10]. It has not been as widely accepted, or routinely used, in the design and analysis of aerospace systems, due mainly to the former lack of direct connection between it and classic aerospace vehicle flight performance analysis [11]. Early seminal work in the area of energy utilization and availability for aerospace airbreathing applications, mainly focused on deriving propulsive availability balances, includes the work of Foa [12], Clarke and Horlock [13], and Lewis [14]. Some notable work done more recently in the area of exergy analysis and aerospace systems includes studies by Arntz et al. [15], Arntz and Hue [16], Ehyaei et al. [17], and Hayes et al. [18].

The global control volume-derived energy utilization analysis and resulting balance described and applied in this (and previous related works) is a form of exergy analysis. However, it is inherently specific to an aerospace vehicle in flight in terms of comprehensively describing the energy utilization associated with onboard propellant and stored energy systems, achieved (force-based) performance, and performance losses associated with that vehicle, including losses incurred in the wake. Techniques for the assessment of vehicle and engine performance have also been developed that do not directly use energy utilization or conventional exergy methods. These efforts have focused on propulsion system/aerospace vehicle performance-centric metrics, and include engine thrust potential [11,19,20], work potential, and kinetic energy efficiency [21–23].

Section 2 of this paper provides a summary description of the global control volume method and the resulting fundamental energy utilization balance that results for a rocket-powered vehicle in flight in the atmosphere. The formal definition of the thermochemical availability of the onboard propellant, which appears in the balance, is also described in this section; the exact quantification of this quantity is generally necessary, particularly for rockets. The correct usage of the force power for “stand-alone” rocket engine energy utilization (i.e., rockets without external aerodynamic losses considered) is also described in this section. Section 3 describes flow modeling methodology used to produce flowfield representations of two legacy rocket systems (F-1 and J-2 rocket engines). These systems are used as application examples throughout this work. Section 4 summarizes the necessary performance parameters and operating range parameters for these two propulsion systems. Section 5 describes the specific application of the energy utilization balance for rockets, and then examines broad energy availability and performance characteristics of the Saturn

V second-stage propulsion system. Metrics, such as an instantaneous effectiveness of energy utilization, are developed. Entropy generation that occurs within the engine flowpath of a rocket and its cascading impact on energy utilization and performance is analytically investigated in Sec. 6. This is done by defining an entropy generation factor in a given engine flowfield, and then studying analytically the impact of parametric variations in the value of that factor in reference engine flowfields on various energy utilization quantities and metrics. Section 7 provides a few representative parametric results for the two Saturn V rocket engines (F-1 and J-2) used in this work; these results are shown as contour maps of entropy generation in the wake and the energy utilization effectiveness metric across flight velocity/altitude/mixture ratio spaces for these systems. This section also provides a time history study of wake entropy generation and energy utilization effectiveness for the flight of the Apollo 11 Saturn V stack from launch to second-stage burnout, incorporating external drag from data and using modeled performance for the engine systems. This case study is for the same legacy access-to-space mission that was examined in Ref. [4]; however, it incorporates the more detailed propulsion models and methodologies necessary for assessing the specific characteristics of energy utilization for specific rocket systems. The final section provides a summary of the work.

## 2. ENERGY UTILIZATION IN A CHEMICAL ROCKET

Consider an isolated aerospace vehicle in flight in the atmosphere, as shown schematically in Figure 1. The vehicle is depicted as a rocket; however, the analysis and resulting energy utilization principles that are described here are completely general [i.e.,

applicable to vehicles with airbreathing propulsion systems, vehicles utilizing collected/ stored energy (batteries), etc.]. Examples of previous work for airbreathing vehicles as well as rockets incorporating these principles can be found in [1–4,9]. The vehicle is embedded within a very large 3-D "global" fluid control volume (or global streamtube), fixed with respect to the vehicle. The surface of the global control volume envelopes all fluid external to the vehicle as well as within the propulsive system (including air induction for airbreathing engines, propellant feed systems, tanks, etc.). The inflow plane to the global control volume is designated $\infty$ (with corresponding inflow conditions $u_\infty$, $P_\infty$, $T_\infty$, etc.). For very large cross-sectional areas of the global streamtube (i.e., in the lateral direction), the side boundaries of the global control volume for analytical purposes are also at $\infty$ conditions. The plane $s$ shown in Figure 1 denotes the plane defined at (or just downstream of) the aftmost closure point of the vehicle solid structure. This plane, which necessarily has distorted flow (nonuniform and out of axial, i.e., multidimensional flow), is referred to as the "vehicle exit plane." It is, by definition, also the inflow plane for the region of the global control volume that encompasses the unconstrained wake (the wake subcontrol volume in Figure 1), downstream of the vehicle. The nonuniform (and energized) flow entering at $s$ and processed within the wake region is then "mixed" (i.e., equilibrated) with the ambient fluid, such that for large-enough length scales, the equilibrated conditions of the fluid at wake exit plane $w$ are uniform, and differentially displaced from that of the freestream $\infty$ conditions. For a rocket at high-enough altitude, the atmosphere becomes increasingly rarefied and the wake equilibration process approaches that of a free expansion process (of the exhaust plume). As shown in Figure 1, the global control volume between $\infty$ and $s$ can be further divided into subcontrol volumes as indicated. For high-

speed flight, the vehicle subcontrol volume (at the minimum spanning the vehicle zone of influence between planes $\infty$ and $s$) can be relatively small in lateral extent. Furthermore, for high-speed flight, the side-bounding subcontrol volumes would be, by definition, at freestream conditions.

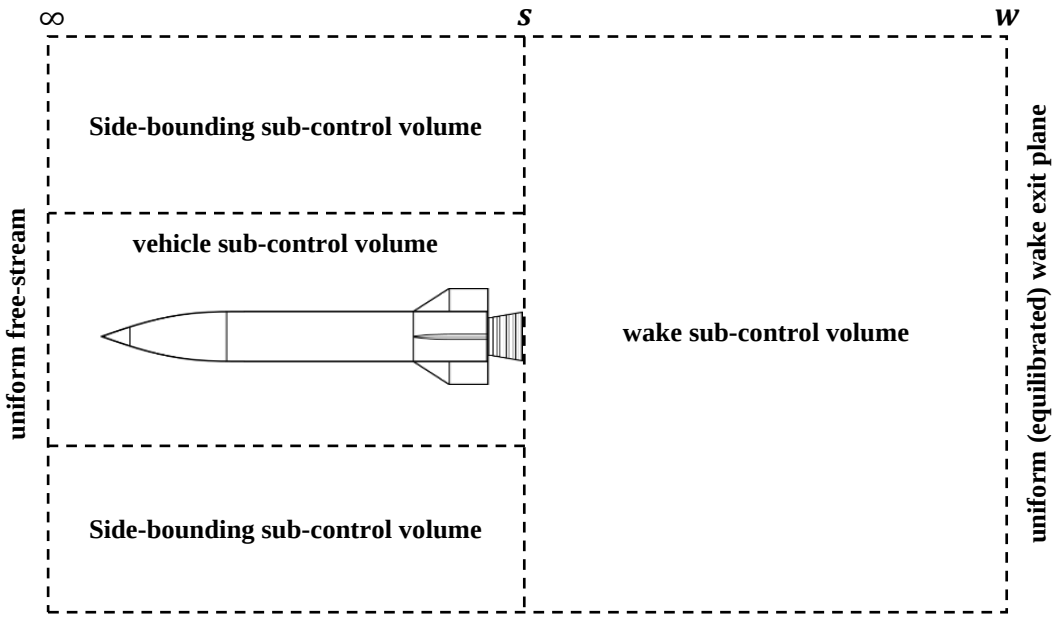


Figure 1. Global control volume for a rocket in flight.

In the analysis and development of the instantaneous energy availability balance for meaningful flight velocities, the flight direction of the vehicle with respect to the direction of gravitational acceleration (line of action of the vehicle weight) is essentially immaterial, that is, the orientation of the vehicle with respect to the center of Earth is arbitrary. However, when the energy availability relationships are combined with vehicle equations of motion, as done in Refs. [2,4], the weight and flight orientation of the vehicle must be considered. The vehicle solid structure is not part of the global control volume;

vehicle surfaces exposed to fluid within the global control volume form internal boundaries adjacent to parts of the global control volume surface. Through and on these "wetted" surfaces of the vehicle, energy interactions with the fluid can occur and forces on the vehicle structure are realized.

The development of the general energy utilization balance for a vehicle in flight at a given altitude proceeds from combining the fundamental principles of mass conservation, momentum (Newton's second law), energy (first law of thermodynamics), and the second law of thermodynamics within this global control volume. The energy availability balance that results constitutes a powerful compilation of all these principles. The detailed derivations and development of the following energy utilization balance relationships (and a number of applications) have been provided in previous work [1–5]. The following is a summary of the relationships and discussion on their implementation for chemical rocket systems as used in the present work.

The general energy utilization balance that results for an aerospace vehicle in flight at a given altitude and flight velocity is given as follows:

$$u_\infty F_{x(\text{flight})} = \dot{E} + \dot{m}_P \left( H^* + \frac{u_\infty^2}{2} \right) - T_\infty \dot{S}_{\text{total}} \tag{1}$$

The left-hand side of the relationship shown in Eq. (1) represents the net instantaneous force power delivered to the vehicle, where $u_\infty$ is the flight velocity magnitude of the vehicle and $F_{x(\text{flight})}$ is the component of the net fluid dynamic force experienced by the vehicle in the direction of flight velocity (i.e., conventionally, thrust minus drag in the absence of thrust vectoring). This net fluid dynamic force is due to all pressure and shear interactions on all wetted surfaces of the vehicle, both external and

internal, including in the propellant feed and tankage systems. The first term on the right-hand side of Eq. (1), $\dot{E}$, denotes any net energy interaction rates to the flow (heat and/or work) from stored energy within the vehicle [i.e., energy not originating from stored thermochemical availability (work potential) associated with the propellant expenditure itself]. The most obvious example would be power supplied to a propellant stream from batteries. However, this term could also represent such phenomena as net heat interaction rates between vehicle and surroundings (i.e., a nonthermally balanced vehicle), etc. In this work, $\dot{E}$ will be considered negligible (zero). The second term on the right-hand side of Eq. (1) is composed of two contributions, both proportional to mass flow rate of propellant. $H^*$, defined in more detail as follows, is the total thermochemical energy availability (chemical potential between propellant in tanks and the ambient surroundings) per unit mass of expended propellant (see [1,4]). The second contribution within the second term on the right-hand side of Eq. (1) is the kinetic energy rate of the stored propellant in the tanks. Therefore, the second term in general represents the total thermal–chemical and mechanical energy availability (work potential) existing between onboard stored propellant and local ambient conditions. The last term on the right-hand side of Eq. (1) is the overall lost work availability rate, $T_\infty \dot{S}_{\text{total}}$, in the global control volume (between $\infty$ and $w$). As shown in Eq. (2), this term can be written as the summation of the entropy generation between the vehicle portion of the global control volume (between $\infty$ and $s$) and the wake portion of the global control volume (between $s$ and $w$); the latter also denoted $\dot{S}_{\text{wake}}$ in subsequent parts of this work. Although the entropy term here is most obviously due to internal irreversibilities occurring in the global control volume, it is also inclusive of any net entropy rates associated with convective and radiative heat transfer (both nonideal and

ideal) to the fluid within the global control volume. Also, as shown in Eq. (2), it can be usefully described as the overall entropy flow rate difference between the wake exit ($w$ plane) and the summation of the entropy flow rate at the inflow plane $\infty$, and the entropy flow rates of propellant exiting the tanks:

$$\dot{S}_{\text{total}} = \left(\Delta\dot{S}_{\infty\to s} + \Delta\dot{S}_{s\to w}\right) = \dot{S}_w - \dot{S}_\infty - \dot{S}_{P(\text{tanks})} \tag{2}$$

The thermochemical energy availability $H^*$ that appears in Eq. (1) for a chemical rocket with separate fuel and oxidizer tanks is defined from the following (see, e.g., [1,4]):

$$\begin{aligned} &\dot{m}_P H^* \\ &= \dot{m}_{\text{fuel}}\left(h_{\text{fuel (tank)}} - T_\infty s_{\text{fuel(tank)}}\right) \\ &+ \dot{m}_{\text{oxidizer}}\left(h_{\text{oxidizer(tank)}} - T_\infty s_{\text{oxidizer(tank)}}\right) + \dot{m}_\infty(h_\infty - T_\infty s_\infty) \\ &- \dot{m}_w(h_w - T_\infty s_w) \end{aligned} \tag{3}$$

In this definition of thermochemical availability, because of the asymptotic computations required for very large global control volume lateral cross-sectional areas, care must be taken to properly evaluate all terms. The mixture enthalpy per mass $h$ and the entropy per mass $s$ of the air entering the global control volume (at station $\infty$ of the global control volume) are evaluated at the ambient temperature and pressure at the given altitude of vehicle operation. Reacted mixture enthalpy (per mass) and entropy (per mass) at the equilibrated exit station $w$ of the global control volume must also be evaluated at the ambient temperature and pressure, while using the proper reacted mixture species mass and mole fractions associated with complete mixing and equilibrium chemistry. (However, due to low ambient temperatures, the assumption of complete reaction is generally entirely sufficient to determine composition at plane $w$.) Fuel and oxidizer contributions in terms

of both enthalpy and entropy per unit mass must be assessed at their respective tank temperatures and pressures; generally, due to phase changes between tank and combustor, appropriate databases must be used for these values. Although (as shown and discussed in Ref. [1]) in principle the global control volume must be made infinitely large to yield an exact limiting analysis relating vehicle performance and entropy production and availability, in practice there is asymptotic convergence to values of interest (vehicle performance, wake entropy generation and thermochemical availability, etc.) using large but finite lateral control volume dimensions [24]. Note that the thermochemical energy availability $H^*$ for a given fuel and oxidizer in a liquid chemical rocket propulsion system is strictly a function of altitude (ambient conditions), tank conditions, and oxidizer/fuel mixture ratio ($O/F$ ratio). The energy utilization balance given in Eq. (1) has been used and validated at all levels of modeling, ranging from simple quasi-1-D flow analysis to multidimensional computational fluid dynamics analysis [1,3,25].

## 3. FLOW MODELING APPROACH

This section provides an overview of the methodology used for modeling the various flowfields (streamtubes) that exist within the global control volume. Because the focus in the present work is on the analysis of the energy utilization of the rocket, as described by Eq. (1), and because the modeling of the flows within these streamtubes is straightforward and conventional (and has been reported in detail in previous work [1–3,5]), the following discussion is relatively brief. The individual streamtubes within the global control volume that require modeling are 1) the wake mixing zone; 2) the rocket

propulsive flowpath (from the tanks to the nozzle exit within the rocket itself); 3) the external (aerodynamic) flow adjacent to the vehicle, defined generally by the zone of influence of the vehicle; and 4) the side-bounding subcontrol volume. In this investigation, flowfields in all streamtubes are analyzed using steady-flow quasi-1-D models. For modeling of fluids in the gaseous phase in all streamtubes, standard NASA polynomial curve fits (Ref. [26]) are used to obtain the required properties of the modeled chemical species.

Although details of the propellant feed systems (pumps, gas generators, valves, etc., between tanks and injection manifolds at the entrance to the combustor) are not modeled explicitly in this work, entropy generation rates and energy considerations (of specific interest in this work) associated with the propellant feed systems can be found directly from known tank and injector manifold conditions. For the main propulsive flowpath (combustor entrance to nozzle exit), the analysis models the flow at three discrete stations, based on given fuel and oxidizer injection manifold conditions at the entrance to the combustor. These stations are the combustor exit, the nozzle throat where the flow is assumed to be choked, and the nozzle exit. Cooling of the main propulsive flowpath is not considered in the modeling for the present work.

The chemistry within the rocket engine is modeled using 1) equilibrium chemical kinetics from combustion chamber to nozzle throat, and 2) chemically frozen flow between the throat and the nozzle exit. This approach is computationally less demanding and is standard practice in preliminary design and analysis [27]. Values of the tank properties for propellant fuels and oxidizers are necessary for calculations of the thermochemical energy availability $H^*$. With the exception of case studies using RP-1 fuel, the conditions of the

fuel and oxidizer in propellant tanks and at entry into the combustion chamber fall outside the limits covered by the NASA polynomials. (Propellants are liquid and in critical states at cryogenic temperatures and high pressures [28–32].) Therefore, the database of the National Institute of Standards and Technology (Ref. [33]) is used to obtain the thermodynamic properties for those conditions. Ambient air at altitude is taken at conditions and chemical composition corresponding to the given altitude of flight, obtained using the NASA MSIS-E-90 Atmosphere Model [34].

Rigorously, the wake exit plane would be modeled such that the chemical composition of the fluid at $w$ is in chemical equilibrium. However, because the temperature at the wake exit is infinitesimally displaced from that of the ambient air and the ambient temperature is generally very low (less than 1000 K for altitudes less than 120 km), the chemical composition at the wake exit plane is very well represented by complete reaction (i.e., simply assuming that all fuel has reacted to yield products). This approximation has been tested up to 1000 km altitude for an $H_2/O_2$ rocket by comparing wake composition utilizing equilibrium chemistry with composition obtained using complete reaction; differences are negligible. The entropy generation occurring in the vehicle wake (from $s$ to $w$) is determined from calculated fluid properties at $w$ (found by conserving integrated total enthalpy and mass flow rates and the integrated stream thrust from $s$ to $w$).

As sketched in Figure 1, the vehicle subcontrol volume, defined as containing the fluid within the vehicle zone of influence from $\infty$ to $s$, is usefully divided into the propulsive flowpath (streamtube) and the external aerodynamic flowpath (streamtube). The summation of the axial (flight direction) force components experienced by all vehicle wetted surfaces in these two flowpaths is then the overall $F_{x(\text{flight})}$ appearing in Eq. (1).

The external aerodynamic flowpath generally produces a net drag force $D$ [a negative contribution to $F_{x(\text{flight})}$] on all external surfaces of the vehicle from vehicle nose to engine nozzle exit ($\infty$ to $s$). The quantification of this external drag force and the generation rate of entropy in the external aerodynamic flowpath for an actual vehicle in flight requires experimental data, modeling, or estimation.

The far-field or side-bounding subcontrol volume extends axially from $\infty$ to $s$, and laterally from the outer boundary of the zone of influence to the far-field side boundary of the global control volume. Nominally, for an actual vehicle in high-speed flight with a well-defined zone of influence, the far-field subcontrol volume will be at identical conditions as those of the freestream inflow $\infty$. However, with the exception of a final study of the Apollo 11 flight, this work specifically only investigates the impact of the (dominant) rocket propulsion system on overall energy utilization, and therefore does not include consideration of aerodynamic losses in the external flowfield (from inflow $\infty$ to plane $s$). For this situation (no consideration of external aerodynamics), the vehicle (external zone of influence) subcontrol volume and the far-field subcontrol volume are combined and assessed as a single streamtube that is isentropically compressed from station $\infty$ to station $s$. The overall cross-sectional area decrease that is associated with this external compression is then identically the exit cross-sectional area of the rocket nozzle exit (designated as plane $e$). In this no-loss (isentropic external aerodynamic) model of the external flow, the external drag for a rocket then becomes simply $P_\infty A_e$ and the overall $F_{x(\text{flight})}$ in Eq. (1) then simply becomes $\dot{m}_P u_e + (P_e - P_\infty)A_e$. This investigation uses this formulation for $F_{x(\text{flight})}$ (with the exception, as noted previously, of the last results

presented for mission analysis of the Apollo 11 launch; these results incorporate available experimental flight data for the external drag).

## 4. DESCRIPTION AND PARAMETERS OF SPECIFIC PROPULSION SYSTEMS USED/MODELED IN THE CURRENT STUDY

In this work, energy utilization in chemical rockets is investigated based on modeling of the relevant propulsion system and wake/plume equilibration processes, as summarized in the previous section. Two legacy systems, both historic and well defined, are used for subsequent parametric and case studies presented here. These systems are, respectively, the first stage and the second stage of the Saturn V rocket stack. The first stage, designated the S-IC, was powered by five Rocketdyne F-1 rocket engines that used liquid RP-1 fuel (a highly refined kerosene-based fuel) and liquid oxygen with a nominal $O/F$ (oxygen/fuel) ratio of 2.27. The second stage, designated the S-II, was powered by five Rocketdyne J-2 rocket engines using liquid hydrogen fuel and liquid oxygen with a nominal $O/F$ ratio of 5.5. For the F-1, tank entropy and enthalpy for the RP-1 fuel are based on nominal tank temperature and pressure of 290 K and 180 kPa; for the oxygen, tank entropy and enthalpy are based on temperature and pressure of 90 K and 170 kPa [28–31]. For the J-2, tank entropy and enthalpy for the hydrogen fuel are based on nominal temperature and pressure of 20 K and 220 kPa; for the oxygen, tank entropy and enthalpy are based on temperature and pressure of 90 K and 260 kPa [28–31]. Rocket engine geometries and configurational requirements in the modeling conform to the listed specifications of the engines in Refs. [28–31].

The propulsive modeling described in the previous section, when applied to these systems, provides the capability to examine performance and energy utilization for these two systems over a large range of operating conditions: from sea level to 200 km altitude, from static operation to a flight velocity of 10 km/s, and across wide ranges of $O/F$ (oxygen/fuel) mixture ratios. The combustion models for these systems are based on equilibrium chemical kinetics and consider only the dominant chemical species involved. Specifically, for the F-1 engine, a surrogate fuel (Jet-A) with similar performance as RP-1 is used to model the chemistry of RP-1 [5]. The chemical species considered in the products for the F-1 engine are $H_2O$; $CO_2$, CO, OH, $O_2$; $H_2$, O, and H. The J-2 chemistry model includes the same product species, excluding carbon dioxide and carbon monoxide.

## 5. ANALYTICAL RESULTS USING THE GENERAL ENERGY UTILIZATION BALANCE FOR ROCKETS

Previous sections and specifically Eq. (1) describe the general energy utilization (rate) balance for an aerospace vehicle (rocket or airbreathing powered) in flight at any given point in the mission of the vehicle. This balance is between 1) the net vehicle force power; 2) thermochemical availability; 3) kinetic energy of the propellant (the sum of 2 and 3 constitutes the total energy availability rate associated with the propellant flow rate, referenced to the surroundings); and 4) total losses, internal and external to the vehicle, including losses incurred in the wake of the vehicle. This section describes the specific application of this balance for rockets, and then examines energy availability characteristics in terms of the J-2 (Saturn V second stage) propulsion system.

For a rocket, the effective exhaust velocity $C$ and the specific impulse $I_{sp}$ are often used to describe thrust-based performance. The thrust force of a rocket $F_{\text{engine}}$ and the corresponding effective exhaust velocity are generally written as follows:

$$F_{\text{engine}} = \dot{m}_P u_e + (P_e - P_\infty)A_e = \dot{m}_P C \tag{4}$$

This definition of rocket thrust is specifically defined for the assumption of a constant ambient pressure on all external rocket surfaces, that is, no external aerodynamic effects are considered. Neglecting pressure terms, which are generally small for higher altitudes, $C$ is approximately equal to the nozzle exit velocity $u_e$. Note also that, by definition, the specific impulse (thrust per weight flow rate of propellant) is $I_{sp} = C/\mathrm{g}_0$. It is important to stress that at a given throttle setting, the propulsive flow in the rocket engine (and hence the engine entropy generation from tanks to the exit plane of the nozzle with supersonic flow) is necessarily fixed across all altitudes (unless the nozzle itself is sufficiently backpressured, a condition which is not relevant to the systems examined in this study). Increase in both thrust and specific impulse with increasing altitude (culminating in vacuum specific impulse) is entirely due to the decreasing ambient pressure, as seen in Eq. (4).

When external drag is neglected or small [such that rocket thrust as defined in Eq. (4) is equal to $F_{x(\text{flight})}$ in Eq. (1)], the flight velocity corresponding to minimum overall entropy generated per mass of propellant at a given altitude ($H^*$ constant) can be found by differentiating Eq. (1) with respect to flight velocity. This condition occurs at a point in flight when the flight velocity $u_\infty$ is exactly equal to the effective exhaust velocity $C$:

$$u_\infty = C \tag{5}$$

(for minimum overall entropy generation in the global control volume)

The condition that the effective exhaust velocity equals the flight velocity of the vehicle for minimum overall entropy generation per unit mass of propellant expended means that (nominally) the exhaust of the rocket is actually at zero velocity relative to the atmosphere through which the rocket is traveling. This means, in turn, that for that condition, there is no gradient in velocity between the rocket exhaust plume and the ambient air (however rarefied), and hence no entropy generation explicitly associated with equilibrating that gradient. This result (minimum overall entropy generation when the flight velocity is equal to the effective exhaust velocity) is complementary to the well-known propulsive condition that for maximum rocket thrust [neglecting external aerodynamics, at a given altitude, and with the thrust force, as defined in Eq. (4)], the static pressure at rocket nozzle exit must be equal to the ambient pressure.

As a specific example using Eq. (1), the distribution of the terms that appear in this balance is examined (vs flight velocity) for the J-2 engine without external aerodynamic effects considered (i.e., neglecting any external drag). The nominal effective exhaust velocity $C$ for this system is 4165 m/s. Figure 2 provides the distribution of the rocket engine (net) force power achieved and the entropy generation rate vs flight velocity for this example. The sum of these two quantities is the overall energy availability associated with the mass flow rate of propellant [Eq. (1)]. As predicted analytically, the minimum entropy generation rate (or entropy per unit mass of propellant) is seen to occur at a flight velocity that is equal to the effective exhaust velocity of the engines (i.e., 4165 m/s).

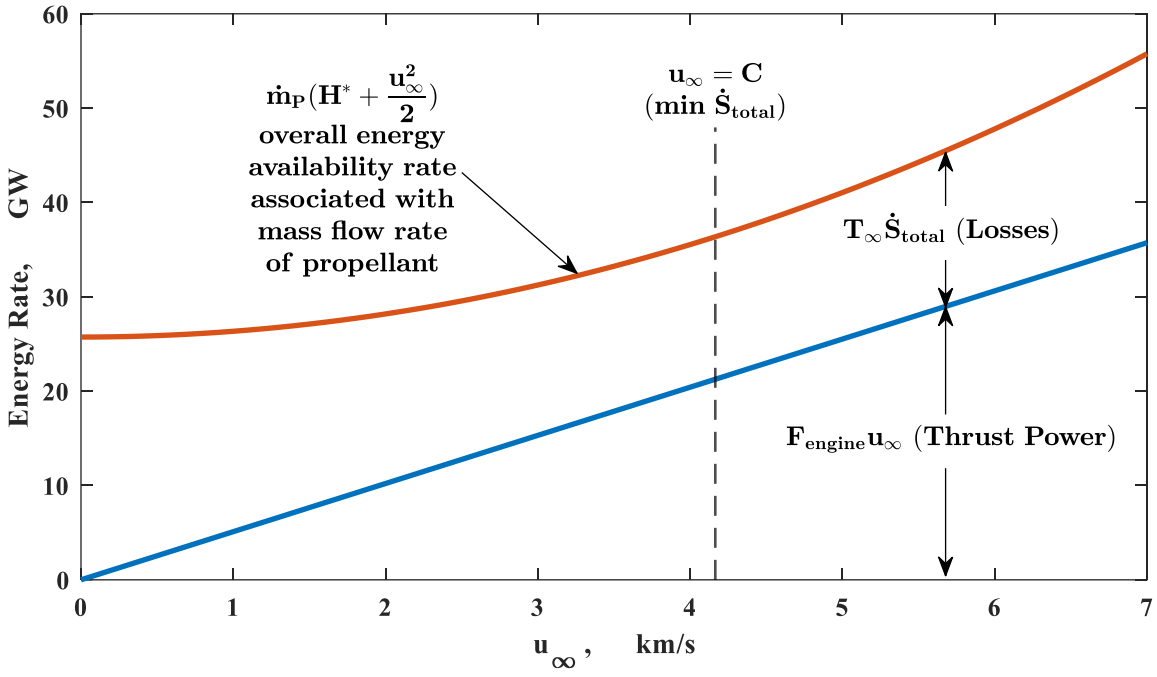


Figure 2. Energy utilization rate of overall energy availability in terms of loss rate and vehicle force (thrust) power rate [Eq. (1)]; stage 2 Saturn V nominal parameters, no atmospheric drag, altitude less than 100 km.

Figure 3 shows the respective contributions of both thermochemical availability $H^*$ and the kinetic energy associated with the stored propellant to the overall energy availability rate. The thermochemical availability term is constant with flight velocity, while the propellant kinetic energy (associated with the stored propellant being carried at the flight velocity of the vehicle) increases with the square of flight velocity. The significant impact of the kinetic energy term at high flight speeds is apparent; at flight velocities above 6000 m/s, the kinetic energy contribution becomes larger than the thermochemical availability contribution. Figure 3 also provides the value of the kinetic energy rate of the propellant at nozzle exit; it is, in fact, about 41% of the thermochemical availability. This quantity (kinetic energy rate of the propellant at nozzle exit) is nominally constant at the indicated value across all ranges of flight velocity and altitude.

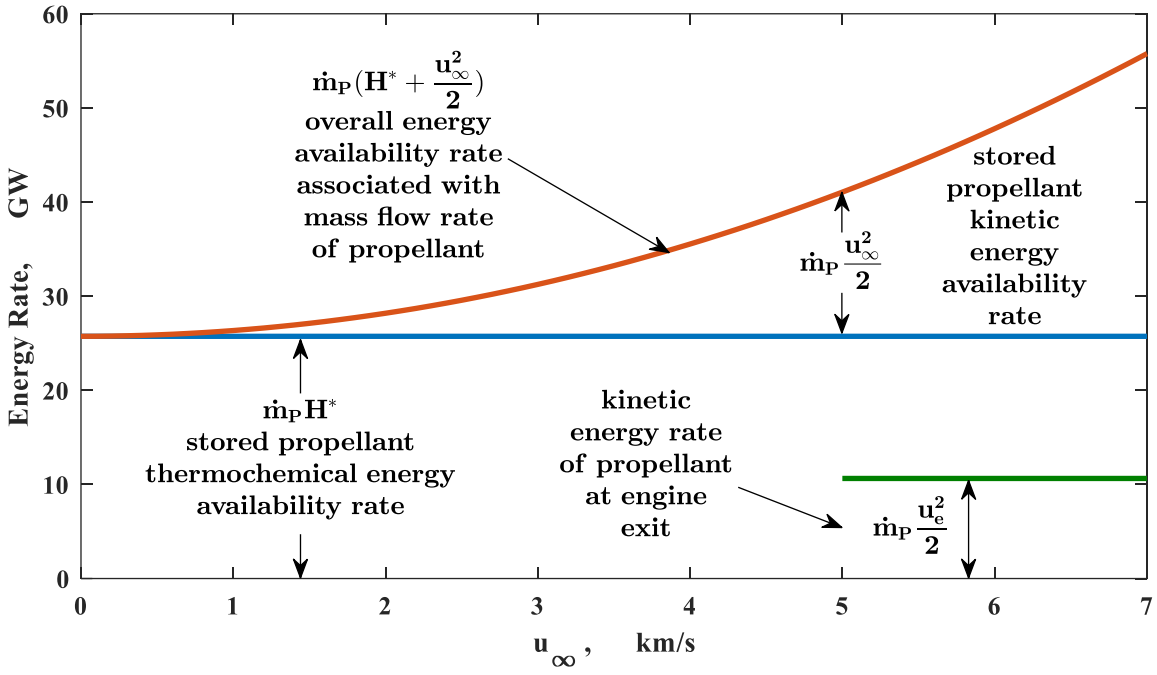


Figure 3. Energy availability rate of propellant in terms of thermochemical availability $H^*$ and kinetic energy of propellant (referenced to surroundings) [Eq. (1)]; stage 2 Saturn V nominal parameters, no atmospheric drag, altitude less than 100 km.

An energy utilization effectiveness $\eta$ based on the Eq. (1) balance is defined; $\eta$ is defined as the ratio of realized vehicle force power to the overall energy availability rate associated with the mass flow rate of propellant:

$$\eta \equiv \frac{F_{\text{engine}} u_\infty}{\dot{m}_P \left( H^* + \frac{u_\infty^2}{2} \right)} = \frac{C u_\infty}{H^* + \frac{u_\infty^2}{2}} \tag{6}$$

Figure 4 plots $\eta$ vs flight velocity for the J-2 rocket engine. By differentiation of Eq. (6) with respect to flight velocity, this effectiveness (assuming negligible drag and operation at constant altitude) can analytically be shown to maximize at the flight velocity corresponding to $\sqrt{2H^*}$:

$$\eta \quad \text{maximized at} \quad u_\infty = \sqrt{2H^*} \tag{7}$$

This condition can be observed in Figure 4 for the J-2 propulsion system ($u_\infty$ for maximum $\eta$ = 6500 m/s). Maximum $\eta$ corresponds to a different (higher) flight velocity than that required for minimization of the entropy generated per mass of propellant; this difference is due to the linear increase in thrust power and the minimum in overall energy availability rate (followed by a quadratic increase) as seen in Figure 2.

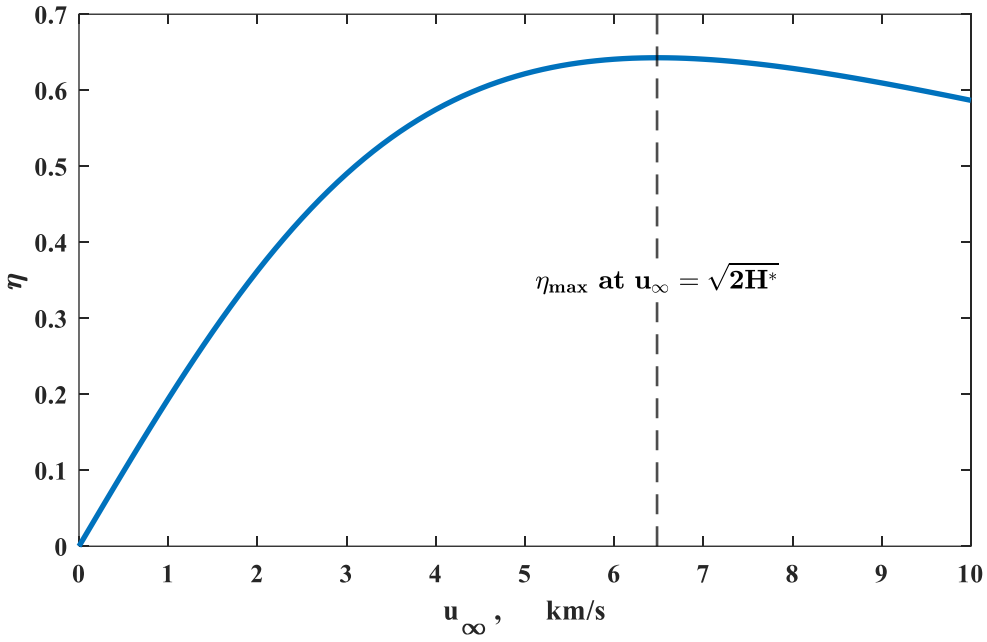


Figure 4. Energy utilization effectiveness $\eta$ vs flight velocity [Eq. (6)]; J-2, no atmospheric drag, 100 km altitude.

## 6. ANALYTICAL INVESTIGATION OF ENGINE ENTROPY GENERATION AND IMPACT ON ROCKET PERFORMANCE

In this section, the entropy generation that occurs within the rocket engine flowpath is investigated in terms of its impact on the following characteristics (at a given flight velocity and altitude): 1) entropy generation in the wake, 2) energy utilization effectiveness

$\eta$ (developed and discussed in the previous section), 3) thrust losses due to entropy generation, and 4) propellant usage associated with overall (engine and wake) entropy generation. This is done by defining a range of reference (analytic) engine flowfields that have varying entropy generations within the engine, increasing from zero (corresponding to a thermodynamic reference "isentropic engine") to large values of entropy generation, such that the actual engine falls within that defined range.

## 6.1. PARAMETRIC ENGINE ENTROPY GENERATION RATIO *K*

A parametric entropy generation ratio, designated $K$, is defined as the ratio of the entropy generation rate in a "reference" engine flowfield with more (or less) entropy generation than an actual engine (with representative engine characteristics and modeling techniques, as discussed earlier) to the entropy generation rate inside the actual engine:

$$K \equiv \frac{\dot{S}_{\text{engine (reference)}}}{\dot{S}_{\text{actual engine}}} \tag{8}$$

This definition implies that, for the actual case, $K = 1$. For the "isentropic reference" flowfield (termed here the "ideal engine"), for which entropy generation in the reference engine flowfield is zero (however still having some entropy generation in the wake), $K$ is by definition zero. For a reference engine with entropy generation greater than that of the actual engine, $K$ is greater than 1. Note that (especially for small $K$) these are, by definition, reference engine flowfields only; for instance, it is not practically feasible to achieve an "ideal reference" ($K = 0$) device based on a rocket configuration, even though it is not thermodynamically excluded by general second law/availability principles. Nevertheless, it ($K = 0$) serves as a fundamental reference from which to measure energy availability

performance. Examination of trends in the vicinity of $K = 1$ is particularly useful. Engine flowfields near $K = 1$ are indeed physically attainable (i.e., through optimization efforts that can decrease $K$ below 1, by reducing entropy generation in the engine, or conversely through design changes that may increase entropy generation, thus increasing $K$ above 1). For this analysis, the chemical composition at nozzle exit is fixed based on the actual engine chemical kinetics, for all values of $K$. This is done in order to isolate and examine the effects of entropy generation within the engine on the quantities of interest (wake entropy generation, effectiveness, lost thrust, and fuel usage).

## 6.2. WAKE ENTROPY GENERATION

For any reference engine flowfield ($K \neq 1$), with more or less entropy generation than that which occurs in the actual engine ($K = 1$), the wake entropy generation necessarily varies. This is because the wake equilibration process is itself dependent on the nozzle exit conditions that are, in turn, dependent on the amount of entropy generation within the engine itself. Thus, to quantitatively evaluate the entropy generation rates in the wakes for all reference engine flowfields with $K \neq 1$, reference nozzle exit properties must be determined. A simple one-step solver, based on fixed propellant tank conditions and a defined entropy flow rate (based on the value of $K$), is used to calculate reference nozzle exit conditions.

## 6.3. THRUST LOSS DUE TO ENTROPY GENERATION IN THE ENGINE

Lost thrust is the direct measure of the thrust force that is not realized by the device due to entropy generation within the engine. Lost thrust is defined in Eq. (9) as the

difference between the thrust ($F_{\text{ideal engine}}$) of the ideal reference device ($K$ = 0) and the thrust of a reference engine of interest with some entropy generation ($K \neq 0$):

$$F_{\text{lost}} = F_{\text{ideal engine}} - F \tag{9}$$

## 6.4. PROPELLANT USAGE ASSOCIATED WITH ENTROPY GENERATION

It is useful to quantify the amount (or fraction) of propellant flow rate that is necessary due to entropy generation occurring within an engine flowfield (from tanks to nozzle exit). For any value of $K$, a ratio $\mu_{\text{engine}}$ is defined as the difference in propellant mass flow rates required between the engine flowfield of interest (where $K \neq 0$) and the ideal reference engine ($K$ = 0), normalized by the overall propellant mass flow rate of the engine flowfield of interest. This parameter can readily be written in terms of the thrust of the engine flowfield of interest ($F$, obtained for some $K$), the propellant mass flow rate of this engine flowfield of interest, and the nozzle exit conditions of the ideal engine:

$$\begin{aligned}\mu_{\text{engine}} &= \frac{\dot{m}_{P,K\neq0} - \dot{m}_{P,K=0}}{\dot{m}_{P,K\neq0}} = 1 - \frac{F - A_e\left(P_{e,\text{ideal engine}} - P_\infty\right)}{u_{e,\text{ideal engine}}\dot{m}_{P,K\neq0}} \\ &= \frac{\dot{m}_{P\text{ associated with entropy generation in engine}}}{\dot{m}_{P\text{ total}}}\end{aligned} \tag{10}$$

It is also useful to quantify the amount of propellant flow rate that is necessary due to all entropy generation associated with a rocket engine, including the wake entropy generation. [Note that the $\mu_{\text{engine}}$ measure defined in Eq. (10) does not include the propellant usage associated with wake entropy generation that occurs even for the $K$ = 0 case.] A completely isentropic device encompassing the global control volume from freestream to wake exit (implying neither any losses within the reference engine flowfield,

nor any losses within the equilibration process in the wake, i.e., mandating full recovery of all onboard energy availability, $\eta = 1$) can therefore be referenced. This is done to quantify the maximum possible thrust force that can be developed with the given onboard energy availability. This global (overall) ideal device, in fact, is the absolute reference point for measuring entropy generation effects. The resulting parameter, $\mu_{\text{overall}}$, is defined in Eq. (11). It can also be written as $1 - \eta$ in terms of the instantaneous energy availability effectiveness defined in the previous section:

$$\mu_{\text{overall}} = 1 - \frac{u_\infty F}{\dot{m}_P \left( H^* + \frac{u_\infty^2}{2} \right)} = \frac{\dot{m}_{P \text{ associated with all entropy generation}}}{\dot{m}_{P \text{ total}}} = 1 - \eta \tag{11}$$

## 6.5. CASE STUDY OF THE EFFECTS OF ENTROPY GENERATION ON ROCKET PERFORMANCE

This subsection provides for the J-2 rocket engine (as described earlier) various parametric impacts of varying engine entropy generation (using the ratio $K$) on the following quantities: wake entropy generation (specifically the ratio of wake to engine entropy generation), energy availability effectiveness $\eta$, lost thrust due to entropy generation, and propellant usage associated with entropy generation as measured using $\mu_{\text{engine}}$ and $\mu_{\text{overall}}$. The actual ($K$ = 1) results are obtained at a nominal operating condition corresponding to flight in the atmosphere at an altitude of 100 km, a flight velocity of 5 km/s, and an oxidizer-to-fuel ratio of 4.5 for a fully open propellant utilization valve (used to vary the mixture ratio) [28]. For the following results, the actual engine flowfield (for $K$ = 1) is obtained with no friction losses assessed in the nozzle, that is, all entropy generation in the engine is due to the chemical kinetics (as well as nominal

propellant feed systems losses, as described earlier). This implies in turn that the case of $K$ = 1 here provides the "best possible" actual performance for a real rocket engine constrained by its design physics; generally, $K$ would be greater than 1, as other losses in the engine are appropriately considered and added.

The parameter $K$ is then varied (based on the actual entropy generation obtained from the model of the actual engine in operation) from 0 (ideal reference engine with no engine entropy generation) to values greater than 1 (entropy generation in the reference engine greater than the actual engine). For values of $K$ decreasing from 1 (i.e., decreasing entropy generation), computed reference exit temperatures and pressures fall progressively, while the exit velocity rises. At low-enough values of $K$ (for $K \lesssim 0.84$), the mandated entropy flow rates are actually too low for all the constituents at the nozzle exit to be assessed entirely in the gaseous phase, mandating the use of a simplified modeled liquid–vapor saturated mixture. The impact of increased entropy generation in the engine over that incurred by the actual engine is modeled by values of $K$ larger than 1. More entropy generation, as expected, drives the reference engine flowfields to choke (exit Mach number reaching unity); this occurs at about $K \approx 1.18$. Therefore, results are shown for a maximum $K$ of 1.15.

Shown in Figure 5 are the impacts of changing entropy generation within the engine (i.e., varying $K$) on resulting entropy generation characteristics in the wake ($\dot{S}_{\text{wake}}$; blue line) and within the overall global control volume ($\dot{S}_{\text{total}}$; orange line). Wake and total entropy generation in this figure across the $K$ range are normalized by the corresponding wake and global entropy generation for the actual engine ($K$ = 1). Both of these ratios increase monotonically with increasing $K$ across the $K$ range; this indicates that the wake

entropy generation always increases as engine entropy generation increases. Note that the total entropy generation ratio (orange line) increases faster than the wake contribution for smaller $K$. This is because this quantity is the summation of both the engine entropy generation (increasing with $K$ by definition) and the wake entropy generation. However, the slopes of the ratios begin to increase significantly (and the ratios merge) for values of $K$ greater than about 0.9, demonstrating the increasing sensitivity of engine performance to entropy generation for meaningful values of $K$ (values around 1). This shows the cascading effect of entropy generation in driving down engine performance in general; losses mount nonlinearly in terms of decreasing performance; a given loss in a flowfield with larger overall entropy generation has a bigger impact than the same loss in a flowfield with less overall entropy generation.

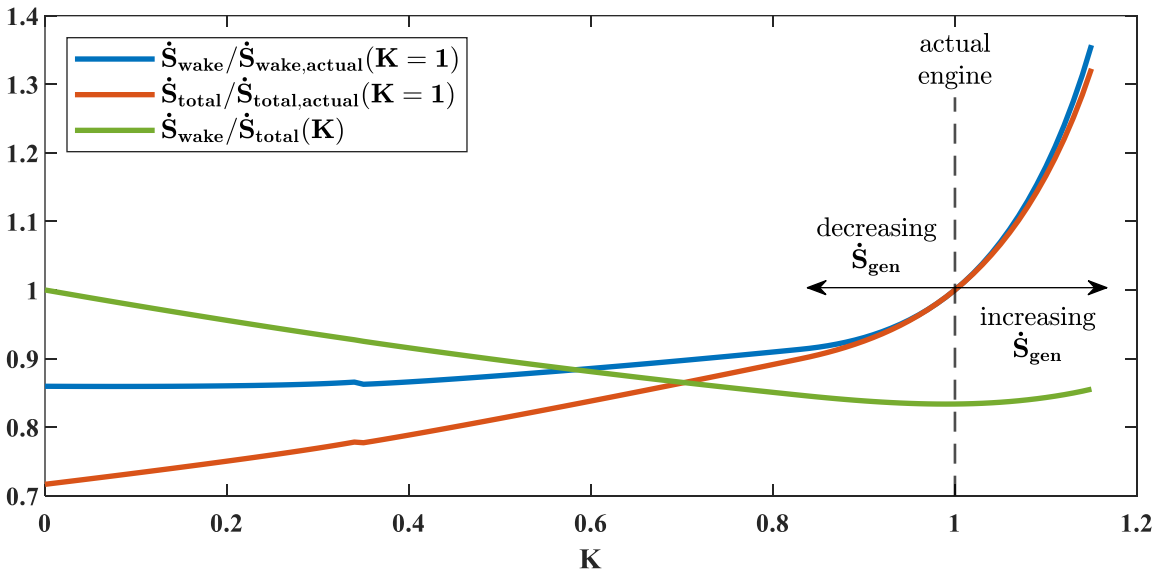


Figure 5. Normalized entropy generation rates with varying entropy generation rate in the engine; J-2,100 km altitude, $u_\infty$ = 5 km/s, $O/F$ = 4.5.

The merging of the wake and total entropy ratios at high $K$ indicates that the wake losses become dominant for high-entropy-generation flowfields. Also shown in Figure 5 is the distribution of the fraction of wake losses to total losses across the $K$ range (the green line); as discussed previously, due to the flight velocity of 5 km/s being close to the computed exit velocity for the $K$ = 1 case, this ratio is minimized very near $K$ = 1 in this figure.

Figure 6 provides the parametric distribution of (normalized) engine thrust developed across the $K$ range as well as the related normalized lost thrust due to engine entropy generation. The ideal reference engine ($K$ = 0) develops 23% more thrust than the actual engine. Increasing entropy generation inside the engine results in an increasing larger drop in thrust (mirrored by the symmetric increase in lost thrust), such that a 15% increase in entropy generation results in an associated thrust drop of about 27%.

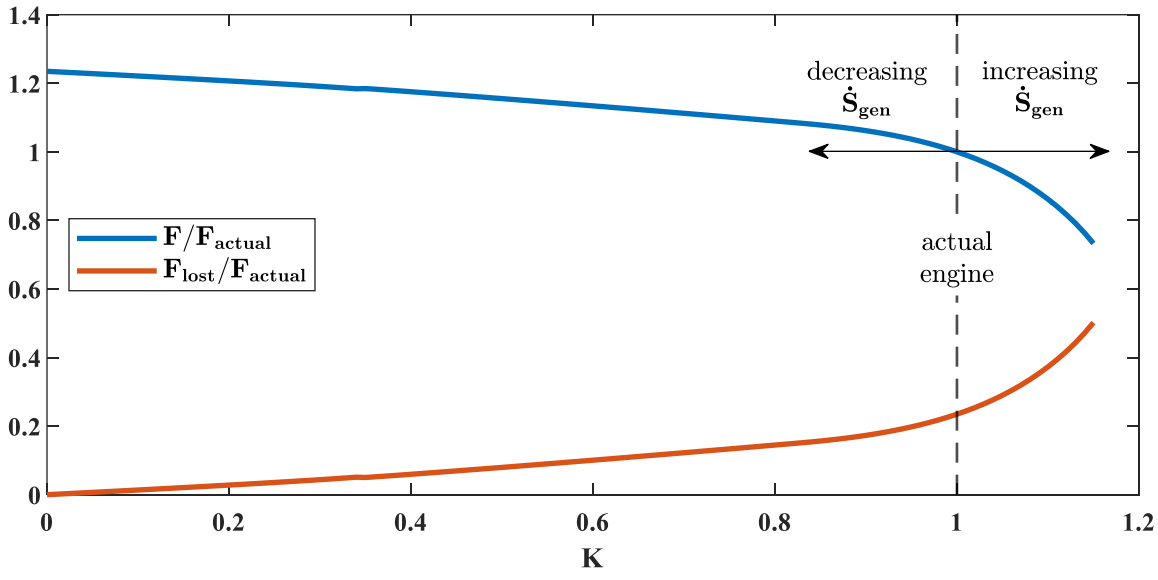


Figure 6. Normalized thrust and normalized lost thrust with varying entropy generation in the engine; J-2,100 km altitude, $u_\infty$ = 5 km/s, $O/F$ = 4.5.

Figure 6 demonstrates the significant and critical nonlinearity of thrust and thrust losses with entropy generation inside the engine. Again, as shown in previous figures, the cascading effect of increasing entropy generation on decreasing engine performance is seen. (Note the rapid thrust loss near $K$ = 1 as entropy generation is increased, compared to that for low $K$ flowfields.)

As described previously, the rate of energy availability expenditure is directly proportional to the propellant mass flow rate; a portion of this mass flow rate is required to overcome entropy generation. In Figure 7, both $\mu_{\text{engine}}$ and $\mu_{\text{overall}}$ are plotted over the range of $K$ from 0 to 1.15.

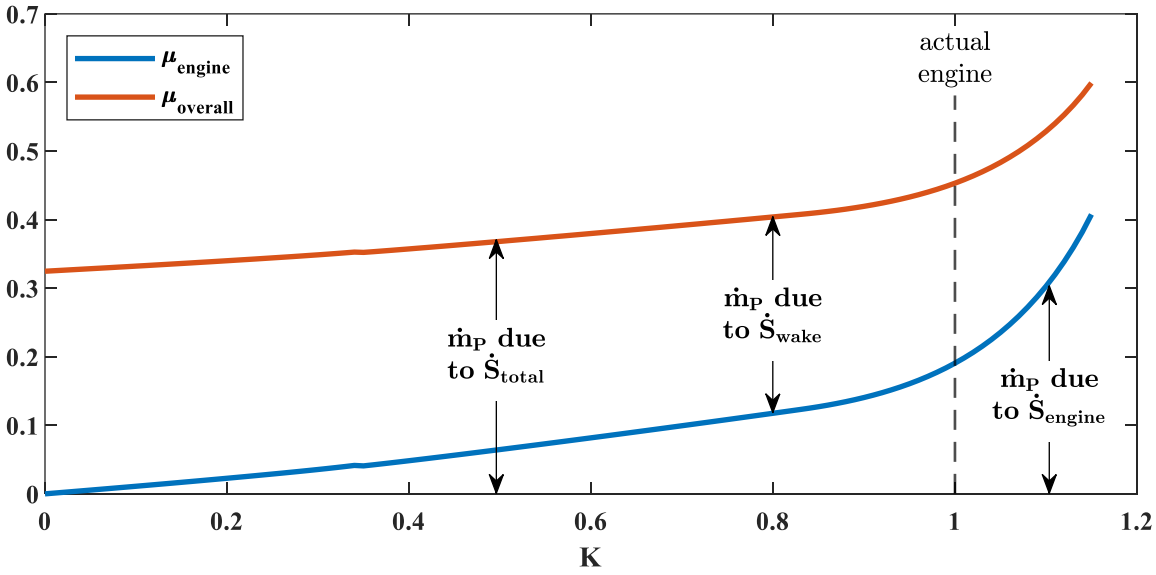


Figure 7. Variation of the fractions of propellant mass flow rate used to overcome losses in the engine and total losses with varying entropy generation in the engine; J-2,100 km altitude, $u_\infty$ = 5 km/s, $O/F$ = 4.5.

For the actual engine, about 19% of the propellant flow rate is used to overcome entropy generation that occurs solely in the engine. In addition, 45% of the propellant

expended by the actual engine is used to overcome all losses (including entropy generation in the wake). For the reference isentropic engine (no entropy generation in the device, $K = 0$), approximately 32% of the propellant mass flow rate is needed to overcome losses, which occur entirely in the wake for that case. As with the other performance parameters presented earlier, the rise in these mass flow rate fractions becomes significantly larger for larger entropy generation rates.

A primary observation in this study is the quantification of the highly nonlinear effect of the entropy generation (that occurs within the engine) on various aspects of performance. At higher levels of entropy generation (particularly for $K > 1$), a given increase in entropy generation results in a significantly larger degradation of performance than an increase in entropy generation of the same magnitude at low levels of entropy generation within the engine ($K < 1$). This is evident in terms of both thrust and the instantaneous effectiveness (and correspondingly for the fractions of propellant used to overcome losses). The results also establish that the entropy-performance penalties for a given engine are entirely dependent on the actual flowfield and entropy generation history that is uniquely associated with that given engine. Also shown is the relatively narrow margin for meaningful improvement within a typical rocket engine, especially when realistic reductions in entropy generation are assessed. For instance, even when considering the thermodynamic reference point of the "ideal reference engine," which cannot practically be achieved of course, the absolute limit to any theoretical benefit is only about 20% in terms of thrust or propellant usage necessary to overcome entropy generation/losses.

# 7. APPLICATION OF ENERGY UTILIZATION ANALYSIS TO LEGACY ROCKET SYSTEMS

This section first provides representative results of a parametric investigation of energy utilization-related quantities for the legacy rocket engine systems that have been modeled in this work (the F-1 and the J-2). The capability developed encompasses operation of these systems in the atmosphere over a wide range of altitudes, flight velocities, and oxidizer-to-fuel mixture ratios (at the nominal operational total mass flow rate of propellant). The three parameters of altitude, flight velocity, and propellant mixture ratio define the point of operation for an engine; the ranges of values chosen for each of the parameters then define the domain of operation. Although a large number of performance parameters of interest in the present study have been evaluated at all operating points, only two representative "slices" of the results are provided and discussed here.

The second part of this section uses engine modeling as described previously, and also rocket trajectory and external drag information as obtained from the Apollo 11 flight data [35], to provide time dependent assessments of entropy generation in the wake and the energy utilization effectiveness $\eta$ from launch to second-stage burnout.

## 7.1. PARAMETRIC STUDY OF THE ROCKETDYNE F-1 AND J-2 ENGINES

Figure 8 provides contours of the ratio of entropy generation rate in the wake to the engine entropy generation rate for the nominal $O/F$ mixture ratio for the J-2 engine across a range of flight velocities from 0 to 10 km/s and for altitudes from 0 to 200 km. These results can also be viewed directly in terms of the trends for "raw" wake entropy generation alone, because the engine entropy generation (from tanks to exit plane of the nozzle) does

not change with either flight velocity or altitude (although it does vary with $O/F$ mixture ratio). The minimum wake entropy characteristics in terms of flight velocity dependence are seen to correspond to where the flight velocity is equal to the effective exhaust velocity of this engine (around 4100 m/s); this result is also predicted analytically in previous sections.

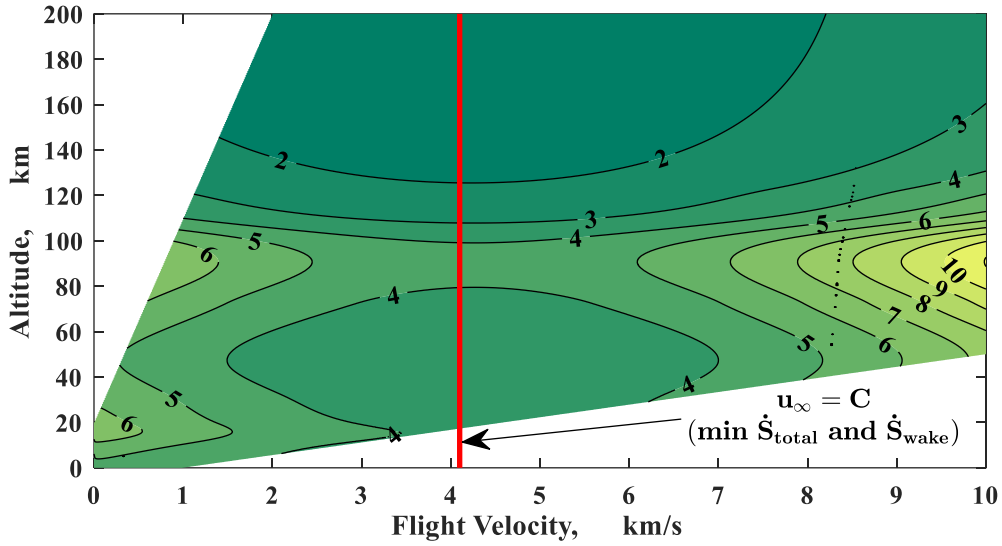


Figure 8. Ratio of entropy generation in the wake to entropy generation in the engine, $\dot{S}_{\text{wake}}/\dot{S}_{\text{engine}}$, over ranges of flight velocities and altitudes. J-2 at $O/F$ = 5.5.

The wake to engine entropy generation ratio also exhibits a dependency on altitude such that the ratio becomes higher at lower atmospheric temperatures, with (two) maxima occurring in the tropopause (~15 km) and in the mesopause (~90 km). Ambient temperature strongly impacts the thermochemical energy availability $H^*$, which in turn strongly impacts entropy generation. The magnitude of entropy generation rate in the wake is always higher than that occurring within the engine; the ratio (wake to engine) can be as

high as 11. These same trends are found for the F-1 engine; however, the ratio (wake to engine) can be as high as 22. These very high ratios of wake to engine entropy generation underscore the relative importance (or rather dominance) of the wake zone in terms of comprehensively measuring and accounting for losses in realizing the thermochemical and kinetic availability of the stored propellant.

Figure 9 provides the parametric variation of the energy availability effectiveness with respect to flight velocity and altitude for the F-1 engine at a nominal $O/F$ mixture ratio of 2.27.

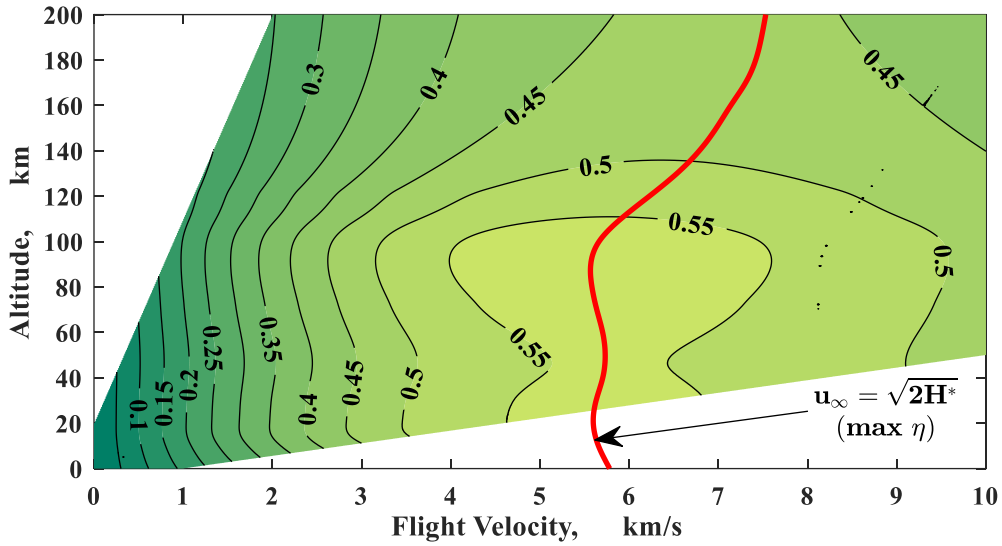


Figure 9. Energy availability effectiveness, $\eta$, over ranges of flight velocities and altitudes. F-1 at $O/F$ = 2.27.

In light of the previous discussion and analysis, the trends observed are seen to correspond to what is expected. Specifically, energy availability effectiveness has been shown to theoretically maximize where $u_\infty = \sqrt{2H^*}$. For the F-1, this corresponds to

approximately 5500 m/s for the nominal $O/F$ ratio, which is mirrored in this figure. Additionally, as altitude increases, $H^*$ tends to increase, which tends to drive the effectiveness down for moderate to high flight velocities, again as seen in the figure. Temperature effects on the effectiveness are also seen at lower flight velocities in this figure; two minima occur at low to midrange flight velocities and at altitudes corresponding to low atmospheric temperatures (tropopause and mesopause). The trends are similar qualitatively for the J-2 engine, however, differ in magnitude. At maximum energy utilization effectiveness, approximately 35–45% of the total available energy is lost (not available to produce vehicle force power) due to overall entropy generation.

## 7.2. SATURN V ASCENT CASE STUDY

The methodology described in earlier sections is now applied to analyze the first- and second-stage flight of the Apollo 11 mission. These results, however, include imposed external drag time histories (and resulting entropy generation) for the vehicle stack (as obtained from the available flight data [35]), that is, they do not represent stand-alone rocket performance as do prior results in this paper. Specifically, in this study, the engine models developed and described earlier are used in conjunction with available trajectory and drag data from the actual mission. Total mass flow rate of propellant is held constant at the nominal/design values for each engine during the flight (rather than modeling nuanced changes in throttle setting during the flight). Shown in Figure 10 is a comparison between actual performance (as obtained from trajectory data) and the performance as calculated by the current models developed for the engines and using the energy availability balance, Eq. (1), to obtain thrust.

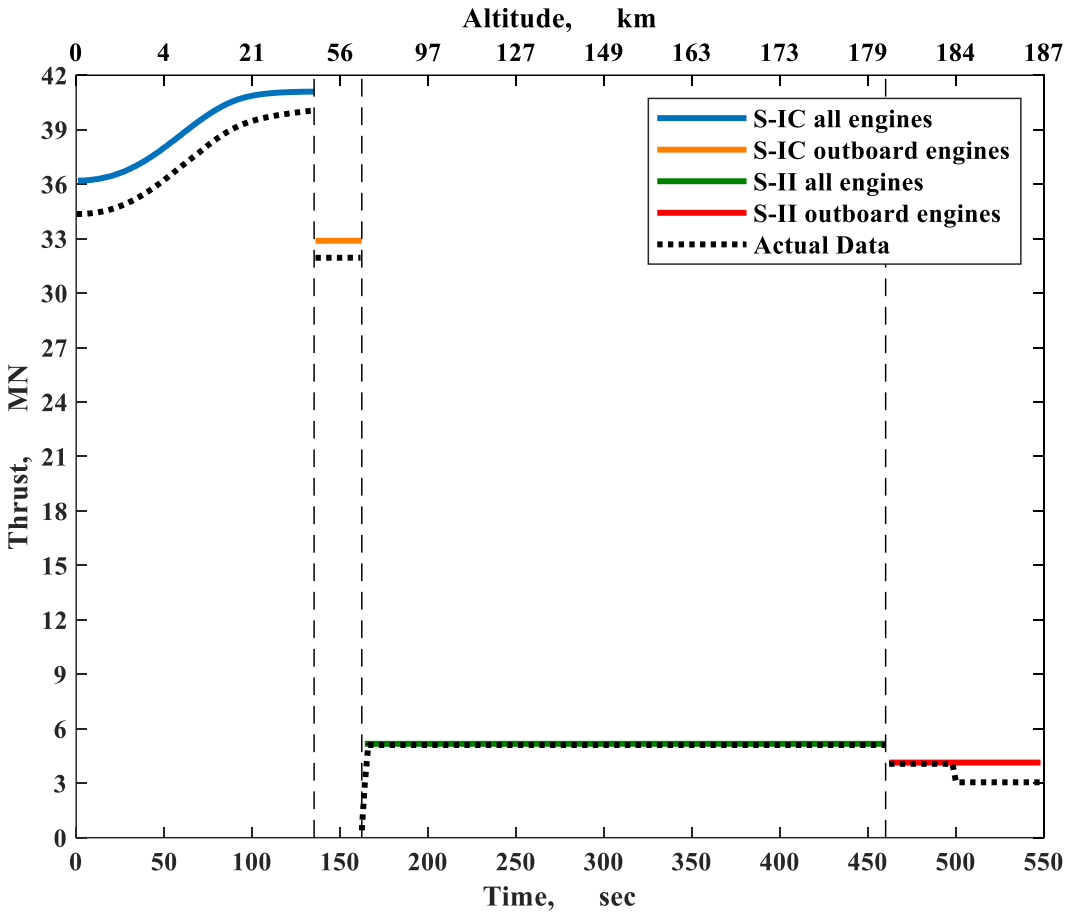


Figure 10. Saturn V first- and second-stage thrust history.

Figure 10 shows the evolution of predicted vs actual engine thrust with mission time. Agreement is good; slight overprediction of thrust in the model is expected due to the approximation used in the current study that all entropy generation in the propulsion system was associated with chemical reaction, that is, other losses due to friction, etc., in the nozzles were not modeled. Note that near the end of the second-stage operation of the flight, the engines in flight were throttled down. However, this is not modeled. (Hence, the step down in thrust is not reflected by the modeled results shown in the present study.) The modeled second-stage performance is more accurate than that of the first stage. This is

attributed to the fact that the simplified hydrogen/oxygen chemistry model better represents actual $H_2/O_2$ combustion processes; the simplified (reduced) model used for the significantly more complex RP-1 chemistry for stage 1 flight is inherently less accurate. Even though these results include external drag (as obtained from the available flight information), and hence associated effects on entropy generation, the entropy generation rate associated with external drag is, as expected, much less than that of the rocket engine and/or the wake. It is small enough that it can generally be neglected without significantly affecting results.

Figure 11 provides a history of the thermochemical availabilities $H^*$ for the flight of the Apollo 11 system from launch to second-stage burnout (taken directly from Ref. [4]). This figure shows the large effect of altitude on the second-stage J-2 engine thermochemical energy availability (driven mainly by ambient temperature at low and intermediate altitudes and by both ambient temperature and pressure at high altitudes), and illustrates the difference between $H^*$ for the F-1 and J-2 propulsion systems. The thermochemical energy availability variance during the mission has an enormous impact on entropy generation in the wake, as shown in the energy utilization balance, Eq. (1). Also shown in this figure for comparison to the $H^*$ are the heating values of the propellants for the respective stages. $H^*$ can be closely approximated by the nominal lower heating value of propellant at lower altitudes, but increases significantly for higher altitudes, mainly due to high ambient temperatures [1,4].

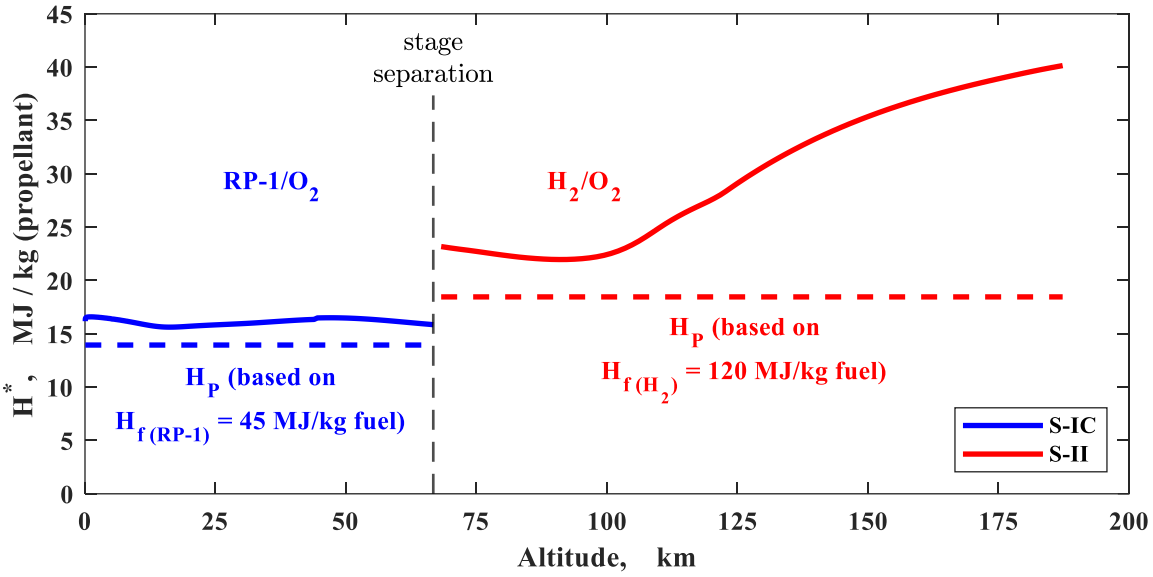


Figure 11. Thermochemical energy availability of propellant $H^*$ for Saturn V first- and second-stage operation (also shown are heating values of propellant $H_P$ based on heating values of fuel $H_f$ evaluated at standard conditions).

The ratio of entropy generation in the wake to that occurring within the engines during the first- and second-stage flight of Apollo 11 is tracked in Figure 12. This ratio is maximized at approximately 7 within the first-stage operation, dropping to a first-stage minimum of about 4.25. The increase in this ratio from time of launch to this maximum of 7 at approximately 95 s is due to the drop in ambient temperature with increasing altitude in this part of the flight. (The work rate loss in the energy utilization balance is proportional to the ambient temperature as well as to the entropy generation rate; hence, entropy generation in the wake increases as ambient temperature drops, with other things being constant.) This decrease in temperature (over this portion of the flight) in fact has a bigger impact on the wake entropy generation than the countering tendency of wake entropy generation to drop as flight velocity approaches nozzle exit velocity. (Note that this trend was explored in an earlier section at a constant altitude, hence at constant ambient

temperature.) For flight past this point, increases in ambient temperature and the fact that the vehicle flight velocity continues to approach the exit velocity of the J-2 engine both tend to drive the entropy generation in the wake lower.

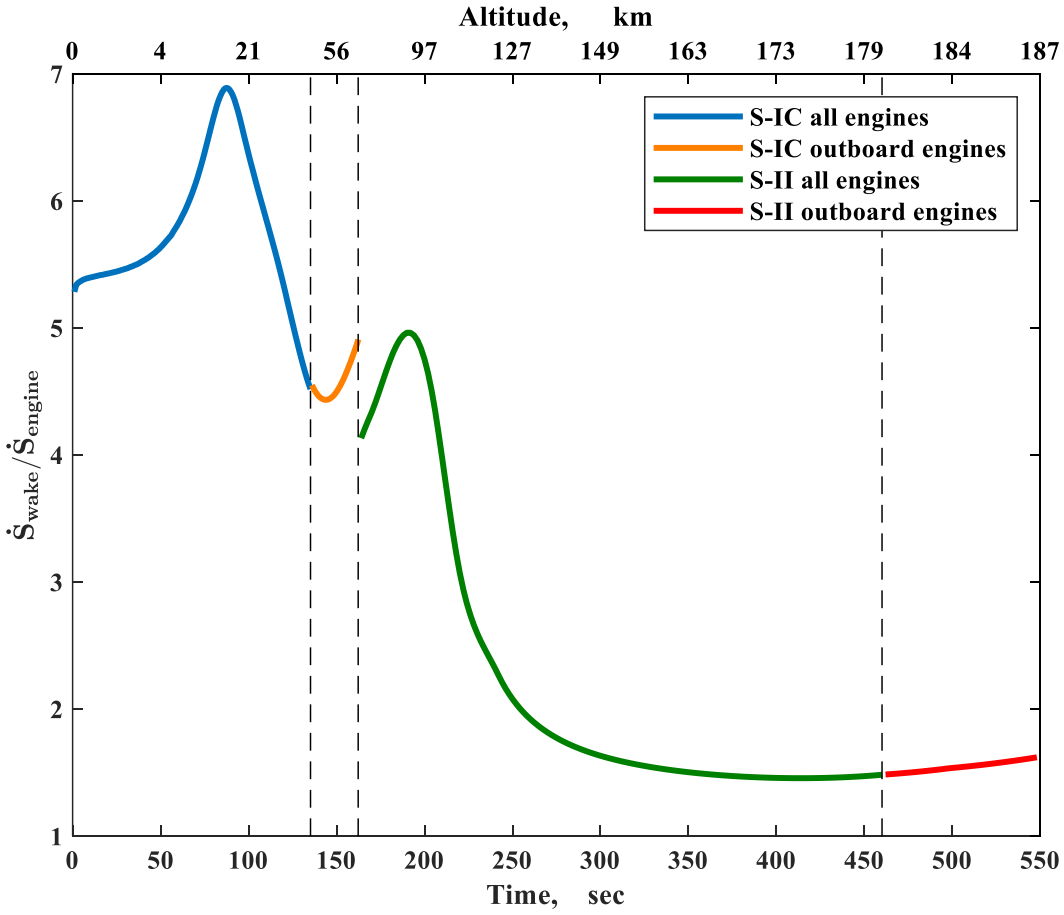


Figure 12. Saturn V first- and second-stage ratio of entropy generation rate in the wake to that in the engine history.

For the second stage, the highest value of the ratio is approximately 5 early on in the second-stage burn, again due primarily to ambient temperature effects. It drops significantly at an altitude of approximately 100 km (nearly 200 s into the flight) and reaches a minimum of about 1.5. This distinct drop in wake entropy generation is primarily

due to the fact that, in this range, the vehicle flight velocity is again approaching the J-2 nozzle exit velocity (around 4500 m/s). Ambient temperature and pressure effects associated with increasing altitude, even though significant in terms of increasing the $H^*$ in this portion of the flight, do not appreciably begin to drive the entropy generation up until flight velocities exceed the effective exhaust velocity. (Note the upturn in the wake entropy generation past about 400 s.)

The time evolution of the instantaneous energy utilization effectiveness of the Apollo 11 stack is shown in Figure 13. This parameter was described previously for nominal flight characteristics in earlier sections. Because the numerator of this effectiveness is vehicle force power, it increases monotonically from launch (as expected) and steadily rises as the flight velocity increases to a first-stage maximum of about 0.4 at first-stage burnout. The thermochemical energy availability does not change appreciably enough (due to ambient temperature changes with altitude) during this part of the flight to significantly affect the trend that $\eta$ will increase as flight velocity increases. It should be recalled that $\eta$ is maximized at a flight velocity of $\sqrt{2H^*}$ or around 5500 m/s for the F-1, which is well above the velocity at first-stage burnout. The instantaneous effectiveness of the J-2 engines during the second-stage operation shows less variation than the F-1 (first stage) engines. It initially increases slightly, then decreases slightly to a minimum of about 0.33 due to (increasing) temperature and (decreasing) pressure with higher altitudes driving the $H^*$ to larger values, then gradually increases to a final value of just over 0.45 as the flight velocity climbs toward the (never achieved) optimal value of $\sqrt{2H^*}$ for the second stage. This final point is the maximum effectiveness achieved across the first- and second-stage operation of the Apollo 11 stack (and corresponds to the highest flight velocity). All

trends in energy utilization observed in this Apollo 11 case study can be readily correlated to the analytical (theoretical) analyses performed in the earlier sections of this paper. Nevertheless, the complex interplay of ambient conditions, flight velocity, propulsion system characteristics, and thermochemical availability considerations results in highly nonlinear performance and effectiveness results across the flight range.

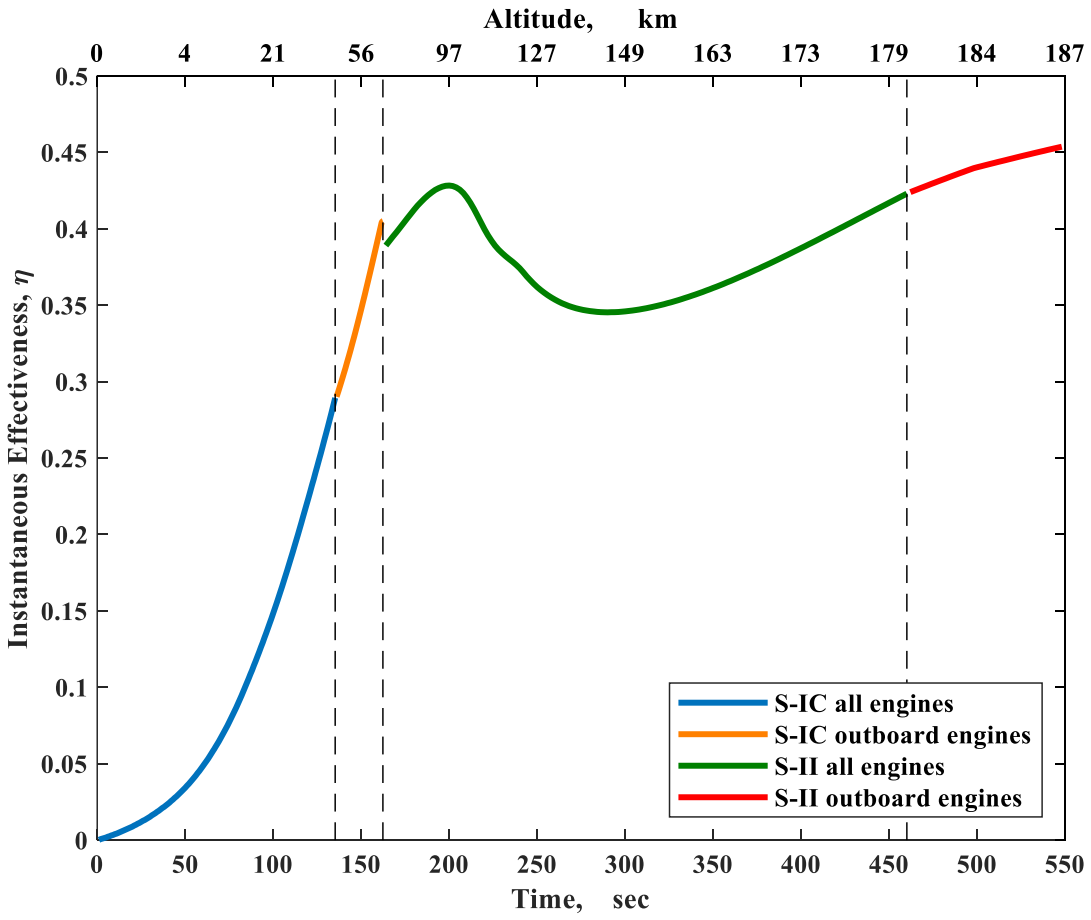


Figure 13. Saturn V first- and second-stage instantaneous energy utilization effectiveness history.

# 8. CONCLUSIONS

This paper provides the detailed description, analysis, and applications of the fundamental relationship between classic vehicle performance, the overall availability and utilization of onboard energy, and entropy generation, with focus on chemical rockets operating in the atmosphere. Utilizing the comprehensive global control volume approach to vehicle flight, the total energy utilization availability associated with the onboard propellant flow rate at any point in the mission of a vehicle is the summation of the thermochemical availability $H^*$ and the directed kinetic energy of the propellant. This overall work availability is measured from the ambient environment in which the vehicle operates (i.e., for atmospheric flight, quiescent air at conditions corresponding to the given altitude). The force power achieved by a vehicle is the productive realization of some fraction of that overall thermochemical and kinetic energy availability. The balance of the overall thermochemical availability that does not produce force power is entirely lost and is directly proportional to the overall generation of entropy in the global control volume.

In developing energy utilization analysis (or availability or exergy analysis) for chemical rockets, it is important that the actual propellant thermochemical and kinetic availability be assessed and used in detailed studies to obtain accurate measures of losses and the impact of entropy generation on vehicle performance. Modeling techniques that are used in the present work for simulating rocket engine performance, as well as the relevant formulations and approaches for evaluating the entropy generation of the vehicle wake and the external aerodynamic flow processes, are described. Example propulsion

systems that are used for case studies and applications of energy utilization in this paper are the Rocketdyne F-1 RP-1/LOX engine and the Rocketdyne J-2 $LH_2$/LOX engine.

Analytical examination of the energy utilization balance that results from control volume analysis is first used to provide fundamental information regarding energy, performance, and losses. The critical importance of the kinetic energy of the stored propellant (due to the propellant in the tanks moving at the flight velocity of the vehicle) is shown, especially for high flight velocities. Differentiation of the energy utilization balance provides the information that the overall entropy generation for rocket-powered vehicles is minimized when the vehicle flight velocity is equal to the effective exhaust velocity of the vehicle; this, in fact, corresponds to a zero gradient in velocity between rocket plume and the ambient environment. This theoretical result is verified using applied models of actual rocket engines in flight. In addition, an instantaneous energy utilization effectiveness $\eta$ is defined to quantify the percentage of (propellant) energy availability rate that is realized as force power developed by the rocket engine. For a given altitude, this effectiveness is found to be a function of flight velocity only, which then permits an analytical solution for the flight velocity that maximizes this effectiveness. The optimum flight velocity in terms of this effectiveness is mathematically equal to $\sqrt{2H^*}$ (without drag). This theoretical result is then verified in applications by utilizing models of actual rocket engines in flight.

The effects of varying entropy generation inside a rocket engine on rocket performance and energy utilization are then analytically investigated. The information obtained are distributions (for varying engine entropy generations) of wake entropy generation, thrust, lost thrust due to entropy generation, and identification of those portions

of the required propellant mass flow rates necessary to overcome 1) engine losses (engine entropy generation) and 2) overall (engine and wake) losses (total entropy generation). The latter propellant mass fraction is shown to be analytically equal to $1 - \eta$.

The impact of entropy generation in the engine on performance and energy utilization parameters is seen to be highly nonlinear, especially in the region of an actual (practical) engine flowfield (i.e., for $K$ near 1 or $K > 1$). In that range, performance losses (degradation) are in (or near) a region of asymptotic growth with increasing $K$, as driven by small increases in entropy generation. Conversely, within that same range, large favorable impacts on performance can be obtained by relatively small decreases in entropy generation (improved design and reduced losses). Results of this analytical study also emphasize the fact that the wake region is dominant in terms of losses (entropy generation) for any amount of entropy generation in the engine. The degree of wake entropy generation is in fact very nonlinear with respect to the entropy generation occurring in the engine itself.

Representative results from the energy utilization balance and related parameters are next shown for ranges of flight velocity, altitude, and oxidizer/fuel ratios ($O/F$) for the F-1 RP-1/LOX engine and the J-2 $LH_2$/LOX engine. These results are given in the form of contour plots. They include contours of the ratio of entropy generation in the rocket wake to entropy generation in the engine across the flight velocity/altitude range. There is, as expected, significant impact on wake entropy generation ratio due to both the ambient temperature (which has large effects on the thermochemical availability $H^*$ and on the lost work term itself in the balance relationship) and the flight velocity. The theoretical result derived previously that entropy generation is minimized at a given altitude when the flight

velocity is equal to the effective exhaust velocity is observed in these results. Contours of the energy utilization effectiveness $\eta$ are provided across the flight velocity/altitude range, again demonstrating the coupled drivers of ambient temperature and flight velocity on the energy utilization balance and the resulting effectiveness definition. This performance map of actual engine performance in terms of $\eta$ provides verification for the theoretical results derived earlier in this paper that the energy utilization effectiveness is maximized when the flight velocity is equal to $\sqrt{2H^*}$. The graphical representation of results in the form of contours, such as shown in this paper, can provide a great deal of information relevant to the energy utilization balance for a rocket engine in flight.

Finally, the fundamental energy utilization balance is applied to and tracked in time for the flight of the Apollo 11 Saturn V rocket stack from launch to second-stage burnout. The time/altitude variation of the thermochemical energy availability $H^*$ during the mission exhibits significant changes across altitude, and hence demonstrates the large impact of altitude on the balance relationship. The energy utilization effectiveness $\eta$ in turn is shown to generally increase throughout the defined mission. The trends in all energy utilization parameters and performance metrics are readily correlated to the theoretical/analytical results obtained earlier, in terms of physical/ functional drivers within the energy utilization balance.

It is important to understand the limitations as well as the potential of energy availability (or exergy) for engineering design of practical aerospace systems. Traditional analysis and performance are properly rooted in (for instance) thrust-to-weight ratios of engines and specific impulses. Thrust (and hence specific impulse) of a rocket engine with fixed $O/F$ ratio and mass flow rate of propellant is essentially constant across the flight

velocity range; it also changes little with altitude. Energy availability and related utilization metrics, however, as viewed from the standpoint of entropy generation (specifically within the wake), are, as shown in this work, highly dependent on both altitude and flight velocity. Furthermore, the effect of entropy generation in the wake is neither directly proportional to the entropy generation in the engine (stand-alone engine or with external drag on the vehicle) nor is it directly proportional to the thrust performance of the vehicle. The energy utilization balance and applications also demonstrate that there is inherently a very large part of the thermochemical energy availability $H^*$ that, because of the physical constraints and physics of a rocket engine, is simply not really available at all to be converted into useful thrust work (at least working within the physical constraints of a rocket engine). However, the actual entropy generated by a rocket engine and downstream wake is thermodynamically a measure of all the thermochemical availability that is not converted into useful thrust work. Properly accounting for and understanding this issue are critical when developing and applying energy utilization (availability/exergy) methods for design and optimization.

The greatest potential of energy utilization analysis (including exergy and availability analysis) for aerospace vehicles is believed to be in overall system-based analysis, design, and optimization of rockets (and aerospace vehicles in general). This is due to the fact that the energy utilization balance for a vehicle in flight provides a single, fundamental, and universal metric (viz. entropy generation) for describing all losses, mechanical, thermal, chemical, electromagnetic, etc., for all vehicle systems and vehicle subsystems, regardless of the degree of integration and fidelity of modeling used. Furthermore, the balance relates this loss metric (entropy generation) directly to

conventional vehicle performance (i.e., thrust). This work and related work in this area demonstrate that the understanding (and the proper accounting) of entropy generation is in fact necessary to a comprehensive understanding of vehicle performance, design, and optimization. Specifically, energy utilization analysis provides the baseline thermofluid dynamic performance references and metrics for consistently measuring all available energy usage and performance (thrust) losses in terms of the single metric of entropy generation. Furthermore, it encapsulates and clarifies the fundamental physics that underlie the principle of flight.

## ACKNOWLEDGMENTS

The authors would like to thank Jose Camberos (U.S. Air Force Research Laboratory, Wright–Patterson Air Force Base) for his invaluable counsel, support, and encouragement in all phases of this and past work involving energy utilization and exergy throughout the years.

## REFERENCES

[1] Riggins, D. W., Moorhouse, D., and Camberos, J., *Entropy Generation and Aerospace Vehicle Performance*, Vol. 238, Progress in Astronautics and Aeronautics Series, Exergy Analysis and Design Optimization for Aerospace Vehicles and Systems, AIAA, Reston, VA, 2011, pp. 181–227, Chap. 6. DOI:10.2514/5.9781600868405.0181.0227

[2] Riggins, D. W., Camberos, J., and Moorhouse, D., *Characterization of Aerospace Vehicle Performance and Mission Analysis Using Exergy*, Vol. 238, Progress in Astronautics and Aeronautics Series, Exergy Analysis and Design Optimization for Aerospace Vehicles and Systems, AIAA, Reston, VA, 2011, pp. 275–307, Chap. 8. DOI:10.2514/5.9781600868405.0275.0307

[3] Riggins, D. W., Camberos, J., Wolff, M., and Bowcutt, K., "Mission-Integrated Exergy Analysis for Hypersonic Vehicles: Methodology and Application," *Journal of Propulsion and Power*, Vol. 29, No. 3, May–June 2013, pp. 610–620. DOI:10.2514/1.B34733

[4] Riggins, D. W., Abbas, M., Wainwright, M., and Camberos, J., "Analysis of Energy Utilization for Chemical Rockets," *Journal of Spacecraft and Rockets*, Vol. 56, No. 3, May 2019, pp. 695–707. DOI:10.2514/1.A34296

[5] Abbas, M., Riggins, D. W., and Watson, M. D., "Entropy-Based Performance Analysis of Chemical Rockets," *AIAA SciTech 2020 Forum*, AIAA Paper 2020-0759, Jan. 2020. DOI:10.2514/6.2020-0759

[6] Watson, M., "System Exergy: System Integrating Physics of Launch Vehicles and Spacecraft," *Journal of Spacecraft and Rockets*, Vol. 55, No. 2, 2018, pp. 451–461. DOI:10.2514/1.A33929

[7] Oswatitsch, K., *Gas Dynamics*, Academic Press, New York, 1956, Chap. 4.

[8] Giles, M., and Cummings, R., "Wake Integration for Three Dimensional Flowfield Computations: Theoretical Development," *Journal of Aircraft*, Vol. 36, No. 2, 1999, pp. 357–365. DOI:10.2514/2.2465

[9] Abbas, M., and Riggins, D. W., "Exergy-Based Performance Analysis of a Turbojet Engine," *52nd AIAA/SAE/ASEE Joint Propulsion Conference*, AIAA Paper 2016-4638, July 2016. DOI:10.2514/6.2016-4638

[10] Bejan, A., "Entropy Generation and Exergy Destruction," *Entropy Generation Minimization: The Method of Thermodynamic Optimization of Finite-Size Systems and Finite-Time Processes*, 1st ed., CRC Press, New York, 1995, pp. 21–47. DOI:10.1201/9781482239171

[11] Riggins, D., "Evaluation of Performance Loss Methods for High-Speed Engines and Engine Components," *Journal of Propulsion and Power*, Vol. 13, No. 2, 1997, pp. 296–304. DOI:10.2514/2.5162

[12] Foa, J., *Elements of Flight Propulsion*, Wiley, New York, 1960, Chap. 13.

[13] Clarke, J., and Horlock, J., "Availability and Propulsion," *Journal of Mechanical Engineering Science*, Vol. 17, No. 4, 1975, pp. 223–232. DOI:10.1243/jmes_jour_1975_017_033_02

[14] Lewis, J. H., "Propulsive Efficiency from an Energy Utilization Standpoint," *Journal of Aircraft*, Vol. 13, No. 4, 1976, pp. 299–302. DOI:10.2514/3.44525

[15] Arntz, A., Atinault, O., and Merlen, A., "Exergy-Based Formulation for Aircraft Aeropropulsive Performance Assessment: Theoretical Development," *AIAA Journal*, Vol. 53, No. 6, 2015, pp. 1627–1639. DOI:10.2514/1.J053467

[16] Arntz, A., and Hue, D., "Exergy-Based Performance Assessment of the NASA Common Research Model," *AIAA Journal*, Vol. 54, No. 1, 2016, pp. 88–100. DOI:10.2514/1.J054127

[17] Ehyaei, M., Anjiridezfuli, A., and Rosen, M. A., "Exergetic Analysis of an Aircraft Turbojet Engine with an Afterburner," *Thermal Science*, Vol. 17, No. 4, 2013, pp. 1181–1194. DOI:10.2298/tsci110911043e

[18] Hayes, D., Lone, M. M., Whidborne, J. F., and Coetzee, E., "Entropy Generation Minimization and Exergy Analysis Approaches for Aerospace Applications—A Review," AIAA Paper 2016-0866, Jan. 2016. DOI:10.2514/6.2016-0866

[19] Riggins, D., McClinton, C. R., and Vitt, P., "Thrust Losses in Hypersonic Engines Part 1: Methodology," *Journal of Propulsion and Power*, Vol. 13, No. 2, 1997, pp. 281–287. DOI:10.2514/2.5160

[20] Riggins, D., "Thrust Losses in Hypersonic Engines Part 2: Applications," *Journal of Propulsion and Power*, Vol. 13, No. 2, 1997, pp. 288– 295. DOI:10.2514/2.5161

[21] Roth, B., "A Work Potential Perspective of Engine Component Performance," *Journal of Propulsion and Power*, Vol. 18, No. 6, 2002, pp. 1183–1190. DOI:10.2514/2.6077

[22] Roth, B., "Comparison of Thermodynamic Loss Models Suitable for Gas Turbine Propulsion," *Journal of Propulsion and Power*, Vol. 17, No. 2, 2001, pp. 324–332. DOI:10.2514/2.5745

[23] Roth, B., "Aerodynamic Drag Loss Chargeability and Its Implications in the Vehicle Design Process," AIAA Paper 2001-5236, Oct. 2001. DOI:10.2514/6.2001-5236

[24] Riggins, D., Taylor, T., and Moorhouse, D., "Methodology for Performance Analysis of Aerospace Vehicles Using the Laws of Thermodynamics," *Journal of Aircraft*, Vol. 43, No. 4, July–Aug. 2006, pp. 953–963. DOI:10.2514/1.16426

[25] Riggins, D., Taylor, T., Moorhouse, D., and Terhune, L., "Methods for the Design of Energy Efficient High-Speed Aerospace Vehicles," *Aeronautical Journal of the Royal Aeronautical Society*, Vol. 111, No. 1119, May 2007, pp. 297–309. DOI:10.1017/S0001924000004541

[26] McBride, B., Zehe, M., and Gordon, S., "NASA Glenn Coefficients for Calculating Thermodynamic Properties of Individual Species," NASA TP-2002-211556, NASA John H. Glenn Research Center at Lewis Field, Cleveland, OH, Sept. 2002.

[27] Oates, G., *Aerothermodynamics of Gas Turbine and Rocket Propulsion*, 3rd ed., AIAA Educational Series, AIAA, New York, 1997, pp. 85–88.

[28] Anon., *NASA Apollo Saturn V News Reference Manual*, NASA, The Boeing Company, Douglas Aircraft Company, International Business Machines Corporation, North American Aviation, Aug. 1967.

[29] *Saturn V Launch Vehicle Flight Evaluation Report-AS-510 Apollo 15 Mission*, NASAMPR-SAT-FE-71-2, Oct. 1971.

[30] Rafferty, C. A., *Altitude Developmental Testing of the J-2 Rocket Engine in Propulsion Engine Test Cell (J-4) (Test J4-1801-23)*, Arnold Engineering Development Center, Air Force Systems Command, Arnold Air Force Station, Tullahoma, TN, June 1968.

[31] Woods, W. D., *NASA Saturn V: 1967-1973 (Apollo 4 to Apollo 17 and Skylab) Owner's Workshop Manual*, Haynes, Sparkford, Somerset, U.K., 2016.

[32] Oefelein, J. C., and Yang, Y., "Comprehensive Review of Liquid Propellant Combustion Instabilities in F-1 Engines," *Journal of Propulsion and Power*, Vol. 9, No. 5, 1993, pp. 657–677. DOI:10.2514/3.23674

[33] Lemmon, E., McLinden, M., and Friend, D., "Thermophysical Properties of Fluid Systems," NIST Chemistry WebBook, NIST Standard Reference Database Number 69, edited by P. J. Linstrom, and W. G. Mallard, National Inst. of Standards and Technology, Gaithersburg, MD, April 2018. DOI:10.18434/T4D303

[34] Kuznetsova, M., and Chulaki, A., "MSIS-E-90 Atmosphere Model," Community Coordinated Modeling Center, NASA, ccmc.gsfc.nasa.gov/modelweb/models/msis_vitmo.php [retrieved 31 Oct. 2019].

[35] Anon., "Apollo/Saturn V Post-Flight Trajectory-AS-506," Boeing Company TR D5-15560-6, Huntsville, AL, Oct. 1969.

## PAPER

# IV. GENERALIZATION AND VALIDATION OF ENERGY AVAILABILITY UTILIZATION METHODOLOGY TO N-STAGE ROCKETS

Mohammad Abbas and David W. Riggins

Department of Mechanical and Aerospace Engineering, Missouri University of Science and Technology, Rolla, MO 65409

## ABSTRACT

The mission-integrated global control volume-based energy availability utilization balance is generalized for an *N*-stage rocket. Terms associated with available energy, losses due to irreversibilities, losses due to discarded mass, and productive energy utilization are formulated for individual stages as well as for an entire mission. The productive energy utilization is defined as the change in kinetic and potential energies of the rocket's payload. The formulation is recast in non-dimensional form and is employed in the study of two special cases: a two-stage rocket 1) operating without drag or gravitational effects, i.e., 'free-space,' and 2) in vertical climb in a constant gravitational field. For both cases, analytical optimization studies are performed that identify the staging velocity which maximizes the productive energy availability utilization for a mandated overall impulse. Application of this analysis to specific configurations for the special cases is then performed. The energy utilization for the free space case is shown to agree with traditional (analytical) mass-based optimization results. The energy utilization approach is shown in

this work to provide a wealth of information relevant to on-board energy usage, losses, and flight performance for rocket-powered vehicles.

## NOMENCLATURE

| Symbol | Description |
|---|---|
| $C$ | Effective exhaust velocity, m/s |
| $E_{\mathrm{AV}}$ | Total energy availability of propellant at beginning of mission, J |
| $F_{x(\mathrm{flight})}$ | Net fluid-dynamic force acting on the vehicle in flight (axial) direction, N |
| g | Gravitational acceleration, m/s$^2$ |
| $H_P$ | Heating value of propellant, J/kg |
| $H^*$ | Total thermochemical energy availability of propellant, J/kg |
| $H^*_{\mathrm{eff}}$ | Effective thermochemical energy availability of propellant (mission integrated), J/kg |
| $h$ | Altitude, m |
| $K$ | Energy availability loss term, J |
| $K^*$ | Non-dimensional energy availability loss term |
| $m$ | Mass, kg |

| | |
|---|---|
| $m_R$ | Instantaneous mass of the rocket, kg |
| $\dot{m}_P$ | Propellant mass flow rate, kg/s |
| $N$ | Total number of stages |
| $n$ | $n$-th stage designator |
| $\dot{S}_{\text{total}}$ | Total entropy generation rate in the global control volume, W/K |
| $T_\infty$ | Ambient/free-stream temperature, K |
| $t$ | Time, s |
| $u_\infty$ | Flight velocity, m/s |
| $V$ | Flight velocity, m/s |
| $\left(\frac{F}{W}\right)_i$ | Thrust-to-weight ratio at the start of a stage's operation |
| $\beta$ | Remaining energy availability, J |
| $\delta$ | Discard mass ratio |
| $\delta^*$ | Discard mass ratio (relative to propellant mass) |
| $\zeta$ | Payload mass ratio |
| $\eta$ | Energy availability effectiveness |
| $\eta_a$ | Accelerator efficiency |

| | |
|---|---|
| $\theta$ | Flight path angle (measured relative to local horizon), degree |
| $\lambda$ | Propellant mass ratio |
| $\tau$ | Time of a specific event (e.g., staging), s |
| $\phi$ | Productive energy availability utilization, J |
| $\phi^*$ | Non-dimensional productive energy availability utilization |

Subscripts

| | |
|---|---|
| $d$ | Discarded mass |
| $f$ | Final |
| $i$ | Initial |
| $n$ | $n$-th stage |
| $P$ | Propellant |
| $s$ | Value at the start of stage operation |

## 1. INTRODUCTION

Rocket staging is a widely used technique in the design and operation of both access-to-space rocket systems and long-range ballistic missiles. Staging offers an

advantage over a single-stage rocket in terms of propellant mass, payload mass, and/or payload final velocity achieved. The work presented in this paper constitutes the application of energy availability utilization and optimization methodology to multi-stage rocket systems. For an accelerating and climbing rocket-powered vehicle, the available energy associated with the propellant is utilized to impart a thrust force whereby the kinetic and gravitational potential energies of the vehicle are increased, representing the productive utilization of initial available energy. The remainder of the available energy is 'lost' in overcoming irreversibilities 1) inside the engines, 2) external to the vehicle (associated with external drag), and 3) in the wake of the vehicle. When structural mass is discarded during staging, the kinetic and gravitational potential energies that have been imparted to the discarded mass (through the use of available energy associated with the propellant) is also 'lost.' The paper establishes a general formulation for the mission-integrated global control volume-based available energy utilization balance for an *N*-stage rocket in both dimensional and non-dimensional forms. The non-dimensional form is employed in the subsequent optimization studies. Two basic cases are analyzed; specifically, the operation of a 2-stage rocket in: 1) free-space (i.e., no gravity, no drag), and 2) in vertical ascent in a constant gravitational field. This is done to identify the staging velocity (for given total impulse required) that would maximize the utilization of available energy for the mission. These cases are treated first analytically in order to provide the energy utilization-based formulations for each; the resulting formulations are then applied to representative examples in order to illustrate the energy utilization methodology.

Entropy and exergy-based analysis and performance improvement as well as optimization based on minimizing entropy generation are well-established for ground-

based systems, such as powerplants. The application of such analysis is far less common and productively utilized for aerospace applications (especially for rocket systems) due mainly to the historical lack of a direct, analytically satisfactory, connection between exergy, entropy generation, and traditional vehicle performance. The global control volume-based energy utilization approach (as well as similar approaches) will be summarized subsequently and establishes a direct relation between traditional vehicle performance metrics and loss in the 'best performance possible,' specifically as quantified by entropy generation. Entropy generation, rooted in the second law of thermodynamics, is the most fundamental and universal metric (currency) describing losses in all components and subsystems as well as on the overall system level of any aerospace vehicle.

The global control volume-based energy availability utilization methodology has been developed mostly over the last decade [1-3]. This methodology directly relates the available energy associated with the propellant to the classic performance of engines and aerospace vehicles. It has been applied to both airbreathing engines [4,5] and chemical rockets [6-8]. Central to the methodology is the instantaneous energy availability utilization balance as developed in Ref. [1], which relates the available energy associated with the propellant to the net work-producing fluid dynamic force on the vehicle and losses due to irreversibilities. A time-integrated form of the balance incorporating the vehicle's equation of motion is also developed [3,6]. The work presented in this paper constitutes further development and generalization of the work presented in Ref. [6], which used a time-integrated approach and showed that entropy generation and losses associated with staging phenomena are directly related to the vehicle's change in kinetic and gravitational potential energies. Reference [6] also presented the time evolution of the energy

availability, losses, and productive energy for a legacy access to space rocket using a simplified model. Reference [8] further utilized the energy utilization methodology as applied to rockets, incorporating more detailed rocket engine and wake entropy generation solvers for both kerosene and hydrogen fueled systems. In Ref. [8], loss characteristics and vehicle performance were explored in greater detail and overall mission effectiveness and optimization metrics were established. Another work, focused on space access rocket systems and partially utilizing the global control volume approach in its formulation, provides system-level and comparative exergy quantification for representative access to space rocket systems [9].

One of the earliest seminal works focused on flight and utilizing a control volume approach considering the second law of thermodynamics is the work of Oswatitsch [10], wherein the drag experienced by an unpowered body immersed in a fluid flow is directly related to the entropy generation in and behind the body. Most of the work involving second-law considerations for aerospace applications has been focused on airbreathing propulsion systems. Giles and Cummings [11] formulated an energy availability relation for an air-breathing powered vehicle that uses a simplified heating model for fuel-air combustion. Abbas and Riggins [5] employed the global control volume-based methodology to study the energy availability utilization characteristics and performance of a turbojet engine as well as the performance of a jet-propelled vehicle where cruising range and endurance performance is directly related to entropy generation. Early work concerning energy availability performance of airbreathing engines, includes the work of Foa [12], Clarke and Horlock [13], Builder [14], and Lewis [15]. Exergy-related studies in the 1990s, which mainly focused on scramjet engines, include the work done by Czysz and

Murthy [16], Murthy [17], and Brilliant [18]. Curran and Craig [19] were pioneers in planting the seed for the thrust-potential methodology that was developed later by Riggins et al. [20-22], with initial focus on high-speed propulsion applications. Roth [23-25] developed a similar methodology utilizing work potential and kinetic energy efficiency applied to engines. In contrast to the global control volume-based energy availability analysis, both thrust potential and work potential methods avoid the wake mixing process and the entropy generation occurring therein, as these methods involve a direct assessment of performance based on the engine flowfield itself. More recent work concerned with exergy for aerospace flight systems is that of Arntz et al. [26], Arntz and Hue [27], Ehyaei et al. [28], Hayes et al. [29], as well as related work focused on turbojet engines [30-36].

Section 2 of this paper first introduces the time-integrated (mission-integrated) energy utilization balance relation incorporating the rocket's equation of motion. A general formulation of the time-integrated balance for an *N*-stage rocket is then developed, with the major loss terms and productive energy utilization term identified. These terms are formulated for the entire mission as well as for the individual stages. Section 2 then introduces useful effectiveness parameters defined in various ways. The mission-integrated balance along with all associated terms are then recast in a non-dimensional form to be used in the subsequent analysis. Section 3 presents an analytic optimization study of two special cases: 1) a two-stage rockets in free space (no gravity, no drag) and 2) a two-stage rockets in a vertical climb in a constant gravitational field. For both cases, analytical formulations are developed that identify the optimal staging velocity that will maximize the productive energy utilization. Section 4 presents the results of two specific case studies that illustrate the validity and usefulness of the analytical formulations and the energy

utilization methodology in general. The last section of this paper constitutes a summary of the work.

## 2. MULTI-STAGE ROCKET ENERGY AVAILABILITY

The energy availability utilization methodology is based on control volume analysis. The aerospace vehicle is considered as embedded in a fluid control volume, as seen in Figure 1, designated the global control volume. This control volume encompasses all fluids internal to the vehicle (i.e., fluid in the propulsive flowpaths, propellant tankage and feed systems, etc.). It also includes the fluid external to the vehicle from free-stream to vehicle exit plane (including, as seen in Figure 1, the vehicle sub-control volume defined by the zone of influence and the side-bounding region, which is characterized by undisturbed free-stream flow. Finally, the control volume also includes the wake zone of the vehicle from $s$ to $w$, including the exhaust plume(s) of the propulsion system. In the axial direction (i.e., direction of flight), the inflow plane to the control volume is the uniform and undisturbed freestream, located sufficiently upstream of the vehicle, and the wake outflow plane is at a location sufficiently downstream of the vehicle such that the flow properties are uniform (and infinitesimally displaced from those at the inflow plane). The analysis invokes the governing equations as applied to the global control volume, namely: the conservation of mass (continuity), the conservation of energy (first law of thermodynamics), the entropy balance (second law of thermodynamics), and the momentum equation. These relations are combined into a single expression designated the

energy availability utilization balance, Eq. (1), which is the central mathematical relation in the energy availability methodology of aerospace systems.

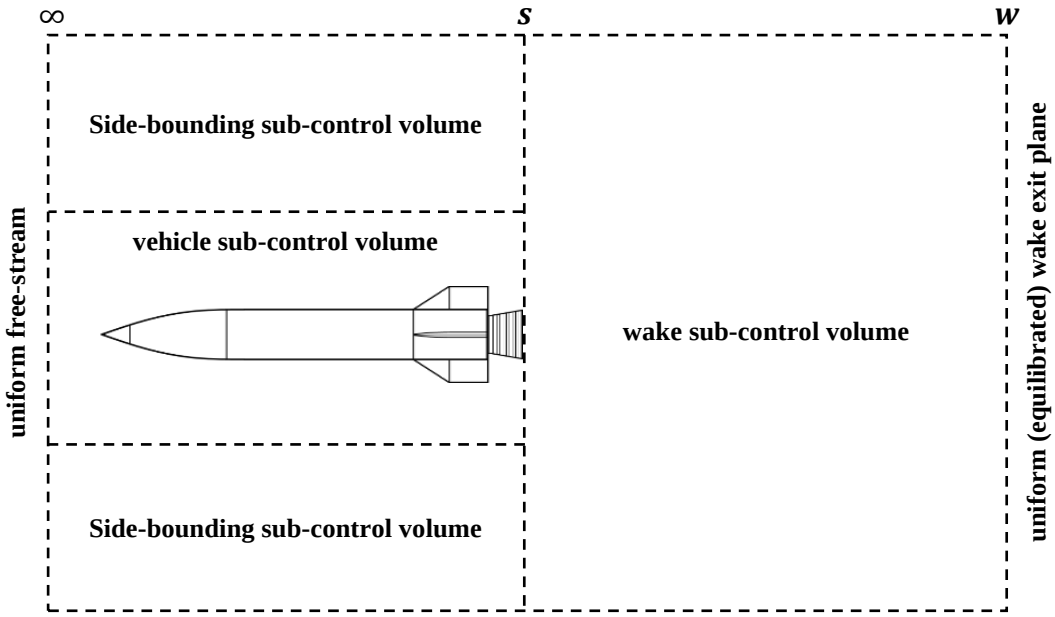


Figure 1. Global control volume for a rocket in flight.

$$\dot{m}_P \left( H^* + \frac{u_\infty^2}{2} \right) - T_\infty \dot{S}_{\text{total}} = u_\infty F_{x(\text{flight})} \tag{1}$$

As developed in Reference [2], for the analysis of a rocket performing a mission, the instantaneous energy utilization balance, Eq. (1), can be combined with the vehicle's equation of motion, Eq. (2). By elimination of the next axial force on the rocket, $F_{x,(\text{flight})}$, the resulting balance is Eq. (3), also see Figure 2.

$$m_R \frac{dV}{dt} = F_{x(\text{flight})} - m_R \text{g} \sin\theta \tag{2}$$

In Equation (2), $\theta$ is the instantaneous flight path angle, i.e., the angle between the rocket's flight velocity $V$ and the local horizon (positive upward).

$$\dot{m}_P H^* - T_\infty \dot{S}_{\text{total}} = \frac{d}{dt}\left(m_R \frac{V^2}{2}\right) + m_R \mathrm{g} \frac{dh}{dt} \tag{3}$$

Equation (3) still represents the instantaneous rate-form energy utilization balance, and it may be integrated over an entire mission or any segment of it. The net power delivered to the vehicle (right-hand side of the equation) integrated over time is equal to the change in the vehicle's mechanical energy: the sum of its kinetic and gravitational potential energies. The energy utilization balance for a vehicle over a mission is then expressed by Eq. (4).

$$H^*_{\text{eff}}\, m_P - \left[\int T_\infty dS_{\text{total}}\right]_{\text{mission}} = m_f \frac{V_f^2}{2} - m_i \frac{V_i^2}{2} + \left[\int m_R \mathrm{g} dh\right]_{\text{mission}} \tag{4}$$

where,

$$H^*_{\text{eff}}\, m_P = \left[\int H^* dm_P\right]_{\text{mission}} \tag{5}$$

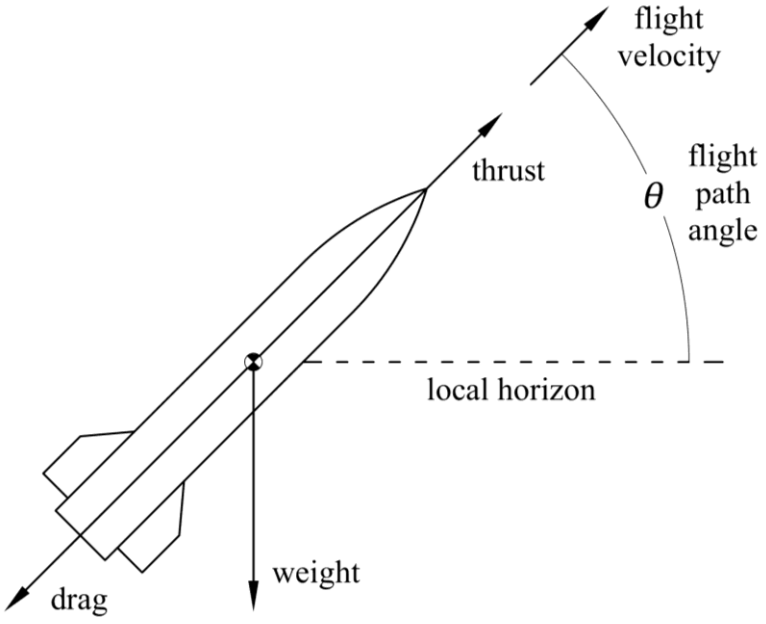


Figure 2. Rocket in flight in the atmosphere.

For rockets in general, and access-to-space launch vehicles in particular, the goal is for the final mass of the rocket, representing the payload, to achieve a certain velocity at a certain altitude. Thus, the productive energy utilization is defined as the change in mechanical energy (kinetic and gravitational potential energies) of the final mass of the rocket, designated here for convenience as the payload (note that this term also includes all structural rocket mass associated with the final flight condition, as well as the mass of any carried cargo/payload):

$$= m_f \left[\frac{1}{2}\left(V_f^2 - V_i^2\right) + \mathrm{g}\left(h_f - h_i\right)\right] \tag{6}$$

An *N*-stage rocket model is now examined where the total mass of the rocket at the start of the mission consists of the mass of all *N* stages in addition to the mass of the payload. For any $n$-th stage, the mass consists of the propellant mass, $m_{p,n}$, and the discard mass, $m_{d,n}$, representing the structural mass of that stage. The final (payload) mass of the rocket can then be expressed in terms of these masses in addition to the initial mass of the rocket:

$$m_f = m_i - \sum_{n=1}^{N}\left(m_{P,n} + m_{d,n}\right) \tag{7}$$

The mass of the rocket at the beginning of any stage $n$ can also be expressed in a similar way:

$$m_{\mathrm{stage},n} = m_i - \sum_{k=1}^{n-1}\left(m_{P,k} + m_{d,k}\right) \tag{8}$$

The energy utilization balance across any $n$-stage burn is then:

$$H^*_{\text{eff},n} m_{P,n} - \left[\int T_\infty dS_{\text{total}}\right]_{\text{stage},n}$$

$$= \left(m_{\text{stage},n} - m_{P,n} - m_{d,n}\right)\frac{V_{nf}^2}{2} - m_{\text{stage},n}\frac{V_{ni}^2}{2} + m_{d,n}\frac{V_{nf}^2}{2} \tag{9}$$

$$+ \left[\int m_R g dh\right]_{\text{stage},n}$$

Summing up the expressions over all *N* stages of the rocket, the total mission-integrated available energy associated with the stored propellants of all *N* stages (which necessarily includes the propellants initial kinetic energy) is then defined in Eq. (10). Note that each stage's propellant has an associated effective thermochemical availability, $H^*_{\text{eff}}$.

$$E_{\text{AV}} \equiv \sum_{n=1}^{N}\left(H^*_{\text{eff},n} + \frac{V_i^2}{2}\right) m_{P,n} \tag{10}$$

where,

$$H^*_{\text{eff},n}\, m_{P,n} = \left[\int H^* dm_{P,n}\right]_{\text{stage},n} \tag{11}$$

## 2.1. THE MISSION-INTEGRATED ENERGY AVAILABILITY UTILIZATION BALANCE FOR AN N-STAGE ROCKET

The energy availability utilization balance over the entire mission is the sum of the individual balances over each stage $n$, Eq. (12). It should be noted that this model assumes that at the end of each stage burn, the structural mass of said stage, $m_{d,n}$ is discarded (instantaneous event), and that the next stage burn follows immediately.

$$
\begin{aligned}
&E_{\mathrm{AV}} \\
&= \sum_{n=1}^{N} \left[ \int T_{\infty} dS_{\mathrm{total}} \right]_{\mathrm{stage},n} + \sum_{n=1}^{N} m_{d,n} \left( \frac{V_{nf}^2}{2} + \frac{V_i^2}{2} \right) \\
&+ \sum_{n=1}^{N} \left\{ \left[ \int m_R \mathrm{g} dh \right]_{\mathrm{stage},n} - \left( m_i - \sum_{k=1}^{N} m_{P,k} - \sum_{k=1}^{n-1} m_{d,\mathrm{k}} \right) \mathrm{g}\left(h_{nf} - h_{ni}\right) \right\} \\
&+ \sum_{n=1}^{N} \mathrm{g}\left(h_{nf} - h_{ni}\right) \sum_{k=n}^{N} m_{d,k} + \phi
\end{aligned}
\tag{12}
$$

This expression delineates how the energy stored initially in the propellant that is available to do work (i.e., exergy) is distributed, and how it is productively used or lost during the operation of the rocket. The first term on the right-hand side represents the available energy that is lost to irreversibilities (exergy destruction), or equivalently it may be viewed as the available energy used to overcome irreversibilities over the mission. The second term describes the change in kinetic energy achieved by the discarded masses and therefore effectively 'lost' from the standpoint of final productive energy utilization. The third term represents the work done by the different stages to lift the propellant to the altitude where it 'leaves' (i.e., is expelled from) the rocket. The fourth term accounts for the change in gravitational potential energy achieved by the discarded masses and therefore also is accounted as 'lost.' The fifth and last term, $\phi$, is the change in kinetic and geopotential energies achieved by the final mass (payload) of the rocket, which is defined as the productive energy utilization. Any amount of utilized energy that does not result in kinetic and/or potential energy changes of the final mass ('payload' mass) is therefore considered lost. This breakdown of the energy utilization can be summarized in Eq. (13), with terms defined in Table 1.

$$E_{\mathrm{AV}} = K1 + K2 + K3 + K4 + \phi \tag{13}$$

Table 1. Description of the terms in Eq. (13).

| Term designator | Description of term | Analytical expression of term |
|---|---|---|
| $E_{\mathrm{AV}}$ | Overall mission-integrated availability (all $N$ stages) | $\sum_{n=1}^{N}\left(H^{*}_{\mathrm{eff},n} + \frac{V_i^2}{2}\right) m_{P,n}$ |
| $K1$ | Available energy used to overcome irreversibilities of all $N$ stages | $\sum_{n=1}^{N}\left[\int T_{\infty} dS_{\mathrm{total}}\right]_{\mathrm{stage},n}$ |
| $K2$ | Kinetic energy loss due to discarded mass of all $N$ stages | $\sum_{n=1}^{N} m_{d,n}\left(\frac{V_{nf}^2}{2} + \frac{V_i^2}{2}\right)$ |
| $K3$ | Work done by all $N$ stages to lift propellant expended | $\sum_{n=1}^{N}\left\{\left[\int m_R \mathrm{g} dh\right]_{\mathrm{stage},n} - \left(m_i - \sum_{k=1}^{N} m_{P,k} - \sum_{k=1}^{n-1} m_{d,k}\right)\mathrm{g}\left(h_{nf} - h_{ni}\right)\right\}$ |
| $K4$ | Work done by all $N$ stages to lift discarded mass | $\sum_{n=1}^{N}\mathrm{g}\left(h_{nf} - h_{ni}\right)\sum_{k=n}^{N} m_{d,k}$ |
| $\phi$ | Productive energy utilization (change in kinetic and geopotential energies of final mass of vehicle) | $m_f\left[\frac{1}{2}\left(V_f^2 - V_i^2\right) + \mathrm{g}\left(h_f - h_i\right)\right]$ |

The productive energy, $\phi$, can be broken up into kinetic energy and geopotential energy changes of the payloads of the rocket's stages, representing the productive energy realized during each stage, Eq. (14). The payload of each stage is the entire mass of all stages above it.

$$\phi = \sum_{n=1}^{N}\phi_n = \sum_{n=1}^{N}\left[m_{ni} - \sum_{k=n}^{N}\left(m_{P,k} + m_{d,k}\right)\right]\left[\frac{1}{2}\left(V_{nf}^2 - V_{ni}^2\right) + \mathrm{g}\left(h_{nf} - h_{ni}\right)\right] \tag{14}$$

The loss terms appearing in Eq. (13) can also be written as the sum of the contributions of the different stages of the rocket, Eq. (15), identified individually in Table 2. The energy utilization balance is then given by Eq. (16).

$$K1 = \sum_{n=1}^{N} K1_n \ , \qquad K2 = \sum_{n=1}^{N} K2_n \ , \qquad K3 = \sum_{n=1}^{N} K3_n \ , \qquad K4 = \sum_{n=1}^{N} K4_n \qquad (15)$$

$$E_{AV} = \sum_{n=1}^{N} (K1_n + K2_n + K3_n + K4_n + \phi_n) \qquad (16)$$

Table 2. Description of the terms in Eq. (16).

| Term designator | Description of term | Analytical expression of term |
|---|---|---|
| $K1_n$ | Available energy used to overcome stage-$n$ irreversibility | $\left[\int T_\infty dS_{\text{total}}\right]_{\text{stage},n}$ |
| $K2_n$ | Kinetic energy loss due to stage-$n$ discarded mass | $m_{d,n}\left(\frac{V_{nf}^2}{2} + \frac{V_i^2}{2}\right)$ |
| $K3_n$ | Work done by stage-$n$ to lift propellant expended | $\left[\int m_R \mathrm{g} dh\right]_{\text{stage},n} - \left(m_i - \sum_{k=1}^{N} m_{P,n} - \sum_{k=1}^{n-1} m_{d,k}\right)\mathrm{g}(h_{nf} - h_{ni})$ |
| $K4_n$ | Work done by stage-$n$ to lift discarded mass | $\mathrm{g}(h_{nf} - h_{ni}) \sum_{k=n}^{N} m_{d,k}$ |
| $\phi_n$ | Productive energy utilization (change in kinetic and geopotential energies of final mass of vehicle) during stage-$n$ burn | $\left[m_{ni} - \sum_{k=n}^{N}(m_{P,k} + m_{d,k})\right]\left[\frac{1}{2}(V_{nf}^2 - V_{ni}^2) + \mathrm{g}(h_{nf} - h_{ni})\right]$ |

## 2.2. ENERGY AVAILABILITY UTILIZATION EFFECTIVENESS

The overall energy availability utilization effectiveness of the rocket stack (all $N$ stages) is defined in Eq. (17) as the ratio of the realized productive energy, $\phi$, to the overall (mission-integrated) energy availability, $E_{\text{AV}}$. As evident from the definition, it is a measure of the amount of energy initially available that is realized by the payload at the end of the mission (in the form of kinetic and gravitational potential energies). Note that

the energy utilization effectiveness as defined is not the same as the thermodynamic first-law efficiency, nor is it the second-law (exergetic) efficiency.

$$\eta_{\text{overall}} \equiv \frac{\phi}{E_{\text{AV}}} = \frac{m_f\left[\frac{1}{2}\left(V_f^2 - V_i^2\right) + \text{g}\left(h_f - h_i\right)\right]}{\sum_{n=1}^{N}\left(H_{\text{eff},n}^{*} + \frac{V_i^2}{2}\right)m_{P,n}} \tag{17}$$

Looking at individual stages, the effectiveness can be defined in a number of different ways. This depends on whether the 'useful' energy for a given stage is considered to be that of the entire rocket's payload (i.e., as associated with its final mass), or whether it is considered to be that of only the stage's payload (i.e., the mass of all subsequent stages, plus the payload). Another way of looking at the effectiveness of a stage would be to reconsider the definition of the denominator. The realized energy, however defined, may be compared to the available energy over the entire mission, or it may be defined with respect to the available energy at the start of the stage itself.

**2.2.1. Stage Effectiveness Defined with Rocket's Payload and Overall Availability.** One obvious way to define the effectiveness of any stage $n$ of the rocket would be as the fraction of the overall initially available energy that was realized as a change in the mechanical energy of the rocket's final mass during the $n$-th stage burn, Eq. (18). For such a definition, the overall effectiveness of the rocket, as defined in Eq. (17), would be the sum of the effectivenesses of the individual *N* stages.

$$\eta_n = \frac{\phi_n}{E_{\text{AV}}} = \frac{m_f\left[\frac{1}{2}\left(V_{nf}^2 - V_{ni}^2\right) + \text{g}\left(h_{nf} - h_{ni}\right)\right]}{\sum_{n=1}^{N}\left(H_{\text{eff},n}^{*} + \frac{V_i^2}{2}\right)m_{P,n}} \tag{18}$$

such that:

$$\eta_{\text{overall}} = \sum_{n=1}^{N} \eta_n \tag{19}$$

**2.2.2. Stage Effectiveness Defined with Rocket's Payload and Availability at the Start of the Stage.** This effectiveness of a stage may also be defined as the fraction of the available energy at the beginning of the stage burn that is realized as a change in kinetic and geopotential energies of the final payload during stage $n$ operation (burn). To find the energy available at any point in time during the rocket's operation, the energy balance may be tracked in time, in which the total energy initially available for the stack, $E_{\text{AV}}$, at any point of time $t$ is the sum of the productive energy $\phi$, the cumulative losses $K$'s, and the remaining available energy $\beta$:

$$E_{\text{AV}} = K1(t) + K2(t) + K3(t) + K4(t) + \phi(t) + \beta(t) \tag{20}$$

Let $t = \tau_{n,n+1}$ be the staging time between stages $n$ and $n$+1, then any loss term $K$ at that time would be the cumulative losses from the start of the mission at $t$ = 0 to the end of the $n$-th stage burn at $t = \tau_{n,n+1}$:

$$K_{n,n+1} = K\left(\tau_{n,n+1}\right) = \sum_{k=1}^{n} K_k \tag{21}$$

Similarly for the productive energy term:

$$\phi_{n,n+1} = \phi\left(\tau_{n,n+1}\right) = \sum_{k=1}^{n} \phi_k \tag{22}$$

The remaining available energy at the beginning of stage $n$ (and end of stage $n-1$) is then:

$$E_{\mathrm{AV},n} \equiv \beta_{n-1,n} = \beta\left(\tau_{n-1,n}\right) = E_{\mathrm{AV}} - \left[K1_{n-1,n} + K2_{n-1,n} + K3_{n-1,n} + K4_{n-1,n} + \phi_{n-1,n}\right] \tag{23}$$

Now, the effectiveness of stage $n$ in terms of the available energy at the beginning of the stage can be written, and the change of kinetic and geopotential energies of the rocket's final mass during this stage's burn:

$$\epsilon_n = \frac{m_f[\frac{1}{2}\left(V_{nf}^2 - V_{ni}^2\right) + \mathrm{g}\left(h_{nf} - h_{ni}\right)]}{E_{\mathrm{AV},n}} \tag{24}$$

Other ways of defining the effectiveness of a stage are also possible. For instance, Eq. (24) can be 'redefined' using the payload of the stage instead of that of the entire rocket (the payload of a given stage is the mass of the rocket's (actual) payload in addition to the masses of all subsequent stages. This would of course be useful if the objective was to analyze a certain stage as a stand-alone mission, with the mission-integrated available energy only accounting for that stage's propellant (and the payload being what the stage is lifting).

## 2.3. NON-DIMENSIONAL DESCRIPTION OF THE ENERGY AVAILABILITY UTILIZATION BALANCE FOR AN N-STAGE ROCKET

It is customary to recast the relations for multi-stage rockets in non-dimensional form when performing generic analysis to study the interplay between certain ratios of interest that would be applicable to any rocket regardless of size. Such analysis can be found in many textbooks dealing with the matter, such as the discussion presented in Ref. [37]. In this section, a non-dimensional form of the energy availability utilization balance is presented along with discussion about the optimization of the productive energy

utilization and its relation to the optimization of the payload mass ratio, as found in traditional analyses.

Let the mass of the rocket at the beginning of stage $n$ be $m_{\text{stage},n} = m_{s,n}$. Now define the following propellant and discard mass ratios for any given stage $n$:

$$\lambda_n \equiv \frac{m_{P,n}}{m_{s,n}} \tag{25}$$

$$\delta_n \equiv \frac{m_{d,n}}{m_{s,n}} \tag{26}$$

For convenience, a different discard mass ratio can be defined, based on the propellant mass (rather than stage mass as in Eq. (25) and (26)), i.e.,

$$\delta_n^* \equiv \frac{m_{d,n}}{m_{P,n}} \tag{27}$$

Therefore, the discard mass ratio defined in Eq. (26) is:

$$\delta_n = \delta_n^* \, \lambda_n \tag{28}$$

Mass quantities are nondimensionalized by dividing them by the initial mass of the rocket, $m_i$. The non-dimensional form of a stage's initial mass, its propellant mass, its discard mass, and the rocket's payload (final) mass are then given by Eq. (29), thru Eq. (32), respectively.

$$\frac{m_{s,n}}{m_i} = 1 - \sum_{k=1}^{n-1} \left[ (\lambda_k + \delta_k) \prod_{j=1}^{k-1} (1 - \lambda_j - \delta_j) \right] \tag{29}$$

Note that $m_i = m_{s,1}$

$$\frac{m_{P,n}}{m_i} = \lambda_n \prod_{k=1}^{n-1} (1 - \lambda_k - \delta_k) \tag{30}$$

$$\frac{m_{d,n}}{m_i} = \delta_n \prod_{k=1}^{n-1}(1 - \lambda_k - \delta_k) \tag{31}$$

$$\frac{m_f}{m_i} = 1 - \sum_{k=1}^{N}\left[(\lambda_k + \delta_k)\prod_{j=1}^{k-1}\left(1 - \lambda_j - \delta_j\right)\right] \tag{32}$$

The energy utilization balance in any of its forms, e.g., Eq. (16), is then nondimensionalized by dividing by the quantity $H^*_{\text{eff},1} m_i$, where $H^*_{\text{eff},1}$ is the mission-integrated effective thermochemical energy availability of the propellant of stage 1. All non-dimensional available energy and loss terms will be denoted by a superscript asterisk, '*' (not to be confused with the asterisk on $H^*$). The non-dimensional form of the energy utilization balance is then given by Eq. (33), with the full form of the terms as presented in Table 3.

$$E^*_{\text{AV}} = \sum_{n=1}^{N}(K1^*_n + K2^*_n + K3^*_n + K4^*_n) + \phi^* \tag{33}$$

It should be noted that the loss term due to irreversibilities for each stage $n$ has been replaced with an equivalent expression using the energy utilization balance for a single stage:

$$\begin{aligned}&\left[\int T_\infty \, dS_{\text{total}}\right]_{\text{stage},n} \\ &= H^*_{\text{eff},n}\, m_{P,n} - \left(m_{nf} + m_{d,n}\right)\frac{V^2_{nf}}{2} + m_{ni}\frac{V^2_{ni}}{2} - \left[\int m_R \text{g}\, dh\right]_{\text{stage},n}\end{aligned} \tag{34}$$

Table 3. Full analytical form of the terms in Eq. (33).

| Term designator | Full analytical form of the term |
|---|---|
| $E^*_{\mathrm{AV}}$ | $\displaystyle\sum_{n=1}^{N}\left\{\frac{H^*_{\mathrm{eff},n}+\frac{V_i^2}{2}}{H^*_{\mathrm{eff},1}}\lambda_n\prod_{k=1}^{n-1}(1-\lambda_k-\delta_k)\right\}$ |
| $K1^*_n$ | $\displaystyle\frac{[\int T_\infty\, dS_{\mathrm{total}}]_{\mathrm{stage},n}}{H^*_{\mathrm{eff},1}\, m_i} = \frac{H^*_{\mathrm{eff},n}}{H^*_{\mathrm{eff},1}}\lambda_n\prod_{k=1}^{n-1}(1-\lambda_k-\delta_k) - \frac{V_{nf}^2}{2H^*_{\mathrm{eff},1}}\left\{1-\sum_{k=1}^{n}\left[(\lambda_k+\delta_k)\prod_{j=1}^{k-1}(1-\lambda_j-\delta_j)\right]+\delta_n\prod_{k=1}^{n-1}(1-\lambda_k-\delta_k)\right\} + \frac{V_{ni}^2}{2H^*_{\mathrm{eff},1}}\left\{1-\sum_{k=1}^{n-1}\left[(\lambda_k+\delta_k)\prod_{j=1}^{k-1}(1-\lambda_j-\delta_j)\right]\right\} - \frac{\left[\int\frac{m_R}{m_i}\mathrm{g}\, dh\right]_{\mathrm{stage},n}}{H^*_{\mathrm{eff},1}}$ |
| $K2^*_n$ | $\displaystyle\frac{\left(\frac{V_{nf}^2}{2}-\frac{V_i^2}{2}\right)}{H^*_{\mathrm{eff},1}}\delta_n\prod_{k=1}^{n-1}(1-\lambda_k-\delta_k)$ |
| $K3^*_n$ | $\displaystyle\frac{1}{H^*_{\mathrm{eff},1}}\left\{\left[\int\frac{m_R}{m_i}\mathrm{g}\, dh\right]_{\mathrm{stage},n} - \mathrm{g}(h_{nf}-h_{ni})\left[1-\sum_{k=1}^{N}\lambda_k\prod_{j=1}^{k-1}(1-\lambda_j-\delta_j)-\sum_{k=1}^{n-1}\delta_k\prod_{j=1}^{k-1}(1-\lambda_j-\delta_j)\right]\right\}$ |
| $K4^*_n$ | $\displaystyle\frac{\mathrm{g}(h_{nf}-h_{ni})}{H^*_{\mathrm{eff},1}}\sum_{k=n}^{N}\delta_k\prod_{j=1}^{k-1}(1-\lambda_j-\delta_j)$ |
| $\phi^*$ | $\displaystyle\frac{\phi}{H^*_{\mathrm{eff},1}\, m_i} = \frac{1}{H^*_{\mathrm{eff},1}}\left\{1-\sum_{k=1}^{N}\left[(\lambda_k+\delta_k)\prod_{j=1}^{k-1}(1-\lambda_j-\delta_j)\right]\right\}\left\{\left(\frac{V_f^2}{2}+\frac{V_i^2}{2}\right)+\mathrm{g}(h_f-h_i)\right\}$ |

## 3. ANALYTIC STUDY OF SPECIAL CASES

In this section, the non-dimensional form of the energy availability utilization balance is applied to simple special cases, where analytical solutions can be obtained and

compared with previous (mass-based) analytical results. Indeed, as shown in Ref. [37], an analytical solution can be found for a rocket in free space (no gravity, no drag). In the traditional analysis, the goal is to either maximize the overall burn $\Delta V$ for a given payload mass ratio, or equivalently, maximize the overall payload mass ratio $m_f/m_i$ for a given burn $\Delta V$. The corresponding optimum number of stages satisfying that and/or the sizing of these stages can then be determined. In the analysis developed in the present work, the function to be optimized is the non-dimensional productive energy utilization $\phi^*$; for a given $\Delta V$, the independent variable would be the staging velocity $V_s$. Two special cases will be investigated, a two-stage rocket in free space, and a two-stage rocket in vertical climb in a constant gravitational field.

### 3.1. TWO-STAGE ROCKET IN FREE SPACE

For a rocket in free space (no gravity or drag), the equation of motion yields the following relationship (rocket equation):

$$\Delta V = C \ln\left(\frac{1}{1-\lambda}\right) \tag{35}$$

where $\lambda$ is the ratio of the propellant mass used in the burn to the total mass of the rocket at the initiation of the burn, and $C$ is the effective exhaust velocity.

Applying the rocket equation to a two-stage rocket, performing a total burn $\Delta V = \Delta V_1 + \Delta V_2$, between initial velocity $V_i$ and final velocity $V_f$ thru an intermediate staging velocity $V_s$, yields the following expressions for the propellant mass ratios of stages 1 and 2:

$$\lambda_1 = 1 - e^{\frac{V_i - V_s}{C_1}} \tag{36}$$

$$\lambda_2 = 1 - e^{\frac{V_s - V_f}{C_2}} \tag{37}$$

It is evident here that the propellant mass ratios are functions of the staging velocity for a given overall $\Delta V$. Applying the relations in Table 3 to a two-stage rocket, the non-dimensional productive energy for the overall burn is then given by Eq. (38), and the non-dimensional overall mission-integrated energy availability is then given by Eq. (39).

$$\phi^* = \frac{1}{H^*_{\text{eff},1}}(1 - \lambda_1 - \delta_1)(1 - \lambda_2 - \delta_2)\left(\frac{V_f^2}{2} - \frac{V_i^2}{2}\right) \tag{38}$$

$$E^*_{\text{AV}} = \lambda_1\left(1 + \frac{V_i^2}{2\,H^*_{\text{eff},1}}\right) + \lambda_2(1 - \lambda_1 - \delta_1)\left(\frac{H^*_{\text{eff},2}}{H^*_{\text{eff},1}} + \frac{V_i^2}{2\,H^*_{\text{eff},1}}\right) \tag{39}$$

The non-dimensional productive energy $\phi^*$ is a function of staging velocity $V_s$ thru the propellant mass ratios $\lambda_1$and $\lambda_2$. In general, the effective thermochemical energy availability of the first stage $H^*_{\text{eff},1}$ is also a function of the staging velocity but to simplify the analysis will be approximated by a constant value, namely $H^*_{P1}$, that is proportional to the heating value of the propellant $H_{P1}$. In addition, again for convenience in presentation of approximate applications and analytical cases, the effective heating value of the propellant can be related to the effective exhaust velocity of the rocket through the use of a bulk 'acceleration efficiency,' $\eta_a$, as defined in Eq. (40). The acceleration efficiency is the ratio of effective exit kinetic energy per mass of the rocket to the effective heating value of propellant.

$$\eta_a = \frac{C^2/2}{H_P} \tag{40}$$

For a given rocket configuration with fixed initial and final velocities and given discard mass ratios, the staging velocity that would maximize the productive energy is the

velocity that satisfies Eq. (41). Note that the maximum non-dimensional productive energy $\phi^*$ for this case corresponds to the maximum overall payload mass ratio $m_f/m_i$ since that is the only variable in Eq. (38).

$$\frac{\partial \phi^*}{\partial V_s} = \frac{1}{H_{P1}^*}\left(\frac{V_f^2}{2} - \frac{V_i^2}{2}\right)\left[-\left(\frac{\partial \lambda_1}{\partial V_s}\right)(1-\lambda_2-\delta_2) - \left(\frac{\partial \lambda_2}{\partial V_s}\right)(1-\lambda_1-\delta_1)\right] = 0 \qquad (41)$$

where,

$$\frac{\partial \lambda_1}{\partial V_s} = \frac{1}{C_1} e^{\frac{V_i - V_s}{C_1}} \qquad , \qquad \frac{\partial \lambda_2}{\partial V_s} = -\frac{1}{C_2} e^{\frac{V_s - V_f}{C_2}} \qquad (42)$$

Only the term in the brackets in Eq. (41) can equal zero. Therefore, substituting the expressions in Eq. (42) and performing some manipulation yields the following relationship:

$$\left(\frac{1}{C_2} - \frac{1}{C_1}\right) e^{\frac{V_i}{C_1} - \frac{V_f}{C_2}} + \frac{\delta_2}{C_1} e^{\frac{V_i}{C_1} - \frac{V_s}{C_2}} - \frac{\delta_1}{C_2} e^{\frac{V_s}{C_1} - \frac{V_f}{C_2}} = 0 \qquad (43)$$

The staging velocity value $V_s$ that satisfies this expression optimizes (maximizes) the productive energy as well as overall payload mass ratio. The corresponding loss terms may be evaluated and are shown in Eq. (44) thru Eq. (47). The $K1^*$ terms represent the losses due to irreversibilities during the operation of each stage, while the $K2^*$ terms represent the losses associated with the kinetic energies of the discarded masses. Note that the loss terms associated with gravity ($K3^*$'s and $K4^*$'s) are identically zero in this free space case.

$$K1_1^* = \lambda_1 - (1-\lambda_1)\frac{V_s^2}{2H_{P1}} + \frac{V_i^2}{2H_{P1}} \qquad (44)$$

$K1_2^*$

$$= \lambda_2(1-\lambda_1-\delta_1)\frac{H_{P2}}{H_{P1}} - (1-\lambda_1-\delta_1)(1-\lambda_2)\frac{V_f^2}{2H_{P1}} + (1-\lambda_1-\delta_1)\frac{V_s^2}{2H_{P1}} \tag{45}$$

$$K2_1^* = \frac{\delta_1}{H_{P1}}\left(\frac{V_s^2}{2} - \frac{V_i^2}{2}\right) \tag{46}$$

$$K2_2^* = \frac{(1-\lambda_1-\delta_1)\delta_2}{H_{P1}}\left(\frac{V_f^2}{2} - \frac{V_i^2}{2}\right) \tag{47}$$

Traditional analysis, such as that presented in Ref. [37], utilize the payload mass ratio $\zeta$ (denoted in Ref. [37] as $\lambda$) instead of the propellant mass ratio $\lambda$, such that:

$$\zeta = 1 - \lambda - \delta \tag{48}$$

The traditional analysis then determines the payload ratios of the rocket's stages that would maximize the overall $\Delta V$. This is equivalent to maximizing the overall payload ratio $\zeta_0$ for a given burn $\Delta V$. Note, for an $N$-stage rocket:

$$\zeta_0 = \prod_{n=1}^{N} \zeta_n \tag{49}$$

The optimization in the traditional analysis is performed by employing the method of Lagrange multipliers subject to the restriction imposed by the relationship above. The case of a two-stage rocket in free space yields:

$$\zeta_1 = \frac{2\delta_1 C_2}{(C_1 - C_2) + \sqrt{(C_1 - C_2)^2 + 4C_1C_2\delta_1\delta_2/\zeta_0}} \tag{50}$$

$$\zeta_2 = \frac{2\delta_2 C_1}{(C_2 - C_1) + \sqrt{(C_2 - C_1)^2 + 4C_1C_2\delta_1\delta_2/\zeta_0}} \tag{51}$$

note,

$$\zeta_1 = 1 - \lambda_1 - \delta_1 = e^{\frac{V_i - V_s}{C_1}} - \delta_1 \tag{52}$$

$$\zeta_2 = 1 - \lambda_2 - \delta_2 = e^{\frac{V_s - V_f}{C_2}} - \delta_2 \tag{53}$$

Substituting these expressions for the payload mass ratios lead to expressions that can be solved for the optimum $V_s$, and it can be shown with some mathematical manipulation that the expressions are equivalent to the one obtained from the availability approach, namely Eq. (43). This demonstrates that both the traditional approach, as well as the energy availability approach yield the same optimization results for the case of a rocket in free space. However, the energy availability approach fundamentally provides much more insight regarding the distribution of the available energy and its utilization during the mission.

## 3.2. TWO-STAGE ROCKET IN VERTICAL CLIMB IN A CONSTANT GRAVITATIONAL FIELD

For a rocket climbing vertically in a constant-g gravitational field, an additional term appears in the rocket equation, Eq. (54), accounting for the gravitational pull. In this expression, a new quantity is identified and utilized, namely the thrust-to-weight of the rocket at the initiation of the burn, $\left(\frac{F}{W}\right)_i$.

$$\Delta V = C \ln\left(\frac{1}{1-\lambda}\right) - \frac{C\lambda}{\left(\frac{F}{W}\right)_i} \tag{54}$$

For a two-stage rocket, the overall burn $\Delta V$ is split again and analytical expressions can be found for the propellant mass ratios of the two stages:

$$\lambda_1 = \left(\frac{F_1}{W}\right)_i \mathbb{W}\left( -\frac{e^{-\left[\frac{(V_s - V_i)}{C_1} + \frac{1}{\left(\frac{F_1}{W}\right)_i}\right]}}{\left(\frac{F_1}{W}\right)_i} \right) + 1 \tag{55}$$

$$\lambda_2 = \left(\frac{F_2}{W}\right)_i \mathbb{W}\left( -\frac{e^{-\left[\frac{(V_f - V_s)}{C_2} + \frac{1}{\left(\frac{F_2}{W}\right)_i}\right]}}{\left(\frac{F_2}{W}\right)_i} \right) + 1 \tag{56}$$

In Eq. (55) and (56), $\mathbb{W}$ is the Lambert W function (also known as the product logarithm function).

The non-dimensional productive energy is then given by Eq. (57) and necessarily includes the change in the geopotential energy of the final mass of the rocket. The expression for the non-dimensional energy availability, $E^*_{\mathrm{AV}}$, is unchanged from the free space rocket case; Eq. (39).

$$\phi^* = \frac{1}{H^*_{\mathrm{eff},1}}(1 - \lambda_1 - \delta_1)(1 - \lambda_2 - \delta_2)\left[\left(\frac{V_f^2}{2} - \frac{V_i^2}{2}\right) + \mathrm{g}\left(h_f - h_i\right)\right] \tag{57}$$

In the case studied here, the initial and final velocities of the rocket are set values, but no such restrictions are imposed on the final altitude of the rocket. Then, the final altitude of the rocket $h_f$ as well as the staging altitude $h_s$ are implicit functions of the staging velocity. The expression for the change in altitude, Eq. (58), is related to the change in velocity via kinematics. The staging velocity is evaluated using Eq. (59).

$$\begin{aligned}
&\mathrm{g}(h_f - h_i) \\
&= \frac{C_1}{\left(\frac{F_1}{W}\right)_i}\left\{V_i\lambda_1 + C_1[(1-\lambda_1)(\ln(1-\lambda_1)-1)+1] - \frac{C_1}{2\left(\frac{F_1}{W}\right)_i}\lambda_1^2\right\} \\
&+ \frac{C_2}{\left(\frac{F_2}{W}\right)_i}\left\{V_s\lambda_2 + C_2[(1-\lambda_2)(\ln(1-\lambda_2)-1)+1] - \frac{C_2}{2\left(\frac{F_2}{W}\right)_i}\lambda_2^2\right\}
\end{aligned} \tag{58}$$

$$h_s = h_i + \frac{C_1}{\mathrm{g}\left(\frac{F_1}{W}\right)_i}\left\{V_i\lambda_1 + C_1[1+(1-\lambda_1)(\ln(1-\lambda_1)-1)] - \frac{C_1}{2\left(\frac{F_1}{W}\right)_i}\lambda_1^2\right\} \tag{59}$$

The optimum staging velocity that would maximize the productive energy utilization has the value that satisfies the following expression:

$$\begin{aligned}
&\frac{\partial\phi^*}{\partial V_s} \\
&= \frac{1}{H^*_{\mathrm{eff},1}}(1-\lambda_1-\delta_1)(1-\lambda_2-\delta_2)\frac{\partial}{\partial V_s}\left[\mathrm{g}(h_f-h_i)\right] \\
&- \frac{1}{H^*_{\mathrm{eff},1}}\left[\left(\frac{V_f^2}{2}-\frac{V_i^2}{2}\right)+\mathrm{g}(h_f-h_i)\right]\left[(1-\lambda_2-\delta_2)\left(\frac{\partial\lambda_1}{\partial V_s}\right)\right. \\
&\left.+ (1-\lambda_1-\delta_1)\left(\frac{\partial\lambda_2}{\partial V_s}\right)\right] = 0
\end{aligned} \tag{60}$$

where the partial derivative terms are given by the following expressions:

$$\left(\frac{\partial \lambda_1}{\partial V_s}\right) = -\frac{\left(\frac{F_1}{W}\right)_i}{C_1}\left[\frac{\mathbb{W}\left(-\frac{e^{-\left[\frac{(V_s-V_i)}{C_1}+\frac{1}{\left(\frac{F_1}{W}\right)_i}\right]}}{\left(\frac{F_1}{W}\right)_i}\right)}{\mathbb{W}\left(-\frac{e^{-\left[\frac{(V_s-V_i)}{C_1}+\frac{1}{\left(\frac{F_1}{W}\right)_i}\right]}}{\left(\frac{F_1}{W}\right)_i}\right)+1}\right] \tag{61}$$

$$\left(\frac{\partial \lambda_2}{\partial V_s}\right) = \frac{\left(\frac{F_2}{W}\right)_i}{C_2}\left[\frac{\mathbb{W}\left(-\frac{e^{-\left[\frac{(V_f-V_s)}{C_2}+\frac{1}{\left(\frac{F_2}{W}\right)_i}\right]}}{\left(\frac{F_2}{W}\right)_i}\right)}{\mathbb{W}\left(-\frac{e^{-\left[\frac{(V_f-V_s)}{C_2}+\frac{1}{\left(\frac{F_2}{W}\right)_i}\right]}}{\left(\frac{F_2}{W}\right)_i}\right)+1}\right] \tag{62}$$

$$\frac{\partial}{\partial V_s}\left[\mathrm{g}(h_f - h_i)\right]$$

$$= \frac{C_1^2}{\left(\frac{F_1}{W}\right)_i}\left(\frac{\partial \lambda_1}{\partial V_s}\right)\left[\frac{V_i}{C_1} - \ln(1-\lambda_1) - \frac{\lambda_1}{\left(\frac{F_1}{W}\right)_i}\right] \tag{63}$$

$$+ \frac{C_2^2}{\left(\frac{F_2}{W}\right)_i}\left[\left(\frac{\partial \lambda_2}{\partial V_s}\right)\left[\frac{V_s}{C_2} - \ln(1-\lambda_2) - \frac{\lambda_2}{\left(\frac{F_2}{W}\right)_i}\right] + \frac{\lambda_2}{C_2}\right]$$

To obtain expressions for the non-dimensional loss terms, the following quantity is utilized, accounting for the change in the rocket's gravitational potential energy over a stage burn:

$$\psi_n \equiv \left[\int \frac{m_R}{m_i}\mathrm{g}dh\right]_{\text{stage},n}$$

$$= \frac{C_n}{\left(\frac{F_n}{W}\right)_i}\left\{V_{ni}\lambda_n - \frac{1}{2}\left(V_{ni} + \frac{C_n}{\left(\frac{F_n}{W}\right)_i}\right)\lambda_n^2 + \frac{1}{3}\frac{C_n}{\left(\frac{F_n}{W}\right)_i}\lambda_n^3\right. \tag{64}$$

$$\left. + \frac{C_n}{4}[(1-\lambda_n)^2\{2\ln(1-\lambda_n) - 1\} + 1]\right\}$$

The expressions for the different loss terms are presented in Table 4. To reiterate, $K1^*$ terms account for the losses due to irreversibilities during the stage burns, $K2^*$ terms account for the losses associated with the kinetic energies of the discarded masses, $K3^*$ terms account for the losses due to lifting the expended propellant, and $K4^*$ account for the losses due to lifting the discarded masses.

Table 4. Full analytical form of the loss terms for a two-stage rocket in vertical climb (constant g).

| Term | Full analytical form of the term |
|---|---|
| $K1_1^*$ | $\lambda_1 - (1-\lambda_1)\frac{V_s^2}{2H_{P1}} + \frac{V_i^2}{2H_{P1}} - \frac{\psi_1}{H_{P1}}$ |
| $K1_2^*$ | $\lambda_2(1-\lambda_1-\delta_1)\frac{H_{P2}}{H_{P1}} - (1-\lambda_1-\delta_1)(1-\lambda_2)\frac{V_f^2}{2H_{P1}} + (1-\lambda_1-\delta_1)\frac{V_s^2}{2H_{P1}} - \frac{(1-\lambda_1-\delta_1)\psi_2}{H_{P1}}$ |
| $K2_1^*$ | $\frac{\delta_1}{H_{P1}}\left(\frac{V_s^2}{2} - \frac{V_i^2}{2}\right)$ |
| $K2_2^*$ | $\frac{(1-\lambda_1-\delta_1)\delta_2}{H_{P1}}\left(\frac{V_f^2}{2} - \frac{V_i^2}{2}\right)$ |
| $K3_1^*$ | $\frac{1}{H_{P1}}\{\psi_1 - \mathrm{g}(h_s - h_i)[1-\lambda_1-\lambda_2(1-\lambda_1-\delta_1)]\}$ |
| $K3_2^*$ | $\frac{1}{H_{P1}}\{(1-\lambda_1-\delta_1)\psi_2 - \mathrm{g}(h_f - h_s)[1-\lambda_1-\lambda_2(1-\lambda_1-\delta_1)-\delta_1]\}$ |
| $K4_1^*$ | $\frac{1}{H_{P1}}\mathrm{g}(h_s - h_i)[\delta_1 + \delta_2(1-\lambda_1-\delta_1)]$ |
| $K4_2^*$ | $\frac{1}{H_{P1}}\mathrm{g}(h_f - h_s)[\delta_2(1-\lambda_1-\delta_1)]$ |

# 4. CASE STUDIES

## 4.1. TWO-STAGE ROCKET IN FREE SPACE

The following case study provides results that utilize the analytical solution for the two-stage free space rocket (no drag or gravity) as developed in Subsection 3.1. In this study, the staging velocity $V_s$ is varied parametrically while fixing other characteristics, including final velocity of the final mass (see Table 5). Energy utilization information is produced for the complete range of staging velocities from initial velocity to final velocity. The non-dimensional formulation for the analysis is used (i.e., Eq. (33), with appropriate terms in the equation modeled using the special case formulation of those terms as given in equations (38), (39), and (44) thru (47)). Given below in Table 5 are the defined (fixed) characteristics of the first and second stages used in this parametric study.

Table 5. Free-space rocket's characteristics.

| Quantity | Value |
|---|---|
| Stage 1 specific impulse | $I_{sp,1}$ = 305.8 s |
| Stage 2 specific impulse | $I_{sp,2}$ = 407.75 s |
| Stage 1 effective exhaust velocity | $C_1$ = 3000 m/s |
| Stage 2 effective exhaust velocity | $C_2$ = 4000 m/s |
| Stage 1 accelerator efficiency | $\eta_{a,1}$ = 1.0 |
| Stage 2 accelerator efficiency | $\eta_{a,2}$ = 1.0 |
| Stage 1 discard mass ratio | $\delta_1$ = 0.10 |
| Stage 2 discard mass ratio | $\delta_2$ = 0.15 |
| Rocket's initial velocity | $V_i$ = 0 m/s |
| Rocket's final velocity | $V_f$ = 5000 m/s |

Figure 3 provides the overall non-dimensional energy utilization results versus staging velocity for this special case, where the first and second stages are denoted by S-I and S-II, respectively. It is important to realize that the total initial available energy associated with stage 1 and stage 2 propellant (at time = 0), i.e., the top line in this figure, varies with staging velocity. This is because this line represents the overall non-dimensional energy availability, $E^*_{\mathrm{AV}}$, which has values of:

$$\left(H_{P1} + \frac{V_i^2}{2}\right) m_{P1} + \left(H_{P2} + \frac{V_i^2}{2}\right) m_{P2} \text{ , normalized by } m_{P1} H_{P1}$$

Hence, as the staging velocity changes, the balance and values of stored propellant on stage 1 and stage 2, respectively, necessarily change.

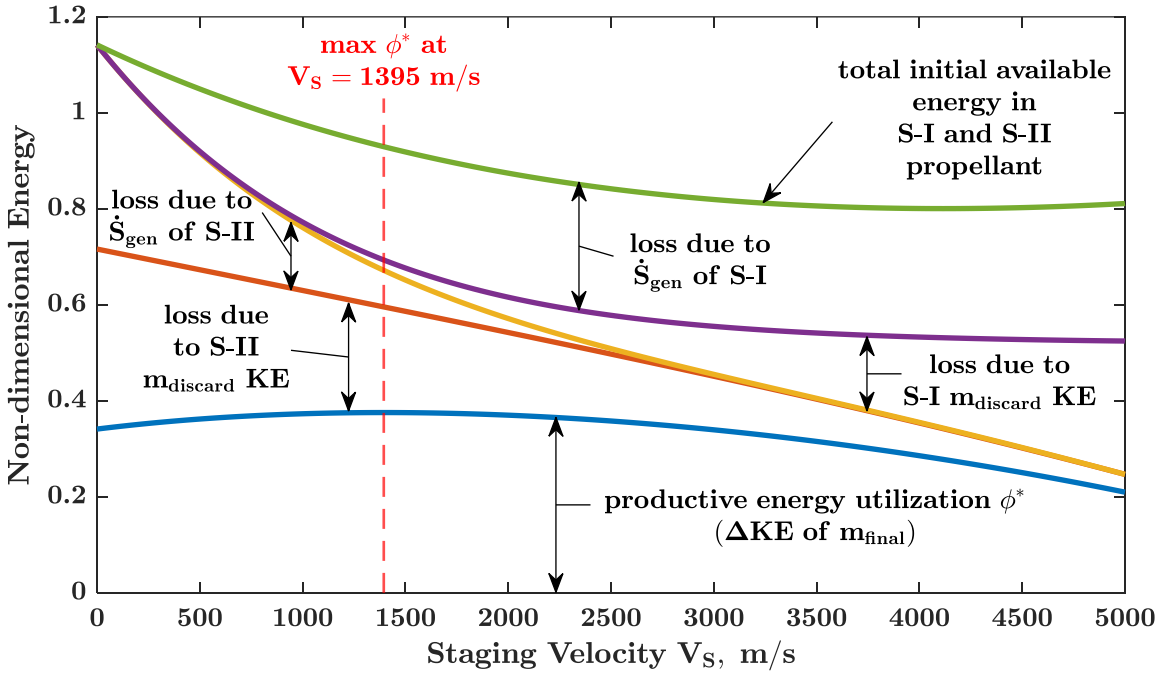


Figure 3. Non-dimensional energy utilization results for two stage 'free-space' rockets for range of staging velocities; stage 1 and stage 2 acceleration efficiencies = 1.

The productive energy utilization (the kinetic energy change of the final vehicle mass, i.e., $\phi^*$ in Eq. (33) as represented by the bottom line in Figure 3) is maximized at a staging velocity of around 1395 m/s, which in agreement with the analytical solution obtained by applying Eq. (43). The corresponding non-dimensional productive energy utilization value at this optimal staging velocity is around 0.376. The balance of energy utilization existing between these two lines is composed of contributions from stage 1 and stage 2 losses (irreversibilities) and 'losses' associated with the kinetic energies of stage 1 and stage 2 discarded structural masses. Note that because this special case does not include gravity, there are no geopotential energy utilization terms associated with either lifting of expended propellant or discarded structural mass. At low staging velocities, stage 2 losses (irreversibilities and kinetic energy associated with discard mass of that stage) are large. As staging velocity increases, stage 1 losses associated with both irreversibilties and discarded mass increase, while corresponding stage 2 losses become smaller.

Figure 4 provides the non-dimensional mass fractions associated with the parametric energy utilization results shown in the previous figure (Figure 3). Here the masses are normalized by the overall initial mass of the vehicle, $m_i$. The final mass of the vehicle is seen to be optimized (maximized) at a staging velocity of 1395 m/s, corresponding to the same optimal staging velocity as obtained for energy utilization. This is expected for free space rockets, since the (maximum) final vehicle kinetic energy at the specified final velocity of 5000 m/s (corresponding to maximum productive energy utilization for a free-space rocket) will necessarily exactly correspond to (maximum) final vehicle mass at that same velocity.

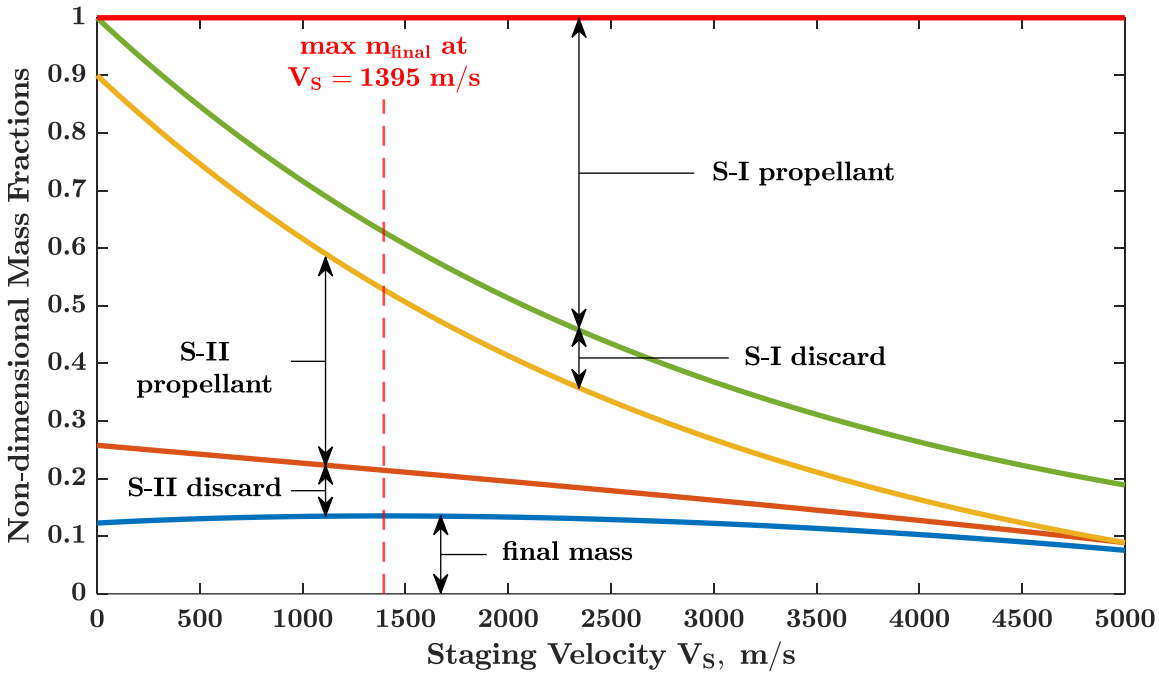


Figure 4. Non-dimensional mass results for two stage 'free-space' rockets for range of staging velocities.

Figure 5 provides energy utilization results for a similar parametric study with the same inputs as used to produce Figure 3, with the exception that both stage 1 and stage 2 acceleration efficiencies are set to 0.8 (i.e., more internal losses are imposed on the propulsion systems in both stage 1 and stage 2). Losses associated with stage 1 and stage 2 entropy generations increase as expected; productive energy utilization therefore decreases across the range with the maximum (non-dimensional) productive energy dropping significantly. However, the optimal staging velocity does not change between Figure 3 and Figure 5. This reflects the fact that decreases in acceleration efficiencies for the free space two stage rocket have no effect on the optimal staging velocity; the balance of losses simply increases equally, proportional to the acceleration efficiencies, across the staging velocity range.

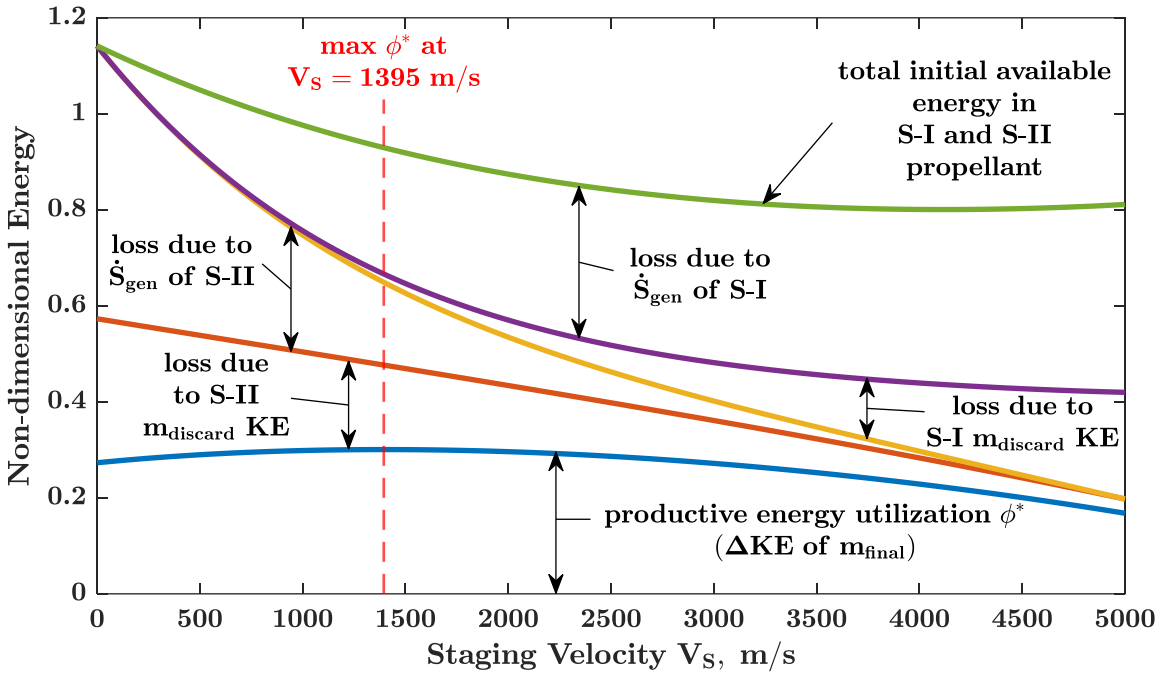


Figure 5. Non-dimensional energy utilization results for two stage 'free-space' rockets for range of staging velocities; stage 1 and stage 2 acceleration efficiencies = 0.8.

## 4.2. TWO-STAGE ROCKET IN VERTICAL CLIMB IN A CONSTANT GRAVITATIONAL FIELD AND NEGLIGIBLE DRAG

This case study provides results that rely on the (special case) analytical solution developed in this work (see Subsection 3.2) for a two-stage rocket in a vertical climb in a gravitational field (but without consideration of external drag). Hence, in the present study, in contrast to the previous results shown in Subsection 4.1, geopotential work is done in lifting expended propellant to altitude, as well as to accelerate and lift discarded structural mass to velocity and altitude at discard (staging). Here the staging velocity $V_s$ is again varied parametrically while other characteristics are fixed, including the final velocity of the final mass. For the characteristics chosen and fixed in the present analysis, the final altitude achieved at this required final vehicle velocity is resultant and therefore varies with staging velocity. Energy utilization information is again produced for the complete range

of staging velocities from initial velocity to final velocity. As in the previous results for a free space rocket, the non-dimensional formulation for the analysis is used (i.e., Eq. (33), with appropriate terms in the equation modeled using the special case formulation of those terms as given in equations (39) and (57), as well as Table 4).

Given in Table 6 below are the defined (fixed) characteristics of the first and second stages used in this parametric study. Note the inclusion of the gravitational acceleration and the stage thrust to initial weight values. The gravitational acceleration constant used is g = 9.81 m/s$^2$ which is assumed to be constant throughout the mission.

Table 6. Vertical climb rocket's characteristics.

| Quantity | Value |
|---|---|
| Stage 1 specific impulse | $I_{sp,1}$ = 305.8 s |
| Stage 2 specific impulse | $I_{sp,2}$ = 407.75 s |
| Stage 1 effective exhaust velocity | $C_1$ = 3000 m/s |
| Stage 2 effective exhaust velocity | $C_2$ = 4000 m/s |
| Stage 1 accelerator efficiency | $\eta_{a,1}$ = 0.5625 (Saturn V stage 1) |
| Stage 2 accelerator efficiency | $\eta_{a,2}$ = 0.5970 (Saturn V stage 2) |
| Stage 1 discard mass ratio (relative to propellant mass) | $\delta_1^*$ = 0.06 (Saturn V stage 1) |
| Stage 2 discard mass ratio (relative to propellant mass) | $\delta_2^*$ = 0.10 (Saturn V stage 2) |
| Stage 1 initial thrust to weight ratio | $\left(\frac{F_1}{W}\right)_i$ = 1.2 |
| Stage 2 initial thrust to weight ratio | $\left(\frac{F_1}{W}\right)_i$ = 1.0 |
| Rocket's initial velocity | $V_i$ = 0 m/s |
| Rocket's final velocity | $V_f$ = 5000 m/s |

Figure 6 provides the overall non-dimensional energy utilization results versus staging velocity for this special case of a two-stage rocket in a vertical climb in a

gravitational field. As discussed for the free-space rocket case results provided in Figure 3, the total initial available energy associated with stage 1 and stage 2 propellant (at time = 0), i.e., the top line in this figure, necessarily varies with staging velocity.

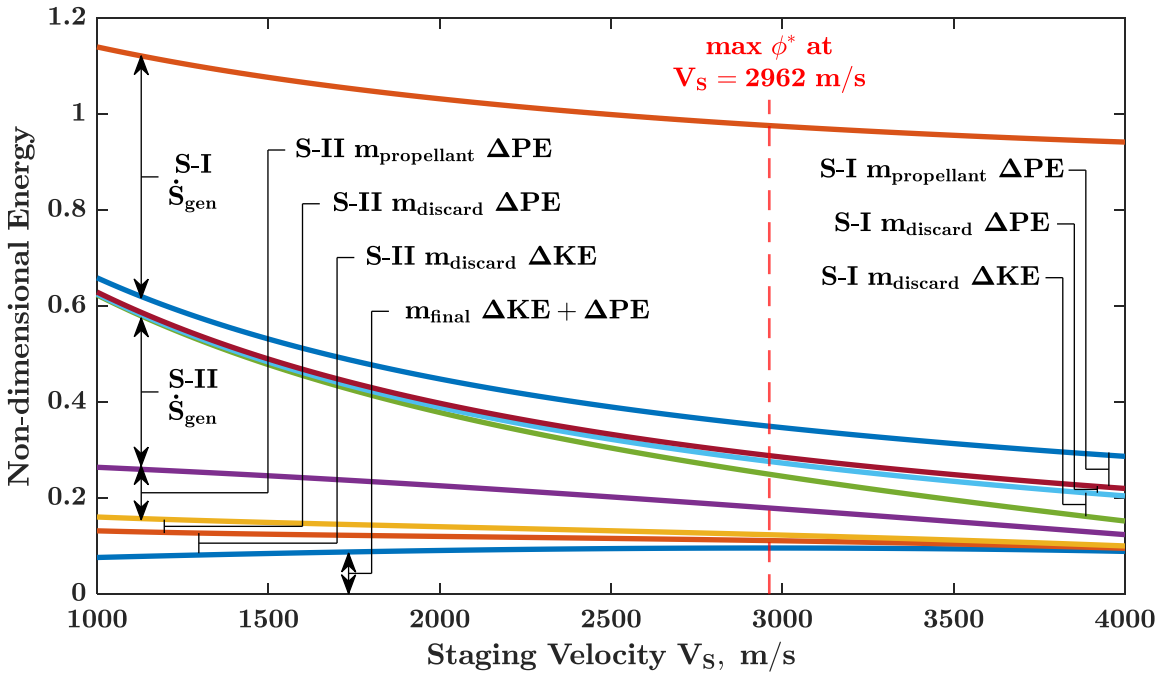


Figure 6. Non-dimensional energy utilization results for two-stage rocket in vertical climb in constant gravitational field for range of staging velocities.

For this case, the productive energy utilization includes both final kinetic energy change of the final vehicle mass, as well as the final potential energy change of the final vehicle mass (corresponding to the final altitude achieved at stage 2 structural mass discard). This value of productive energy utilization is given by $\phi^*$ in Eq. (57) and is represented by the bottom line shown in Figure 6. The balance of energy utilization shown at a specific staging velocity (energy utilization contributions shown in Figure 6 that lie between the initially available energy associated with loaded propellant - the top line in the

figure - and the productive energy utilization - the bottom line in the figure) is composed of the various labeled contributions. These contributions are energy utilization associated with stage 1 and stage 2 losses (irreversibilities), work done to lift expended propellant to altitude for both stage 1 and stage 2, and 'losses' associated with the kinetic energies and geo-potential energies of the stage 1 and stage 2 discarded structural masses. Again, as seen for the free space rocket, at low staging velocities, stage 2 losses (irreversibilities and kinetic and potential energy utilization associated with discarded mass) of that stage are large. Similarly, as staging velocity increases, stage 1 losses associated with both irreversibilties and discarded mass increase, while corresponding stage 2 losses become smaller. Due to the additional contributions to energy utilization associated with gravitational effects (geopotential work done in lifting expended propellant to altitude and lifting discarded structural mass), the productive energy utilization is significantly smaller across the staging velocity range for this case, in comparison to a free-space rocket, as should be expected.

As shown in Figure 5, the optimal staging velocity for maximizing the productive energy utilization for this two-stage rocket example is 2962 m/s, corresponding to a maximum (non-dimensional) value of 0.096 for the productive kinetic and potential energy of final vehicle mass. This result is agreement with the solution to Eq. (60) for the parameters' values of this case study. Recall that the product of initial rocket mass and the effective heating value of stage 1 propellant was used to non-dimensional raw energy utilization. Hence, for any given initial rocket mass at launch and given stage 1 propellant type, there is no other staging velocity that gives higher productive utilization of initially available energy associated with the initially loaded propellant in the stack. For the energy

utilization-optimized staging velocity of 2962 m/s, the final altitude achieved by the rocket at the end of stage 2 burn is 1173 km. (Final) mass ratio for this staging velocity is 0.032 (i.e., this value is the ratio of the rocket final mass after stage 2 burnout and mass discard to the initial rocket mass).

The mass fraction analysis (mass increments made non-dimensional by the initial vehicle mass) for the same problem is shown in Figure 7; as staging velocity is increased, stage 1 propellant mass increases while stage 2 propellant mass decreases, etc. The staging velocity for maximum final rocket mass occurs at 2090 m/s, i.e., with the given inputs and defined requirement of a 5000 m/s final velocity, this staging velocity yields a maximum final mass at stage 2 burnout and structural mass discard. The value of this final (maximum) mass ratio is 0.0328, yielding a higher final mass than that obtained for the staging velocity that maximizes productive energy utilization. However, the value of the productive energy utilization (the sum of kinetic and potential energy achieved by the final rocket mass) for the mass-optimized staging velocity of 2090 m/s is 0.09196, which is lower than the maximum energy-optimized value achieved at a staging velocity of 2962 m/s. This lower productive energy utilization for the mass-optimized case is in fact due to a lower final altitude achieved at stage 2 burnout (1011 km) as opposed to the final altitude achieved for maximum productive energy utilization (1173 km). Therefore, the energy-optimized staging velocity choice yields higher productive energy utilization at the mandated final velocity; the mass-optimized staging velocity choice yields higher mass at the mandated final velocity.

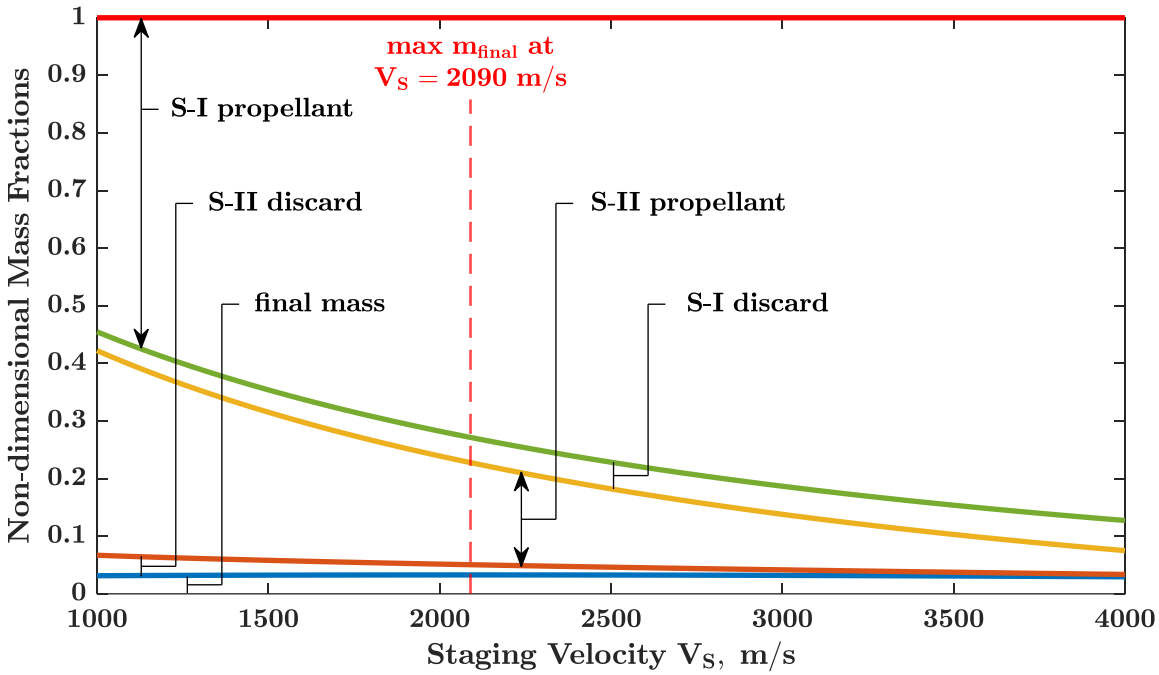


Figure 7. Non-dimensional mass results for two-stage rocket in vertical climb in a constant gravitational field for range of staging velocities.

However, if the altitude for the mass-optimized case is subsequently increased (through modeling an additional vertical constant velocity burn) to equal 1173 km (such that both cases then have both the same final velocity of 5000 m/s and final altitude of 1173 km), the final mass ratio for the originally mass-optimized case is, in fact, less than the final mass ratio of the original energy-optimized case.

This example demonstrates the usefulness of utilizing/considering energy utilization in design, analysis, and optimization. However, it must be noted that these results are predicated on the specific inputs chosen and particularly the specific mandated requirement of a given final vehicle velocity (without a required altitude requirement) within the analysis. Hence, if both final vehicle velocity and final altitude are mandated (with, for instance, thrust to initial weight of stage 2 taken as an output rather than a given

required value), the mass and energy utilization analyses necessarily will then both produce the same optimal, i.e., would both produce the same optimal stage velocity. Nevertheless, the results that are shown here underscore that explicit analysis of energy utilization can be informative and useful in the design and optimization of rockets, especially in applications in which both kinetic and potential energy changes are significant.

## 5. CONCLUSIONS

The energy availability utilization methodology directly relates the available energy (exergy) associated with the propellant to vehicle performance and losses that are associated with irreversibilities (entropy generation), energy imparted on any structural mass that is discarded, and energy used to lift the propellant. It should be noted that the 'global' control volume encapsulates all fluid inside and external to the vehicle as well as the wake region (which includes the exhaust plume). The mission-integrated formulation of the energy availability utilization balance incorporates the vehicle's equation of motion, such that the productive energy utilization is explicitly the change in the payload's kinetic and gravitational potential energies. The work presented in this paper establishes the general formulation of the mission-integrated energy availability utilization balance for an *N*-stage rocket in both dimensional and non-dimensional forms. The non-dimensional formulation is subsequently employed to conduct analytical staging optimization studies. Specifically, an analytical staging optimization study is performed for two special, simple cases: two-stage rocket operating in 1) free space and 2) vertical climb in a constant gravitational field. The optimization studies are aimed at finding the staging velocity that

would maximize the productive energy utilization (kinetic and gravitational potential energies imparted on the payload) for a mandated final velocity. This then indirectly determines the proportionality of the two stages. Two case studies are then conducted (corresponding to the aforementioned special cases) to graphically illustrate the energy utilization breakdown for the entire range of staging velocities. These case studies also serve as a validation for the analytic optimization studies.

The results of the analytic optimization study show that for the free-space case, both the energy utilization-based optimization and the traditional mass-based optimization yield the same result. This is further illustrated in the case study results. This is not surprising, as the productive energy utilization in this case is only the kinetic energy of the payload (no gravity), and since the final velocity is mandated, the only varying parameter in that term is the payload (final) mass. Therefore, maximizing the payload mass is maximizing the final kinetic energy. The results for the vertical climb in a constant gravitational field case, on the other hand, show subtle differences between mass based and energy-based approaches. In this case, the productive energy utilization consists of both the final kinetic energy as well as the final gravitational potential energy. The final altitude, unlike the final velocity, is not mandated, as doing so would over constrain the problem. As a result, the energy-based optimization and the mass-based optimization yield somewhat different results; specifically giving different payload masses and final altitudes. The mass-optimized approach, though yielding a higher payload mass than the energy-optimized case, has a lower final altitude. If then the final altitude is required to be the same as that of the energy-optimized case, by conducting a constant velocity burn, the final mass would then be less than that of the energy-optimized case. It is important to emphasize, however,

that this observation from this example is predicated on the specification of desired final conditions for the final rocket mass. When both final altitude and velocity are mandated, traditional mass-based analysis and energy utilization analysis yield identical optimization information. Nevertheless, the energy utilization analysis provides a significant amount of additional detail as to where losses actually occur and quantifies those losses in relative and absolute terms.

The work presented in this paper constitutes a further extension of previous work employing the global control volume-based energy availability utilization methodology. Such investigations are intended to develop an understanding of aerospace vehicle performance and the mechanics of flight from an energy availability perspective as rooted in fundamental principles of thermodynamics. This is in contrast to the traditional momentum-based viewpoint. However, the intention is not to supplant the traditional approach, but rather to supplement it. The energy availability approach provides unique insight and sheds light on the causal dependence of the degradation in performance on irreversibilities, which is inherent to all real processes. It does so while providing a direct and explicit relation between losses, as measure by entropy generation, and vehicle performance. Irreversibilities, quantified by entropy generation, are the chief reason why the available energy (exergy) is not realized by real systems as mechanical work. Entropy generation is indeed the most basic measure of losses for irreversibilities of any nature at any level of the system, from individual components, like turbopumps, to the entire vehicle in flight. Identifying a single currency/metric to quantify the degradation of performance - relative to the ideal/maximum theoretical- of components, subsystems, and systems of all types is viewed as advantageous for system-level optimization. In addition, efforts made

to improve the energy efficiency of aerospace systems and related studies and investigations can benefit greatly from an exergy-centric approach. As energy is a valuable 'commodity,' and especially with the recent interest in moving away from fossil fuels towards 'renewable' energy, understanding and applying energy utilization methodologies to complex aerospace systems could, in principle, potentially inspire innovative designs and concepts.

## REFERENCES

[1] Riggins, D.W., Moorhouse, D., Camberos, J., "Entropy Generation and Aerospace Vehicle Performance", Chapter 6, Volume 238, AIAA Progress in Astronautics and Aeronautics Series, *Exergy Analysis and Design Optimization for Aerospace Vehicles and Systems***,** AIAA, 2011, Reston, Virginia, pp. 181-227. DOI: 10.2514/5.9781600868405.0181.0227

[2] Riggins, D.W., Camberos, J., Moorhouse, D., "Characterization of Aerospace Vehicle Performance and Mission Analysis Using Exergy", Chapter 8, Volume 238, AIAA Progress in Astronautics and Aeronautics Series, *Exergy Analysis and Design Optimization for Aerospace Vehicles and Systems***,** AIAA, 2011, Reston, Virginia, pp. 275-307. DOI: 10.2514/5.9781600868405.0275.0307

[3] Riggins, D. W., Camberos, J., Wolff, M., Bowcutt, K., "Mission-Integrated Exergy Analysis for Hypersonic Vehicles: Methodology and Application", *AIAA Journal of Propulsion and Power*, Vol. 29, No. 3, pp. 610-620, May-June 2013. DOI: 10.2514/1.B34733

[4] Abbas, M., and Riggins, D. W., "Exergy-based performance analysis of a turbojet engine," Proceedings of the 52nd AIAA/SAE/ASEE Joint Propulsion Conference (2016, Salt Lake City, UT), American Institute of Aeronautics and Astronautics (AIAA), Jul 2016. DOI: 10.2514/6.2016-4638

[5] Abbas, M., and Riggins, D. W., "Analysis of Energy Utilization and Losses for Jet-Propelled Vehicles," *Aerospace*, vol. 8, no. 11, article no. 342, MDPI, November 2021. DOI: 10.3390/aerospace8110342

[6] Riggins, D.W., Abbas, M., Wainwright, M., Camberos, J., "Analysis of Energy Utilization for Chemical Rockets," *Journal of Spacecraft and Rockets*, vol. 56, no. 3, pp. 695-707, American Institute of Aeronautics and Astronautics (AIAA), May 2019. DOI: 10.2514/1.A34296

[7] Abbas, M., Riggins, D. W., and Watson, M. D., "Entropy-Based Performance Analysis of Chemical Rockets," AIAA SciTech 2020 Forum (Orlando, FL), AIAA, Jan 2020. DOI: 10.2514/6.2020-0759

[8] Abbas, M., Riggins, D. W., and Watson, M. D., "Utilization and Loss of Available Energy for chemical Rockets in Atmospheric Flight," *Journal of Spacecraft and Rockets*, Articles in Advance, August 2021. DOI: 10.2514/1.A35100

[9] Watson, M., "System Exergy: System Integrating Physics of Launch Vehicles and Spacecraft," *Journal of Spacecraft and Rockets*, Vol. 55, No. 2, 2018, pp. 451–461. DOI: 10.2514/1.A33929

[10] Oswatitsch, K., *Gas Dynamics*, Academic Press, New York, 1956, Chap. 4.

[11] Giles, M., and Cummings, R., "Wake Integration for Three-Dimensional Flowfield Computations: Theoretical Development," *Journal of Aircraft*, Vol. 36, No. 2, 1999, pp. 357–365.

[12] Foa, J., *Elements of Flight Propulsion*, Wiley, New York, 1960, Chap. 13.

[13] Clarke, J., and Horlock, J., "Availability and Propulsion," *Journal of Mechanical Engineering Science*, Vol. 17, No. 4, 1975, pp. 223-232. DOI: 10.1243/jmes_jour_1975_017_033_02

[14] Builder, C. H., "On the Thermodynamic Spectrum of Air-Breathing Propulsion," *1st Annual Meeting*, AIAA Paper 64-243, Washington, DC, June 1964. DOI: 10.2514/6.1964-243

[15] Lewis, J. H., "Propulsive Efficiency from an Energy Utilization Standpoint," *Journal of Aircraft*, Vol. 13, No. 4, 1976, pp. 299–302. DOI: 10.2514/3.44525

[16] Czysz, P. and Murthy, S. N. B., "Energy Analysis of High-Speed Flight Systems," Chapter 3 in *High-Speed Flight Propulsion Systems*. Progress in Astronautics and Aeronautics Series, AIAA, Volume 137.
DOI: 10.2514/5.9781600866104.0143.0235

[17] Murthy, S. N. B., "Effectiveness of a Scram Engine," *30th Joint Propulsion Conference and Exhibition*, AIAA Paper 94-3087, Indianapolis, IN, June 1994. DOI: 10.2514/6.1994-3087

[18] Brilliant, H. M., "Analysis of Scramjet Engines Using Exergy Methods," *31st Joint Propulsion Conference and Exhibition*, AIAA Paper 95-2767, San Diego, CA, June 1995. DOI: 10.2514/6.1995-2767

[19] Curran, E. T. and Craig, R. R., "The Use of Stream Thrust Concepts for the Approximate Evaluation of Hypersonic Ramjet Engine Performance," Air Force Aero Propulsion Laboratory, Technical Report AFAPL-TR-73-38, July 1973.

[20] Riggins, D. W., "The Thermodynamic Continuum of Jet Engine Performance; The Principle of Lost Work due to Irreversibility in Aerospace Systems," *International Journal of Thermodynamics*, Vol. 6, No. 3, 2003, pp. 107–120. DOI: 10.5541/ijot.1034000113

[21] Riggins, D., McClinton, C. R., and Vitt, P., "Thrust Losses in Hypersonic Engines Part 1: Methodology," *Journal of Propulsion and Power*, Vol. 13, No. 2, 1997, pp. 281–287. DOI: 10.2514/2.5160

[22] Riggins, D., "Thrust Losses in Hypersonic Engines Part 2: Applications," *Journal of Propulsion and Power*, Vol. 13, No. 2, 1997, pp. 288–295. DOI: 10.2514/2.5161

[23] Roth, B., "A Work Potential Perspective of Engine Component Performance," *AIAA Journal of Propulsion and Power*, Vol. 18, No. 6, 2002, pp. 1183-1190. DOI: 10.2514/2.6077

[24] Roth, B., "Comparison of Thermodynamic Loss Models Suitable for Gas Turbine Propulsion," *Journal of Propulsion and Power*, Vol. 17, No. 2, 2001, pp. 324–332. DOI: 10.2514/2.5745

[25] Roth, B., "Aerodynamic Drag Loss Chargeability and Its Implications in the Vehicle Design Process," AIAA Paper 2001-5236, Oct. 2001. DOI: 10.2514/6.2001-5236

[26] Arntz, A., Atinault, O., Merlen, A., "Exergy-Based Formulation for Aircraft Aeropropulsive Performance Assessment: Theoretical Development", *AIAA Journal*, Vol. 53, No. 6, 2015, pp. 1627-1639. DOI: 10.2514/1.J053467.

[27] Arntz, A., Hue, D., 2015. "Exergy-Based Performance Assessment of the NASA Common Research Model", *AIAA Journal*, Vol. 54, No. 1, 2016, pp. 88-100. DOI: 10.2514/1.J054127

[28] Ehyaei, M., Anjiridezfuli, A., Rosen, M. A., 2013. "Exergetic analysis of an aircraft turbojet engine with an afterburner", *Thermal Science*, Vol. 17, No. 4, 2013, pp. 1181–1194. DOI: 10.2298/tsci110911043e

[29] Hayes, D., Lone, M. M., Whidborne, J. F., and Coetzee, E., "Entropy Generation Minimization and Exergy analysis approaches for aerospace applications - A review". AIAA 2016-0866, January 2016. DOI: 10.2514/6.2016-0866

[30] Marley, C., and Riggins, D., "The thermodynamics of Exergy Losses and Thrust Production in Gas Turbine engines," 47th AIAA/ASME/SAE/ASEE Joint Propulsion Conference & Exhibit, AIAA Paper 2011-6130, San Diego, CA, July 2011. DOI: 10.2514/6.2011-6130

[31] Marley, C., and Riggins, D., "Exergy Analysis of a Turbojet Engine Modeled as a Lumped Parameter System," 50th AIAA Aerospace Sciences Meeting including the New Horizons Forum and Aerospace Exposition, AIAA Paper 2012-1122, Nashville, TN, January 2012. DOI: 10.2514/6.2012-1122

[32] Bastani, M., Jafari, R., and Ghasemi, H., "Exergy Analysis of an Aircraft Turbojet Engine," *International Journal of Engineering Sciences and Research Technology*, Vol. 4, No. 4, April 2015, pp. 380 – 386.

[33] Karakoc, T., and Turan, O., "Exergetic Destruction Effects of Operating Conditions on the Turbojet Engine Components," *Applied Mechanics and Materials*, Vols. 110-116, October 2011, pp. 2390-2394.

[34] Turan, O. and Karakoc, T., "Exergetic and Energetic Response Surfaces for Small Turbojet Engine," *Applied Mechanics and Materials,* Vol. 110-116, pp. 1054-1058.

[35] Yuksel, B., Balli, O., Gunerhan, H., Hepbasli, A., and Atalay, H., "Exergetic and Environmental Analyses of Turbojet Engine," 7th Global Conference on Global Warming (GCGW-2018), June 24-28, 2018, Izmir, Turkey.

[36] Gronstedt, T., Irannezhad, M., Lei, X., Thulin, O., and Lundbladh, A., "First and Second Law Analysis of Future Aircraft Engines," *Journal of Engineering for Gas Turbines and Power*, Vol. 136, March 2014, pp. 031202 1-10.

[37] Oates, G., *Aerothermodynamics of Gas Turbine and Rocket Propulsion*, AIAA Educational Series, 3rd ed., New York, 1997, pp. 68-70.

# SECTION

# 2. CONCLUSIONS AND RECOMMENDATIONS

## 2.1. CONCLUSIONS

This work has significantly expanded the theoretical basis and physical understanding of the control volume-based energy availability (or utilization of energy) methodology as originally formulated for aerospace vehicles in flight. It has also provided the techniques and capability for a number of applications within aerospace, covering both jet engine and rocket propelled flight. The methodology is based on global control volume analysis for a vehicle (or propulsion system) in flight and directly describes the fundamental relationships between exergy losses (entropy generation) and classic vehicle performance. It is essentially an extension of traditional exergy analysis but specialized to aerospace vehicles in flight. The work features analysis and applications involving 'stand-alone' propulsive systems (for which no airframe or non-propulsion system is considered), as well as 'complete' vehicles with integrated airframe and propulsion system.

The characteristics of a modeled stand-alone gas-turbine engine from an energy availability standpoint were analyzed over a wide range of operating conditions. The exergetic performance of jet-propelled aircraft in cruise was also investigated by integrating the modeled engines with a suitable airframe. The analytical link between entropy generation and cruise performance was established; this result is believed to represent the first explicit proof and demonstration of this link. Specifically, at flight conditions that minimize the entropy generation rate, endurance is shown to be maximized,

both theoretically and in application. Furthermore, at flight conditions that minimize entropy generation per distance traveled, the range is maximized, again shown both theoretically and in example application. Furthermore, these results focused on range and endurance are shown to be in agreement with the well-established traditional criteria for optimal cruise performance. However, the results obtained from the energy utilization approach are exact, whereas the traditional criteria (related to the lift-to-drag ratio of the vehicle) are approximate.

Also investigated in this work, both theoretically and through applications, are the energy utilization characteristics of chemical rockets operating across a wide range of flight conditions. It was shown based on energy utilization methodology that the entropy generation rate is necessarily minimized (for negligible aerodynamic drag) at a flight velocity equal to the effective exhaust velocity of the rocket propulsion system. Conversely, optimizing the productive utilization of available energy was found to occur at a significantly higher flight velocity, which is an explicit function of the overall thermochemical availability of the propellant. The effects of varying entropy generation inside a rocket engine on overall performance were also investigated. It was found that the trends are highly non-linear. Specifically, a given reduction in entropy generation for a ‘high-loss’ engine results in a much larger improvement in performance than seen by a ‘low-loss’ engine. This means that there is a trend of ‘diminishing returns’ for achieving meaningful loss reductions in rocket engines. The work done here provides direct insight (based on the energy utilization methodology and the fundamental considerations of the global control volume approach which inherently includes the wake in the analysis) into

the non-linearity of entropy generation that occurs inside the engine, in terms of its impact on vehicle performance.

The research presented here has also developed the techniques and theory for describing and quantifying in detail the energy availability aspects for a rocket-powered vehicle operating over a mission. Although focus in the present work has been on characterizing energy utilization in acceleration and climb missions for rockets (i.e., access-to-space), the techniques and methodologies are general and can be applied to other types of missions as well. The energy availability associated with the propellant at the beginning of the mission is not all realized as productive force-power on the vehicle. It is of course this force-power acting on the vehicle over the mission that results in change in the mechanical energy (kinetic and gravitational potential energies) of the final (payload and residual structure) mass. By far the largest portion of the initial energy availability associated with the on-board propellant is lost due to irreversibilities (entropy generation) inside the engines, external to the rocket (associated with aerodynamic drag), and in the wake mixing region where the rocket wake and exhaust plume equilibrate with the surroundings. The wake entropy generation is in fact massive in comparison with entropy generation in the propulsion system and over the vehicle itself. In addition, the inclusion of the wake entropy generation within the analysis is necessary to adequately assess losses for the rocket; the energy utilization approach taken in this work allows the direct assessment to be made. Other losses that are quantified by the energy utilization method include that portion of the energy availability that is used to lift the propellant to the altitude where it is expelled from the rocket. For rockets that utilize staging, a portion of the energy initially available is lost in imparting kinetic and gravitational potential energies on the

discarded mass. The work done here has formulated the theory and approach to applications and demonstration of applications that allow the exact quantification of all losses in available energy for rocket missions. This methodology has been generalized to *N*-stage systems and has also been applied to special cases in which optimization is examined.

The efforts undertaken in this scholarly work were aimed at increasing understanding of the energy availability and energy utilization aspects of powered flight. This methodology offers a unique perspective for assessing vehicle performance that is rooted in the fundamental laws of thermodynamics and can, in fact, be characterized as lying at the intersection of thermodynamics and classic vehicle performance. Specifically, the method is based on a different viewpoint than that generally taken in the well-established and universally accepted momentum-based approach. It also provides the exact proper analytical linkage between exergy analysis and classic vehicle performance concepts such as thrust, drag, change in kinetic and potential energies across a mission, and range and endurance. The objective of this research is not to 'replace' or supplant the traditional methodology for vehicle design, analysis, and optimization, but is instead to augment it, i.e., provide additional information. The energy utilization method as developed and applied within this work fundamentally provides an enormous wealth of additional information for the vehicle designer or analyst.

In summary, the theory, methodology, and applications developed and provided in this work provide the explicit analytical link between entropy generation and aerospace propulsion system and vehicle performance. Entropy generation is the fundamental universal metric/'currency' for all losses, no matter the type of loss mechanism or the

spatial location (at any level of sub-component, component, sub-system, or system) that a given loss occurs. The global control volume-based energy utilization approach for a vehicle in flight enables the consistent quantification and full accounting of vehicle and mission performance losses, in terms of the entropy generation. It has been shown to provide a significant amount of additional information beyond traditional methodologies that should be inherently useful to a vehicle designer and analyst. It has also provided clarification of (and the theoretical basis for) linking entropy generation characteristics to important elements of classic vehicle performance. Based on these results and observations, it is believed that the methodology has significant promise in facilitating and informing aerospace system-level design and optimization efforts.

## 2.2. RECOMMENDATIONS

The methodology can be further developed. One obvious extension is to adjust the energy availability utilization balance to allow analysis of spacecraft operating external to an atmosphere. It would be interesting to amalgamate the methodology with orbital mechanics in order to investigate energy availability utilization for interplanetary operation. This, of course, requires adjustments in the derivation of the relations. Extensions to vehicles utilizing other types of propulsion systems that are not chemical (in terms of relying on combustion-generated heat release, i.e., electric, nuclear) are also of potential interest.

As stated in the conclusions and elsewhere in this work, this methodology has the immediate ability to inform present system-level design and optimization techniques (in terms of providing a large amount of additional information within a given

design/optimization process). For optimization methodology that is based directly on the approach itself, an initial investigation could be useful in which a relatively simple problem is posed considering an aircraft with mandated performance capabilities and mission requirements. Initially, only the ‘major’ subsystems need be considered; propulsive, aerodynamic, and structural, and low fidelity models employed. The methodology would have to be integrated into an optimization routine where the entropy generation associated with the different subsystems is evaluated, with consideration of the wake issues, and then directly linked utilizing the energy utilization methodology to the overall performance of the vehicle. Comparison with existing design and optimization methods and approaches would then allow evaluation of the energy utilization approach.

# BIBLIOGRAPHY


[1] Carnot, N. L. S., et al., *Reflections on the Motive Power of Fire and Other Papers on the Second Law of Thermodynamics*, Dover Publications, New York, 1960.

[2] Bejan, A., "Entropy Generation and Exergy Destruction," *Entropy Generation Minimization: The Method of Thermodynamic Optimization of Finite-Size Systems and Finite-Time Processes*, 1st ed., CRC Press, New York, 1995, pp. 21–47. DOI:10.1201/9781482239171

[3] Hayes, D., Lone, M., and Whidborne, J., "Entropy Generation Minimization and Exergy Analysis Approaches for Aerospace Applications—A Review," AIAA Paper 2016-0866, Jan. 2016.

[4] Clarke, J., and Horlock, J., "Availability and Propulsion," *Journal of Mechanical Engineering Science*, Vol. 17, No. 4, 1975, pp. 223–232. DOI: 10.1243/JMES_JOUR_1975_017_033_02

[5] Lewis, J. H., "Propulsive Efficiency from an Energy Utilization Standpoint," *Journal of Aircraft*, Vol. 13, No. 4, 1976, pp. 299–302. DOI: 10.2514/3.44525

[6] Foa, J., "Efficiencies: Propulsive Cycles," *Elements of Flight Propulsion*, Wiley, New York, 1960, pp. 274–287.

[7] Doty, J., Camberos, J., and Moorhouse, D., "Benefits of Exergy-Based Analysis for Aerospace Engineering Applications: Part 1." *40th Thermophysics Conference*, AIAA Paper 2008-4355, Seattle, WA, June 2008. DOI: 10.2514/6.2008-4355

[8] Etele, J. and Rosen, M. "Sensitivity of Exergy Efficiencies of Aerospace Engines to Reference Environmental Selection", *Exergy, An International Journal*, Vol. 1, Issue 2, 2001, pp. 91-99. DOI: 10.1016/S1164-0235(01)00014-0

[9] Arntz, A., Atinault, O., and Merlen, A., "Exergy-Based Formulation of Aircraft Aeropropulsive Performance Assessment: Theoretical Development," *AIAA Journal*, Vol. 53, No. 6, June 2015, pp. 1627-1639. DOI: 10.2514/1.J053467

[10] Builder, C. H., "On the Thermodynamic Spectrum of Air-Breathing Propulsion," *1st Annual Meeting*, AIAA Paper 64-243, Washington, DC, June 1964. DOI: 10.2514/6.1964-243

[11] Brilliant, H. M., "Analysis of Scramjet Engines Using Exergy Methods," *31st Joint Propulsion Conference and Exhibition*, AIAA Paper 95-2767, San Diego, CA, June 1995. DOI: 10.2514/6.1995-2767

[12] Roth, B., and Mavris, D., “Comparison of Thermodynamic Loss Models Suitable for Gas Turbine Propulsion,” *Journal of Propulsion and Power*, Vol. 17, No. 2, 2001, pp. 324–332. DOI: 10.2514/2.5745

[13] Ehyaei, M., Anjiridezfuli, A. and Rosen, M.. "Exergetic Analysis of an Aircraft Turbojet Engine with an Afterburner." *Thermal Science*, Vol. 17, No. 4, pp. 1181-194. DOI: 10.2298/TSCI110911043E

[14] Bastani, M., Jafari, R., and Ghasemi, H., “Exergy Analysis of an Aircraft Turbojet Engine,” *International Journal of Engineering Sciences and Research Technology*, Vol. 4, No. 4, April 2015, pp. 380–386.

[15] Karakoc, T., and Turan, O., “Exergetic Destruction Effects of Operating Conditions on the Turbojet Engine Components,” *Applied Mechanics and Materials*, Vols. 110-116, October 2011, pp. 2390-2394.

[16] Turan, O. and Karakoc, T., “Exergetic and Energetic Response Surfaces for Small Turbojet Engine,” *Applied Mechanics and Materials*, Vol. 110-116, pp. 1054-1058.

[17] Yuksel, B., Balli, O., Gunerhan, H., Hepbasli, A., and Atalay, H., “Exergetic and Environmental Analyses of Turbojet Engine,” *7th Global Conference on Global Warming (GCGW-2018)*, June 24-28, 2018, Izmir, Turkey.

[18] Riggins, D.W., Camberos, J., and Moorhouse, D., “The Characterization of Aerospace Vehicle Performance and Mission Analysis Using Thermodynamic Availability”, *AIAA Journal of Aircraft*, Vol. 47, No. 3, 2010, pp. 904-916. DOI: 10.2514/1.46420

[19] Riggins, D. W., Moorhouse, D., and Camberos, J., *Entropy Generation and Aerospace Vehicle Performance*, Vol. 238, Progress in Astronautics and Aeronautics Series, Exergy Analysis and Design Optimization for Aerospace Vehicles and Systems, AIAA, Reston, VA, 2011, pp. 181–227, Chap. 6. DOI:10.2514/5.9781600868405.0181.0227

[20] Oates, G., *Aerothermodynamics of Gas Turbine and Rocket Propulsion*, AIAA Educational Series, 3rd ed., New York, 1997, pp. 68-70.

# VITA

Mohammad Abbas was born in Kuwait City, Kuwait in 1992 and completed his basic and secondary education there. He received a Bachelor of Science degree in Mechanical Engineering, Summa Cum Laude, from Missouri University of Science and Technology, with a minor in Aerospace Engineering, in May 2015. He received a Master of Science degree in Aerospace Engineering from Missouri University of Science and Technology in May 2017 and received a Doctor of Philosophy degree in Aerospace Engineering from Missouri University of Science and Technology in May 2022. Between August 2012 and May 2015, he worked as a Peer Learning Assistant at the Physics Learning Center, at Missouri S&T, as part of the university's Learning Enhancement Across Disciplines program. He continued to routinely volunteer in the Physics Learning Center between August 2015 and April 2020. He worked as a Graduate Teaching Assistant for the Mechanical Engineering Capstone Design course for three consecutive semesters between August 2017 and May 2018. He was subsequently employed by the Mechanical and Aerospace Engineering Department at Missouri S&T as a class instructor between January 2019 and May 2022. In that capacity, he was the instructor for one section of sophomore-level Dynamics for three consecutive semesters and of sophomore-level Thermodynamics for the following four semesters.